LEABHARLANN CHOLÁISTE NA TRÍONÓIDE, BAILE ÁTHA CLIATH | TRINITY COLLEGE LIBRARY DUBLIN
Ollscoil Átha Cliath | The University of Dublin

Terms and Conditions of Use of Digitised Theses from Trinity College Library Dublin

Copyright statement

All material supplied by Trinity College Library is protected by copyright (under the Copyright and Related Rights Act, 2000 as amended) and other relevant Intellectual Property Rights. By accessing and using a Digitised Thesis from Trinity College Library you acknowledge that all Intellectual Property Rights in any Works supplied are the sole and exclusive property of the copyright and/or other IPR holder. Specific copyright holders may not be explicitly identified. Use of materials from other sources within a thesis should not be construed as a claim over them.

A non-exclusive, non-transferable licence is hereby granted to those using or reproducing, in whole or in part, the material for valid purposes, providing the copyright owners are acknowledged using the normal conventions. Where specific permission to use material is required, this is identified and such permission must be sought from the copyright holder or agency cited.

Liability statement

By using a Digitised Thesis, I accept that Trinity College Dublin bears no legal responsibility for the accuracy, legality or comprehensiveness of materials contained within the thesis, and that Trinity College Dublin accepts no liability for indirect, consequential, or incidental, damages or losses arising from use of the thesis for whatever reason. Information located in a thesis may be subject to specific use constraints, details of which may not be explicitly described. It is the responsibility of potential and actual users to be aware of such constraints and to abide by them. By making use of material from a digitised thesis, you accept these copyright and disclaimer provisions. Where it is brought to the attention of Trinity College Library that there may be a breach of copyright or other restraint, it is the policy to withdraw or take down access to a thesis while the issue is being resolved.

Access Agreement

By using a Digitised Thesis from Trinity College Library you are bound by the following Terms & Conditions. Please read them carefully.

I have read and I understand the following statement: All material supplied via a Digitised Thesis from Trinity College Library is protected by copyright and other intellectual property rights, and duplication or sale of all or part of any of a thesis is not permitted, except that material may be duplicated by you for your research use or for educational purposes in electronic or print form providing the copyright owners are acknowledged using the normal conventions. You must obtain permission for any other use. Electronic or print copies may not be offered, whether for sale or otherwise to anyone. This copy has been supplied on the understanding that it is copyright material and that no quotation from the thesis may be published without proper acknowledgement.

Kinetic Studies on Biliverdin-IXα Reductase

A dissertation submitted to Trinity College, Dublin for the degree of Doctor of Philosophy

by

Edward Franklin

School of Biochemistry and Immunology
University of Dublin
Trinity College
Dublin 2
Ireland

March 2006

TRINITY COLLEGE
10 NOV 2006
LIBRARY DUBLIN
THESIS
7990

Dedicated with love to my parents,

Peter and Patricia Franklin.

TABLE OF CONTENTS

Declaration		**(i)**
Acknowledgements		**(ii)**
Abstract		**(iii)**
Abbreviations		**(iv)**
Chapter 1	**Introduction**	
1.1	**Haem and tetrapyrroles**	**1**
1.2	**The nomenclature and structure of tetrapyrroles**	**1**
1.3	**The evolutionary origins of haem**	**2**
1. 4	**Precursors and formation of tetrapyrroles**	**3**
1.5	**The localization of haem synthesis**	**4**
1. 6	**The haem degradation pathway**	**5**
1.7	**Physiological significance of haem degradation**	**8**
1.8	**Biliverdin in plants and bacteria**	**9**
1.9	**Haem Oxygenase**	**10**
1.10	**Biliverdin Reductase**	**12**
Chapter 2	**Materials and Methods**	
2.1	**DNA Purification and Manipulation Techniques**	**19**
2.1.1	**Electrophoresis of DNA**	**19**
2.1.2	**Determination of the concentration and purity of nucleic acids**	**19**

2.1.3	Digestion of DNA	20
2.1.4	Ligation of DNA fragments	20
2.1.5	Purification of plasmid DNA and PCR products	21
2.1.6	Large scale purification of plasmid DNA from overnight cultures	21
2.1.7	Small scale purification of plasmid DNA from overnight cultures	22
2.1.8	Purification of amplified PCR products	22
2.1.9	DNA Sequencing	23
2.1.9a	Terminator Cycle Sequencing Ready Reaction	23
2.1.9b	Preparation of Sequencing Gel	24
2.1.10	Total RNA Purification and Reverse Transcriptase Polymerase Chain Reactions	25
2.1.10a	The isolation of total RNA from animal tissues	25
2.1.10b	First Strand cDNA synthesis	25
2.1.10c	PCR from primer specific first strand cDNA aliquots	26
2.1.11	Site directed mutagenesis of plasmid cDNA inserts	28
2.2	Bacterial strains and culturing techniques	28
2.2.1a	Preparation of fresh competent cells for storage	28
2.2.1b	Transformation of competent cells	28
2.2.1c	Preparation and transformation of *E. coli* cells by electroporation	29
2.2.2	Preparation of *E.coli* cells for SDS-PAGE	29
2.3	Protein electrophoresis and immunoblotting	30
2.3.1	Sodium dodecyl sulphate – polyacrylamide gel electrophoresis (SDS-PAGE) sample preparation	30
2.3.2	Gel preparation and electrophoresis	30
2.3.3	Staining and de-staining procedures	31
2.3.4	Raising antisera	31
2.3.4a	Preparation of protein for immunisation schedule	31
2.3.4b	Determination of antibody titre using a dot blot assay	32
2.3.5	Western Blotting	33
2.4	Protein expression and purification	33
2.4.1	Activity measurements of recombinant	

	glutathione-S-transferase fusion proteins	33
2.4.2	Protein purification techniques	34
2.4.3	Purification of *Synechocystis PCC 6803* biliverdin-IXα reductase	35
2.4.4	Preparation and purification of human biliverdin IXα reductase	36
2.4.5	Purification of murine BVR-A (ppMAL expression vector)	37
2.4.6	Purification of Rat Biliverdin-IXα Reductase	38
2.4.7	Preparation of cytosolic fractions from murine tissue	39
2.4.8	Desalting protein samples using Sephadex G-25 gel filtration	40
2.4.9	Chromatofocusing of BVR-A	40
2.4.10	Protein concentration techniques	
2.4.11a	Protein Determination	41
2.4.11b	Bradford protein determination in multiwell plates	42
2.5	Kinetic and ligand binding studies	42
2.5.1	Kinetic studies on biliverdin IX-α reductase	42
2.5.2	Recording of CD spectra and stopped flow CD measurements	43
2.5.3	Absorbance spectrum measurements	44
2.5.4	Measurement of stopped flow absorbance kinetic traces	44
2.5.5	Fluorescence Binding Studies on BVR-A	45
2.5.6	Determination of protein bound zinc by atomic absorption spectrophotometry	45
2.5.7	Preparation of biliverdin IXα	46
2.5.7b	Preparation of biliverdin ditaurate	47
2.5.8	Separation of adenine nucleotides and nicotine adenine dinucleotides	47
2.5.9a	Separation of adenine nucleotides and nicotine adenine dinucleotides on DEAE	47
2.5.9b	Separation of adenine nucleotides and nicotine adenine dinucleotides on HPLC	48
2.5.9c	Separation of nicotine adenine dinucleotides on PEI cellulose	48

2.5.10 Synthesis of [P^{32}] NADPH 49

2.6 The identification of biliverdin-IXα reductase cDNA from various organisms 49

2.7 The crystalisation of human, and murine biliverdin reductase 50

Chapter 3 A phylogenetic survey of biliverdin -IXα reductase

3.1 Introduction 51

3.2 'In silico' sequence analysis, and the identification of putative biliverdin reductases from various species 54

3.3 Amplification of *Xenopus tropicalis* BVR-A sequence 55

3.3.1 Digestion and ligation of *Xenopus* cDNA into pGEX-KG 56

3.3.2 Screening for the presence of *Xenopus* BVR-A insert in transformed cells 56

3.4 Amplification of the *Danio rerio* (zebrafish) BVR-A sequence 57

3.4.1 Digestion and ligation of zebrafish cDNA into pET41a-Mod and pGEX-KG 57

3.4.2 Screening for the presence of zebrafish BVR-A insert in transformed cells 58

3.5 Identification and cloning of the putative murine biliverdin- IXα reductases 59

3.5.1 The Isolation of RNA from murine tissues 59

3.5.2 Amplification of murine BVR-A c-DNA 60

3.5.3 Digestion and ligation of Murine cDNA into ppMAL and pGEX-KG 60

3.5.4 Screening for the presence of murine BVR-A insert in transformed cells 60

3.5.6 Sequence analysis of the murine BVR-A cDNA ppMAL construct 61

3.7 The tissue and gender distribution of *Murine*

	Biliverdin-IXα reductase	61
3.8	Cloning of human biliverdin- IXα reductase	62
3.8.1	Amplification of human BVR-A c-DNA	62
3.8.2	Digestion and ligation of human cDNA into pET41a-Mod	62
3.8.3	Screening for the presence of human BVR-A insert in transformed cells	63
3.8.4	Sequence analysis of human cDNA in the plasmid pET-41aMod	63
3.9	Investigation of a putative avian biliverdin- IXα reductase	63
3.9.1	The *Gallus gallus* genomic sequence	63
3.9.2	Preparation of erythrocyte lysate from packed turkey red blood cells	64
3.10	Protein expression and purification	64
3.10.1	Purification of recombinant human BVR-A	65
3.10.2	Purification of recombinant murine BVR-A	65
3.10.3	Purification of recombinant *Synechocystis* and rat BVR-A	66
3.11	Chapter 3 Discussion	67

Chapter 4 The nature of the dual pH-cofactor specificity of BVR-A

4.0	Introduction	75
4.1	Effect of pH on the stability, activity and cofactor selectivity of biliverdin-IXα reductases from various species	77
4.1.1	The effects of pH on the stability of various BVR-As	77
4.1.2	The effect of pH on the activity of BVR-A	78
4.2	Studies on phosphate activation of human BVR-A	79
4.2.1	The effects of various anions on the activity of human BVR-A	79
4.2.2	The effects of phosphate on the NADH dependent activity of human BVR-A	80
4.2.3	The effect of phosphate on the burst rate constant of human BVR-A	81

4.2.4 The effect of pH on the anion activation of human BVR-A using NADH as cofactor 82

4.3 Studies on phosphate activation of rat BVR-A 82

4.3.1 Identification of a putative 2'-phosphate binding site 82

4.3.2 Site-directed mutagenesis of residues in the 2'-phosphate pocket 83

4.3.3 Effect of phosphate concentration on the activity of wild type and "2'-phosphate pocket" mutants of rat BVR-A 83

4.3.4 Comparision of the kinetic parameters for NADH and NADPH with the wild type and S43A mutants and R44A mutants of rat BVR-A 84

4.3.5 The effect of phosphate on the dissociation constant of NAD^+ with BVR-A 84

4.4 The effect of pH and biliverdin-IXα concentrations on the initial rate using NADPH as cofactor 85

4.5 Chapter 4 Discussion 86

Chapter 5 Spectral and kinetic studies on biliverdin-IXα reductase

5.1 Introduction 88

5.2 Separation of nucleotides 90

5.2.1 Separation of nucleotides using DEAE column chromatography 91

5.2.2 Separation of nucleotides using PEI cellulose TLC 91

5.2.3 Separation of nucleotides using HPLC 93

5.2.4 Synthesis of [adenylate-^{32}P] NADH 93

5.2.5 Synthesis of 2'-[^{32}P]-NADPH 94

5.2.6 The temperature dependent inactivation of human BVR-A 96

5.2.7 The assay of human BVR-A using 2'-[^{32}P]-NADPH as cofactor 96

5.3 Investigating the nature of the biliverdin binding pocket 97

5.3.1 Probing the nature of substrate specificity of human biliverdin-IXα reductase using conformationally locked biliverdin substrates 97

5.3.2 Initial rate studies with biliverdin sulphonate,

5.3.3 biliverdin ditaurate and the dimethyl ester of biliverdin-IXα 99

5.3.4 The CD spectrum of biliverdin-IXα and bilirubin-IXα bound to BVR-A 99

5.3.5 Discussion 100

Chapter 6 Is biliverdin-IXα reductase a zinc metalloprotein, and does it have a leucine zipper type DNA binding domain?

6.1 Introduction 105

6.2 Determination of protein bound zinc by atomic absorption spectrophotometry 106

6.3 Discussion 108

Chapter 7 General discussion

General discussion 112

Appendix I 115
Appendix II 116
Appendix III 121
Appendix IV 129
Appendix V 140

References

Declaration

This thesis is submitted by the undersigned to the University of Dublin for the examination of Doctorate in Philosophy. The work herein is entirely my own and has not been submitted as an exercise for a degree in any other university. The library at Trinity College, Dublin, has my full permission to lend or copy this thesis on request.

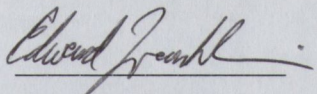

Edward Franklin

March 2006

Acknowledgements

Sincere thanks to my supervisor Dr. Tim Mantle for his never ending support, advice guidance enthusiasm and friendship. Thanks for all the opportunities past and present. I owe you a great deal. I have come to one conclusion regarding enzyme kinetics:-

Anyone who isn't confused about enzyme kinetics
really doesn't understand kinetics.

A very special thanks to my family especially my parents Peter and Patricia. You have given me everything, and without your support this would have been impossible. So this is dedicated to both of you with love.

To my brother Peter, and sisters Eleanor, Marcia and Irene. Thanks for everything ye have done for me. When times were tough you made the road much easier. Enjoy the read because I think some of your sweat and tears have gone into this too. Thanks also to Darragh, Brian and Frankie, for all the laughs and friendship. You all kept my family busy enough so that I had time to finish my writing. To Olivia, very special thanks for your love understanding and support through the years.

Great gratitude is due to all in Tim's lab past and present. To the International DJ, Seamus (you would have avoided the traffic cone too) Browne, my long suffering friend;-The surf is finally up! Thanks for so many laughs. Just a few things to say: your gorilla hallucination from a Rhode Island bed wasn't a hallucination! I'm never sitting in a Boston cab with you again (we get a limo next time you decide I'm getting married). Thanks also for ruining any postdoc prospects we had with a very imminent tetrapyrrole researcher. Thanks for the toilet blockage and the toilet engineer, the stairs inside my hall door, the late night security phone calls, the dirty screensaver, the Wednesday nights, the carpet burns the tendonitis and the plumbers cleavage, the skittle machine in the toilet, a broken rib, and for introducing me into the world of bouncers and security. It's onwards and upwards from here. Thanks also to Gavin McMess Manus, a gentleman, a friend and now a scholar. The memories just keep flooding back. It was nice to have someone with height, muscle and attitude visiting the Junior Dean. Thanks also for the floods in Spain. It seems that you are a man who likes to walk on water. You kept me on *terra ferma* through the years even when chatting up waitresses. So finally we can finally go for that curry. A big thanks to Coilín for making sure the lab didn't explode and that my columns were there when I needed them. Thanks for 'the sun' in the morning the smell of toasted cheese sandwiches at lunch, and the smell of *E.Coli* in the evening. You provided invaluable help through the years. To Bertie, a Mexican by birth, a Munster man by heart. Thanks for the good friendship and patience, and also for the bouncy castles and all the craic. Blue hair and boots really suit you! To Jerard 'Don Juan' Hayes. Roses rolleys and letterboxes…! Stop denying it, she was at least fifty. Stay with the science, gardening just isn't your thing. Thanks for all the bruises questions and laughs. To Vini and Tania for the advice support and scandal. To Valeria for the tiramisu, the friendly ear, and all the tears. A big thanks to MaryAnne for your, friendship and all the fun. Thanks to Joe for, all the diversions, and Jeff for giving me angina every week during soccer. Thanks to Orla, Geraldine, Arlene and Veronica for the endless supply of crosswords, fish, staples and laughs. Thanks to cuz Caroline for stressing me out and reminding me that I should have written up a long time ago, and Michelle for the dinners and a pillow during my frequent lab breaks. Last but not least, thanks to all members of the department for putting up with me for so long.

Abstract

The species distribution of biliverdin-IXα reductase (BVR-A) has been reinvestigated. It appears increasingly likely that birds and amphibia have the potential to express an active biliverdin-IXα reductase. The full length cDNAs encoding human, *Danio rerio*, murine, and *Xenopus* BVR-A were successfully amplified and cloned into various expression vectors. To date human BVR-A pET41a-Mod, murine BVR-A ppMAL, and *Xenopus* BVR-A pGEX-KG transformed cultures have been induced with IPTG resulting in the expression of recombinant proteins which display the appropriate molecular weights. The cloning and expression of an active *Xenopus* BVR-A in this study and the detection of biliverdin reductase activity in turkey erythrocyte cytosol extends the phylogenetic distribution of BVR-A to include amphibians and possibly birds.

Phosphate has been shown to enhance NADH binding by human BVR-A as the apparent K_m for NADH is decreased over 100-fold with no change in the apparent V_{max}. Replacement of residues around the nucleotide's 2' phosphate binding pocket was used to investigate the nature of phosphate activation. It was shown that the R44A mutant not only abolished the kinetic discrimination between NADH and NADPH, but also the activation by phosphate during the NADH dependent reaction. It is clear that NADH binding is augmented by inorganic phosphate "mimicking" the 2'-phosphate of NADPH. The kinetics of the mammalian enzymes have been distorted by the effects of substrate inhibition and by the activation of NADH dependent activity by phosphate. It now seems likely that the nature of the dual pH-cofactor specificity is due to the pH dependence of substrate inhibition which is additionally complicated by phosphate activation with NADH as cofactor. In order to overcome the effects of substrate inhibition hampering the full characterisation of these enzymes it was decided to develop a radiolabelled assay for BVR-A. It has been shown that the synthesis of radiolabelled 2'-[^{32}P] NADPH with a specific activity of 243mCi/mmol is possible and that the TLC separation of $NADP^+$ from NADPH and NAD^+ from NADH on PEI cellulose provides a convenient method to assay the activity of this enzyme.

The substrate specificity of BVR-A was investigated in the hope of gaining an insight into factors determining substrate binding. These studies suggest that the most important determining factors for substrate binding are the charged propionate moiety on two

central pyrrole rings. In addition, biliverdin-IXα dimethylester was shown not to be a substrate for human BVR-A, while the reaction using biliverdin-IXα sulphonate as substrate was catalytically productive. Further studies using biliverdin isomers with conformational restraints suggest that significant modifications on the conformational volume occupied by the outer pyrroles of biliverdin do not impede substrate binding. This may be interpreted in a model where the outer pyrroles are not intimately associated with the enzyme surface.

It has been suggested that BVR-A has functions beyond its recognised catalytic activity. One such function is based on the enzymes ability to associate with zinc and as a result it has been suggested that BVR-A may play a role in either Zn^{2+} storage, or in the regulation of gene. Atomic absorbance spectroscopy measurements show that Zn^{2+} can indeed associate with human BVR-A, however the molar ratio of zinc to protein of 0.28:1 is of the same order as that seen with a control protein (BSA) not normally considered to be a zinc protein. Under the same conditions alcohol dehydrogenase was shown to have a zinc to protein ratio of 1.8 to 1 in agreement with its known zinc stoichiometry (2:1). The mouse enzyme is 'stickier' for zinc with a molar ratio of 0.67 to 1. Based on the crystal structure data for the rat enzyme there is no evidence for a zinc binding site and suggestions that BVR-A could function as a zinc finger protein or as a leucine zipper like protein are therefore unlikely.

Abbreviations

ALA	5-aminolevulinic acid
Abs	Absorbance
bp	base pairs
BSA	Bovine serum albumin
BVR-A	Biliverdin-IXα reductase
BVR-B	Biliverdin-IXβ reductase
°C	degrees celsius
Da	Daltons
DNA	Deoxyribonucleic acid
dNTP	deoxyribnucleotide triphosphate
DTT	dithiothreitol
EDTA	ethylenediaminetetra-acetic acid
EtBr	Ethidium bromide
Fig	Figure
GSH	Glutathione
GST	Glutathione-*S*-transferase
HO	Heme oxygenase
g	Gram
h	hour
IPTG	isopropylthio-β-glactoside
Kb	Kilobase pairs
Kda	Kilodalton
L	Litre
LB	Lauria Bertani broth
M	milli
M	Molar
mg	milligram
μg	microgram
min	minute
ml	mililitre
Mr	Relative molecular mass
ng	nanogram

nM	nanomolar
NAD(P)H	nicotinamide adenine dinucleotide (phosphate) reduced form
$NAD(P)^+$	nicotinamide adenine dinucleotide (phosphate) oxidised form
PBS	phosphate buffered saline
PCR	polymerase chain reaction
RNA	ribonucleic acid
rpm	revolutions per minute
SDS	Sodium dodecyl sulphate
SDS-PAGE	SDS-polyacrylamide gel electrophoresis
TAE	Tris-acetate/EDTA electrophoresis buffer
TEMED	N,N,N',N'-tetramethylenediamide
Tris	2-amino-2-(hydroxymethyl)-propane-1,3,-diol
TBS	Tris buffered saline
UV	ultraviolet
V/v	volume per volume
W/v	weight per volume

1.1 Haem and tetrapyrroles.

Tetrapyrroles are found as prosthetic groups in virtually all organisms. They fulfil a wide range of essential functions including oxygen transport and storage, energy metabolism, detoxification of foreign compounds, light gathering and electron transport during photosynthesis. The functionality of the molecule is provided by the ability to co-ordinate different metal ions at its centre with multiple oxidation states (Fe^{2+} and Fe^{3+}), conferring on them a very functional diversity. For example hemo proteins are involved in a broad spectrum of crucial biological functions including oxygen binding (hemoglobins), oxygen metabolism (oxidases, peroxidases, catalases, and hydroxylases), and electron transfer (cytochromes). The functions of tetrapyrroles are not restricted to metabolic functions as organisms use these molecules in a myriad of very different ways from their use as camouflage pigments to antioxidants and signalling molecules.

1.2 The nomenclature and structure of tetrapyrroles

The haem molecule is composed of four N-heterocyclic pyrrole residues linked by single bridging carbon atoms in the form of methene bridges. Overall, the basic structure is a planar, highly conjugated system as seen in Figure 1.1. The commonly used Fisher numbering system (Fisher & Orth, 1937; cited in Lemberg & Legge, 1949 and Dolphin, 1979) has been adopted to identify each of the four pyrrole rings. The rings are designated I, II, III, and IV (or alternatively A, B, C, D) and the methene bridges referred to as α, β, γ and δ (Figure 1.1). Porphyrins are tautomeric with respect to the location of the two hydrogen atoms not involved in the peripheral conjugated system. The two hydrogen atoms may be associated with any two of the four nitrogen atoms. So traditionally the representation of one tautomeric form does not imply the absence of another. The porphyrin ring of haem is cleaved enzymatically at the α-methene bridge by haem oxygenase to form biliverdin-IXα.

Linear tetrapyrroles are often referred to as bilins. The carbon bridges of these bilins exist in either saturated (-CH_2-), or unsaturated (-CH=) forms. Bilenes, bilidienes and bilitrienes are structures with one, two, and three unsaturated bridges respectively. These linear

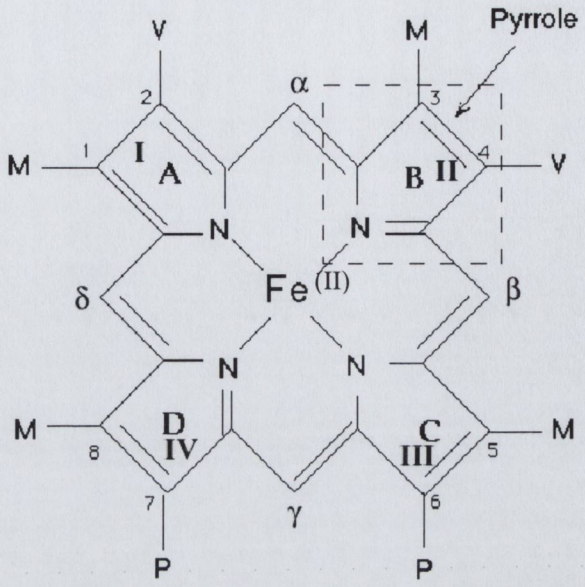

Figure 1.1 The structure of haem (Protoporphyrin IX) and the Fischer labeling system.

Haem has four pyrrole rings interlinked by methene bridges denoted α, β, γ and the δ. The pyrrole rings (A, B, C and D or alternatively I, II, III and IV) co-ordinate an iron atom (Fe^{2+}), at the center of the porphyrin complex. The letters M, V and P represent the conjugated groups along the tetrapyrrole moiety where M represents methyl groups (CH_3), V represents vinyl ($CH=CH_2$) groups and P represents the propionate (CH_2-CH_2-COOH) groups.

tetrapyrroles (or bilins) also have significant biological functions, being present in bile pigments of animals, in light harvesting pigments of algae and photosynthetic cyanobacteria and as the chromophore of the light sensing pigments the phytochromes. In animals linear tetrapyrroles exist either as precursors in the formation of haem or as the catabolic products of haem degradation. There is increased interest in linear tetrapyrroles in animals as they have been shown to have strong antioxidant properties and may be involved in signalling pathways (Stocker, 1990; Falchuck *et al.*, 2002; Montorzi *et al.*, 2002; Maines, 2003).

1.3 The evolutionary origins of haem

Studies on the round worm *Ascaris lumbricoides* have revealed some interesting insights into the origins of haem and haemoglobin. Both structurally and functionally, *Ascaris* haemoglobin is related to bacterial and mammalian haemoglobins. Haemoglobin in bacteria developed to destroy NO (the 'primordial gas' which evolved before atmospheric oxygen became abundant) while in mammals, haemoglobin evolved mainly as a carrier for oxygen and NO. In addition to its oxygen transport function, red blood cell haemoglobin forms NO complexes in the lung transporting NO to capillaries where, through activation of guanylate cyclase, NO causes expansion of the capillaries facilitating increased oxygen transfer (Ignarro, 1992). Since *Ascaris* haemoglobin binds oxygen 25,000 times more tightly than human equivalent (Minning *et al.*, 1999), its ability to deliver oxygen efficiently is hindered due to the fact that oxygen is so tightly bound that its dissociation is extremely low. Minning *et al.*, (1999) showed that oxygen is removed through a novel enzymatic reaction with nitric oxide to produce nitrate. In essence the *Ascaris* haemoglobin acts as a deoxygenase, using NO to detoxify the oxygen around it. It appears that *Ascaris* haemoglobin is primarily involved in the elimination of oxygen protecting the worm from NO which is present in the host gut or produced by the host's immune system. This ability to metabolize NO is very similar to the haemoglobin of early bacteria, but the *Ascaris* may not be able to do it quite as efficiently. This view would be consistent with the evolutionary appearance of simple bacterial haemoglobin when the earth's early atmosphere was anoxic, and toxic due to a high NO content.

1. 4 Precursors and formation of tetrapyrroles

The biosynthesis of all haem and tetrapyrroles begins with an initial pathway whereby two molecules of 5'-aminolaevulinic acid (ALA) combine to form porphobilinogen (PBG). Four molecules of porphobilinogen are then condensed to form a linear tetrapyrrole, preuroporphyrinogen, and this subsequently undergoes ring closure and rearrangement to produce uroporphyrinogen III. From here the pathway diverges and different modifications are introduced onto the macrocycle ring. This biosynthetic pathway is represented by the detailed schematic presented in Figure 1.2. In the late 1940s and early 1950s, the laboratories of Shemin and Neuberger investigated the basic aspects of haem biosynthesis and showed that glycine and succinyl CoA were the source of all haem. The use of isotopic tracers demonstrated that the haem nitrogen atoms and eight of the carbon atoms are derived from glycine (Shemin *et al*, 1948). Further studies (Shemin *et al.*, 1950; Muir & Neuberger, 1950) showed that the C-2 carbon atom of glycine was incorporated into 8 of the positions in the haem macrocycle. The remaining 26 carbon atoms of haem were found to be derived from succinyl CoA (Gibson *et al.*, 1958). We now understand that animals, yeast and purple photosynthetic bacteria use glycine and succinyl-CoA in the production of ALA, while glutamate is incorporated into ALA in plants and most bacteria (Beale & Castelfranco 1974a Beale & Castelfranco 1974b). ALA synthesis takes place in the mitochondria with the condensation of glycine and succinyl-CoA which is catalysed by the pyridoxal phosphate-containing enzyme δ-aminolevulinic acid synthase (ALA-S). This reaction is both rate-limiting and is the most regulated reaction of the entire pathway.

It has been shown that there are differences in the regulation and rates of haem synthesis in erythroid and non-erythroid cells. There are 2 different genes for ALA synthase, one of which is expressed ubiquitously (ALA-S1), while the other (ALA-S2) is expressed in erythroid cells (Ponka *et al.*, 1981 & Bishop 1990). The 5'-untranslated region of the erythroid-specific ALA-S2 mRNA contains the iron-responsive element (Melefors *et al.*, 1993), and as a result iron is responsible for the translational induction of erythroid ALA-S2. The availability of iron controls protoporphyrin IX levels in hemoglobin-synthesizing cells. In non-erythroid cells the ALA-S1 catalysed rate-limiting step of haem production is in fact feedback-inhibited by haem (Shoolingin-Jordan, 1994). Some time before this,

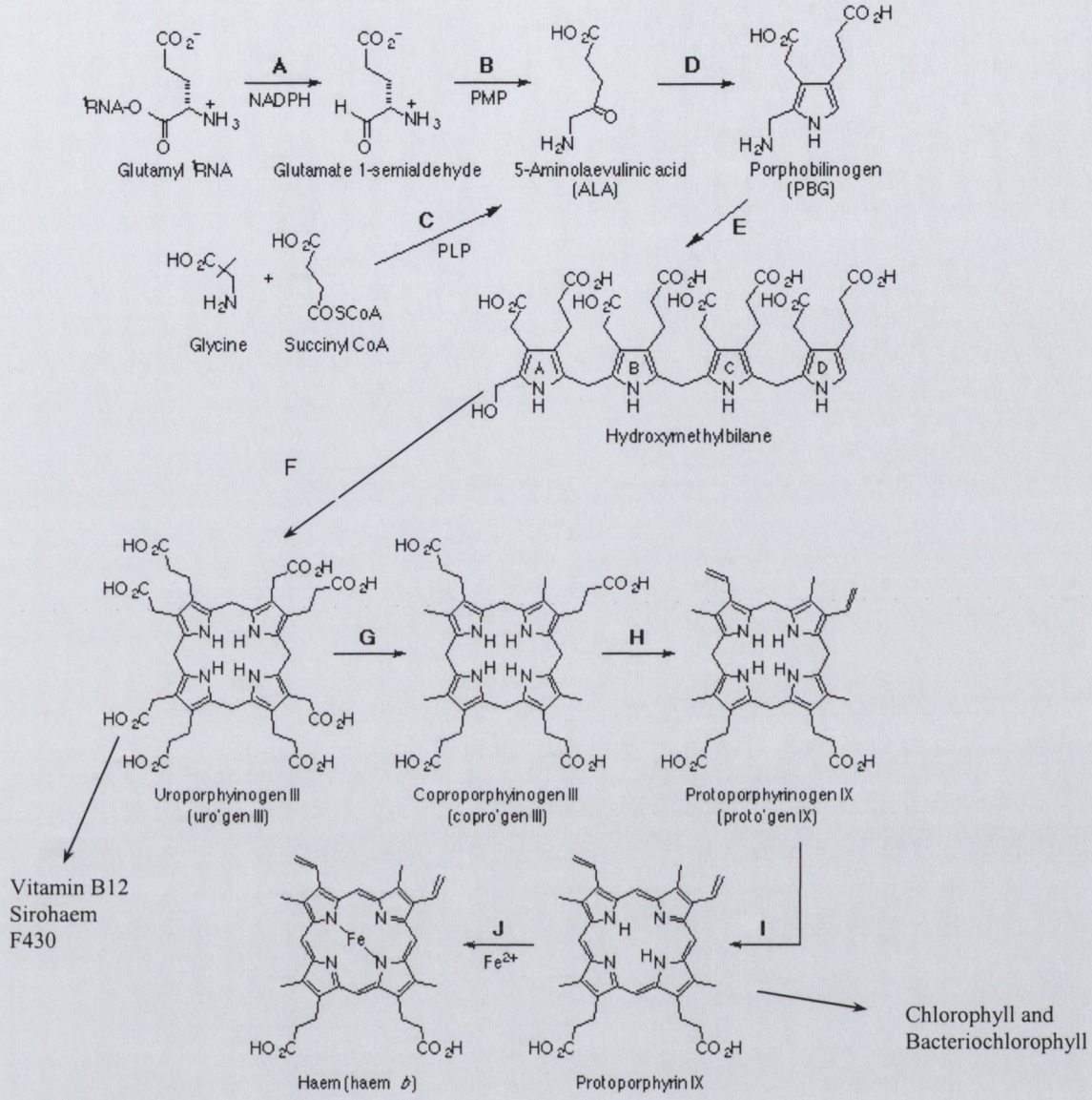

Figure 1.2 The intermediates and the enzymes involved in the haem synthetic pathway.

A: Glutamyl tRNA reductase

B: Glutamate semialdehyde aminomutase

C: 5-Aminolaevulinic acid synthase; located in the mitochondria.

D: Porphobilinogen synthase (ALA dehydratase) located in the cytosol.

E: Hydroxymethylbilane synthase (PBG deaminase) located in the cytosol.

F: Uroporphyrinogen III synthase (cosynthetase) located in the cytosol.

G: Uroporphyrinogen decarboxylase located in the cytosol.

H: Coproporphyrinogen oxidase; located in the mitochondria.

I: Protoporphyrinogen oxidase; located in the mitochondria.

J: Ferrochelatase; located in the mitochondria.

studies by Granick *et al.*, (1975), showed that haem levels as low as 0.1 to 0.3 μM decreased the level of ALA-S by one-half in cultured chick embryo liver cells.

Mitochondrial δ-aminolevulinic acid (ALA) is transported to the cytosol, where ALA dehydratase (also called porphobilinogen synthase or hydroxymethylbilane synthase) condenses 2 molecules of ALA to produce porphobilinogen. Porphobilinogen deaminase then catalyses the polymerization of four molecules of porphobilinogen to produce pre-uroporphobilinogen. Uroporphyrinogen synthase catalyses the cyclisation of pre-uroporphobilinogen forming uroporphobilinogen III, which is the universal precursor of all cyclic and linear tetrapyrroles. Apart from the first step in tetrapyrrole biosynthesis, the pathway leading to the formation of uroporphyrinogen III is similar in all living systems.

1.5 The localization of haem synthesis

Although haem is synthesized in virtually all tissues, there are two principal sites of synthesis. Erythroid cells produce about 85% of the haem being made in humans while the majority of the remaining 15% is synthesized in the hepatocytes. In hepatocytes, haem is required mainly for incorporation into cytochromes, in particular, the P450 class of cytochromes, which are important in cellular detoxification, and also the cytochromes of the oxidative-phosphorylation pathway. In erythroid cells all of the haem is synthesized for incorporation into hemoglobin and this synthesis occurs once the cells have differentiated into reticulocytes (immature erythrocytes). On maturation of the red cells synthesis of haem and hemoglobin ceases and as a result, haem must survive over the life time of the erythrocyte (~ 120 days).

Hemoglobin synthesis requires the coordinated production of haem and globin. Globin is the protein that surrounds, protects and gives functionality to the haem molecule as an oxygen transporter. In haemoglobin there are two distinct pairs of globin chains (*i.e.* four individual chains, each chain contains one haem molecule). Of these 4 chains, one pair is generally composed of alpha globin chains while the second pair are non-alpha chains. The combination of two alpha chains and two beta chains forms adult hemoglobin. Adult hemoglobin becomes the predominant haemoglobin within about 18 to 24 weeks of birth.

Other globins (zeta globin) are expressed during the first few weeks of embryogenesis, thereafter the alpha globin gene product takes over. Of the other non-alpha type chains the epsilon gene is also expressed initially during embryogenesis while the gamma gene is expressed during fetal development. Around the time of birth, the production of gamma globin declines while there is a rise in beta globin synthesis. A significant amount of fetal hemoglobin persists for seven or eight months after birth. Most adults have only trace amounts, if any, of fetal hemoglobin after infancy. The predominant hemoglobin tetramers are hemoglobin A which is the normal 'adult' hemoglobin that exists after birth and comprises of a tetramer with two alpha chains and two beta chains ($a_2\beta_2$). Hemoglobin A2 is a minor component of the hemoglobin found in red cells after birth and during adulthood and it consists of two alpha chains and two delta chains ($a_2\delta_2$). Hemoglobin A2 generally comprises less than 3% of the total red cell hemoglobin. Hemoglobin F is the predominant hemoglobin during fetal development. The molecule is a tetramer of two alpha chains and two gamma chains ($a_2\gamma_2$) (Bunn & Forget, 1986).

1. 6 The haem degradation pathway

The normal human erythrocyte has a life span of about 120 days in adults and 70 days in infants after which time it is removed from circulation and degraded by the reticulo-endothelial system (spleen, liver and kidney). Eventually the apoprotein of hemoglobin will be hydrolyzed to its constituent amino acids while the haem moiety is cleaved at the α-meso carbon of the haem by the microsomal enzyme haem oxygenase. This is the first step in the haem degradation process and results in the production of iron, carbon monoxide, and biliverdin-IXα. For a full description of the haem degradation refer to Figure 1.3. Due to the asymmetric nature of the side chains, cleavage at any one of the methene bridges will produce one of four possible isomers of the linear tetrapyrrole biliverdin (biliverdin-IXα, -IXβ, -IXγ and -IXδ) as shown in Figure 1.4. The predominant naturally occurring isomer however is the biliverdin-IXα produced by haem oxygenase. All the eukaryotic and cyanobacterial haem oxygenases characterized to date produce biliverdin-IXα so it is interesting that Caignan *et al.*, (2002), reported a haem oxygenase from *Pseudomonas aeruginosa* which produced biliverdin-IXα (70%) and biliverdin-IXβ (30%) isomers. The natural occurrence of other isomers is not unknown as biliverdin-IXδ has been found in the ovaries of the marine snail *Turbo cornutu* (Benedikt *et al.*, 1988) and

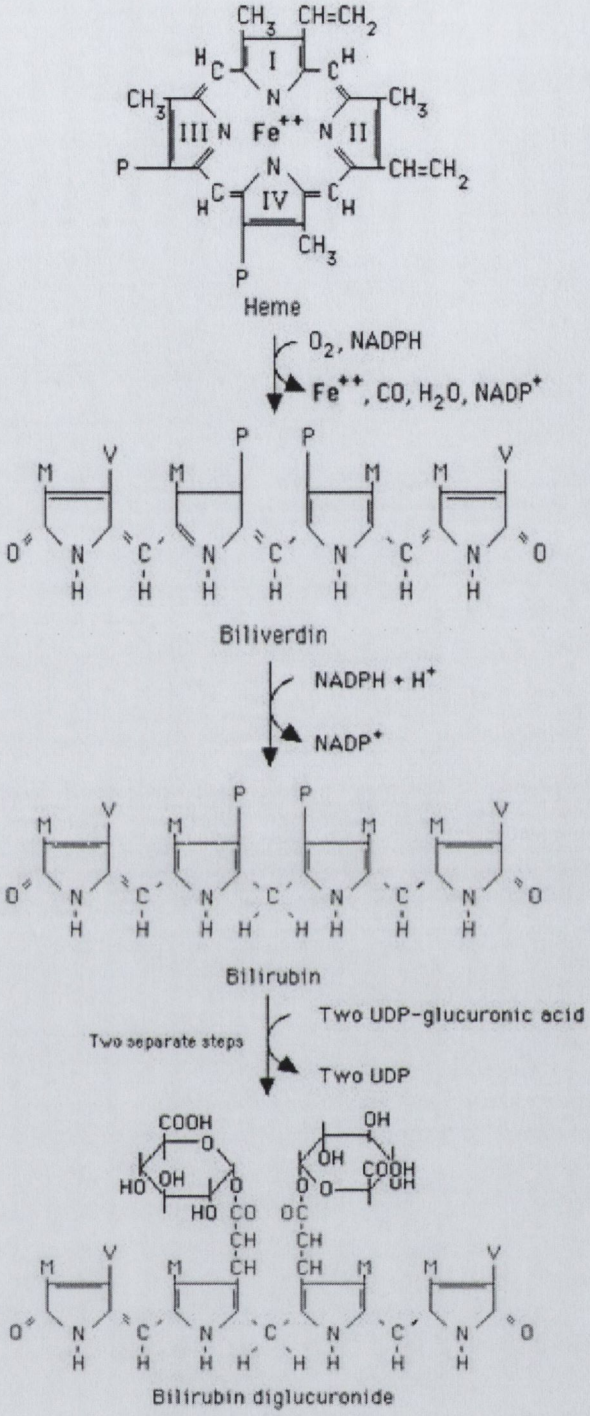

Figure 1.3 The haem degradation pathway.

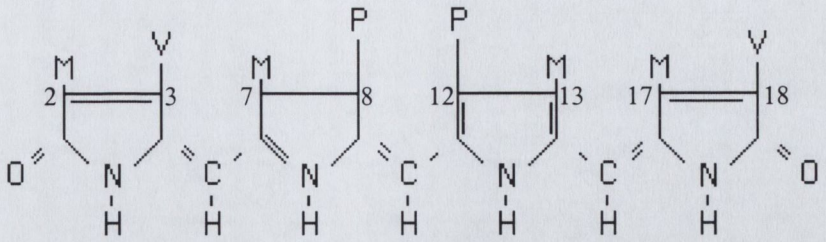

(a)

Biliverdin or bilirubin	β-Substituent Position							
	2	3	7	8	12	13	17	18
IXα	M	V	M	P	P	M	M	V
IIIα	V	M	M	P	P	M	M	V
XIIIα	M	V	M	P	P	M	V	M
XIβ	M	P	P	M	M	V	M	V
IXγ	P	M	M	V	M	V	M	P
IXδ	M	V	M	V	M	P	P	M

(b)

Figure 1.4 The basic structure of the linear bilin skeleton.

(a) The structure of biliverdin-IXα. M represents methyl groups (CH_3), V represents vinyl ($CH=CH_2$) groups and P represents the propionate (CH_2-CH_2-COOH) groups.

(b) Cleavage of haem at any one of the methene bridges will produce one of four possible isomers of the linear tetrapyrrole biliverdin (biliverdin-IXα, -IXβ, -IXγ and -IXδ). The predominant naturally occurring isomer however is the biliverdin-IXα produced by haem oxygenase. The other isomers shown in the table above differ by the positioning of the β-substituents on the numbered carbons.

biliverdin-IXγ in the butterfly *Pieris brassicae* (Rudiger *et al.*, 1969). The precise origins of these isomers are unknown but the idea that novel heam oxygenases exist which could produce biliverdin IXβ, IXγ and IXδ is an intriguing possibility.

Biliverdin is reduced to bilirubin by the enzyme biliverdin reductase using NADPH as cofactor. This is discussed in greater detail in Section 1.10. Bilirubin can adopt a folded conformation like that of a ridge tile type structure as displayed in Figure 1.5. This occurs as the dipyrrole sub-units rotate about the central methylene bridge and the structure becomes stabilized as the carboxyl groups of the propionic acid side chains hydrogen bond to the terminal pyrrole ring lactams (Figure 1.5). There are six hydrogen bonds in this conformation and it has a greatly reduced polarity as the acid groups within the molecule are hidden. This conformation accounts for bilirubins lipophilic properties, allowing it to cross physiological barriers such as the placenta and the blood-brain barrier. The molecule is therefore virtually insoluble in water and has remarkably high pK_a values (both above 8.0). Ionization or conjugation of the –COOH groups breaks the hydrogen bonding network, allowing it to interact with water (McDonagh & Lightner, 1985).

Although haem oxygenase functions in many cells it is particularly important in the reticuloendothelial system which is composed of monocytes and macrophages located in the reticular connective tissue of the spleen. Haem degradation capabilities are not just limited to the spleen however as Kupffer cells (hepatic resident macrophages) of the liver also function in this regard.

Bilirubin being lipophilic complexes to albumin with a K_d of approx. 10^{-8}M, and this bound form circulates in blood plasma. Once the albumin bound bilirubin reaches the hepatic sinusoids the complex migrates across the sinusoidal endothelium into the space of Disse (Figure 1.6). There, any bilirubin released from albumin is taken by up by carrier-mediated active transporters on the basolateral membrane of the hepatocytes (Bissell, 1972). These organic anion transporters (OATPs), transport both unconjugated and conjugated bilirubins from the space of Disse into hepatocytes. Once inside the hepatocyte, the intracellular bilirubin is bound to the α-class glutathione S-transferase (Zucker *et al.*, 1995) or Z-protein. In the hepatocyte the bilirubin is conjugated at the smooth endoplasmic reticulum (ER) with glucuronic acid, to form bilirubin monoglucuronide and also bilirubin

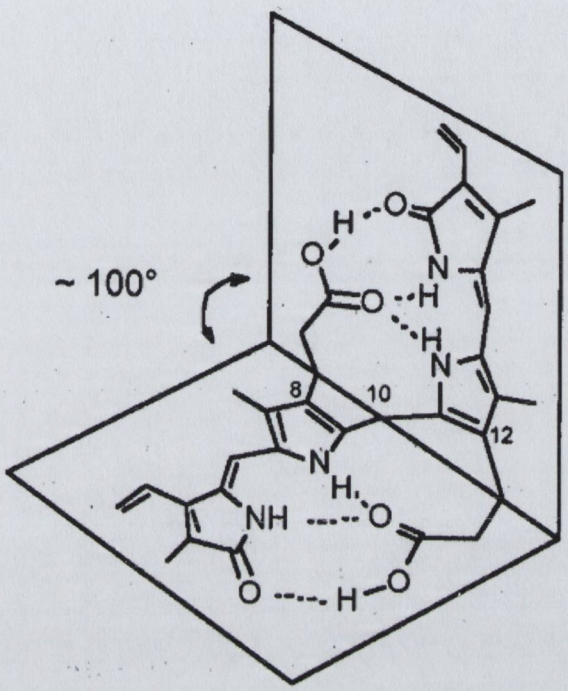

Figure 1.5 The ridge-tile conformation of bilirubin.

The dipyrrole sub-units rotate about the central methylene bridge and the structure becomes stabilized as the carboxyl groups of the propionic acid side chains hydrogen bond to the terminal pyrrole ring lactams. The resulting folded conformation adopts a ridge tile type structure.

Figure 1.6 Haem degradation pathways in the liver

a Bilirubin is formed mainly by the reticuloendothelial system and is transported via blood circulation to the liver, where it is conjugated and excreted. Bilirubin forms a stable complex with albumin in blood plasma which facilitates its circulation in blood to liver. Bilirubin is conjugated and removed from the bloodstream by the liver and eliminated via the bile duct, passing from the liver into the intestines.

b Cartoon diagram showing the close association of hepatocytes with sinusoids (hepatic blood capillaries). This cellular organisation facilitates a rapid passage of nutrients from the blood to the peri-sinusoidal space ('Space of Disse'). Unconjugated bilirubin and its albumin complex freely cross the sinusoidal endothelium into the space of Disse. Unconjugated bilirubin within hepatocytes is complexed to ligandin (GST-B). This helps the transfer of unconjugated bilirubin to the smooth endoplasmic reticulum where it is conjugated using glucuronic acid by the specific bilirubin-UDP glucuronosyl transferase (UGT1A1). Organic anion transporters transport both unconjugated and conjugated bilirubins from the space of Disse, while bilirubin conjugates are secreted into the bile by MRP2 (cMOAT), one of the organic anion transporters present in the canalicular membranes.

OUTLINE - BILE PIGMENT PRODUCTION PATHWAY IN HEALTH

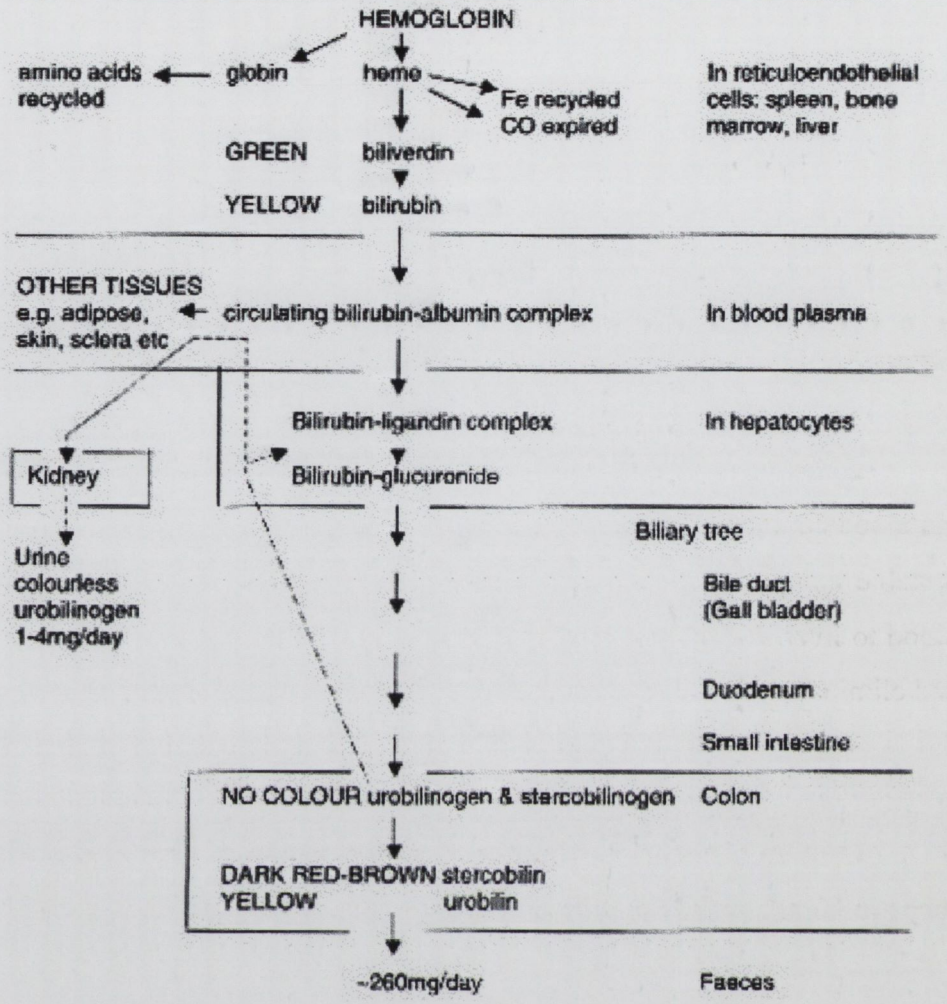

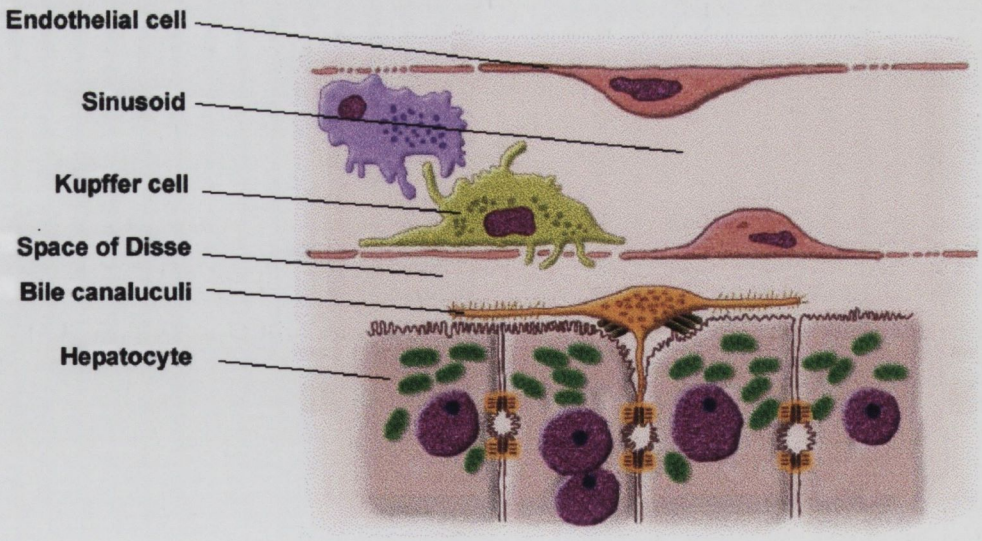

diglucuronide (Figure 1.7), in a reaction catalysed by bilirubin UDP-glucuronyl transferase (UGTIA1) another microsomal enzyme (Jansen *et al.*, 1977). Approximately 90% of the glucuronides formed are diglucuronides and 10% are monoglucuronides. These conjugates are more water-soluble than bilirubin, and have a conformation that more readily passes to the biliary canaliculi. A small proportion of this will find its way back into the blood plasma but in healthy individuals this tends to be very small, accounting for <5% of the total plasma bilirubin concentration. Once formed the bilirubin conjugates are secreted into the bile canaliculi by the ATP-dependent transporter MRP2 (also known as the canalicular multispecific organic anion transporter, cMOAT). Bilirubin diglucuronide normally accounts for about 80% of the bilirubin conjugates in the bile of adult humans, while monoconjugates predominate in newborns. A tiny fraction (less than 2%) of the total bilirubin in normal bile is unconjugated and this is mainly due to the hydrolysis of the secreted conjugates.

Bilirubin conjugates then pass with the bile successively from the canaliculi, through the bile ductules, and eventually make their way to the gall bladder where they are stored before being emptied into the duodenum. In the small intestine, conjugated bilirubins are poorly absorbed, but are often hydrolyzed to unconjugated bilirubin by β-glucuronidases from the enterocytes, (cells of the intestinal epithelium) and also from enteric bacteria. In the colon the action of anaerobic intestinal bacteria results in the deconjugation of the bilirubin and with further modifications they produce the colourless urobilinogen, stercobilingogen and mesobilinogen, which all contain saturated methene bridge carbons. In the lower intestinal tract these urobilinogens spontaneously oxidise at the central methene bridge to form their corresponding bile pigments, stercobilin, mesobilin and urobilin, which are orange-brown in colour. These pigments are responsible for stool coloration. Some urobilinogen, which is water-soluble can be reabsorbed from the intestine into portal blood, taken up by liver and re-excreted. A small portion (~1% of total bile pigments) however can find its way into the circulation but is excreted by kidneys into the urine. On exposure to air the colourless urobilinogen is slowly oxidised to yellow urobilin.

It is reported that about 3.8 $mg.kg^{-1}$ of bilirubin is produced per day in normal adults, and that 70% - 80% is from erythroid breakdown. The remainder originates from non erythroid sources such as haemoproteins, cytochrome P450 and catalase and a small portion of daily

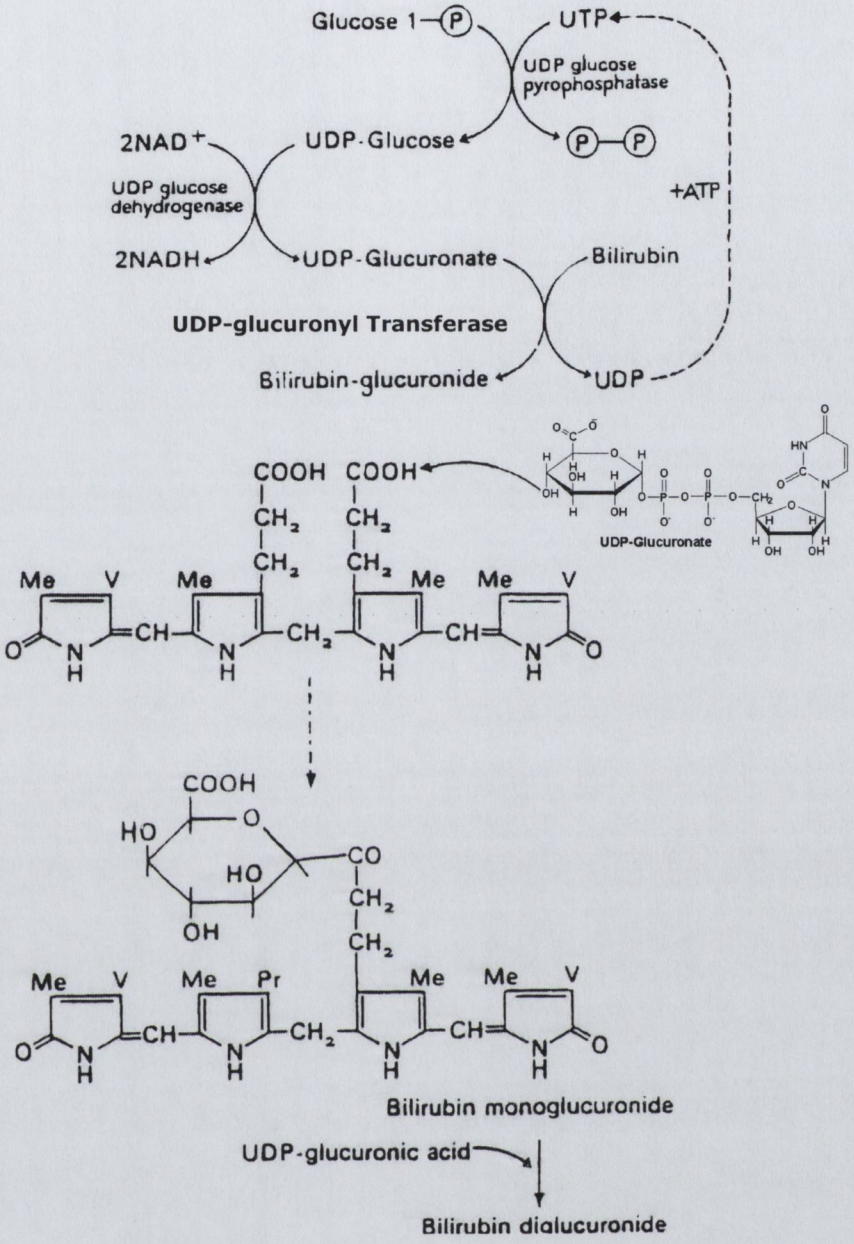

Figure 1.7 The conjugation reactions involving bilirubin.

Bilirubin is made more water-soluble once conjugated with glucuronic acid. The enzyme catalyzing this reaction is bilirubin-UDP glucuronosyl transferase (UGT1A1) Ionization or conjugation of the –COOH groups breaks the hydrogen bonding network, allowing it to interact with water.

bilirubin is derived from the destruction of young or developing erythroid cells (Granick & Beale, 1978).

1.7 Physiological significance of haem degradation

Recent studies on haem oxygenase and other constituents of the haem degradation pathway have underlined the important protective functions of various components within cells. The protection provided comprises of anti-inflammatory, anti-apoptotic, and anti-proliferative actions (Otterbein *et al.*, 2003) which are mediated by haem oxygenase, haem and the degradation products, carbon monoxide (CO), biliverdin, bilirubin and free iron (Fe^{2+}) (Berberat *et al.*, 2003; Ryter *et al.*, 2004, Nakano *et al.*, 2004, Ott *et al.*, 2005, and Zuckerbraun *et al.*, 2003).

Bilirubin has been shown to suppress p38 MAPK which in turn has anti proliferative effects. Similar effects have been reported with the upregulation of HO-1 (Lavitrano *et al.*, 2004). Studies also show that individuals with high normal or slightly elevated levels of bilirubin have less atherosclerosis-related diseases than individuals with low normal levels of bilirubin (Novotny & Vitek 2003). When biliverdin is administered to a cell, biliverdin reductase is induced and Kravets *et al.*, (2004) reported that biliverdin functions as a transcription factor leading to the induction of HO-1. Bilirubin has been shown to be an effective scavenger of peroxyl radicals generated *in vitro* (Stocker *et al.*, 1987; Stocker & Ames 1990). Sedlak & Snyder (2004) recently showed that a mechanism of bilirubin to biliverdin recycling results in cytoprotection through the elimination of reactive oxygen species. Such protective effects arise when lipophilic reactive oxygen species oxidise bilirubin back to biliverdin. Bilirubin is again produced through the actions of biliverdin reductase and this protective cycling process is allowed to continue. Sedlak & Snyder (2004) proposed that this is an extremely efficient system and that bilirubin has the potential to detoxify a 10000-fold excess of oxidants.

Interleukin 10 (IL-10) is a potent anti-inflammatory molecule and acts on macrophages and other cells. It is known to suppress TNF-α expression in stimulated macrophages. This suppression requires the presence of HO-1 (Lee *et al.*, 2002) and in the absence of IL-10 the expression of HO-1 or the introduction of CO or biliverdin to the macrophages produced the same effect as IL-10.

Another product of the haem oxygenase catalysed reaction, Fe^{2+} leads to the opening of channels which exports Fe^{2+} from the cell. It also causes an increase in the ferritin synthesis as Fe^{2+} binds the IRP repressor protein which prevents translation of ferritin mRNA which has an iron response element (IRE). Also the formation of carbon monoxide during the haem oxygenase reaction may have potential downstream effects and may function in a similar manner to nitric oxide. The mRNA encoding HO-2 was found to co-localise in the brain with mRNA for soluble guanyl cyclase, while zinc protoporphyrin-IX which is a potent inhibitor of HO, was shown to deplete endogenous guanosine 3',5'-monophosphate (cGMP) (Verma *et al.*, 1993). Carbon monoxide was shown to modulate secretion of corticotrophin releasing factor from rat hypothalamic cultures (Pozzoli *et al.*, 1994).

1.8 Biliverdin in plants and bacteria.

Plants are light sensitive and have evolved to respond to the intensity, direction, spectrum, and periodicity of light in the environment. They have achieved this feat through light sensors or photo-receptors. Studies, mainly with *Arabidopsis* have revealed the presence of a multiplicity of receptors, which respond to light stimuli (Fankhauser 2001). One such group of photoreceptors are the phytochromes of which there are five types *phyA–phyE.* They absorb mainly red/far-red light although *PhyA* is an exception which responds to broad-spectrum light (Quail, 2002).

These photoreceptors proteins occur as homo-dimers of approximately 124kDa and each unit has covalently attached a linear tetrapyrrole chromophore. The phytochromes contain a very highly conserved photosensory domain which is responsible for the covalent attachment of the tetrapyrrole via thio-ether linkages to cysteine residues.

It has also been shown that significant conformational changes occur in the phytochrome protein upon light excitation. Phytochromes exist in two spectral forms, Pr and Pfr. Absorption of a photon of red light triggers the "Z" to "E" isomerization of the C-15 double bond between rings C and D of the linear tetrapyrrole in the inactive Pr (red light absorbing form) to the active Pfr form (far-red light absorbing). Conformational changes in the protein backbone are required to maintain this high energy state Pfr, however it can

reconvert to Pr by a slow non-photoinduced reaction (dark reversion) or much faster upon absorption of further far-red light.

The precursor of the linear tetrapyrroles found in cyanobacteria is haem (Cornejo & Beale 1991). The ubiquitous haem oxygenase (ferredoxin-linked in cyanobacteria) cleaves haem at the IXα position resulting in biliverdin-IXα production. Biliverdin-IXα has two possible fates; the reduction of biliverdin-IXα by the cyanobacterial biliverdin reductase to yield bilirubin IXα, or the biliverdin is used in the synthesis of phycobilin molecules necessary for light harvesting in the cyanobacteria (Figure 1.8). Schluchter & Glazer (1997) show that blocking the conversion of biliverdin to bilirubin interferes with normal phycobiliprotein biosynthesis in cyanobacteria. This implicates the cyanobacterial biliverdin-IXα reductase in the control of light sensing in cyanobacteria.

1.9 Haem Oxygenase

The first step in the haem degradation is the cleavage of its alpha-methene bridge to form the linear tetrapyrrole biliverdin-IXα, catalyzed by haem oxygenase. Tenhunen *et al.*, (1968) were the first to report a haem oxygenase activity in the microsomal fraction from liver, spleen and kidney of rat. The enzyme catalyses the rate limiting production of equimolar amounts of biliverdin-IXα and carbon monoxide. Braggins *et al.* (1986) described the discovery of two forms of haem oxygenase designated HO-1 and HO-2, and more recently a third form HO-3 was described (McCoubrey *et al.*, 1997). Haem oxygenase is membrane bound however some groups have expressed a soluble recombinant rat and human HO-1 which lacks the 23 carboxy terminal amino acid membrane anchor (Wilks & Ortiz de Montellano 1993). The HO-1 catalysed oxidation of haem involves sequential α-meso-hydroxylation, oxygen dependent fragmentation of the α-mesoverdohaem to verdohaem and oxidative cleavage of verdohaem to biliverdin (Figure 1.9). The α-meso-hydroxylation proceeds via the P450 reductase dependent reduction of the iron to the ferrous state. Most naturally occurring haem is in the form of protoporphyrin IX.

HO-1 is induced by stress factors such as cytokines, heavy metals, hypoxia and oxygen-free radicals resulting from a variety of disease conditions including ischemia reperfusion

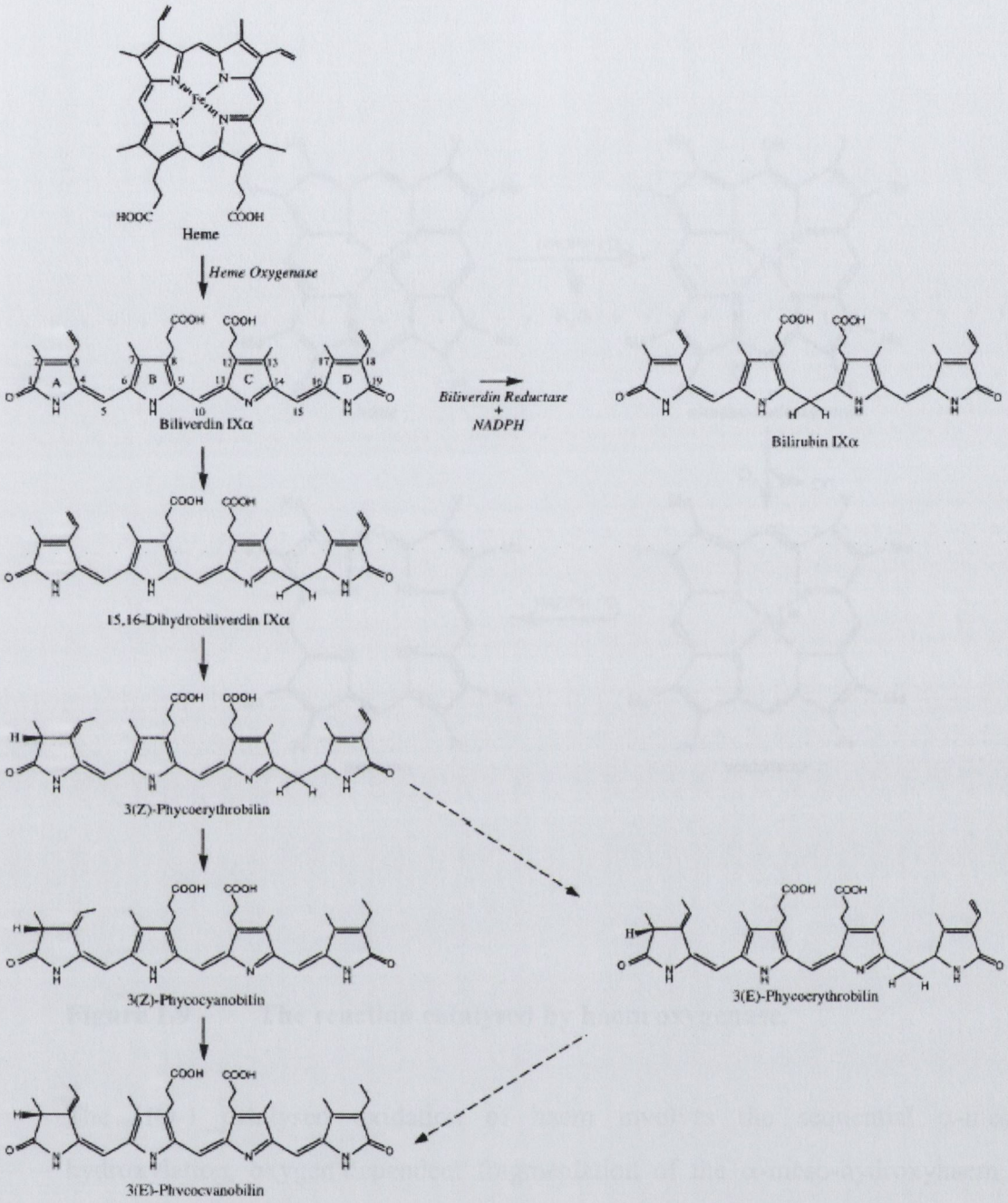

Figure 1.8 The proposed phycobilin biosynthetic pathway in plants

Biliverdin-IXα has two fates in the cyanobacterial biliverdin reductase (from Schluchter & Glazer, 1997). Biliverdin-IXα can be used to synthesise phycobilin molecules which are necessary for light harvesting in the cyanobacteria or it can be reduced by the cyanobacterial BVR-A.

(Tacchini *et al.*, 1993, Choi *et al.*, 1996 and Lee *et al.*, 1996) and also by haem itself. With exposure to stress stimuli, HO-1 increases in all of these cell types, potentially increasing the levels of endogenous CO.

The regulation and expression differences between the HO isoforms are due to differences in their respective promoter regions. The HO-1 promoter contains the heat-shock elements AP-1, a cyclic nucleotide-response element, and metal regulatory element, whereas the HO-2 promoter contains only a single glucocorticoid response element. A report by Immenschuh (1998) indicated that cyclic guanosine monophosphate (cGMP), a second messenger up-regulated by nitric oxide (NO), can stimulate transcriptional regulation of HO-1 through activation of cyclic nucleotide-response element and AP-1.

The electrons required for catalytic turnover of the enzyme are provided, in mammalian systems, by NADPH-cytochrome P450 reductase (Yoshida *et al.*, 1980 and reviewed by Maines 1997). The enzyme binds an equivalent of haem, thus forming a haem-protein complex in which the haem iron is coordinated to a histidine in a manner similar to that seen in myoglobin. The distal site of the haem is then used to coordinate and activate oxygen that leads to the regiospecific hydrogenation of the α-meso carbon of the haem. This is the first of three cycles of oxygenation reactions catalysed by haem oxygenase. At the second oxygenation step, the enzyme converts the α-hydroxyhaem to verdohaem with the release of CO by consuming one equivalent of oxygen and electron. In the final oxygenation step, the verdohaem is converted to biliverdin-iron complex, which is released from the enzyme as ferrous iron and biliverdin to conclude the turnover (Oritz de Montellano, 1998, Liu & Ortiz de Montellano, 1999)

Wang & Ortiz de Montellano (2003) provided evidence that P450 reductase and biliverdin reductase bind competitively to HO-1. They also established that the binding sites for the two proteins partially overlapped and defined some of the residues involved. Since biliverdin reductase accelerates the catalytic turnover by promoting product (biliverdin) release (Liu & Ortiz de Montellano, 2000), it is possible that the cytosolic concentrations of biliverdin reductase may have regulatory effects on the activity of HO-1. Wang & Ortiz de Montellano (2003) remind us that HO-1 and P450 reductase are membrane-bound proteins, whereas biliverdin reductase is a cytosolic protein and the localisation of the first

two proteins in the membrane would effectively concentrate them and this is likely to enhance their interaction at the expense of the interaction of HO-1 and biliverdin reductase.

1.10 Biliverdin Reductase

Biliverdin reductases are small cytoplasmic oxidoreductases, which are ubiquitously expressed, and catalyse the reduction of biliverdin to bilirubin. There are two types of biliverdin reductases, biliverdin-IXα reductase (BVR-A), the major component of human adult liver, and biliverdin–IXβ reductase (BVR-B). Yamaguchi *et al.*, (1993) were the first to report cytosolic biliverdin-IXβ reductase activity in human liver. It was later shown that biliverdin-IXβ reductase and flavin reductase were identical, and it was confirmed that biliverdin-IXβ reductase has the ability to reduce riboflavin (Shalloe *et al.*, 1996). Biliverdin-IXβ is produced after haem cleavage at the β-meso position, while biliverdin-IXα is produced on cleavage at the α-meso position (see Figure 1.4 for the differences between isomers). Kinetic studies on these enzymes indicate that BVR-B has the ability to reduce β, γ and δ isomers of biliverdin more efficiently than BVR-A, however BVR-B is unable to reduce biliverdin-IXα (Yamaguchi *et al.*, 1994).

It has been shown that in the human fetus, bilirubin-IXβ is the major catabolite of haem degradation, and is detectable at 14-15 weeks (Blumenthal *et al.*, 1980) and remains as the major bile pigment at 20 weeks (Yamaguchi and Nakajima 1995). It is also interesting that BVR-B activity is considerably lower than BVR-A activity in the adult liver, however at 26 weeks of fetal gestation the activity of both BVR-A and BVR-B is approximately equal. Because of the increased solubility of bilirubin-IXβ, the fetus does not need the conjugation system catalysed by UDP-glucuronyltransferase, to eliminate the bilirubin produced. UDP-glucuronyltransferase is not expressed until the first week of birth, and a delay in its expression results in the onset of the condition known as neonatal jaundice. The switch in haem degradation from the IXβ pathway to the IXα pathway may be coupled to the switch from fetal to adult hemoglobin as described in Section 1.5.

BVR-A is found in most mammals but also in fish (Elliot & Mantle 1995, Fang & Lai, 1987) and in the cyanobactera *Synechocystis sp.* 6803 (Schluchter & Glazer, 1997) and *Nostoc sp.* PCC 7120 which will be discussed in this report. In all species the liver, spleen

and kidney tissue seem to have the highest distribution of BVR-A (Colleran & O'Carra, 1977) however there is wide variation of the enzyme present when comparing like tissues of different species (Rigney *et al.*, 1988). It is worth noting that BVR-A has been detected in tissue which are not particularly associated with haem degradation such as lungs, brain, intestine, and muscle (Tenhunen *et al.*, 1970a).

BVR-A occurs as a cytosolic monomer of molecular weight 34 kDa in rat, pig and ox kidney (Kutty & Maines 1981: Noguchi *et al.*, 1979: Phillips & Mantle 1981). The human enzyme was shown to exhibit a slower mobility on SDS-PAGE, migrating with an apparent Mr of 40,000 Da, even though the predicted Mr according to its amino acid sequence is ~34,000Da. The difference in molecular weight has been attributed to post–translational modifications (Maines *et al.*, 1996).

The gene encoding rat BVR-A is 12,270 bp in length and consists of 5 exons and 4 introns (McCoubrey *et al.*, 1995). The promoter region was also reported to contain binding sites for AP-1 (activated c-jun / c-fos dimer), HNF-5 (hepatic nuclear factor 5) and INF-1 (initiation factor 1). Meera-Khan *et al.*, (1993), localised the gene for human BVR-A to chromosome 7 (7p14-cen: 43,764,797 – 43,83,457)), meanwhile the Jackson laboratory (available on line at http://www.informatics.jax.org/) has recently mapped the mouse BVR-A gene to chromosome 2 (cM position 62.0: 126584521 - 126610938).

Maines *et al.*, (1996) have suggested that human BVR-A is a zinc metalloprotein which contains one atom of zinc per enzyme molecule. This was based initially on the primary sequence of the enzyme which has similarity with a zinc binding domain. Using atomic absorption spectroscopy and also ^{65}Zn-exchange analysis of both tissue purified enzyme and recombinant enzyme they have shown experimentally the presence of zinc. However the determination of the crystal structure of the rat enzyme (Kikuchi *et al.*, 2001) shows clearly that there cannot be coordination of zinc in the αM helix of the rat enzyme, which corresponds to the zinc binding domain proposed in the human enzyme (Figure 1.10). Maines *et al.*, (1996) also reported that zinc inhibits NADPH-dependent but not NADH-dependent activity and so proposed that the NADH and NADPH binding regions are differentiated due to their ability to interact with Zn. Ahmad & Maines (2002) proposed that human biliverdin-IXα reductase is a leucine zipper-like DNA-binding protein and

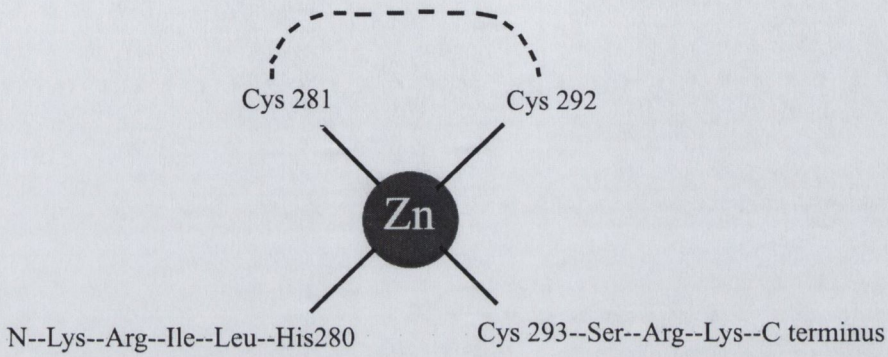

Figure 1.10 (a) The proposed zinc binding domain of human BVR-A

The zinc binding domain of human BVR-A proposed by Maines *et al.*, (1996). This observation is based primarily on the primary structure of the enzyme.

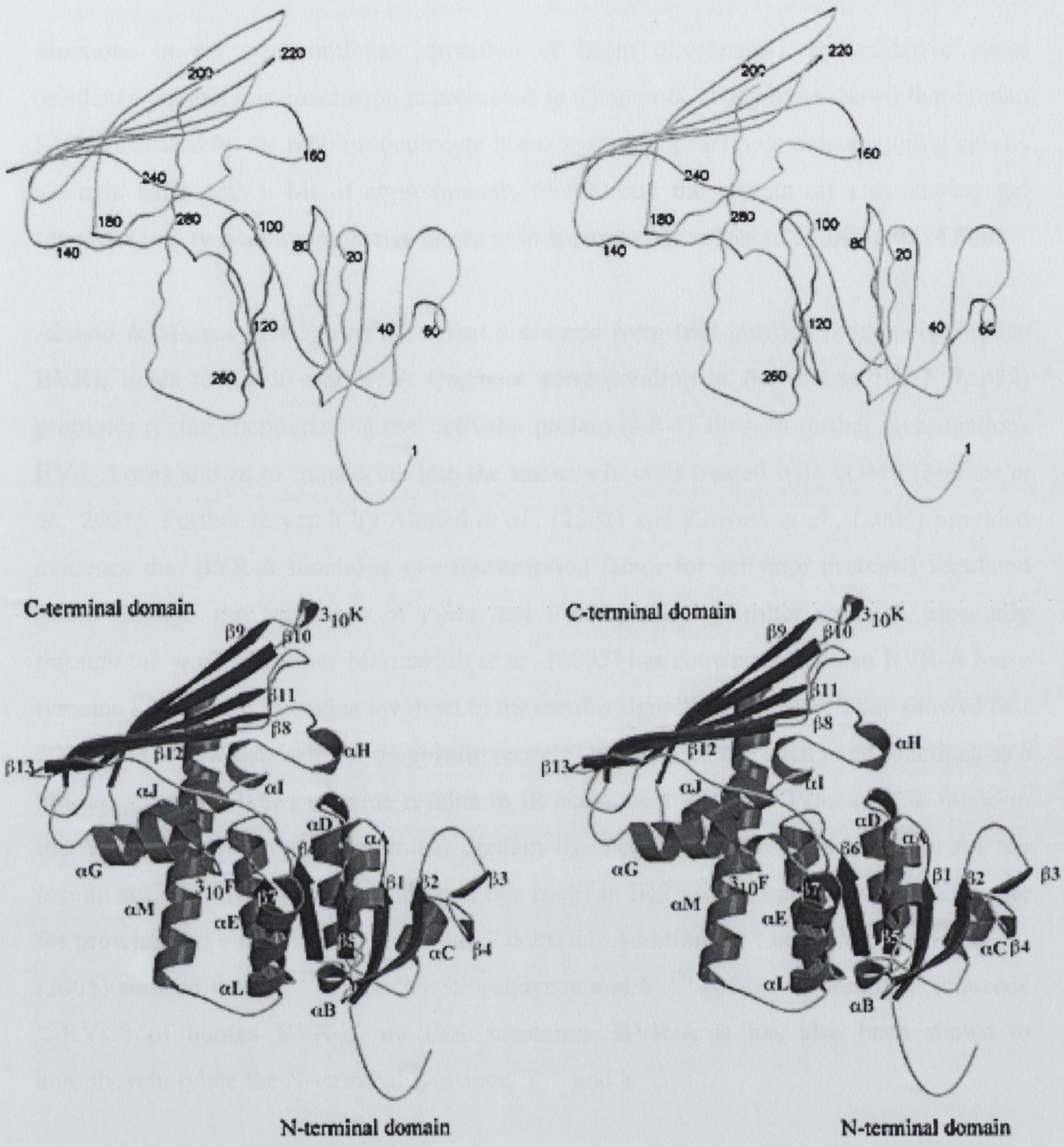

Figure 1.10 (b) **The structure of rat biliverdin-IXα reductase**

Stereo views of rat biliverdin-IXα reductase with all helices and sheets labelled. Every 20th Cα carbon atom is also identified. This picture was reproduced from Kikuchi *et al.*, 2002).

carbon. The C-10 then undergoes a nucleophilic addition of hydride from the NADPH cofactor bound at the active site. The kinetic characterization of BVR-A has been complicated by the fact that the enzyme is subject to profound substrate inhibition even at low micro molar concentrations. To further compound matters the product bilirubin, has limited solubility in solution due to the formation of intramolecular hydrogen bonds. Another interesting kinetic observation associated with biliverdin reductase which is apparently unique among all enzymes is the fact that it displays a dual pH/ cofactor-dependency, preferring NADH at pH 6.7 and NADPH at pH 8.5 (presented in Figures 1.11 and 1.12). The cyanobacterial enzyme however exhibits a distinctive pH activity profile, the pH optimium for both NADPH and NADH dependent enzyme activities being 5.8 as shown in Figure 1.14 (Schluchter & Glazer 1997).

Two different groups have looked at the role of cysteine residues (C73, C280, and C291) in the rat and human enzymes (McCoubrey *et al.*, 1994 and Kikuchi *et al* 2001). McCoubrey found that the modification of the Cys73, to alanine completely inactivated the enzyme with NADH at pH 6.75 and NADPH at pH 8.7 and suggested that the loss of activity was not due to changes in three-dimensional characteristics of the protein. They also suggested that although the two mutations near the C-terminus (Cys 280 and Cys 291) significantly reduced activity with both the cofactors, these mutations did not inactivate the enzyme. Comparison of K_M values for these mutations suggest that Cys 280 functions in biliverdin binding, whereas Cys 291 is predominantly involved in cofactor binding. This data is at variance with Kikuchi's later experiments where the Cys 73 Ala mutation had only moderate effects on the enzyme's activity relative to that of the wild type.

The unusual properties associated with BVR-A, its substrates and products have conspired against the complete kinetic characterisation of this enzyme. In fact the basic kinetic constants associated with BVR-A still remain obscure. Firstly, the reaction product bilirubin-IXα is relatively insoluble. Although there are several strong polar groups present with two oxydipyrryl moieties (lactams), and two carboxyl groups, it is the formation of internal hydrogen bonds between the propionate side chains and the terminal lactams which severely decrease the solubility of bilirubin in aqueous solution. In contrast bilirubin in its di-anion form shows little tendency towards aggregation. Brodersen (1979) showed that the logarithm of solubility varies linearly with pH, and although insoluble in acidic

water, soluble bilirubin concentrations greater than 10mM in alkaline water were measured. To alleviate the aggregation problems especially at lower pH values, BSA has been traditionally added to bind bilirubin-IXα. The addition of BSA however increases the extinction coefficient of bilirubin from 27,000 M^{-1} cm^{-1} to 55,000 $M^{-1}.cm^{-1}$ (Phillips 1981). A larger extinction coefficient provides increased sensitivity for the detection of bilirubin at 460nm which is clearly an advantage for initial rate studies of BVR-A as the measurement of initial rates for substrate concentrations as low as 1 μM are feasible. There are disadvantage to making BSA additions to the assay mix however as BSA also binds the substrate biliverdin-IXα and in effect reduces the free concentration of biliverdin. This proves problematic when calculating kinetic constants for BVR-A as biliverdin concentrations need to be adjusted to provide a better estimation of the concentration of free biliverdin in solution. This is important as the free biliverdin-IXα concentration is the crucial variable when studying initial rate kinetics. The enzyme suffers from potent substrate inhibition (even at low micromolar concentrations of biliverdin) which hampers attempts to kinetically characterise the enzyme. At physiological pH, biliverdin concentrations as low as 2 μM display inhibitory effects. Attempts to fit curves to initial rate data exhibiting substrate inhibition at low concentrations of biliverdin are thwarted by the lack of data on the ascending limb of saturation curves. Consequently, the conventional spectrophotometric assay precludes reliable estimation of parameters such as the Michaelis constant for biliverdin. The development of a new assay which would allow the detection of sub micro molar quantities of the products of this reaction would be extremely informative. The ability to monitor the BVR-A catalysed reaction using nanomolar biliverdin would provide much needed data regarding BVR-A activity and would overcome the limitations of the conventional assay. It would also help in the enzymatic determination of biliverdin levels in vivo (which are probably sub micromolar). This is not feasible with the current spectrophotometric methods. The development of such an assay was initiated over the course of this work.

The most unusual feature associated with the kinetics of BVR-A is the fact that it is said to have two distinct pH optima. NADH is preferentially used between pH 6 and 7 while NADPH is the preferred cofactor between pH 8.5 and 8.7. Both native and recombinant human and rat BVR-A enzymes (Maines *et al.*, 1983, Yamaguchi *et al.*, 1994, Maines *et al.*, 1996, and Kutty & Maines 1981) the ox kidney enzyme, (Rigney *et al.*, 1986) and the

pig spleen enzymes (Noguchi *et al.*, 1979) all share this interesting pH dependent behaviour. Of the non mammalian enzymes studied the salmon liver has a slightly lower pH optimum between 5.5 and 6.2, while its NADPH dependent activity displayed increasing activity at the extremes of the pH ranges studied, and showed minimal activity at physiological pH. Although all the enzymes mentioned can use both cofactors to catalyse the reduction of biliverdin-IXα, it is important to note that of the biliverdin-IXα reductases examined from various species NADPH is the preferred cofactor with apparent K_M values close to two orders of magnitude below that for NADH.

The crystal structures resolved by Kikuchi *et al.*, (2001) and Whitby *et al.*, (2002), show that there is only one nucleotide binding site in BVR-A, which is defined by the Rossmann fold which comprise of the residues found spanning the loop located between β1 and αA. It has been reported that the nicotinamide moieties of both NADH and NADPH are proposed to extend into the active site of BVR-A in a well defined position and orientation (Kikuchi *et al.*, 2001). If there is only one binding site for both the nucleotides, and the C4 carbon positioning of the NADH and NADPH nicotinamide rings are identical, one must question why there is such a difference in activity when using each nucleotide as cofactor over the pH ranges studied.

1.11 Proposed Study

On the basis of the advances made in genomic and EST sequence information in recent years it is proposed that a phylogenetic survey would provide a greater insight into the distribution of BVR-A in many organisms. This may shed some light on the intriguing observation that while ancient cyanobacteria clearly express a BVR-A that is related to the "vertebrate" forms, there is no evidence for BVR-A in lower eukaryotes from yeast to worms and indeed there is a question as to whether birds, reptiles and amphibians express a functional BVR-A. Due to ongoing efforts within our group to construct a BVR-A knock out mouse I propose to clone and express the mouse enzyme and raise antibodies against it to facilitate the characterization of the mouse enzyme.

I also propose to investigate the nature of the two distinct pH optima and determine why NADH is preferentially used between pH 6 and 7 while NADPH is the preferred cofactor

between pH 8.5 to 8.7 for the mammalian enzymes. A comparison with the cyanobacterial enzyme will also be made in this regard.

An investigation into the nature of the biliverdin binding site will also be undertaken. The substrate specificity of BVR-A using a number of biliverdin isomers, some of which have conformational restraints, are to be analysed. This study is to be further extended encompass the analysis of CD spectra to determine whether a particular 'chiral' form of biliverdin-IXα is adopted in the substrate binding pocket of the various BVR-A's enzymes. The development of a radioactive assay that utilizes [^{32}P]-labelled NADPH will be undertaken to help kinetic studies at low concentrations of biliverdin-IXα and also to provide a means to enzymatically measure biliverdin levels in tissues.

A re-evaluation of the levels of zinc in mouse and human BVR-A will clarify whether BVR-A is a zinc metalloprotein. In tandem a structural review of the proposed BVR-A DNA binding domains will be examined.

Chapter Two

Materials and Methods

2.1 DNA Purification and Manipulation Techniques

2.1.1 Electrophoresis of DNA

DNA was routinely subjected to electrophoresis through 1% agarose gels, which were made by melting 100 ml of 1% (w/v) agarose in TAE buffer (40 mM Tris-HCl, 20 mM acetic acid, 1 mM EDTA pH 8.5). The melted agarose/TAE was then poured and allowed to set in an 'ATTO AE-6100' (8 cm x 10 cm) gel box. Samples 20 µl (not exceeding 50 ng DNA) were mixed with 5 µl sample volume of loading dye (0.4% orange G, 0.03% bromophenol blue, 0.03% xylene cyanol, 15% Ficoll, 0.625% SDS, 50 mM EDTA, 10 mM Tris-HCl pH 8), and were then loaded into the gel wells submersed in TAE buffer. Gels were run at 100V for approximately 1 hour using an 'ATTO Crosspower 3500' power pack.

2.1.2 Determination of the concentration and purity of nucleic acids

The purity of DNA and RNA was determined by establishing the A_{260}/A_{280} ratio using a Heλios Thermo-Spectronic spectrophotometer. Pure DNA and RNA solutions show a A_{260nm} /A_{280nm} ratio of between 1.6-1.9. A high absorbance at A_{280nm} indicates contamination with proteins. For all spectrophotometric measurements, 10 mM sodium phosphate pH 7.5 was used as diluent. The absorbance of RNA and DNA solutions was measured at 260 nm and an approximate concentration was calculated using the following conversion factors:

Pure dsDNA: A_{260nm} X Dilution factor X 50 = dsDNA Concentration (µg/ml)

Pure ssDNA: A_{260nm} X Dilution factor X 37 = ssDNA Concentration (µg/ml)

Pure ssRNA: A_{260nm} X Dilution factor X 40 = ssRNA Concentration (µg/ml)

Approximate molecular weight of nucleic acids:

MW of ssRNA = (length in nucleotides x 320.5) + 159.0

MW of ssDNA = (length in nucleotides x 303.7) + 79.0

MW of dsDNA = (length in nucleotides x 607.4) + 157.9

pM = ((ng/ml) x 10^6) / MW

The concentration and purity of DNA/RNA samples was also estimated by direct comparison to standard markers of known concentration on 1% agarose gels as described in Section 2.1.1.

2.1.3 Digestion of DNA

All restriction endonucleases used in this study were obtained from Roche Diagnostics Ltd. DNA fragments and vectors (0.1 – 1 μg) were generally digested with 10-20 units of the required restriction enzyme for at least 3 hours at 37°C in the recommended reaction buffer.

Component	**μl**
Nuclease free water	X
Endonuclease A	0.5
Endonuclease B	* (0.5)
10 X Sure Cut Buffer	5
DNA (typically between 100ng and 1μg)	5
Total Volume	50

**Supplement with nuclease free water during sequential digests.*

The final volume for each reaction was 50 μl recommended 'sure/cut' reaction buffer. Sequential digestions were performed in cases where the endonucleases were mutually incompatible in the recommended individual reaction buffers.

2.1.4 Ligation of DNA fragments

All ligations were performed using the 'Takara Ver. 2.1 DNA Ligation Kit'. Vector and insert DNA were initially digested with the appropriate restriction enzyme as described in Section 2.1.3. To prevent self ligation of the plasmid during the ligation reaction, the vector DNA was treated with Takara Bacterial Alkaline Phosphatase (BAP) to remove 5' phosphates. Following heat inactivation of the restriction enzymes at 65°C for 15 minutes, 1 μl BAP was added to the restriction digest reaction and then incubated for 1 hour at 55°C. Prior to ligation, both the digested insert and vector were purified using the 'QIAquick PCR purification kit', following the standard protocol outlined in Section 2.1.8. Ligations were typically performed by incubating 300 ng of insert to 100 ng vector in a 10 μl volume with 'Takara ligation solution I' and incubated overnight at 16°C.

2.1.5 Purification of plasmid DNA and PCR products

Small (up to 5 μg) and large scale (70 – 100 μg) purification of plasmid DNA was achieved using the Promega Wizard Plus SV Miniprep DNA purification system and the '*Qiagen Plasmid Midi Kits'* which allowed the isolation of between 70 and 100 μg of pure plasmid DNA. For a summary of these purifications, see Sections 2.1.6 and 2.1.7.

2.1.6 Large scale purification of plasmid DNA from overnight cultures

A single colony of the selected bacterial strain transformed by the desired plasmid was used to inoculate 5 ml LB medium (10 g/l Bacto tryptone, 10 g/l sodium chloride, and 5 g/l yeast extract) containing the appropriate selective antibiotic. This starter culture was then incubated for ~8 hours at 37°C with shaking at 270 rpm. After this time 50μl of the starter culture was used to inoculate 25 ml of selective LB medium. This culture was then grown at 37°C for 16 hours with shaking at 270 rpm. Bacterial cells were harvested by centrifugation at 6000 x *g* for 15 min at 4°C. The supernatant was removed and the bacterial pellet re-suspended in 4 ml of the *Qiagen Plasmid Midi Kit* Buffer P1. Once fully resuspended 4 ml Buffer P2 (lysis buffer) was added. The suspension was then mixed thoroughly by inverting the sealed tube 6 times, and then incubated at room temperature (15–25°C) for 5 min. Chilled Buffer P3 (4 ml) was added and mixed immediately by inverting the tube 6 times. Chilled P3 precipitates genomic DNA, proteins, and other cell debris. The suspension was then incubated on ice for 15 min and then centrifuged at 20,000 x *g* for 40 min at 4°C. The supernatant containing plasmid DNA was removed promptly and loaded onto a pre-equilibrated 'QIAGEN-tip 100' (the column was equilibrated by applying 4 ml 'Buffer QBT' and allowing the column to empty by gravity flow). Once the sample was loaded the 'QIAGEN-tip' was allowed to drain completely by gravity flow. The 'QIAGEN-tip' was then washed with 2 x 10 ml 'Buffer QC'. The plasmid DNA was eluted by the addition of 5 ml Buffer QF. DNA was precipitated by adding iso-propanol (3.5 ml) at room-temperature to the eluted DNA. Once mixed the suspension was centrifuged immediately at 15,000 x *g* for 30 min at 4°C. The supernatant was carefully removed and the iso-propanol treated pellets washed with 70% ethanol (2 ml) and centrifuged at 15,000 x *g* for 10 min. Again the supernatant was carefully

Strain	Genotype
BL21(DE3)	*hsdS gal (lcIts857 ind1 Sam7 Nin5 lacUV5-T7 gene 1)*
TG1	*supE hsd△5 thi △ (lac-proAB) F[traD36 proAB+ lacIq lacZ△M15]*
DH5α	*supE44 △lacU169 (080 lacZ△M15) Hsd R17 recA1 endA1 gyr△96 thi-1 relA1*
XL1-Blue	*15 F' ::Tn 10 proA+ B+ lacI^{q}, Δ(lacZ)M15/recA1, endA1, gyrA96, (Nalr), thi, hsdR17(r_K^- m_K^+), glnV44, relA1, lac*
BL21 (DE3)	*F– ompT gal [dcm] [lon] hsdSB (r_B^- m_B^-; an E. coli B strain) with DE3, a l prophage carrying the T7 RNA polymerase gene*
BL21(DE3)-RIL	*Strain[a]: E. coli B F– ompT hsdS(r_B– m_B–) dcm+ Tet^{r} gal λ (DE3) endA Hte [argU ileY leuW Cam^{r}]**

Table 2.1 Genotypes of *E. coli* strains used in recombinant DNA experiments

removed. The resulting pellet was air-dried for 10 min, and finally the DNA was re-dissolved in 100 µl nuclease free water.

2.1.7 Small scale purification of plasmid DNA from overnight cultures.

A single colony of the desired bacterial strain transformed with the appropriate plasmid was used to inoculate a culture of LB medium (5 ml) containing the appropriate selective antibiotic. The culture was then incubated for 16 hours at 37°C with shaking at 270 rpm. After this time the bacterial cells were harvested by centrifugation at 6000 x *g* for 15 min at 4°C. The supernatant was removed and the pellet resuspended with 250 µl cell resuspension solution from the 'Wizard Miniprep Kit' (Promega). Cell lysis solution was then added and the solution inverted 4 times to mix. Alkaline protease solution (10 µl) was added, and the solution incubated for 5 minutes at room temperature. Neutralisation solution (350 µl) was then added and mixed by inverting 4-6 times. The solution was centrifuged at maximum speed in a bench top centrifuge at room temperature for 10 minutes. The supernatant was transferred into the provided 'Wizard' spin columns and centrifuged at top speed for 1 minute at room temperature. The flow through was discarded and the column reinserted into the collection tube. Wash solution (750 µl) was added to the column followed by centrifugation for 1 minute. The flow through was discarded and the wash step repeated once again with 250 µl of the wash solution and centrifuged for 2 minutes at room temperature. The spin column was placed in a new 1.5ml microcentrifuge tube and 100 µl of nuclease free water was added to the spin column and let stand for 1 minute. The column was centrifuged for 1 minute at top speed and the eluent containing DNA was stored at -20°C.

2.1.8 Purification of amplified PCR products.

PCR products were purified using the 'QIAquick PCR purification kit'. The manufacturer's protocol was followed at all stages. In summary 5 volumes of binding 'buffer PB' were added to 1 volume of the PCR sample mix. The mixture was then applied to a 'QIAquick spin column' which was contained in a 'collection tube'. The column was centrifuged for 60 seconds at 13,000 rpm in a bench top centrifuge. The flow through was discarded and the column placed back into the collection tube. 'PE wash buffer' was then

added to the column which was centrifuged for 60 seconds. The flow through was discarded, and the column centrifuged for an additional 60 seconds to remove all traces of ethanol. The column was placed into a clean 1.5 ml microcentrifuge tube and the bound DNA was eluted with 50 µl 'EB elution buffer'.

2.1.9 DNA Sequencing

2.1.9a Terminator Cycle Sequencing Ready Reaction

All sequencing reactions were carried out using the 'ABI PRISM BigDye Terminator Cycle Sequencing Ready Reaction Kit' (Perkin Elmer Applied Biosystems Division, Foster City, CA). Separate reactions for forward and reverse primers were set up as follows:

BIG DYE Terminator V1.1 Cycle Seq RR-100 (ABI 436774)	8µl
Plasmid miniprep (DNA ~500ng)	3µl
Primer (2pmol/µl)	1.6µl
Nuclease free water	7.4µl
Total Volume	20µl

Terminator sequencing reactions were then subjected to the following cycling program using an 'MJ Research PTC-200 Peltier Thermal Cycler'.

1	96°C	10sec
2	50°C	5 sec (or normal annealing temperatures for that primer)
3	60°C	4 minutes
4	Goto step 1	25 times
5	4°C	

After amplification, unincorporated dye terminator was removed using a Qiagen 'DyeEx 2.0' spin column. These mini columns contain ready to use pre-hydrated gel filtration resin. On centrifugation unincorporated dye terminators contained in sequencing reactions are retained in the gel-filtration material while the DNA fragments are recovered in the flow-through. In summary, these spin columns were vortexed gently to re-suspend the

resin and placed in a 2 ml collection tube. Columns were then centrifuged for 3 min at 3000 rpm in an 'Eppendorf 5415D' centrifuge before being transferred to a clean centrifuge tube. Each 20 µl terminator cycle sequencing reaction was applied to the centre, and just proud of the column gel bed. The columns were centrifuged for 3 min at 3000 rpm and the eluate containing the purified DNA was retained and dried using a 'Thermo Savant SpeediVac'. Before sample loading, 6 µl of sample loading dye (250 µl of 50 mg/ml blue dextran + 1250 µl deionised formamide) was added to each sample and boiled for 2 minutes to denature the DNA.

2.1.9b Preparation of Sequencing Gel

Gel plates were washed, rinsed thoroughly with distilled water and allowed to dry. The bottom plate was placed at one end of the gel pouring apparatus, with the inside surface facing up. Spacer strips were placed and aligned to the long edge of the plate and clamped in position. The other sequencing glass plate was placed at the end of the first plate in preparation for gel pouring. A 5% acrylamide gel was then prepared as follows. Urea (11 g) was dissolved in 16 ml nuclease free water and stirred until fully dissolved. To this, 3 ml Long Ranger Gel Mix (Cambrex) was added, followed by 3ml 10X TBE. The solution was stirred gently and filtered through a Nalgene 115ml filtration device (0.2 µm). Fresh 10% (w/v) ammonium persulphate (150 µl) and finally 21 µl of TEMED were added to the mixture while swirling to mix. The solution was then loaded into a 50 ml syringe and as quickly as possible, the mixture was dispensed onto the plates, while moving the top plate over the bottom plate until the two plates were fully aligned. Extreme care was taken not to introduce bubbles while pouring the gel. The plates were clamped and the comb was inserted into the top of the gel. Freshly poured gels were let stand for at least 2 hours until set. The exterior plate surfaces were washed to remove particulate matter and allowed to dry. The plate was inserted into the gel holding apparatus and locked into position with the heating block overlaid on an ABI 377 DNA sequencer. Buffer trays were attached and filled to the mark with 1 X TBE. The comb was inserted about 1mm into the gel. The gel was pre-run for ~ 1 hour to reach the recommended operating temperature of 52°C, followed by the plate check run. Into individual wells, 1 µl of each sample was loaded between the comb teeth. The gel was run over a 7 hour period to facilitate full sequence acquisition.

2.1.10 Total RNA Purification and Reverse Transcriptase Polymerase Chain Reactions

2.1.10a The isolation of total RNA from animal tissues

A Balb/c strain mouse was sourced through the Bioresources Unit, Trinity College Dublin. Following sacrifice by cervical dislocation, the required tissues were quickly removed, stripped of excess connective tissue using scissors and washed with RNase free water (Ambicon). Care was taken to minimise transfer of connective tissue and excess blood. The tissue was sliced into small pieces on a petri dish containing RNA Later solution. All solutions and tubes used were sourced as RNase free grade materials, while dissection and homogenisation materials used for during this process were rendered RNase-free by treatment with RNaseZap. Tissue (100 mgs of each) was weighed and placed in RNase free microcentrifuge tubes. 1ml Trizol solution was added to the tissue samples and homogenised with a hand held homogenizer. The homogenate was stored for 5 minutes at room temperature, after which time 0.1 ml of BCP (1-bromo-3-chloropropane) was added. BCP is used in place of chloroform, and minimises the contamination of the RNA with DNA (Chomczynski & Mackey K (1995). It is also less toxic. The suspension was shaken vigorously for 15 seconds and then let stand at room temperature for 5 minutes and then centrifuged at 12000g for 15 minutes at 4°C. The aqueous phase (RNA separates into the upper aqueous phase) was removed and the RNA precipitated by the addition of iso-propanol (0.5ml). The samples were stored at room temperature for 5-10 minutes followed by centrifugation at 12000 x *g* for 8 minutes at 4°C. The RNA pellet was washed with 75% ethanol and centrifuged at 7500 x *g* for 5 minutes at 4°C. The RNA pellet was then air dried for 5 minutes. The pellet was resuspended in 100 µl RNase free water and heated to 60°C for 10 minutes to fully dissolve the RNA.

2.1.10b First Strand cDNA synthesis

First strand cDNA synthesis was performed using the Invitrogen SuperScript™ III Reverse Transcriptase Kit. Gene specific primers were designed with a GC content $\leq$50% and between 21 to 25 base pairs in length.

To a sterile minifuge tube the following components were added:

1 µl of a 2 pmol/µl stock gene specific primer

1 µg total RNA

1 µl 10 mM dNTP mix

The volume was then adjusted to 14 µl with sterile distilled water.

The mixture was then heated to 65°C for 5 minutes followed by incubation on ice for 1 minute. The mixture was centrifuged briefly to collect the material and the following components were added and mixed by pipetting up and down:

4 µl 5X strand buffer

1 µl 0.1M DTT

1 µl SuperScript™ III RT (200 units/ul)

The mixture was incubated for 1 hour at 55°C to allow cDNA synthesis followed by heat inactivation of the reverse transcriptase at 70°C for 15 minutes. To remove template RNA 1 µl of RNase A (Qiagen 7 units/ul) was added, mixed and incubated for 10 minutes at room temperature. A 'Qiaquick PCR Purification Kit' was then used to purify the newly synthesised cDNA. The 'Qiaquick Spin' handbook instructions were followed throughout this purification procedure to the final elution step when 50 µl of the 'Qiaquick elution buffer' was used to elute the cDNA from the spin column.

2.1.10c PCR from primer specific first strand cDNA aliquots.

The concentration and purity of the final preparation of total RNA was analysed as described in Section 2.1.2. Initial PCR mixtures such as that outlined below were prepared and run over a gradient program. Template concentration was also varied until clean PCR products were produced after examination on 1% agarose gels as described in Section 2.1.1.

Component	Volume l
Nuclease free water	40.5µl
10 X Pfu DNA polymerase reaction buffer	5µl
dNTPs (25mM each dNTP)	0.5µl
DNA template	1µl
Forward Primer (100ng/ul)	1µl
Reverse Primer (100ng/ul)	1µl
Pfu Turbo DNA polymerase (2.5units/µl)	1µl

Cycle Number	Conditions	Time (Minutes)
1	95°C	1
2	95°C	1
3	54°C to 60°C	1
4	68°C	2
5	Go to step 2, 21 times	
6	68°C	5
7	Hold at 4°C	

2.1.11 Site directed mutagenesis of plasmid cDNA inserts

The introduction of site directed mutations into plasmid DNA was achieved by amplification of the plasmid using *PfuTurbo* DNA polymerase (Stratagene). Two complimentary oligonucleotides of 27 base pairs were synthesized (MWG) incorporating the required base pair changes in their sequences. Details of primer design are presented in Figure 4.13. On annealing and primer extension incorporation of the oligonucleotide primers generates a mutated plasmid containing staggered nicks. Following the amplification reaction, the product is treated with *Dpn* I. The *Dpn* I endonuclease (recognition sequence: 5′-G^{M}A^TC-3′ where ^ represents the digestion site and ^{M}A represents methylated adenine) is specific for methylated and hemimethylated DNA and is therefore used to digest the parental DNA template. Upon digestion the intact vector DNA containing the desired mutations is transformed into XL1-Blue super-competent cells.

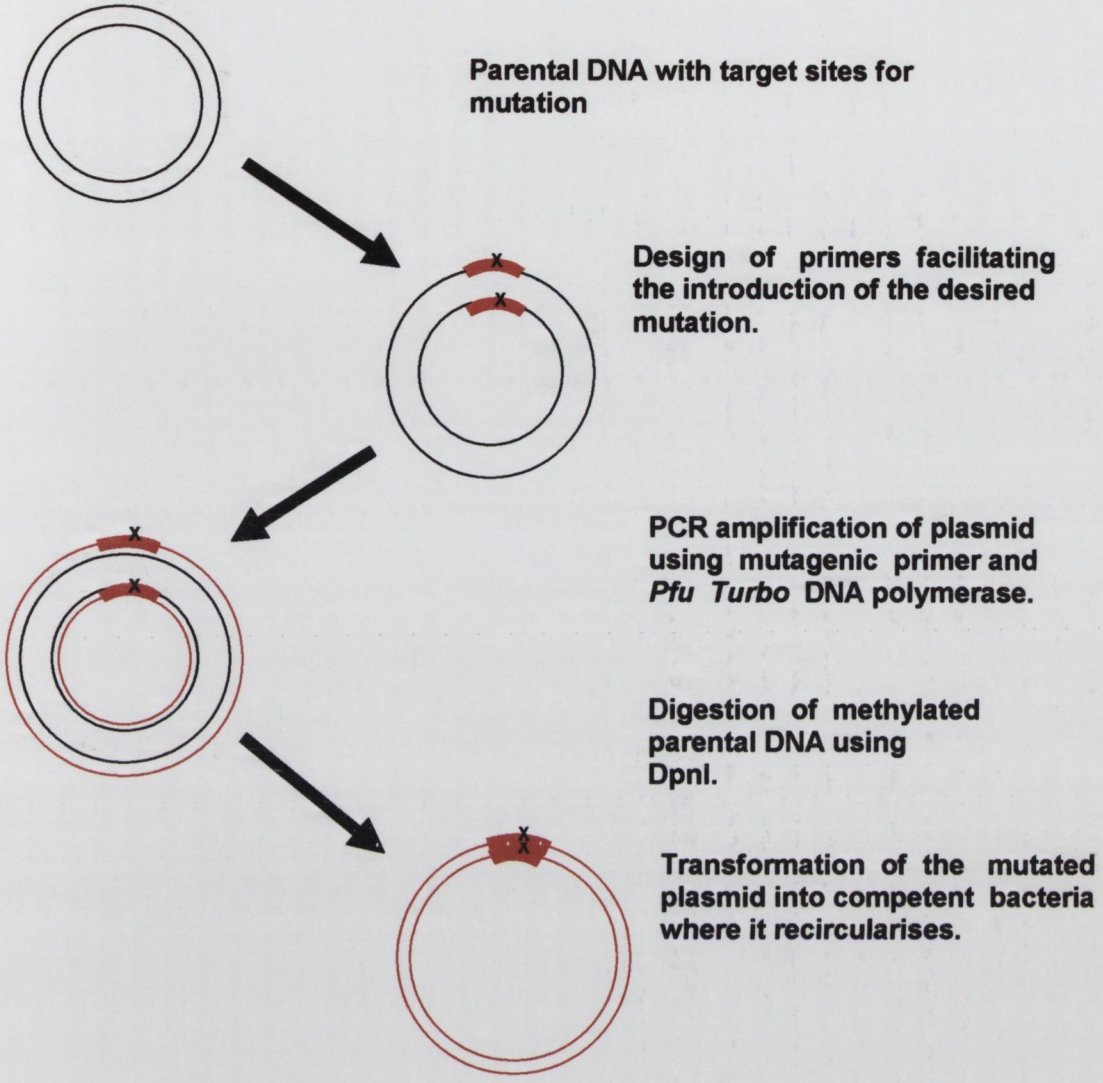

Figure 2.2 Site directed mutagenesis of plasmid DNA encoding biliverdin IXα reductase

Synthetic primers containing the desired mutation are extended during temperature cycling by *PfuTurbo* DNA polymerase. Incorporation of the oligonucleotide primers generates a mutated plasmid containing staggered nicks. The PCR product is treated with *Dpn* I (specifically digests methylated DNA) which results in the digestion of the parental DNA template. DNA containing the desired mutations is then transformed into XL1-Blue supercompetent cells.

2.2 Bacterial strains and culturing techniques

2.2.1a Preparation of fresh competent cells for storage

Competent *E. coli* were prepared by treatment of cells with rubidium chloride, as described by Inoue *et al.* (1990). The bacterial strains used are detailed in Table 2.1. An overnight culture (5 ml) was used to inoculate 500 ml Psi broth (detailed in the table below) which was incubated at 37°C with aeration to an absorbance at 600 nm of 0.5. At this point the cultures were placed on ice for 15 min. The cells were pelleted at 5000 x g for 5 minutes. The supernatant was discarded and 200 ml buffer I (30 mM potassium acetate, 100mM rubidium chloride, 10 mM calcium chloride, 50 mM manganese chloride, 15% (v/v) glycerol, pH 5.8 with dilute acetic acid) was added to resuspend the pellet. The suspension was then left on ice for 15 min. The suspension was then centrifuged at 4000 x *g* for 5 minutes and the pellet re-suspended in 20 ml buffer II (10mM MOPS, 75mM calcium chloride, 10mM rubidium chloride, 15% (v/v) glycerol and the pH adjusted to 6.5 with 0.5N NaOH). The suspension was left on ice for 15 minutes. The cells were then aliquoted into 250 µl samples and snap frozen in either an ethanol-dry ice bath, or liquid nitrogen. Once frozen aliquots were transferred to a -70°C freezer.

Psi broth	
Bacto yeast extract	5 g / L
Bacto tryptone	20 g / L
Magnesium sulfate	5 g / L
pH to 7.6 with potassium hydroxide	

2.2.1b Transformation of competent cells

The required cells were thawed on ice just before individual transformations. DNA (30-200 ng) samples were added to 50µl aliquots of these cells, and the suspension subjected to heat shock treatment (30 min on ice, 2 min at 42°C and finally 2 min on ice). 1ml of LB broth was then added and the cells incubated at 37° for 1 hour. The cells were then centrifuged briefly and resuspended in 100 µl LB and plated onto LB plates containing 100µg/ml of the desired antibiotic. The plates were incubated overnight at 37°C.

Generally transformation of 50 µl cells with 2-10 µl of a ligation reaction yielded between $1x10^8$ to $1x10^9$ cfu's/µg plasmid DNA (pET41aMod).

2.2.1c Preparation and transformation of *E. coli* cells by electroporation.

A single colony of the desired *E. coli* strain was used to inoculate a 5 ml culture of LB. This starter culture was grown overnight at 37°C with shaking at 270 rpm. The starter culture was then used to inoculate a 500 ml flask of LB, which was grown to an absorbance of 0.5 units at 600 nm. The culture was then placed on ice for 10 minutes and centrifuged at 5,000 x g for 15 min at 4°C, in pre-chilled centrifuge tubes. The cell pellet was resuspended gently in 5 ml of ice cold water. Once fully resuspended, 500 ml of ice cold sterile distilled water was added and the cells were gently mixed and centrifuged for 15 minutes at 5,000 x *g*. Care was taken at every step to ensure the cells and all equipment were maintained at 4°C throughout the centrifugation steps. The cells were once again resuspended and washed in 500 ml ice cold sterile distilled water. The pellet was then suspended in 10 ml of ice cold water and centrifuged at 4°C in a sterile pre-chilled polypropylene tube at 5000 x g for 10 minutes. The resulting pellet was gently resuspended in 500 µl ice cold sterile distilled water. Aliquots (50 µl) of the cell suspension were placed into pre-chilled electroporation cuvettes containing 1 µl DNA sample (30-200 ng plasmid DNA). The cuvette was placed in the sample unit of a Gene Pulse electroporator and the pulse was applied (25 µF 2.5 kV and 200 ohms). The cell suspension was then incubated at 37°C in 1 ml SOC medium for 1 h with shaking at 270 rpm. The cells were then plated onto LB plates containing the appropriate antibiotic and incubated at 37°C overnight.

2.2.2 Preparation of *E.coli* cells for SDS-PAGE

The volume of *E.coli* culture required to give an A_{600} reading of 0.2 (compared to an LB reference blank) was centrifuged at 12,000 x *g* for 5 minute at room temperature. The supernatant was discarded and the pellet was resuspended in 20 µl of SDS sample buffer. Samples were boiled for 5 minutes immediately before being loaded onto the gel.

2.3 Protein electrophoresis and immunoblotting

2.3.1 Sodium dodecyl sulphate – polyacrylamide gel electrophoresis (SDS-PAGE) sample preparation

Samples were prepared for electrophoresis by boiling the required amount of protein sample (routinely 5 μg for pure protein samples and 100 μg for lysates) in sample buffer for 3 minutes. The sample buffer consisted of 2% (w/v) SDS, 0.5% (v/v) 2-mercaptoethanol, 25 mM Tris-HCl, pH 6.8, 0.0012% (v/v) bromophenol blue and 10% (v/v) glycerol. Dilute solutions of protein were concentrated by precipitation with ice-cold 12.5% (w/v) trichloroacetic acid (TCA) for 20 minutes. The precipitate was centrifuged at 7500 x *g* for 5 minutes. The pellet was washed twice in ice cold acetone (0.8 ml) and allowed to dry before being resuspended in sample buffer. Dilute samples were also concentrated in a freeze drier.

2.3.2 Gel preparation and electrophoresis

SDS-PAGE was carried out by the method of Laemmli (1970). In summary all of the components of the resolving gel were mixed and poured into an ATTO slab gel mould and covered with a layer of water while polymerising. Once set the water was removed, the stacking gel added and a 1mm thick Teflon comb with 12 wells was inserted. Once set the comb was removed and the wells were washed with distilled water before use. All gels were run in an ATTO AE-6400 minigel system. The electrophoresis buffer contained 400 mM glycine, 0.1% (w/v) SDS, 50 mM Tris-HCl pH 8.3. Electrophoresis was carried out at 30 mA/gel until the tracking dye reached the bottom of the gel (approx. 45 minutes).

12% Acrylamide Resolving Gel

Total volume (10ml)	**ml**
H2O	3.3
30% Acrylamide Mix	4
1.5M Tris-HCl (pH8.8)	2.5
10% SDS	0.1
10% ammonium persulphate	0.1
TEMED	0.004

5% Acrylamide Stacking Gel

Total volume (4ml)	**ml**
H2O	2.7
30% Acrylamide Mix	0.67
1.5M Tris-HCl (pH8.8)	0.5
10% SDS	0.04
10% ammonium persulphate	0.04
TEMED	0.004

Solutions for preparing resolving gels for Tris-glycine SDS-polyacrylamide gel electrophoresis are detailed in the table above. Generally individual gel lanes were loaded with 5 μg protein in sample buffer. Sample buffer contained 2% (w/v) SDS; 10% glycerol; 0.001% (w/v) bromophenol blue and 5% 2-mercaptoethanol in 25 mM Tris-HCl pH 6.8. Samples were denatured by boiling for 2-3 minutes at 100°C.

2.3.3 Staining and de-staining procedures

Gels were stained for 10 – 15 minutes in a solution of 10% (v/v) acetic acid; 50% (v/v) methanol and 1.25% (w/v) Coomassie Blue R for 10 minutes. Destaining was carried out overnight in 10% (v/v) acetic acid and 30% methanol.

2.3.4 Raising antisera

2.3.4a Preparation of protein for immunisation schedule

Antisera were raised against the recombinant protein in New Zealand White Rabbits. On the day before commencing the schedule a 10 ml blood sample was taken from the rabbit. This was used to prepare a sample of pre immune serum. The blood sample was allowed to clot at room temperature for 1 hour. The clot was detached from the walls of the glass container and stored overnight to allow the clot to retract. Serum was decanted and centrifuged at 10000 x *g* for 10 minutes to remove any remaining blood cells. The resulting supernatant was stored at -20°C in 0.5ml aliquots. Between 250 and 400 μg of pure protein in 10mM sodium phosphate pH 7.2 was mixed with an equal volume of Freund's complete adjuvant (final volume of 1.2 ml). The mixing was carried out by placing the solutions in a tightly capped 20 ml glass bottle which was firmly attached to a vortex whirl mixer at full speed for 2 hours at room temperature. The emulsion formed (0.5 ml) was injected into multiple sites on the back of the rabbit on day one of the immunisation schedule. On day 21 a booster injection was prepared in the same manner except that Freund's incomplete adjuvant was used. The emulsion was injected intramuscularly into the leg. A second booster was prepared in the same way and injected on day 31 of the schedule. On day 38 a test bleed was carried out in which 10 ml of blood was taken from the rabbit. The serum was prepared as described above with the pre-immune serum. A dot blot assay was used to

determine the antibody titre of this serum. If the titre was sufficiently high the rabbit was exsanguinated by cardiac puncture under anaesthetic on day 39. If the titre was lower than desired a third booster injection was prepared in an identical manner to the previous booster and administered on day 53. Exsanguination was carried out one week after this and the collected blood treated as described above.

2.3.4b Determination of antibody titre using a dot blot assay

Nitrocellulose paper was cut into 5 strips (7 x 4cm). Nine dots were marked with a lead pencil on each strip leaving at least 1 cm between each dot. Samples (2 μl) containing varying amounts of BVR-A (1 ng -1 μg) in 10mM sodium phosphate pH 7.2 was applied directly onto the marked dots on each strip. As a control, 2 μl 10 mM sodium phosphate pH 7.2 containing no enzyme was applied onto the first dot on each strip. The strips were allowed to dry at room temperature and were then placed in TTBS blocking solution (3% Marvel in TTBS (0.5 M NaCl, 0.05% (v/v) Tween 20 in 20 mM Tris-HCl buffer, pH 7.5)) and incubated overnight as detailed in Section 2.3.5. Pre-immune serum (1:20) was made up in 1% (w/v) Marvel in TTBS. The first nitrocellulose strip was soaked in pre-immune serum solution and the remaining strips placed in antibody solution diluted 1:20, 1/200, 1/500 and 1/1000 in 3% Marvel TTBS. The nitrocellulose strips were incubated in these antibody solutions for 1.5 hours and then rinsed briefly in TTBS. The strips were then washed for 15 minutes in TTBS, followed by three 5 min washes in TTBS. The nitrocellulose strips were incubated for 1.5 hours in a 1:1000 dilution of secondary antibody (goat anti-rabbit IgG peroxidase conjugate) solution in 1% (w/v) Marvel in TTBS. Finally, the strips were washed for 5 min, three times in TBS (500mM NaCl, 20 mM Tris-HCl pH 7.5). The protein dots were developed by incubating the blot in 'Sigma FAST DAB' solution'. This solution was made by dissolving one of each kit tablet in 5 ml water. This yielded a ready-to-use buffered solution containing DAB (3,3'-diaminobenzidine tetrahydrochloride). Dots normally appeared within 5-10sec.

2.3.5 Western Blotting

Directly after SDS-PAGE, protein bands were transferred electrophoretically from the polyacrylamide gel onto nitrocellulose using a 'semi-dry' transfer unit (Hoefer Scientific Instruments, Model no. TE70). The gel and nitrocellulose were sandwiched in the cassette

according to the manufacturer's instructions. Before use the filter paper was soaked in transfer buffer (190 mM glycine, 13 mM SDS, 15% v/v methanol 25mM Tris-HCl pH 8.3. Transfer was achieved by applying a constant current of 110 mA for 1hour. During this time the complete transfer of pre-stained protein markers (NEB Broad Range: Cat No P7708S) was evident, which indicated an efficient transfer. Immuno-detection of biliverdin reductase on nitrocellulose was carried out using rabbit anti-BVRA antiserum as the primary antibody. These antibodies were raised against the various purified recombinant BVR-As as described in Sections 2.4. After transfer, the nitrocellulose sheets were washed overnight in TTBS containing 5% Marvel skimmed milk powder. The following morning the blot was rinsed 3 times with TTBS and then incubated for 1 hour in a solution of the primary antibody (1/1000 primary antibody) in TTBS containing 5% (w/v) Marvel. Again the blot was washed 3 times in TTBS, taking 5 minutes for each wash. A 1/1000 dilution of goat anti rabbit IgG conjugated horse radish peroxidase in 5% w/v Marvel in TTBS was added to the blot, and rolled at 4°C for 1 hour. The blot was given 3 final washes, in TBS buffer. The protein bands were developed by incubating the blot in 'Sigma FAST DAB' solution' as described in Section 2.3.4b.

2.4 Protein expression and purification

2.4.1 Activity measurements of recombinant glutathione-S-transferase fusion proteins

Glutathione-S-transferase activity was assayed using 1-chloro-2, 4-dinitrobenzene (CDNB) as substrate, as described by Haibig *et al.* (1974). Production of DNP-glutathione is detectable by monitoring the increase in absorbance at 340 nm. The reaction mixture had a final volume of 2 ml and contained 1 mM glutathione, 1 mM CDNB and 50 µl enzyme fraction in 1.85 ml of 100 mM sodium phosphate pH 6.7. All reactions were carried out at 30°C. Stock solutions of 40 mM glutathione in reaction buffer, and 40mM CDNB in 100% ethanol were used. On addition of the CDNB (50 µl) to the buffer the solution went cloudy but with rapid mixing the CDNB went into solution

2.4.2 Protein Purification Techniques

Four 5ml cultures were prepared by aseptically inoculating each vial with a single bacterial colony. The LB medium contained a final concentration of 100 μg/ml ampicillin (or other desired antibiotic). The cultures were incubated overnight at 30°C with shaking at 270 rpm and then transferred into four sterile 500 ml flasks of LB also containing 100 μg/ml ampicillin. The A_{600} was monitored at half hourly intervals and when the absorbance reached 0.4 expression of the fusion protein was induced by the addition IPTG to a final concentration of 0.2 mM. The cells were induced overnight at 30°C with shaking at 270 rpm.

The cells were harvested by centrifugation at 7,700 x *g* for 10 minutes. The supernatant was decanted and the pellets were frozen overnight to weaken the cell walls. On thawing, the pellet was resuspended in ice cold PBS (0.9% sodium chloride in 10 mM sodium phosphate pH 7.2 containing 0.1 mM DTT). To this suspension lysozyme was added to a final concentration of 40 μg/ml cell resuspension. The cells were then allowed to stand for 1 hour at 4°C. Full cell wall lysis was achieved by sonication with a Braun microprobe for 5 second bursts over a period of 5 minutes, keeping the suspension on ice at all stages of this treatment. The sonicated cells were then centrifuged at 19,000 x g for 45 minutes, and the resulting supernatant transferred to a cool clean tube for further manipulation. The supernatant was retained and loaded onto a glutathione affinity column (1.8 x 15cm containing 15 ml gel) to bind the glutathione-*S*-transferase/biliverdin reductase fusion protein. Once loading was complete the column was washed extensively with PBS until the A_{280} reached less than 0.03. The fusion protein was then eluted with 200 ml of 50mM Tris-HCl pH8 containing 10mM reduced glutathione. Fractions collected were monitored for BVR-A activity and fractions showing peak activity and high A_{280} values were pooled.

Dialysis tubing (SiC visking tubing (24/32") was prepared by boiling in 250 μM EDTA for 5 minutes. The tubing was extensively washed in deionised distilled water before use. Purified fusion protein was dialysed overnight against 25 litres of 10 mM sodium phosphate pH 7.2. While dialysing thrombin cleavage was also achieved. Lyophilised human thrombin (1000 units) was dissolved in 1 ml PBS giving a final concentration of 1unit / μl. From this stock solution 1 unit of thrombin was added for each mg fusion protein purified. The thrombin was included in the dialysis tubing with the fusion protein.

The cleaved protein was then passed through a glutathione affinity column pre-equilibrated with 200 ml 10mM sodium phosphate pH 7.2. On loading the non-bound fractions were collected. Peak protein fractions were determined by measuring the A_{280} and pooled after retaining a small sample which was then subjected to SDS-PAGE analysis (see Section 2.3.2).

2.4.3 Purification of *Synechocystis PCC 6803* biliverdin-IXα reductase.

The pHisP1 plasmid coding for the archaebacterium *Synechocystis* BVR-A (a cyanobacterial biliverdin-IXα reductase) was kindly provided by Dr.Wendy Schluchter, of the Department of Molecular and Cell Biology, University of California, Berkeley, California. LB medium, 4 x 500ml flasks were prepared and autoclaved. A 1.5 x 10 cm column was packed with a 10ml bed volume of $Ni2^{+}$ agarose and equilibrated with 200 ml loading buffer (20 mM Tris-HCl, 100 mM NaCl, 20 mM imidazole, pH 8). Each starting culture (4 x 10ml LB with 100 μg/ml final concentration of spectinomycin) was inoculated with *E.coli BL21 DE3* transformed by the pHisP1 plasmid coding for *Synechocystis* BVR-A and incubated overnight in an orbital shaker at 30°C and at 270 rpm. These 10 ml overnight cultures were then transferred to 500 ml flasks of LB containing spectinomycin at a final concentration of 100 μg/ml. The cells were incubated at 30°C with shaking at 270 rpm until the absorbance at 600 nm reached 0.6 - 0.7, at which point IPTG (400 μM final concentration) was added to each flask and the incubation continued for a further 8 hrs at 30°C. The cells were spun down at 8000 x *g* for 15 minutes at 4°C. The supernatant was discarded and the pellets frozen overnight. The cells were re-suspended in 100 ml ice cold resuspension buffer (100 mM sodium chloride in 50 mM Tris-HCl pH 7.8). Lysozyme was then added to the cell suspension to a final concentration of 40 μg/ml. The suspension was then incubated on ice for 1 hour. The cells were sonicated on ice with a DAWE Soniprobe 7532A with micro-tip output setting 4, over a period of 5 minutes with 5 second bursts. Once sonication was complete the suspension was centrifuged at 19000 x g for 45 min at 4°C to remove cell debris. The supernatant was transferred immediately to 50 ml tubes stored on ice and samples taken for SDS PAGE and measurements of BVR-A activity analysis. Nickel agarose (5 ml) was added to each tube and rolled at 4°C for 20 minutes on a bench top roller. The suspension was then loaded into a scintered glass column (1.8 x 15cm) and washed with loading buffer until the absorbance at 280 nm reached 0.03. The

column was then washed with 50 ml of 100 mM NaCl, 50 mM imidazole, 20 mM Tris-HCl pH 8, followed by 50 ml of 100 mM NaCl, 200 mM imidazole, 20mM Tris-HCl, pH 8. The eluted fractions were analysed using SDS PAGE as outlined in Section 2.3.1. Peak fractions were pooled and imidazole removed by gel filtration on a G-25 column as described in Section 2.4.8

2.4.4 Preparation and purification of human biliverdin IXα reductase

Each starting culture (4 x 10ml LB with 50μg/ml final concentration of kanamycin and 50μg/ml chloramphenicol) was inoculated with *E.coli* BL21 DE3 RIL transformed with human BVR-A pET41aMod plasmid and incubated overnight at 30°C with shaking at 270rpm in an orbital shaker. Details of the construction of this his-tagged GST fusion protein are presented in Section 3.8. The 10ml overnight cultures were then transferred to 500ml flasks of LB containing 50 μg/ml chloramphenicol and kanamycin at a final concentration of 50 μg/ml, and incubated at 30°C with shaking at 270rpm until the absorbance at 600 nm reached 0.6-0.7. At this point IPTG (200 μM final concentration) was added to each flask and allowed to incubate for a further 10 hrs at 20°C with agitation. The suspension was centrifuged at 8000 x g for 15 minutes at 4°C. The supernatant was discarded and the pellets frozen overnight. The cells were resuspended in 100 ml of ice cold buffer A (100 mM sodium chloride, 1% glycerol, 50 mM sodium phosphate pH 7.8), containing lysozyme (40 μg/ml of the cell resuspension). The suspension was incubated on ice for 1 hour before sonication on ice with a DAWE Soniprobe 7532A with microtip over a period of 5 minutes, with sonication for 5 seconds followed by 5 seconds without sonication. Once sonication was complete the suspension was centrifuged at 19000 x g for 45 min at 4°C to remove cell debris. The supernatant was transferred immediately to 50ml tubes stored on ice and samples taken for SDS PAGE and measurement of BVR-A activity. To the supernatant, 6 ml of *S*-hexyl glutathione Sepharose (3ml settled gel in 3ml Buffer A) was added and rolled for 30mins at 4°C. The suspension was then loaded by gravity flow into a column (1.5 x 10cm) and with a 'safety layer' of 5ml of *S*-hexyl glutathione Sepharose. The affinity resin was washed with 10 bed volumes of Buffer A until the absorbance at 280nm was less than 0.03. The 6xHis tagged GST-hBVR-A fusion protein was eluted with 200 ml of 5mM *S*-hexyl glutathione in Buffer A and collected in 3ml fractions. The absorbance at 280 nm of each fraction was determined and peak

fractions were pooled. Thrombin (1unit/mg) of protein was added and the samples were dialysed over 9 hours with 3 changes against 5 litres of 50 mM sodium phosphate, 100 mM sodium chloride 1% glycerol pH 7.8 at 4°. Dialysis tubing (SiC visking tubing (24/32") was prepared by boiling in 250 μM EDTA for 5 minutes. The tubing was extensively washed in deionised distilled water before addition of protein sample. The sample was then passed through a Ni^{2+} agarose affinity resin column which removed the His-tagged GST which had been cleaved from the h-BVR-A moiety. The flow through absorbance at 280 nm was monitored and peak protein containing samples were concentrated by centrifuging through a centricon filtration device as described in Section 2.4.9.

2.4.5 Purification of murine BVR-A (ppMAL expression vector).

Starter cultures of LB (5ml; supplemented with 100 μg/ml ampicillin) were inoculated with a single colony of *E.coli* BL21 transformed with mouse BVR-A/ppMAL plasmid (see Section 3.5 for details of the construction of the mBVR-A/ppMAL vector). These starting cultures were incubated overnight at 27° with orbital shaking at 270 rpm. Overnight cultures were then transferred into sterile 500 ml flasks of LB also containing 100 μg/ml ampicillin. The absorbance at 600 nm was monitored at half hourly intervals, and once the absorbance reached 0.7, expression was induced by the addition of a final concentration of 0.2 mM IPTG. The cells were induced for 12 hours at 27°C with shaking at 270 rpm.The cells were harvested by centrifugation at 7,700 x g for 10 minutes. The supernatant was decanted and the pellets were frozen overnight. On thawing, the pellet was re-suspended in ($1/20^{th}$ original culture volume) ice cold 50 mM sodium phosphate pH 7.8 containing 100 mM sodium chloride and 0.1 mM DTT. To this suspension, lysozyme (40μg/ml of the cell resuspension) was added and the cells allowed stand for 1 hour at 4°C. Cell wall lysis was achieved by sonication with a DAWE Soniprobe 7532A (micro-tip output setting 4), over a period of 5 minutes with 5 second bursts. The suspension was kept on ice at all stages. The sonicated cells were then centrifuged at 19,000 x g for 45 minutes. The supernatant was promptly removed, and loaded onto amylose affinity column (1.5 x 10cm scintered glass column) to bind the MBP/BVR-A fusion protein. Once loading was complete the column was washed extensively with 50 mM Tris-HCl, 150 mM NaCl, 1 mM EDTA, 1 mM DTT, pH 7 until the absorbance at 280nm of the wash fractions fell below 0.03. The ppMAL fusion protein was eluted at this point with 10 mM maltose in 50 mM Tris-HCl, 150 mM

NaCl, 1 mM EDTA, 1 mM DTT, pH 7. The eluate was tested for BVR-A activity and the absorbance at 280 nm was measured to determine protein content and the peak fractions were pooled. PreScission™ Protease from Amersham Biosciences (1 unit cleaves 0.8mg fusion protein over 16 hours at 4°C in the elution buffer used) was supplied in a 2 units/μl stock. PreScission™ Protease specifically cleaves the MBP fusion tag between the Gln and Gly residues of the recognition sequence LeuGluValLeuPheGln/GlyPro which has been engineered in the fusion protein linker domain of ppMAL expressed proteins. After the overnight incubation with PreScission™ Protease the sample was dialyzed against three 5L changes of 25 mM NaCl, 20 mM Tris-Cl pH 8 for at least 2 hours each. A column (1.5 x 10cm) of DEAE-cellulose was pre-equilibrated with 25mM NaCl, 10mM Tris-HCl, pH 8 (200ml). The fusion protein cleavage mixture was loaded onto the column while collecting 2.5 ml flow-through fractions and subsequently washed with 50 ml of the equilibration buffer. A gradient (2 x 30ml) from 25 mM NaCl to 500 mM NaCl in 20 mM Tris-HCl pH 8 was used to separate the mBVR-A from the MBP. Peak fractions were analysed using SDS PAGE described in Section 2.3.1.

2.4.6 Purification of Rat Biliverdin-IXα Reductase.

The pHis-Parallel 1 plasmid coding for rat BVR-A was kindly provided by Professor John Phillips, University of Utah, Salt Lake City. LB medium, 4 x 500 ml flasks were prepared and autoclaved. A 1.5 x 10cm column was packed with a 10 ml bed volume of $Ni2^{+}$ agarose and equilibrated with 200 ml loading buffer (20 mM Tris-HCl, 100 mM NaCl, 20 mM imidazole, pH 8). Each starting culture (4 x 10ml LB with 100 μg/ml final concentration of ampicillin) was inoculated with *E.coli BL21 DE3* transformed by the pHis-Parallel 1 plasmid coding for rat BVR-A and incubated overnight in an orbital shaker at 30°C and at 270 rpm. These 10 ml overnight cultures were then transferred to 500 ml flasks of LB containing ampicillin at a final concentration of 100 μg/ml. The cells were incubated at 30°C with shaking at 270 rpm until the absorbance at 600 nm reached 0.6-0.7, at which point IPTG (200μM final concentration) was added to each flask and the incubation continued overnight at 30°C. The cells were spun down at 8000 x *g* for 15 minutes at 4°C. The supernatant was discarded and the pellets frozen overnight. The cells were re-suspended in 100 ml ice cold resuspension buffer (100 mM sodium chloride in 50 mM Tris-HCl pH 7.8). Lysozyme was then added to the cell suspension to a final

concentration of 40µg/ml. The suspension was then incubated on ice for 1 hour. The cells were sonicated on ice with a DAWE Soniprobe 7532A with micro-tip output setting 4, over a period of 5 minutes with 5 second bursts. Once sonication was complete the suspension was centrifuged at 19000 x g for 45 min at 4°C to remove cell debris. The supernatant was transferred immediately to 50 ml tubes stored on ice and samples taken for SDS PAGE and measurements of BVR-A activity analysis. Nickel agarose (5 ml) was added to each tube and rolled at 4°C for 20 minutes on a bench top roller. The suspension was then loaded into a scintered glass column (1.8 x 15 cm) and washed with loading buffer until the absorbance at 280 nm reached 0.03. The column was then washed with 50 ml of 100 mM NaCl, 100 mM imidazole, 20mM Tris-HCl pH 8, followed by 50 ml of 100 mM NaCl, 150mM imidazole, 20 mM Tris-HCl, pH 8, and finally with 100 mM NaCl, 200mM imidazole, 20 mM Tris-HCl, pH 8. The eluated fractions were analysed using SDS PAGE as outlined in Section 2.3.1. Peak fractions were pooled and imidazole removed by gel filtration on a G-25 column as described in Section 2.4.8

2.4.7 Preparation of cytosolic fractions from murine tissue

Tissue cytosols were prepared essentially by the method of Habig *et al.,* (1974a). Tissues were removed from the mice and washed in ice cold homogenising buffer (0.25M sucrose, 1mM EDTA in 10 mM Tris-HCl pH 7.2), weighed and homogenised in three volumes of homogenisation buffer using an Ultra-turrax T-25 homogeniser. The homogenates were centrifuged at 49,460 x *g* for 45 min at 4°C in a fixed angle rotor, using a Sorval RC-5B centrifuge. The resulting supernatants were filtered through glass wool to remove lipid, prior to protein determination and BVR-A activity measurements.

2.4.8 Desalting protein samples using Sephadex G-25 gel filtration.

Gel filtration on Sephadex G-25 was used to desalt protein solutions and to separate protein from low molecular weight substances such as glutathione and imidazole. The resin initially was swollen in water according to the manufacturer's instructions (1g swells to 5 ml bed volume). The column (62 x 3.2 cm) was poured and equilibrated with 100mM NaCl in 10mM sodium phosphate buffer pH 7.2 at 4°C. The included and excluded volumes were determined using solutions of p-nitrophenol (10mg/ml) and blue dextran (5 mg/ml) respectively. As a general rule a sample volume height of no more than half the

column diameter was loaded at any time. The column flow rate was established to be ~1ml/minute. Eluted fractions were monitored through the absorbance at wavelengths of maximum extinction for each sample.

2.4.9 Chromatofocusing of BVR-A.

The polybuffer exchanger PBE-94 (Sigma) was pre-equilibrated with start buffer (25 mM imidazole/HCl pH 7.4) before packing the column (30 x 1.5 cm containng a 50 ml bed volume PBE). Once poured the column was washed with 400 ml of start buffer and finally the pH of the run through was checked making sure that the pH of the run through was the same as that of the starting buffer. All samples to be chromatofocused were dialysed against start buffer (25mM imidazole pH 7.4/HCl). Prior to loading the sample, 5 ml of eluent Polybuffer 74 (1/8 dilution of Poly buffer 74; pH 4) was run through the column. The sample was applied (< 0.5 bed volumes) at a flow rate of 1 ml/min. Elution was achieved by running 14 column volumes of eluent buffer through the column. Fractions were analysed using the Bradford protein assay as described in Section 2.4.10. A sample (20 µl) of each fraction was taken and run on SDS PAGE as described in Section 2.3.1. Regeneration of the poly buffer exchanger was achieved by washing at least 5 bed volumes of 1M NaCl through the column. The column was then re-equilibrated with start buffer, until the eluent pH matched that of the washing buffer.

2.4.10 Protein concentration techniques

Disposable Amicon Centriplus 15 ml YM-10 centrifugal filter devices with a molecular weight cut off of 10 KDa were used when it was necessary to concentrate protein samples. The filtration devices were initially rinsed with deionised water and centrifuged until at least 7 ml passed through the membrane. The remaining deionised water was discarded and 15 ml of the sample to be concentrated was loaded into the filtration reservoir. The device was then spun at 3,000 x g for approximately 2 hours at 4°C. The sample was checked at half hour intervals to ensure that the reservoir did not dry due to excessive centrifugation. An absorbance at 280 nm gave an indication of the concentration of protein. A Markwell protein assay, as described in Section 2.4.10a, was performed to obtain a more precise protein concentration value for these concentrated samples.

For crystallisation purposes the smaller Millipore microcon centrifugal filter devices were used. These have a maximum sample volume of 0.5 ml and again were centrifuged at 3000 x g in an Eppendorf 5415R bench-top centrifuge.

2.4.11a Protein Determination

For routine column monitoring the absorbance of fractions was measured at 280 nm and a value of 1 was assumed to be equivalent to a protein concentration of 1 mg/ml (Thorne, 1978). When required protein concentrations were determined using the method of Markwell *et al.,* (1978). Bovine serum albumin was used as the standard protein and a series of standards were made up ranging from 0 -100 μg of protein. Reagent C was prepared by mixing reagent A (100 ml: 2% (w/v) sodium carbonate, 0.4% (w/v) sodium hydroxide, 0.16% (w/v) potassium tartrate and 1% (w/v) SDS and reagent B (1 ml, 4% copper sulphate). BSA standard or unknown protein sample (0.5ml) was added to reagent C (1.5 ml), in duplicate. These samples were allowed to stand at room temperature for 10 minutes before Folin-Ciocalteau's phenol reagent (0.3 ml: 50% w/v) was added. The colour change was allowed to develop for 45minutes and the absorbance at 660 nm was determined. The BSA standards were used to construct a standard curve from which the protein concentration of the unknown samples was determined.

2.4.11b Bradford protein determination in multiwell plates

This assay was used to determine protein concentration in samples eluted from the various chromatography columns described. This assay was performed in a 96 well plate. BSA standards, 5 μl of 0.1-1.0 mg/ml solutions were added in triplicate to separate wells, while 5μl sample buffer (used as blank) and 5 μl unknowns were added to individual wells. To each well 250 μl of the Bradford Reagent was added and mixed on a shaker for approximately 30 seconds. The samples were incubated at room temperature for 20 minutes after which time the absorbance at 595nm was measured. The BSA standards were used to construct a standard curve from which the protein concentration of the unknown samples was determined.

2.5 Kinetic and ligand binding studies

2.5.1 Kinetic studies on biliverdin IX-α reductase.

The standard assay for monitoring BVR-A activity contains:

100mM	sodium phosphate pH 7.2
100μM	NADPH (or 700μM NADH)
20μM	biliverdin IX-α
37μM	BSA

All reactions were performed at 30°C. Reactions were generally started by the addition of enzyme. The Beer-Lambert Law (A= ϵ.c.l) was used to obtain exact concentrations of nucleotide and biliverdin IXα. Extinction coefficients for these substrates are:

Biliverdin IX-α at 660nm $\epsilon = 12.5 \times 10^3 \text{l.mol}^{-1}.\text{cm}^{-1}$

NAD(P)H at 340nm $\epsilon = 6.22 \times 10^3 \text{l.mol}^{-1}.\text{cm}^{-1}$

For saturation kinetics data points were fitted to the Michaelis equation outlined in Equation 2.1 using the least squares fitting program 'WinCurve Fit, version 1.3' (Kevin Raner Software, Mt. Waverley, Australia).

Equation 2.1 $$v_o = \frac{V_{max}[S]}{K_M + [S]}$$

The rectangular hyperbolas generated by these fits were used to obtain values for the apparent K_m and V_{max} .

2.5.2 Recording of CD spectra and stopped flow CD measurements

Both steady state and kinetic CD spectra were collected on an Applied Photophysics π*-180 Fluorimeter/CD/Stopped Flow Spectrophotometer using either the equilibrium sample handling unit (ESHU) or the kinetic sample handling unit (KSHU). Instrument hardware was set up as outlined in the Applied Photophysics π*-180 users manual. During kinetic CD applications the most intense lamp for the wavelength of interest was fitted to the system and the instrument control panel was set up to 'kinetics mode' with 'circular

dichroism' selected as signal. The xenon lamp was fitted to the system where equilibrium CD spectra were measured. The polariser was set across the instrument light path for all CD detection experiments and with recordings below 200 nm, the instrument was purged with nitrogen at a flow rate of 3 litres per minute. All buffers used during these studies were degassed and filtered through '*Sarstedt Filtropur S 0.2μm*' filtration devices before use. On the software spectrometer control panel the spectrum mode was selected and circular dichroism activated on the signal section of the control panel. The monochromator was set at the desired wavelength range, and a step size of 1nm for the spectrum required was set in the details window. The monochromator entrance and exit slit widths were then set at 1nm standard or 2 nm for far UV spectra applications. The AutoPM button was activated to switch on the automatic CD detector high voltage adjustment within the instrument. An appropriate scan time was then set by entering a suitable number of samples per step of the scan. Blank solutions were loaded in the sampling handling unit and a baseline recorded for the sample. In situations where automatic baseline subtraction was desired the 'enable baseline option' was selected. Samples of interest were then loaded into the sample handling unit and the absorbance spectrum measured. During kinetic measurements, once the sample was loaded onto the KSHU the flow circuit was primed with sample before measurements were taken. Generally a minimum of 5 shots were measured and averaged during each measurement.

2.5.3 Absorbance spectrum measurements

Instrument hardware was set up as outlined in the Applied Photophysics π*-180 users manual. In the software 'Spectrometer Control Panel' spectrum mode was activated. Absorbance was then selected in the signal section of the control panel and following this the CD detector was ticked in the absorbance signal section. The desired wavelength range and step size for the spectrum was set in the monochromator details window. Also in his window the monochromator entrance and exit slit width were set to 1nm. Appropriate scan times were set by entering a suitable number of samples to be recorded at each step of the scan. The appropriate blank solution was loaded into the sample handling unit and in the absorbance signal section of the Control Panel, the calibrate button was activated to record a baseline for the blank. Samples to be measured were then loaded in the sampling handling unit and the absorbance spectrum was recorded.

2.5.4 Measurement of stopped flow absorbance kinetic traces

Absorbance stopped-flow kinetic traces were collected using the KSHU. Instrument hardware was set up as outlined in the Applied Photophysics π*-180 users manual. Once kinetics mode in the software control panel was selected, absorbance in the signal section was then activated. The CD detector was then ticked in the absorbance signal section of the control panel. The desired wavelength for the measurement was set under the monochromator details window, and entrance and exit slit widths was set to the recommended 1nm width. The appropriate blank solution was then loaded into the KSHU and washed through the sample circuit. The instrument was then calibrated to register a baseline for the sample. The reaction to be measured was loaded into the KSHU and again the flow circuit was primed. At least 6 measurements were taken and averaged.
The results of stopped flow experiments discussed in Section 4.4 were fitted to a curve of single exponential with slope (see Eqution 2.2).

Equation 2.2 $$y = a.e^{(-k.x)} + b.x + c$$

2.5.5 Fluorescence Binding Studies on BVR-A

Nucleotide binding to BVR-A was monitored by studying the quenching of the protein fluorescence using a Perkin-Elmer luminescence spectrophotometer (LS 50B). Data was processed using the Perkin Elmer FL WinLab scan application. The excitation wavelength was set at 295nm (half band width, 5nm) and the emission wavelength was set to scan from 310nm to 400nm (half band width, 5nm). All solutions used in fluorescence experiments were filtered through a 0.45μm filter before use and an acid washed quartz cuvette was used throughout to minimise noise interference. BVR-A enzymes (1μM final concentration) were diluted in 100mM of the desired buffer to a final volume of 2 ml. Quenching of protein fluorescence was achieved by the sequential addition of $NADP^+$ (from a 100μM stock) and NAD^+ (from a 1mM stock). The fluorescence intensity (F_{meas}) was measured after each addition of nucleotide. The F_{meas} was corrected for the 'inner filter effect' as described by Levine (1977) using a correction factor:

$$F_{corr} = F_{meas} \text{ X antilog } ((\epsilon_{excit} + \epsilon_{emiss})[\text{nucleotide}](\text{pathlength}/2))$$

Where ϵ_{excit} and ϵ_{emiss} are the molar extinction coefficients of the nucleotide at the excitation and emission wavelengths, respectively, and the pathlength is 1cm. Once the peak of the protein fluorescence had been determined from an initial scan, F_{meas} was measured at the wavelength after the addition of nucleotide. The extinction coefficients were then determined at 295nm and at 345/350nm by detecting the absorbances of known concentrations of nucleotide in 100mM sodium phosphate pH 7.5, under conditions where Beer's law is obeyed. The dissociation constants K_d were calculated from a titration plot of ΔF (the change in fluorescence upon each addition of nucleotide) against nucleotide concentration.

2.5.6 Determination of protein bound zinc by atomic absorption spectrophotometry

Absorption spectrophotometry was used to measure zinc levels. The technique has been extensively reported since Hackley *et al.*, 1968. The highest quality reagents available and distilled deionised water were used in the making of all solutions. A model 357 AA/AE spectrophotometer (Instrumentation Laboratory) with an oxygen/acetylene flame, a hollow cathode current of 3 mA, 1nm band pass and a monochromatic wavelength of 213.9 nm was used for zinc detection. The system was calibrated using the buffered solutions without protein. The sample absorption characteristics were integrated by the spectrophotometer over 3 s and the resulting readings were recorded. $ZnCl_2$ was used to create a standard curve over the range 0-0.5 ppm. Bovine serum albumin, equine liver alcohol dehydrogenase, human and murine biliverdin-IXα reductase were all analysed for the presence of zinc. Human BVR-A was expressed in *E.coli* using LB supplemented with 100μM $ZnCl_2$, and also in non-supplemented LB. Expressed BVR-A was then purified to homogeneity. Samples (1.5 ml; 0.5-1 mg/ml) which had been supplemented with $ZnCl_2$ were dialysed against a 200 times volume of 100μM $ZnCl_2$ in 100mM Tris-HCl pH 7.2 for 3 hours. These samples were then passed through 5 ml HiTrap™ Desalting Column (Amersham). The eluent fractions were collected and analysed for protein content and also for zinc using atomic absorption spectroscopy.

2.5.7 Preparation of biliverdin IXα

Biliverdin-IXα was prepared from commercial bilirubin-IXα by the method of McDonagh (1979). Bilirubin (450mg) were dissolved in 100 ml of nitrogen purged DMSO. The bilirubin was oxidised by the addition of (377mg) 2,3-dichloro-5,6-dicyano-p-benzoquinone (DDQ) while stirring. The reaction was terminated after 2 minutes by adding 1.5L of ice cold distilled water. Precipitated biliverdin IXα was recovered by centrifugation at 13,500 x g for 20 minutes at 2°C. The pellet was washed 4 times with 100 ml of ice cold water, and dried overnight in a freeze drier. Silica gel 60G (15g) was resuspended in methanol acetone (1:1, v/v) and packed in a 4x4 cm scintered glass column. The dried biliverdin-IXα, 100mg, was dissolved in the above solvent and applied to the equilibrated silica bed. The column was washed with solvent until a clear eluent was obtained. Application of (70:30:0.3, v/v) chloroform-methanol-acetic acid was used to elute the dark green band of biliverdin. This material was dried overnight under reduced pressure in a desiccating vessel. Purity of the fraction was ascertained by thin layer chromatography on a 20 x 20 cm Silica plate using chloroform-methanol-acetic acid (90:10:1, v/v) as the mobile phase.

2.5.7b Preparation of biliverdin ditaurate

Bilirubin-IXα ditaurate (53mg) was dissolved in 20 ml sterile distilled water in a round bottomed flask. To this 30mg of DDQ was added and mixed. The solution was allowed to react for 5 minutes after which time Silica gel (3g) was added to the flask. The biliverdin ditaurate was dried onto the silica gel by rotary evaporation. A silica gel 60G column of 20 ml bed volume was equilibrated in ethyl acetate (100 ml). To this the dried biliverdin ditaurate / silica material was loaded onto the column. The column was washed with 300 ml ethyl acetate to remove the hydrogenated quinine. The column was then washed with 150 ml of ethyl acetate methanol (4:1, v/v) to elute unreacted quinone and unreacted bilirubin ditaurate. Finally the biliverdin ditaurate was eluted with 100% methanol and dried to a powder by rotary evaporation.

2.5.8 Separation of adenine nucleotides and nicotine adenine dinucleotides

The potent substrate inhibition encountered during kinetic analysis of BVR-A has proved to be a major stumbling block in fully understanding its enzymatic behaviour, and the determination of many of its kinetic parameters (discussed in Chapter 4). Since [^{32}P]-NADPH is not commercially available, it was necessary to develop a convenient method which would produce [^{32}P] labelled NADPH and NADH. Furthermore on assaying biliverdin reductase the development of a fast, effective and analytical method which would allow the detection of the reaction products was also necessary.

2.5.9a Separation of adenine nucleotides and nicotine adenine dinucleotides on DEAE

One of the methods studied primarily due to its capacity to bind nucleotides was the technique of ion exchange chromatography using DEAE mini-columns. A 10 ml plastic mini-column (Biorad) was filled with a 50% DEAE 52 suspension which had been equilibrated overnight in multiple changes of 200mM potassium phosphate pH 7.5 (i.e. until the pH remained constant at pH 7.5). Once settled the 5 ml bed volume in the column was washed extensively with 150 ml of 10mM Tris-HCl pH 7.5. Solutions (1mM) of the following nucleotides NAD^+, NADH, $NADP^+$ and ATP were made in 10mM Tris-HCl pH 7.2. A sample of each (200 µl) was loaded onto the column and washed with 10mM Tris-HCl pH 7.2 (18 ml) followed by elution with a 2 x 50 ml gradient (50 mM KCl and 400mM KCl in 10mM Tris-HCl pH 7.2). The absorbance at 260nm and 340nm (for the reduced nucleotides NADH and NADPH) was determined and the elution volumes were recorded.

2.5.9b Separation of adenine nucleotides and nicotine adenine dinucleotides on HPLC

The purification of various nucleotides during the synthesis of [adenylate ^{32}P]-NADPH was achieved using the HPLC technique described by Markham *et al.* (2004). The reaction mixture from the synthesis reaction (Section 2.5.10) was fractionated on a Shimadzu LC-10AL system (Kyoto, Japan) with a Supelco Discovery C18 HPLC column (25cm x 4mm)

attached via a 500µl injection loop. Elution from the column was achieved using the gradient program Buffer A (100mM potassium phosphate pH 6.0), Buffer B (60% Buffer A with 40% MeOH), Buffer C (100 % MeOH) at a flow rate of 0.8 ml/min. Eluant was monitored at 254 nm and the elution profile recorded using a Shimadzu C-R8A chromatopack.

2.5.9c Separation of nicotine adenine dinucleotides on PEI cellulose

PEI cellulose (polyethyleneimine-modified microcrystalline cellulose) was also evaluated for the separation of nucleotides substrates and products of the biliverdin reductase assay. The PEI cellulose was cut into rectangular strips (5cm x 10cm). A pencil (soft tip) was used to mark the line of origin. Care was taken not to score these plates during the experimental setup. During the technique evaluation, and mobile phase tests, 2µl of a 2mM solution of NAD^+, NADH, $NADP^+$, NADPH were spotted on plates at the origin. Various mobile phases were examined and it was found that for NADH, NAD^+ applications 50mM $CaCl_2$ in 50mM Tris-HCl pH7.2 provided the best separation, while for $NADP^+$ and NADPH, 200mM $CaCl_2$ in 50mM Tris-HCl pH 7.2 as mobile phase provided good separation. Plates were run in lined containers with a lid at room temperature until the front reached the end of the plate. The plates were then removed and air dried, and separated nucleotides visualised under an ultraviolet source (excitation at 254nm). Where [^{32}P] labelled nucleotides were employed the plates were wrapped in cling film and used to exposed to X-ray film (Kodak). On development the separated radiolabelled nucleotides spots were visualised.

2.5.10 Synthesis of [P^{32}] NADPH

The conversion of NAD to [^{32}P]-NADP is now possible by utilising the recombinant *E.coli* NAD^+ kinase which was cloned, expressed and available from Dr. Seamus Browne of the Biochemistry Department in Trinity College, Dublin. The conversion of NAD^+ to $NADP^+$ was essentially performed according to the method of Kawai (2001). The reaction mixture consisted of 1mM NAD^+, 16µM ATP, 16µM γ-[^{32}P] ATP, 5mM $MgCl_2$, 100µg NAD^+ kinase in 100mM NaCl, 100mM KCl, 100mM Tris-HCl at pH 7.8. The total reaction volume of 500µl was necessary to minimise dilution and sample loss during HPLC separation of the reaction products (Section 2.5.9b).

The $NADP^+$ dependent alcohol dehydrogenase from *Thermoanaerobium brockii* (Sigma) was used to synthesise 2'-[^{32}P]-NADPH from 2'-[^{32}P]-$NADP^+$. Components of the ADH reaction used to synthesise 2'-[^{32}P]-NADPH were 2'-[^{32}P]-$NADP^+$ (7.7μM), 0.5mM propan-2-ol, 20μM $NADP^+$, 0.1 units ADH and in 100mM sodium phosphate pH 7.8. The reaction mixture was incubated at 40°C for 30 minutes to allow conversion of $NADP^+$ to NADPH.

2.6 The identification of biliverdin-IXα reductase cDNA from various organisms

Searches of the various EST (expressed sequence tags) databases produced a number of sequences showing very high similarities with biliverdin-IXα reductase. Some of these are outlined in Section 3.2. The manipulation tools necessary to examine these sequences are found at *http://www.ebi.ac.uk/Tools*. The nucleotide sequence restriction digest program, pDraw32 for PC use was downloaded as freeware from *http://www.acaclone.com/*. The GenBank sequence database, provided by the National Center for Biotechnology Information (NCBI) available online at *http://www.ncbi.nlm.nih.gov/* . The Sanger Institute available at *http://www.sanger.ac.uk/Projects/X_tropicalis/blast_server.shtml*) was scanned for nucleotide sequences and their protein translations.

2.7 The crystalisation of human, and murine biliverdin reductase

Firstly the purified proteins were concentrated to at least ~5 mg/ml. In attempts to crystallize the purified protein the vapour diffusion hanging drop method was employed. A protein droplet (2 μl) and crystallisation buffers (2 μl) were placed onto crystallisation slides. The slide was inverted and used to cover the greased reservoir face containing 1 ml precipitant of the same precipitant. The slides and crystallisation chambers were sealed with vacuum grease to ensure a closed system. The droplet initially contains an insufficient concentration of precipitant for crystallization to occur, but as water vaporizes from the drop and transfers to the reservoir, the precipitant concentration increases which often induces crystal formation and growth. Duplicate sample plates were incubated at 4°C and at room temperature, while monitoring plates over a number of weeks. The precipitant

screens were first set up using the Emerald products EBS-WIZ-F (Wizard I and II) screening kits.

Chapter Three

A phylogenetic survey of biliverdin -IXα reductase

Chapter 3 A phylogenetic survey of biliverdin -IXα reductase

3.1 Introduction

For many years it was generally accepted that bilirubin is found solely in vertebrates, while biliverdin is found not only in vertebrates and invertebrates, but also in some micro-organisms. It was also widely accepted that both biliverdin and bilirubin had no physiological importance, being merely waste products of haem catabolism. Recent findings as discussed in the introduction clearly refute this, with several new functions being recently attributed to these linear tetrapyrroles. However, despite recent advances many questions remain unanswered. There is a void in our knowledge as to why the evolution of the haem degradation pathway in many higher organisms simply did not stop with the production of biliverdin. Since biliverdin is readily excreted into bile in many species and therefore easily enters the intestine, one must ask why the pathway evolved as it did; using valuable reducing equivalents to make the insoluble, and potentially toxic by-product bilirubin. Additionally, bilirubin requires further modification by the glucuronyl transferase system before it can be excreted. Superficially the extra steps involved in bilirubin production and its elimination appear to have no role *in vivo*. However there is an increasing body of evidence that bilirubin functions as a major physiological antioxidant and cytoprotectant (Baraňano *et al*, 2002, Yamaguchi *et al* 1994, Stocker, *et al* 1987, and McDonagh 1972). Baraňano *et al* (2002) showed that bilirubin very potently protected brain cultures from H_2O_2 neurotoxicity, with as little as 10 nM bilirubin protecting against a 10,000-fold stoichiometric excess of H_2O_2. It is important to note that all these studies have concentrated on the elucidation of mammalian pathways. In the case of birds, reptiles, and amphibians, biliverdin is widely accepted as being the predominant end product of the haem degradation pathway. Consequently, for many years, few resources have been dedicated to determine, whether or not, these organisms actually express or have the capacity to express an active biliverdin-IXα reductase.

Without doubt biliverdin seems to be the major final product of haem degradation in many species, however we should not assume that where biliverdin-IXα is the sole catabolic haem by-product that there is an absolute absence of BVR-A activity. In this regard attention must be drawn to reports that bilirubin and bilirubin conjugates have been found

in chickens, turkeys, alligators, turtles (Lin *et al.*, 1974; Himes & Cornelius, 1975; Dolphin, 1979) and frogs (Lester *et al.*, 1971: Cole & Little 1983 a; Cole & Little 1983 b). Indeed the products of amphibian haem catabolism are under a renewed degree of scrutiny after recent studies by Falchuk and co-workers (Falchuk *et al.*, 2002; Montorzi *et al.*, 2002). They have shown that biliverdin plays a vital role in *Xenopus laevis* embryogenesis. Biliverdin-IXα is broken down once irradiated with either 254 or 366 nm UV light. Irradiation of frog embryos at these wavelengths is known to affect dorsal axis development. Falchuk *et al.*, 2002, described how *Xenopus* embryos, after irradiation treatment, could be rescued if supplemented with biliverdin-IXα, but not if supplemented with either irradiated biliverdin-IXα or biliverdin dimethyl ester.

Another interesting study by When-Qi & Yong Long 2004, detected a biliverdin reductase activity in the soluble fraction homogenates of adult worms of *Schistosoma japonicum*. This is an interesting observation in light of the fact that worms are one of the few organisms which do not have the necessary enzymes to synthesise haem (Rao *et al.*, 2005). Cornelius (1981) also points out that there is a wide variation in hepatic bilirubin-IX-α uridine diphosphate (UDP) glucuronyl, glucosyl and xylosyl transferase activities among yellow rat snakes, pin fish, chickens, turkeys, sea turtles, alligators, nutria and rats. Lower hepatic enzyme activities were observed in fish, snakes, turtles, and avian species with intermediate enzyme activities present in the livers of nutria and alligators. Interestingly hepatic glycosyltransferase activities were greater in the biliverdin-excreting species which are known to excrete an exogenous bilirubin load. Bilirubin is found in chickens and the levels vary throughout the lifecycle. For instance in a study by Vajro *et al.*, (1995) 11.5% of the total bile pigment in embryos of white Leghorn hens and this decreased to 2.5% of the total as the embryo developed. They found that bilirubin existed almost entirely (98%) in esterified form, mainly as glucosides, glucoronides and xylosides in the ratios 6:3:1 respectively. Mizobe *et al.*, (1997) also detected biliverdin, bilirubin and bilirubin conjugates in pericardial fluid from jaundiced broilers.

With respect to those species which excrete predominantly biliverdin, such as chickens, are the small quantities of bilirubin and conjugated bilirubin simply a product of a very low biliverdin reductase activity or is it a product of an alternative mechanism of biliverdin reduction that does not utilise BVR-A? To further confuse matters it seems that not all

avian species share similar tetrapyrrole excretion characteristics. The house sparrow is reported to have serum bilirubin levels in the same range reported for human serum ~1mg/dL (Parrish & Mote, 1984) while turkeys are reported to have a total of 5.2 mg bilirubin / dL bile (Himes & Cornelius 1975). These differences are not just avian phenomena. Most fish have serum and bile that is yellow, and excrete bilirubin in a manner similar to mammals. Other species have blue-green serum due to the presence of biliverdin. In many fishes including cod and atlantic salmon, the bile colour changes from yellow to green during starvation (Talbot, 1982). Is this change due to a down regulation or inactivation of the BVR-A? Makos & Youson, (1988) demonstrated that the serum of sea lampreys has elevated levels of bilirubin late in the life cycle, when biliary atresia occurs and concluded that over the course of the lamprey life cycle different avenues of bile pigment storage and elimination were utilized. Noonan *et al.*, (1979) reported unconjugated hyperbilirubinemia in all species of normal indigo snakes. The plasma clearance of large organic anions like bilirubin was markedly delayed when compared to other snake species.

What is the source of bilirubin in these species? If putative biliverdin reductases could be identified, their amplification and cloning into expression vectors, and subsequent purification would allow a phylogenetic study of biliverdin reductase function in much greater detail.

With an unprecedented degree of genetic information available from genome and EST databases, it was felt that some answers as to why biliverdin-IXα reductase is absent in some species might be provided and it may shed some light in establishing why the evolutionary progression of haem degradation within different species developed as it did. It may be true that biliverdin is the major end product of haem degradation in many organisms, but this may not necessarily imply that biliverdin reductase is without activity or function in many of these organisms.

During the course of this study, it was decided to revisit some of the species reputed not to have biliverdin reductase activity, and perform an extensive search of all available EST and genomic databases in an attempt to identify nucleotide sequences displaying a high degree of similarity to the mammalian and cyanobacterial enzymes.

As described in the introduction another objective of this work was to clone and express the murine biliverdin IXα reductase enzyme. Currently attempts are being made to construct both conditional and complete BVR-A knockout mice. The murine biliverdin reductase however has never been studied. Clearly, this enzyme needs to be characterised as a prelude to the knock out work, and would not only provide the necessary assay conditions for all activity measurements, but would also facilitate immunisation of rabbits with the recombinant enzyme, allowing polyclonal antibody production.

3.2 'In silico' sequence analysis, and the identification of putative biliverdin reductases from various species.

The Basic Local Alignment Search Tool (BLAST) provided by the 'National Centre for Biotechnology Information' (NCBI available at http://www.ncbi.nlm.nih.gov/) finds regions of local similarity between sequences. This program was used to compare BVR-A nucleotide and protein sequences to those in databases and to retrieve statistically significant matches.

In an attempt to identify nucleotide sequences displaying a high degree of similarity to known biliverdin reductases, the Expressed Sequence Tags (EST), and High-Throughput Genome Sequences (HTGS) data of the GenBank sequence database was queried using the nucleotide and protein sequences of the human, rat and *Synechocystis* enzymes. Positive results from these searches were subsequently re-submitted and further analysed. This provided a more in-depth data set of related proteins of the mammalian enzymes. All blast hit sequences were aligned using the Clustalw tool available on the European Bioinformatics Institute (EBI) website (http://www.ebi.ac.uk/clustalw/index.html#). Phylograms were constructed using the Treeview application (Page 1996) which is available online at http://taxonomy.zoology.gla.ac.uk/rod/treeview.html. From Figures 3.1(a) and 3.1(b) it is clear that there are two distinct groups with a gene and/or EST evidence for the presence of biliverdin reductase. The first are the archaic cyanobacteria with *Anabaena variabilis* ATCC 29413, *Trichodesium erythraeum* IMS101, Crocosphaera watsonii WH 8501, Gloebacter violaceus PCC 7421 and 2 species of Nostoc (*Nostoc punctiforme* PCC 73120 and *Nostoc sp.* PCC 7120) all sharing a high degree of sequence identity with the characterised *Synechocystis* BVR-A enzyme (alignment scores are

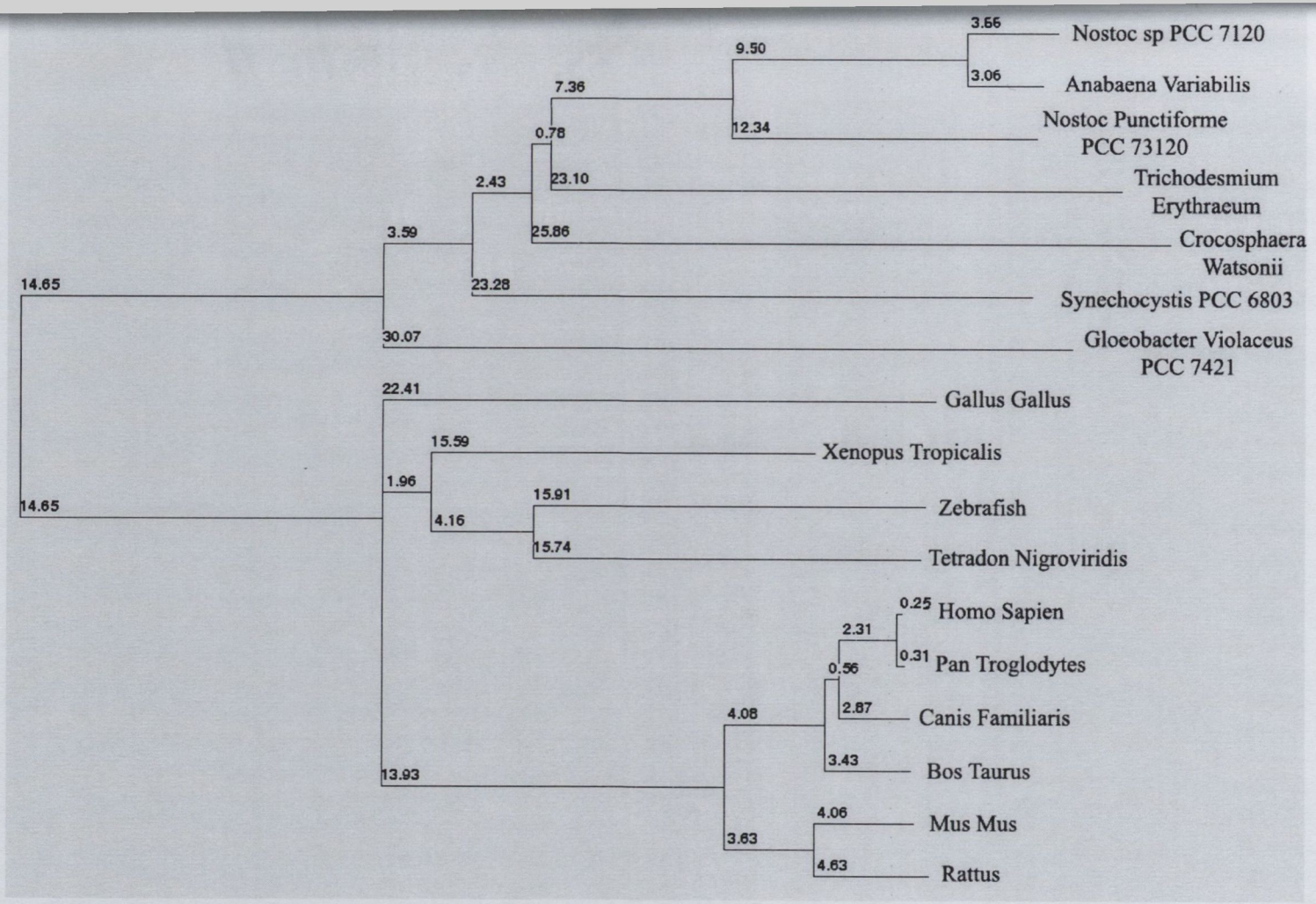

Figure 3.1 (a) **The evolutionary divergence of biliverdin-IXα reductase.**

Results of the biliverdin-IXα reductase blast analysis (Section 3.2) were used to construct this unrooted phylogenetic tree using the 'Treeview' application. Branch distances are highlighted.

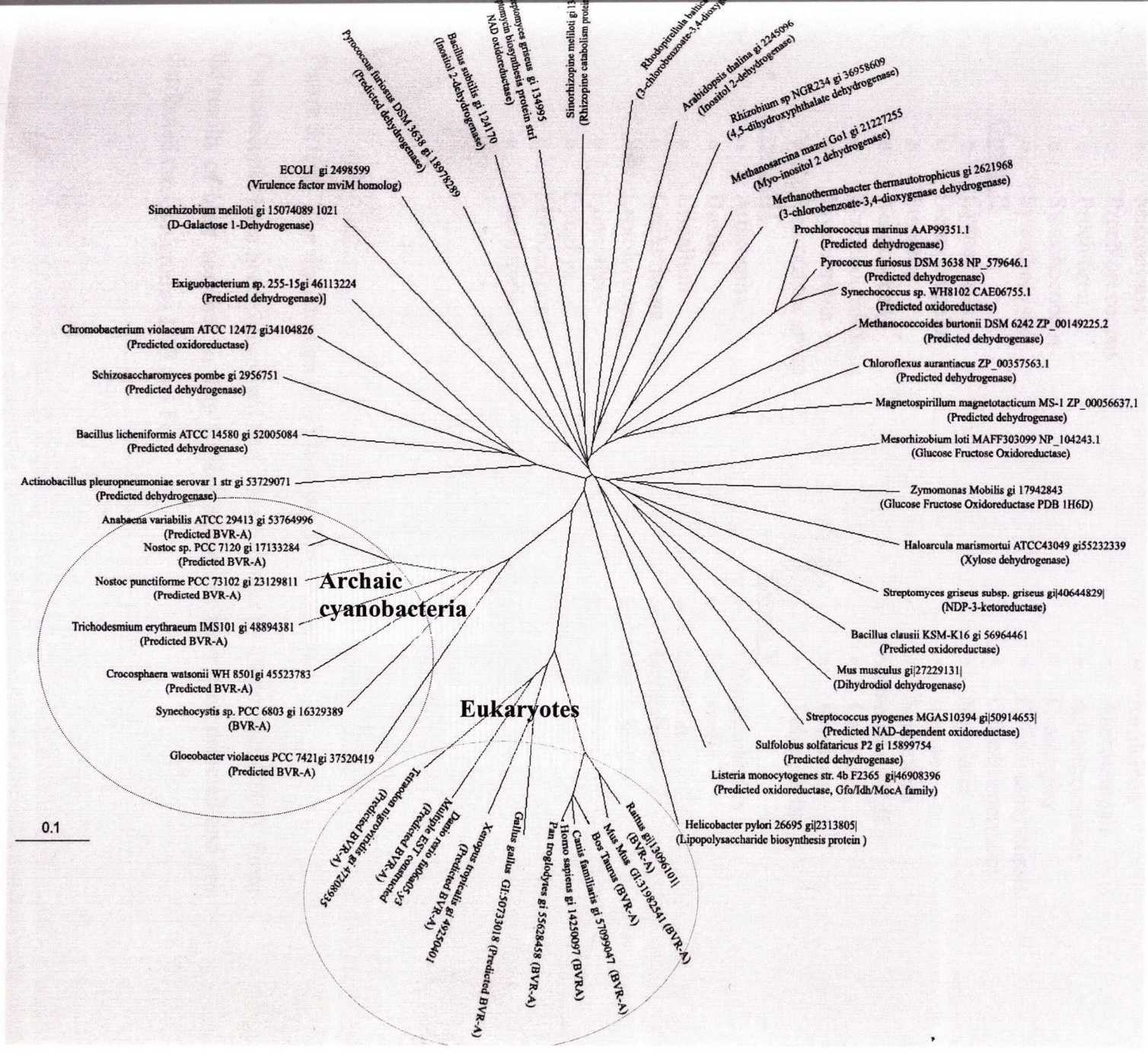

Figure 3.1 (b)

An unrooted tree constructed with proteins displaying sequence similarity to the mammalian and synecochystis biliverdin reductases.

The emergence of two main groups, the archaic cyanobacteria, and those of the eukaryotic enzymes are evident. No other procaryotic organisms showing homology to biliverdin reductase were identified.

Cyanobacteria

- **Group I**
  - Chamaesiphon
  - Chroococcus
  - Cyanobacterium
  - Cyanobium
  - Cyanothece
  - Dactylococcopsis
  - **Gloeobacter**
  - Gloeocapsa
  - Gloeothece
  - Microcystis
  - Prochlorococcus
  - Prochloron
  - Synechococcus
  - **Synechocystis**
- **Group II**
  - Cyanocystis
  - Dermocarpella
  - Stanieria
  - Xenococcus
  - Chroococcidiopsis
  - Myxosarcina
  - Pleurocapsa group
- **Group III**
  - Arthrospira
  - Borzia
  - Crinalium
  - Geitlerinema
  - Leptolyngbya
  - Limnothrix
  - Lyngbya
  - Microcoleus
  - Oscillatoria
  - Planktothrix
  - Prochlorothrix
  - Pseudanabaena
  - Spirulina
  - Starria
  - Symploca
  - **Trichodesmium**
  - Tychonema
- **Group IV**
  - **Subsection IV.I**
    - **Anabaena**
    - Anabaenopsis
    - Aphanizomenon
    - Cyanospira
    - Cylindrospermopsis
    - Cylindrospermum
    - Nodularia
    - **Nostoc**
    - Scytonema
  - **Subsection IV.II**
    - Calothrix
    - Rivularia
    - Tolypothrix
- **Group V**
  - Chlorogloeopsis
  - Fischerella
  - Geitleria
  - Iyengariella
  - Nostochopsis
  - Stigonema

Figure 3.1(c) The distribution of BVR-A in *Cyanobacteria*.

Cyanobacteria have been categorised into 5 main groups by Castenholz (2001). From the results of blast searches to date BVR-A sequences have been detected and are distributed through groups I, III and IV.

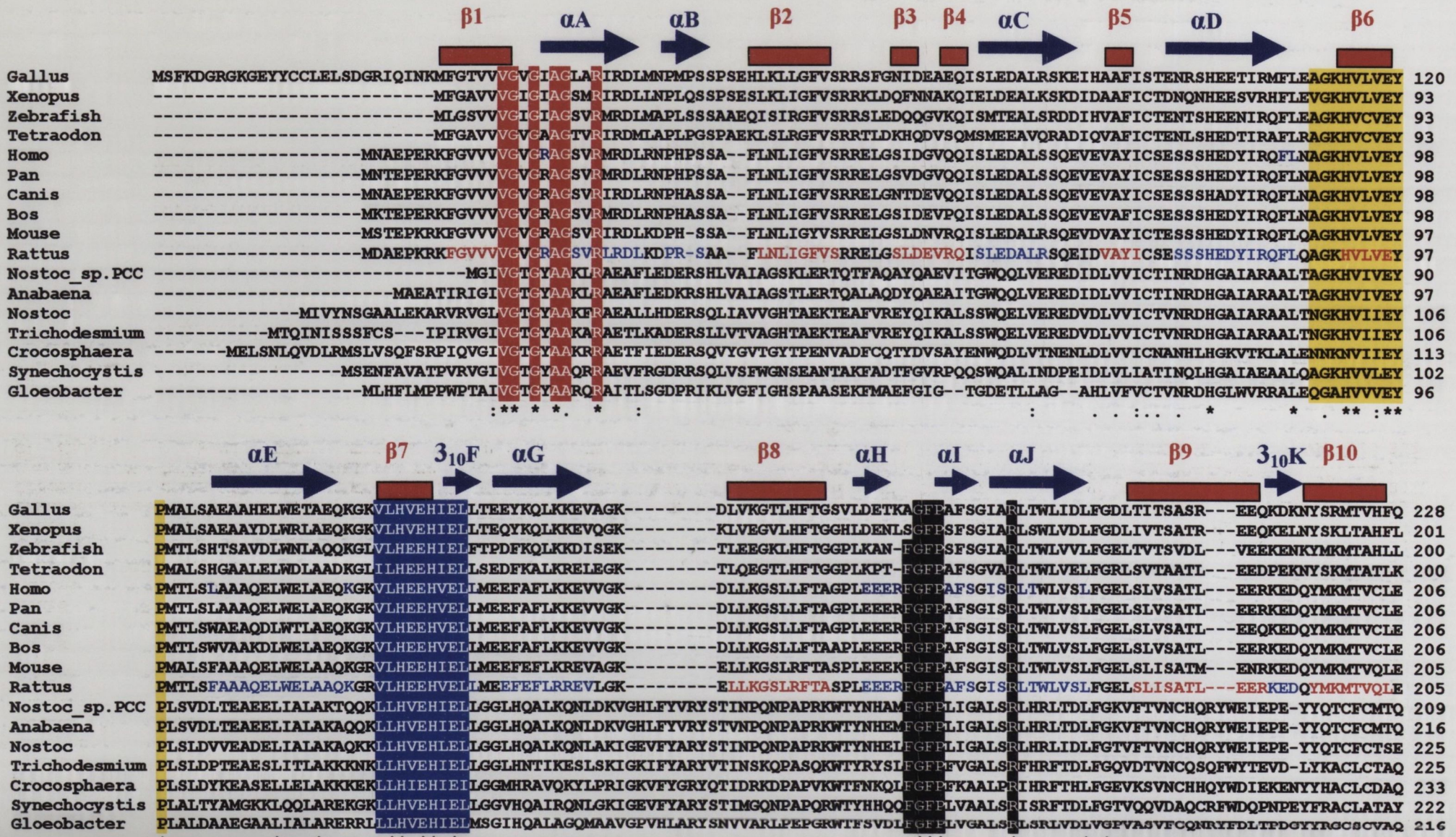
β1 αA αB β2 β3 β4 αC β5 αD β6
Gallus MSFKDGRGKGEYYCCLELSDGRIQINKMFGTVVGVGIAGLARIRDLMNPMPSSPSEHLKLLGFVSRRSFGNIDEAEQISLEDALRSKEIHAAFISTENRSHEETIRMFLEAGKHVLVEY 120
Xenopus MFGAVVVGIGIAGSMRIRDLLNPLQSSPSESLKLIGFVSRRKLDQFNNAKQIELDEALKSKDIDAAFICTDNQNHEESVRHFLEVGKHVLVEY 93
Zebrafish MLGSVVVGIGIAGSVRMRDLMAPLSSSAAEQISIRGFVSRRSLEDQQGVKQISMTEALSRDDIHVAFICTENTSHEENIRQFLEAGKHVCVEY 93
Tetraodon MFGAVVVGVGAAGTVRIRDMLAPLPGSPAEKLSLRGFVSRRTLDKHQDVSQMSMEEAVQRADIQVAFICTENLSHEDTIRAFLRAGKHVCVEY 93
Homo MNAEPERKFGVVVVGVGRAGSVRMRDLRNPHPSSA--FLNLIGFVSRRELGSIDGVQQISLEDALSSQEVEVAYICSESSSHEDYIRQFLNAGKHVLVEY 98
Pan MNTEPERKFGVVVVGVGRAGSVRMRDLRNPHPSSA--FLNLIGFVSRRELGSVDGVQQISLEDALSSQEVEVAYICSESSSHEDYIRQFLNAGKHVLVEY 98
Canis MNAEPERKFGVVVVGVGRAGSVRIRDLRNPHASSA--FLNLIGFVSRRELGNTDEVQQISLEDALSSQEVEVAYICSESSSHADYIRQFLNAGKHVLVEY 98
Bos MKTEPERKFGVVVVGVGRAGSVRMRDLRNPHASSA--FLNLIGFVSRRELGSIDEVPQISLEDALSSQEVEVAFICSESSSHEDYIRQFLNAGKHVLVEY 98
Mouse MSTEPKRKFGVVVVGVGRAGSVRIRDLKDPH-SSA--FLNLIGYVSRRELGSLDNVRQISLEDALRSQEVDVAYICTESSSHEDYIRQFLQAGKHVLVEY 97
Rattus MDAEPKRKFGVVVVGVGRAGSVRLRDLKDPR-SAA--FLNLIGFVSRRELGSLDEVRQISLEDALRSQEIDVAYICSESSSHEDYIRQFLQAGKHVLVEY 97
Nostoc_sp.PCC MGIVGTGYAAKLRAEAFLEDERSHLVAIAGSKLERTQTFAQAYQAEVITGWQQLVEREDIDLVVICTINRDHGAIARAALTAGKHVIVEY 90
Anabaena MAEATIRIGIVGTGYAAKLRAEAFLEDKRSHLVAIAGSTLERTQALAQDYQAEAITGWQQLVEREDIDLVVICTINRDHGAIARAALTAGKHVIVEY 97
Nostoc MIVYNSGAALEKARVRVGLVGTGYAAKFRAEALLHDERSQLIAVVGHTAEKTEAFVREYQIKALSSWQELVEREDVDLVVICTVNRDHGAIARAALTNGKHVIIEY 106
Trichodesmium MTQINISSSFCS---IPIRVGIVGTGYAAKARAETLKADERSLLVTVAGHTAEKTEAFVREYQIKALSSWQELVEREDVDLVVICTVNRDHGAIARAALTNGKHVIIEY 106
Crocosphaera MELSNLQVDLRMSLVSQFSRPIQVGIVGTGYAAKRRAETFIEDERSQVYGVTGYTPENVADFCQTYDVSAYENWQDLVTNENLDLVVICNANHLHGKVTKLALENNKNVIIEY 113
Synechocystis MSENFAVATPVRVGIVGTGYAAQRRAEVFRGDRRSQLVSFWGNSEANTAKFADTFGVRPQQSWQALINDPEIDLVLIATINQLHGAIAEAALQAGKHVVLEY 102
Gloeobacter MLHFLMPPWPTAIVGTGYAARQRAITLSGDPRIKLVGFIGHSPAASEKFMAEFGIG--TGDETLLAG--AHLVFVCTVNRDHGLWVRRALEQGAHVVVEY 96
αE β7 3₁₀F αG β8 αH αI αJ β9 3₁₀K β10
Gallus PMALSAEAAHELWETAEQKGKVLHVEHIELLTEEYKQLKKEVAGK---------DLVKGTLHFTGSVLDETKAGFPAFSGIARLTWLIDLFGDLTITSASR---EEQKDKNYSRMTVHFQ 228
Xenopus PMALSAEAAYDLWRLAEQKGKVLHVEHIELLTEQYKQLKKEVQGK---------KLVEGVLHFTGGHLDENLSGFPSFSGIARLSWLVDLFGDLIVTSATR---EEQKELNYSKLTAHFL 201
Zebrafish PMTLSHTSAVDLWNLAQQKGLVLHEEHIELFTPDFKQLKKDISEK---------TLEEGKLHFTGGPLKAN-FGFPSFSGIARLTWLVVLFGELTVTSVDL---VEEKENKYMKMTAHLL 200
Tetraodon PMALSHGAALELWDLAADKGLILHEEHIELLSEDFKALKRELEGK---------TLQEGTLHFTGGPLKPT-FGFPAFSGVARLTWLVELFGRLSVTAATL---EEDPEKNYSKMTATLK 200
Homo PMTLSLAAAQELWELAEQKGKVLHEEHVELLMEEFAFLKKEVVGK---------DLLKGSLLFTAGPLEEERFGFPAFSGISRLTWLVSLFGELSLVSATL---EERKEDQYMKMTVCLE 206
Pan PMTLSLAAAQELWELAEQKGKVLHEEHVELLMEEFAFLKKEVVGK---------DLLKGSLLFTAGPLEEERFGFPAFSGISRLTWLVSLFGELSLVSATL---EERKEDQYMKMTVCLE 206
Canis PMTLSWAEAQDLWTLAEQKGKVLHEEHVELLMEEFAFLKKEVVGK---------DLLKGSLLFTAGPLEEERFGFPAFSGISRLTWLVSLFGELSLVSATL---EEQKEDQYMKMTVCLE 206
Bos PMTLSWVAAKDLWELAEQKGKVLHEEHVELLMEEFAFLKKEVVGK---------DLLKGSLLFTAAPLEEERFGFPAFSGISRLTWLVSLFGELSLVSATL---EERKEDQYMKMTVCLE 206
Mouse PMALSFAAAQELWELAAQKGRVLHEEHIELLMEEFEFLKREVAGK---------ELLKGSLRFTASPLEEEKFGFPAFSGISRLTWLVSLFGELSLISATM---ENRKEDQYMKMTVQLE 205
Rattus PMTLSFAAAQELWELAAQKGRVLHEEHVELLMEEFEFLRREVLGK---------ELLKGSLRFTASPLEEERFGFPAFSGISRLTWLVSLFGELSLISATL---EERKEDQYMKMTVQLE 205
Nostoc_sp.PCC PLSVDLTEAEELIALAKTQQKLLHVEHIELLGGLHQALKQNLDKVGHLFYVRYSTINPQNPAPRKWTYNHAMFGFPLIGALSRLHRLTDLFGKVFTVNCHQRYWEIEPE-YYQTCFCMTQ 209
Anabaena PLSVDLTEAEELIALAKAQQKLLHVEHIELLGGLHQALKQNLDKVGHLFYVRYSTVNPQNPAPRKWTYNHEMFGFPLIGALSRLHRLTDLFGKVFTVNCHQRYWEIEPE-YYQTCFCMTQ 216
Nostoc PLSLDVVEADELIALAKAQKKLLHVEHLELLGGLHQALKQNLAKIGEVFYARYSTINPQNPAPRKWTYNHELFGFPLIGALSRLHRLIDLFGTVFTVNCHQRYWEIEPE-YYQTCFCTSE 225
Trichodesmium PLSLDPTEAESLITLAKKKNKLLHVEHIELLGGLHNTIKESLSKIGKIFYARYVTINSKQPASQKWTYRYSLFGFPFVGALSRFHRFTDLFGQVDTVNCQSQFWYTEVD-LYKACLCTAQ 225
Crocosphaera PLSLDYKEASELLELAKKKEKLLHIEHIEILGGMHRAVQKYLPRIGKVFYGRYQTIDRKDPAPVKWTFNKQLFGFPFKAALPRIHRFTHLFGEVKSVNCHHQYWDIEKENYYHACLCDAQ 233
Synechocystis PLALTYAMGKKLQQLAREKGKLLHVEHIELLGGVHQAIRQNLGKIGEVFYARYSTIMGQNPAPQRWTYHHQQFGFPLVAALSRISRFTDLFGTVQQVDAQCRFWDQPNPEYFRACLATAY 222
Gloeobacter PLALDAAEGAALIALARERRILLHVEHIELMSGIHQALAGQMAAVGPVHLARYSNVVARLPEPGRWTFSVDLFGFPLVGALSRLSRLVDLVGPVASVFCQNRYFDLTPDGYYRGCSCVAQ 216

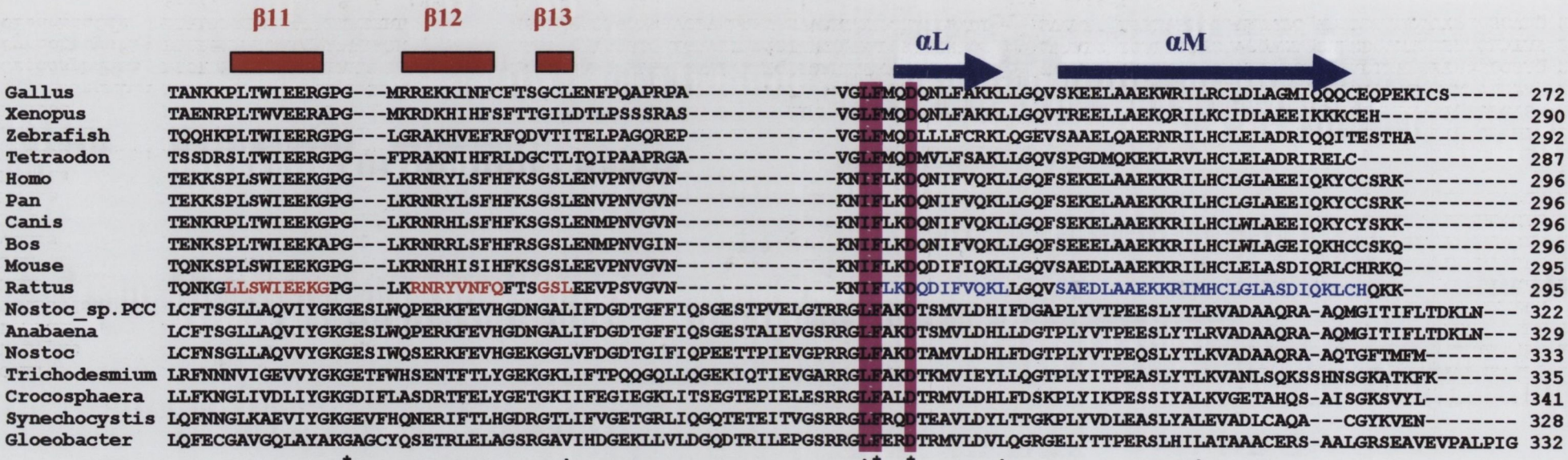

Figure 3.2 **Amino acid sequence alignments of rat human and *synechocystis PCC6803* biliverdin-IXα reductases, with the proposed enzymes of similar function.**

Clustalw alignment of all the BVR-A sequences identified through the blast searches described in Section 3.2. Structural features of rat BVR-A (from the crystal structure reported by Kikuchi *et al.*, 2001) are also shown above the alignments. A set of 5 highly conserved motifs have been colour coded red yellow blue grey and purple for clarity. Shaded columns represent the most conserved regions.

presented in Appendix III Figure I). To date BVR-A like sequences have been identified in 3 members of the 5 cyanobacterial groups classified by Castenholz (2001) detailed in Figure 3.1(c). Schluchter & Glazer (1997) found that the conversion of biliverdin to bilirubin was important for normal phycobiliprotein biosynthesis. BVR-A could well serve similar functions across all the cyanobacterial groups mentioned. Figures 3.1(a) and (b) also show that there is a wide distribution of BVR-A encoding sequences among eukaryotes also. The most interesting observations to be made here are regarding biliverdin reductase like sequences in the chicken (*Gallus gallus*) and the frog (*Xenopus tropicalis*), which are reputed not to have a biliverdin-IXα reductase.

3.3 Amplification of *Xenopus tropicalis* BVR-A sequence

The putative *Xenopus tropicalis* biliverdin-IXα reductase was amplified from the I.M.A.G.E cDNA clone (IMAGE:5308696) which was acquired from UK HGMP-RC, Hinxton, Cambridge CB10 1SB, UK, one of the appointed distributers of I.M.A.G.E. clones (http://image.llnl.gov/image/html/idistributors.shtml). This cDNA clone, the nucleotide sequence of which is shown in Figure 3.3, was prepared from RNA extracted from embryo of *Silurana tropicalis*, gastrula (stages 10-13). Other full length BVR-A like sequences from *Xenopus tropicalis* for example TEgg035m18 (Accession Number: CR761396), have been prepared from mRNA of *Xenopus* eggs, which suggests that BVR-A may be expressed through various stages of *Xenopus* development.

Using the primers outlined in Table 3.1(a), a series of amplification reactions were performed to establish suitable PCR conditions for the amplification of *Xenopus* BVR-A cDNA. Since Pfu has proofreading (3'-5' exonuclease activity) which allows the polymerase to remove mispaired bases and make perfectly blunt ends (Cline *et al.*, 1996), it was the polymerase of choice for all amplification purposes described herein. The components of the successful PCR reactions used to amplify the *Xenopus* cDNA are presented in Table 3.1(b). A cDNA product of the expected size (~882 base pairs) was amplified from the *Xenopus* cDNA clone (IMAGE:5308696) the results of which are presented in Figure 3.4(a).

```
1    gagcttccac acgctgacac aggcttgtgc agaaagggtt cagcgacccc ctcccctggt
61   gcctctgctg tatcctgccc tatacagaaa cgctatcttc agaggataat aaaatgtttg
121  gcgcagtagt ggtgggaatt ggcattgctg gctctatgag aattcgggac ctcctcaacc
181  cattgcagtc cagcccctca gagagtctga aacttattgg ctttgtatca aggagaaaac
241  ttgaccagtt taataatgca aagcaaattg agctggatga agcactgaaa agtaaagata
301  ttgatgctgc ttttatttgt acagataatc agaaccacga agaaagtgtc aggcatttcc
361  tagaggttgg taaacatgtc ctggtggagt accctatggc gttgtcagca gaagcagcat
421  atgatttatg gagacttgct gagcagaaag gaaaagtcct gcacgtggaa cacatagagc
481  tgcttacaga gcaatacaag caactgaaga aggaagtaca gggcaaaaag cttgtggaag
541  gggtgttgca ttttactgga gggcatctag atgagaacct ttctggattc ccatctttta
601  gtggcattgc tcgactgagc tggcttgttg atctgtttgg tgatctaatc gtcacctcag
661  ccacaagaga ggagcaaaaa gaactgaact actccaaact tacagcacat ttcctgactg
721  ctgaaaacag gccgctgacc tgggttgaag aaagggcacc aggcatgaaa cgggataagc
781  atatccactt ctctttcacg acgggcattc tggacacatt gccttcatcc agcagggcat
841  cagttgggct ttttatgcaa gatcaaaact tatttgcaaa gaaactccta gggcaagtaa
901  ccagggagga gctgctagca gagaagcaac gaatcttaaa atgcattgac cttgctgaag
961  agatcaaaaa gaaatgtgag cattaatgtg ttaatacagt acaaagggtg gtactgtgta
1021 aagtggatct gtgaactaag catttcctca cttttaagta tataataatt tcaaatagtg
1081 gcagtgtttt ttacatagaa ctctaaaaga tgagcggtaa ctgcattttc tttgaaagta
1141 actactgttt tccagcgaaa gtggatcacg tttttaaaac aagatttgaa acaagatata
1201 ttatgttaca cataaaagtt taacatttta aagcgttggt aaacttgttt gctgagctgc
1261 aactgggaaa catgagaaag agaaaagaaa tcctattcat ttttatactg ttagaaaact
1321 agtgacaata ataagaatag aaagcaattt tcaaaaaatt gttatttgtg ggagcccgca
1381 gttaaatctt ccctaaaaaa tcctcagaaa aagaccacaa gtaaaaccta ttacatcagg
1441 cagtctggct taacagcagg gaaatgtgaa ggatgacctt tttttccttg gttaagtcag
1501 attgctgtaa taggttttgc atcagacaat cttaaagggc acctatcacc ctgaaattgc
1561 ttccccctcc aggtgcagaa aaaagaaaaa aaaaaaaaaa
```

Figure 3.3 Sequence analysis of the putative *Xenopus tropicalis* biliverdin-IXα reductase

The sequence of the IMAGE clone (Accession No: IMAGE:5308696 MGC:69310), which is a full length cDNA generated from gastrula stages 10-13 of the *Xenopus tropicalis (Silurana tropicalis)* embryo. The full length *Xenopus BVR-A* protein aligned in Figure 3.2 is the protein product of this cDNA.

Expression Vector	Primer Name	Direction	Sequence
pGEX-KG	Xenopus For BamHI	Forward	GGATGGATCCATGTTTGGCGCAGTAGT
pGEX-KG(NcoI & XhoI)	XenoNcoIXhoIRev	Reverse	CCTCGAGCCATGGTTAATGCTCACATTTC

(a)

Nuclease free water	39µl
10X pfu reaction buffer	5µl
Forward primer (XenopusBamHIFor 10pmol/µl)	1µl
Reverse primer (XenopusNcoIXhoIRev 10pmol/µl)	1µl
dNTPs (10mM each nucleotide)	2µl
Xenopus BVRA pCMV-Sport 6.1 (20ng~1/700 dilution of stock)	1µl
Pfu DNA polymerase	1µl

(b)

Step Number	Temperature	Time
1	95°C	1 minute
2	95°C	1 minute
3	62°C	1 minute
4	68°C	1.5 minutes
5	Go to step 2	28 more times
6	68°C	5 minutes
7	4°C	Hold

(c)

Table 3.1 The PCR components and cycling parameters used to amplify the putative *Xenopus* BVR-A cDNA.

(a) The primers used to amplify target cDNA. Primers were designed from the cDNA sequence presented in Figure 3.3.

(b) The components of the PCR reaction mixture.

(c) The cycling parameters used with the successful amplification of the *Xenopus* BVR-A cDNA.

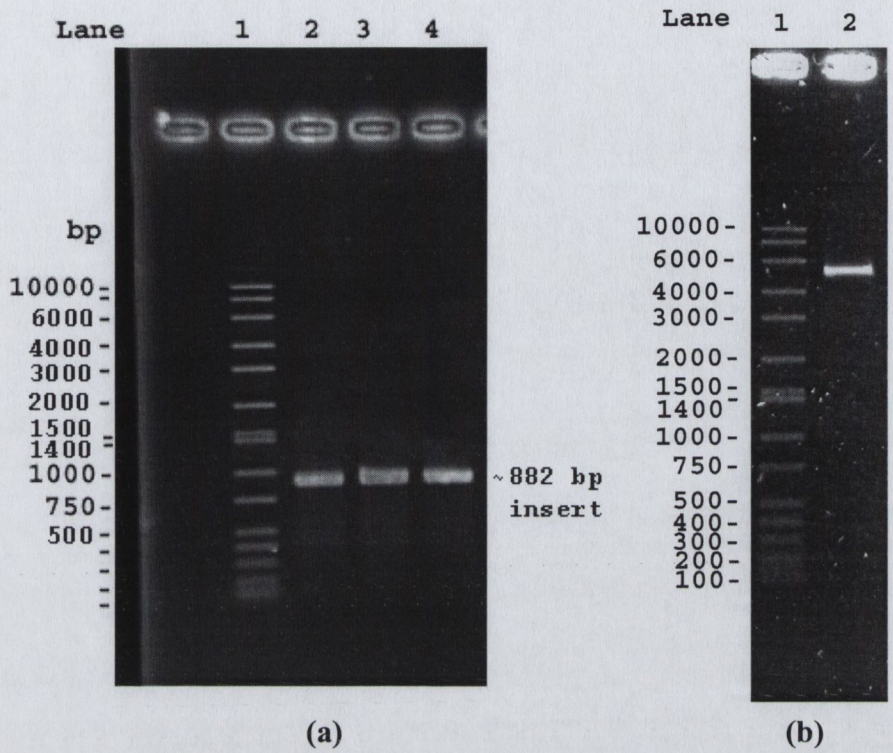

(a) (b)

Figure 3.4 (a) **Amplification of the putative biliverdin-IXα reductase from *Xenopus tropicalis*.**

Xenopus tropicalis cDNA from the IMAGE clone (IMAGE:5308696) was used as template for the amplification of the putative BVR-A insert. Lane 1 contains molecular weight markers from Sigma (D-7058). Lanes 2, 3 and 4 contain PCR products from the optimised amplification conditions detailed in Table 3.1.

Figure 3.4 (b) **Digestion of the pGEX-KG plasmid in preparation for insertion of the Xenopus BVR-A cDNA insert.**

Lane 1: Contains 5µl of sigma markers (D-7058). Lane 2: Contains a sample of the double digest of pGEX-KG (using BamHI and XhoI) which was purified using the QIAquick PCR purification kit (Section 2.2.8).

3.3.1 Digestion and ligation of *Xenopus* cDNA into pGEX-KG

The pGEX-KG plasmid (shown in Appendix II Figure 3) was transformed into *E.coli* XL1 Blue cells as described in Section 2.2.1. The pGEX-KG plasmid was subsequently purified (~100 μg) of from these cells using 'Qiagen Midi Kits' and the protocol detailed in Section 2.1.6. The purified pGEX-KG plasmid (1 μg) was then prepared for insertion of the amplified *Xenopus* cDNA by digestion with 20 units BamHI and XhoI using (1 x) 'Sure Cut Buffer B' (Roche) in a total volume of 50 μl. Restriction digests were incubated for 6 hours at 37°C. Following this 6 hour incubation, 2 units of bacterial alkaline phosphatase (Takara) was added to the plasmid digests and incubated between 60-65°C for 1 hour to remove the overhanging 5' phosphates. Purified and digested (BamHI and XhoI) pGEX-KG was analysed by electrophoresis in a 1% agarose gel (Figure 3.4b). The digested plasmid ran with the expected size ~5006 bp's and appeared to cut with 100% efficiency. The amplified *Xenopus* BVR-A cDNA insert was digested in a similar fashion except there was no treatment with bacterial alkaline phosphatase. Both plasmid and insert were purified using the procedure outlined in Section 2.1.8 prior to the ligation reaction.

The digested and purified insert was ligated into pGEX-KG plasmid using the Takara DNA Ligation Kit Version 2.1 (see Section 2.1.4). A series of ligation reactions containing various ratios of insert to vector in a total volume of 10 μl were set up. Vector to insert ratios used were 20 ng, 50 ng, 100 ng insert to 100 ng vector. Control ligations contained 100 ng insert DNA without vector DNA and 100 ng vector DNA without insert DNA. To each reaction 10 μl of the 'Takara Ligation Kit-Solution 2' was added, mixed and then incubated at 16°C overnight. As described in Section 2.2.1b, 200μl aliquots of competent XL1 Blue cells were transformed with the ligation mix, and plated onto ampicillin plates which were incubated overnight at 37°C.

3.3.2 Screening for the presence of *Xenopus* BVR-A insert in transformed cells.

The antibiotic resistant colonies from the transformation plates were streaked onto fresh ampicillin plates and incubated overnight at 37°C. A single colony of each population was used to inoculate individual 5 ml cultures containing the desired antibiotic, and these were grown for 16 hours at 37°C with shaking at 270rpm. DNA was isolated from these cultures

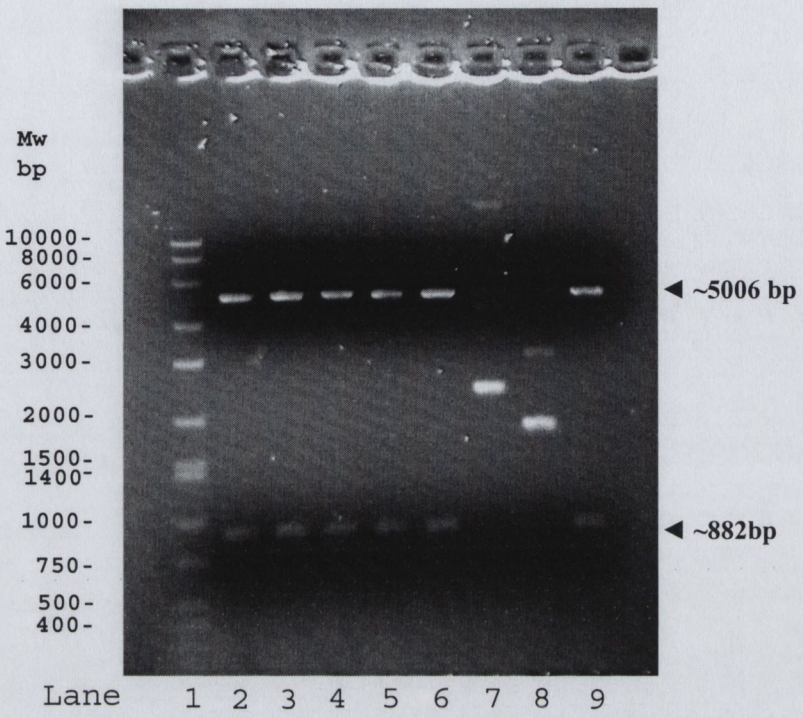

Figure 3.5 **Screening for the presence of putative *Xenopus* BVR-A insert in transformed cells.**

Plasmid purified from single colonies from successful ligation plates were screened for the presence of a *Xenopus* cDNA insert through restriction digest analysis as described in Section 3.3.2. Lane 1: Sigma (D-7058) molecular weight markers. Lanes 2-9: Double digests of clones using restriction enzymes BamHI and XhoI. Successful clones resulted in a ~882bp insert being cut from the construct leaving linearised pGEX-KG (5006bp).

as described in Section 2.1.7 using the Wizard Plus SV Miniprep DNA purification system. Each clone was screened for the presence of a *Xenopus* cDNA insert through restriction digest analysis using BamHI and XhoI. DNA (500 ng) was digested in a final volume of 50 µl using (1X) 'Sure Cut Buffer B' (Roche). The results of this screening are shown in Figure 3.5. A large number of successful transformants were obtained. Clearly lanes 2-6 and 9 all contained the putative *Xenopus* BVR-A cDNA inserts (882bp). Transformants (shown in lanes 2-6 and lane 9) were replated and later analysed for protein expression.

3.4 Amplification of the *Danio rerio* (zebrafish) BVR-A sequence

The putative zebrafish biliverdin-IXα reductase was amplified from the I.M.A.G.E cDNA clone (IMAGE:5304464) which was acquired from RZPD Deutsches Ressourcentrum, Heubnerweg 6, D-14059 Berlin. The cDNA for this clone was made from mRNA purified from whole ovaries collected from zebrafish and had an average insert size 2 kb.

The culture slopes obtained from I.M.A.G.E. were re-streaked on agar plates containing 100 µg / ml ampicillin and grown overnight at 37°C. Individual colonies were used to inoculate 25 ml cultures as described in Section 2.1.6, from which plasmid was purified. As a range of insert sizes were reported by RZPD the insert size was determined by digestion of the pCMV-Sport6 plasmid containing the insert with NotI and SalI prior to use of the clone. This gave a band corresponding to ~1.6 kb and results of the RZPD sequencing revealed that the 5' sequence resembled that of a putative biliverdin reductase. This led to the conclusion that a full open reading frame for zebrafish BVR-A was contained within this clone. It was decided to use this as cDNA target to amplify the zebrafish cDNA and ligate it into an expression plasmid. Primers for the amplification of zebrafish cDNA were designed using the full length sequence presented in Figure 3.6.

Using the primers outlined in Table 3.2, a series of amplification reactions were performed to establish suitable PCR conditions for the zebrafish cDNA insert. The thermo cycling conditions and reaction components detailed in Table 3.2 (b) and (c) were used to amplify the zebrafish BVR-A cDNA of the expected size ~890 bp as shown in Figure 3.7. PCR products were cleaned and prepared for digestion with the 'QIAquick PCR Clean Up Kit' as described in Section 2.5.

```
   1 gcggttacga aaaaagagtt atgaaagtag tttcctgagt cacagttgat gaatgtcatt
  61 atcgttctca tttcgctgac gttgcgtaag aaaaccacat caaaggctgt gaggggacat
 121 tcacaggaat catgctggga tcagtggttg ttggaattgg aattgcagga tctgtgagga
 181 tgagagattt aatggctcct ctctcgtcca gcgccgcaga acagatcagc atcaggggct
 241 ttgtgtccag gaggagtctt gaagatcagc agggtgtgaa gcagatcagc atgactgaag
 301 cgctgagcag agacgacatc catgtggcat ttatatgcac agaaaacacc agccatgaag
 361 agaacatcag gcagtttctg gaggcaggaa agcatgtgtg tgtggagtat cccatgaccc
 421 tcagccacac ctctgctgtg gatctgtgga atctggctca acagaagggt ctggtgcttc
 481 atgaggaaca catcgagctg ttcactcctg acttcaaaca gctgaaaaaa gacatttctg
 541 aaaaaacact ggaggaagga aagctgcact tcaccggtgg tcctctaaag gcaaactttg
 601 gcttcccgtc tttcagtggt atcgccagac tgacgtggct ggtggttctg tttggagagc
 661 tcacagtcac ttcagtagat ctggtggagg agaaagagaa caagtacatg aagatgacgg
 721 cacacttact gactcaacag cacaagcctc tgacgtggat tgaagaacgg ggtccgggtc
 781 tgggcagagc caaacacgtg gagtttcgct ttcaggatgt gacgatcaca gagcttccag
 841 caggtcagcg tgagccggtc ggactcttca tgcaggatct gctgctgttc tgccggaagc
 901 tgcaggggga agtttcagct gcagagctcc aggcggagag aaacaggatc ttacactgtc
 961 tggagctagc agaccgcatt cagcagatca ccgaaagcac tcacgcctga acattaactc
1021 acactaccaa acattcattc taatgtggca cacacagact gtgtatagag acagataact
1081 gaagtgctaa gtcagattaa aatcattaaa
```

Figure 3.6 The full length sequence of a putative *Danio rerio* (zebrafish) biliverdin IXα reductase)

The sequence of a 1110 bp cDNA clone (XM_682507.1 GI:68356867) from *Danio rerio* made from whole ovaries collected from zebrafish aged 4-5 months, 1 and 2 years. This was used in the amplification of the Zebrafish BVR-A. This sequence displays similarity to 5 other zebrafish EST's.

Expression Vector	Primer Name	Direction	Sequence
ppMAL and pET41aMod	Zebrafish For BamHI	Forward	CGCGGATCCATGCTGGGATCAGTGGTTG
ppMAL and pET41aMod	ZebrafishRevHindIII	Reverse	GTGTAAGCTTTCAGGCGTGAGTGC

(a)

Nuclease free water	39 µl
10X Pfu reaction buffer	5 µl
Forward primer (Zebrafish For BamHI 10pmol/µl)	1 µl
Reverse primer (ZebrafishRevHindIII 10pmol/µl)	1 µl
dNTPs (10mM each nucleotide)	2 µl
Xenopus BVRA pCMV-Sport 6.1 (10ng~1/800 dilution of stock)	1 µl
Pfu DNA polymerase	1 µl

(b)

Step Number	Temperature	Time
1	95 °C	1 minute
2	95 °C	1 minute
3	62 °C	1 minute
4	68 °C	1.5 minute
5	Go to step 2	28 more time
6	68 °C	5 minute
7	4 °C	Hold

(c)

Table 3.2 PCR components and cycling parameters used to amplify the putative *Danio rerio* BVR-A cDNA.

(a) The primers used to amplify target cDNA. Primers were designed from the cDNA sequence presented in Figure 3.6.

(b) The components of the PCR reaction mixture.

(c) The cycling parameters used with the successful amplification of the *Danio rerio* cDNA.

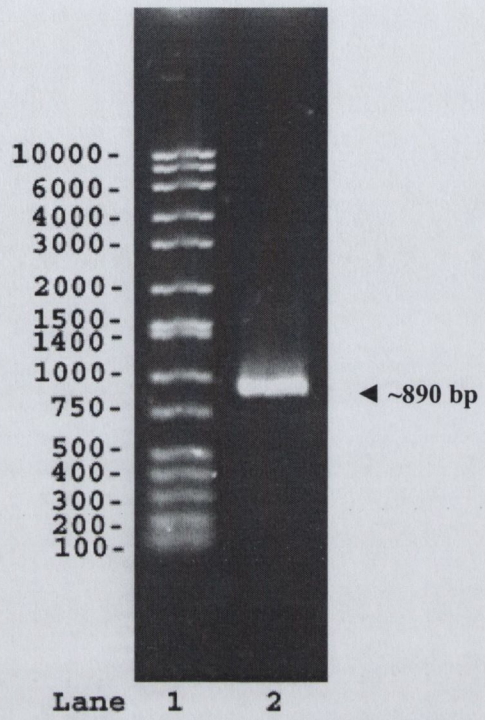

Figure 3.7 Amplification of the putative biliverdin IXα reductase from *Danio rerio* (Zebrafish).

Zebrafish BVR-A cDNA from the IMAGE clone (IMAGE: 5304464, Gen Bank Acc BI983742) was used as template for the amplification of the putative BVR-A insert as described in Section 3.4. Lane 1 contains molecular weight markers from Sigma (D-7058). Lane 2 contains 10 µl of the PCR product from the optimised amplification conditions described in Table 3.2.

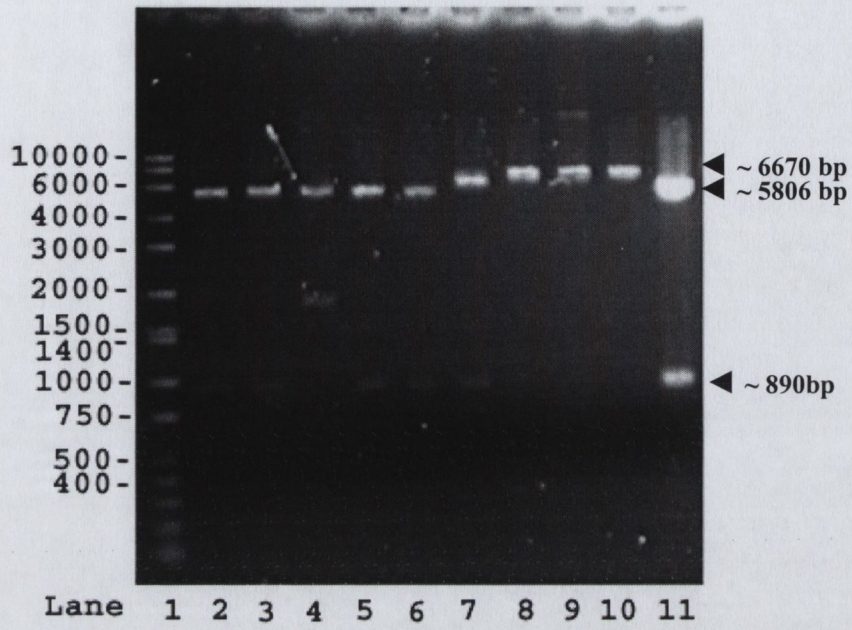

Figure 3.8 Screening transformants for correctly ligated *Danio rerio* BVR-A cDNA insert.

The amplified, digested and purified, *Danio rerio* BVR-A cDNA insert was ligated into ppMAL and transformed into competent XL1Blue *E.coli*. Plasmid was purified from the positive transformants and screened by restriction digest analysis using BamHI and HindIII as detailed in Section 3.4.2. Lane 1: Contains 5µl of Sigma markers (D-7058). Lanes 2 to 6 and 11 contain pET41aMod digests. Lanes 7 to 10 contain ppMAL digested plasmid. The appearance of a zebrafish insert of ~890bp indicates a clone containing zebrafish BVR-A.

3.4.1 Digestion and ligation of zebrafish cDNA into pET41a-Mod and pGEX-KG

The pET41a-Mod plasmid (Appendix II Figure 4), was transformed into *E.coli* XL1 Blue cells as described in Section 2.2.1b. From over night cultures of these cells 100 μg of plasmid was purified using the Qiagen Midi Kits detailed in Section 2.1.6.

Digestion was performed with 20units BamHI and HindIII using 1 X 'Sure Cut Buffer B' in a total volume of 50μl, containing 1 μg plasmid DNA. Restriction digests were incubated for 6 hours at 37°C. Following this 6 hour incubation, 2 units of bacterial alkaline phosphatase (Takara) was added to the plasmid digests and incubated between 60-65°C for 1 hour to remove the overhanging 5' phosphates. The amplified zebrafish BVR-A cDNA insert was digested in similar fashion but without BAP treatment.

Before continuing to the ligation steps, plasmid digests were checked for complete cutting by agarose gel electrophoresis. Digested products were cleaned and prepared for ligation with the 'Qiagen PCR Clean Up Kit as described in Section 2.5. The digested and purified inserts were ligated into ppMAL, and pET41a-Mod plasmids using the Takara DNA Ligation Kit Version 2.1. A series of ligation reactions similar to that previously described in the *Xenopus* cDNA ligation section, which contained an excess of insert in 10 μl were set up. To each reaction 10 μl of Takara ligation Kit solution 2 was added, mixed and then incubated at 16°C overnight. As described in Section 2.2.1b, 200 μl aliquots of competent XL1 Blue cells were transformed with the ligation mix and plated onto ampicillin (ppMAL ligations) and kanamycin (pET41aMod ligations) plates which were incubated overnight at 37°C.

3.4.2 Screening for the presence of zebrafish BVR-A insert in transformed cells.

The antibiotic resistant colonies from the transformation plates were streaked onto fresh ampicillin and kanamycin plates and were incubated overnight at 37 °C. A single colony of each population was used to inoculate individual 5 ml cultures containing the desired antibiotic, and these were grown for 16 hours at 37 °C with shaking at 270 rpm. DNA was isolated from these cultures as described in Section 2.1.7 using the Wizard Plus SV

Miniprep DNA purification system. Each clone was screened for the presence of zebrafish cDNA insert with a restriction digest using BamHI and Hind III. Plasmids (500 ng) were digested in a final volume of 50 µl using '1X Sure Cut buffer B' (Roche). The results of this screening are shown in Figure 3.8. Ligation into the pET41a-Mod vector was very successful with 6 out of 7 transformants having the zebrafish cDNA insert of ~890 bp (Lanes 2, 3, 5, 6 and 11). Of the ppMAL-zebrafish cDNA ligations the excision of insert is seen in lane 7 (Figure 3.8).

3.5 Identification and cloning of the putative murine biliverdin- IXα reductases

3.5.1 The Isolation of RNA from murine tissues.

As described in Section 2.1.10a, a Balb/c strain mouse was sacrificed, and RNA isolated using Trizol Reagent™. The air dried pellet was resuspended in 100 µl RNase free water and heated to 60°C for 10 minutes to fully dissolve the RNA. First strand cDNA synthesis was performed using the Invitrogen SuperScript™ III Reverse Transcriptase Kit. The specific primer used in the amplification was TGAAGCTTCCTCCTCACTGCTTCCGG. Components of the reaction consisted of 2pmol/µl stock gene specific primer (1 µl), total RNA (1 µg) and 10 mM dNTP mix (1 µl).

The volume was then adjusted to 14 µl with sterile distilled water. The mixture was heated to 65°C for 5 minutes followed by incubation on ice for 1 minute. The mixture was centrifuged briefly to collect the material, and to it (4 µl) 5X Strand Buffer, 0.1M DTT (1 µl) and SuperScript™ III RT (200 units/µl) 1 µl were added and mixed by pipetting up and down. The mixture was incubated for 1 hour at 55°C. This cDNA synthesis step was followed by heat inactivation of the reverse transcriptase at 70°C for 15 minutes. To remove template RNA, 1 µl of 'Qiagen RNase A' (7 units/µl) was added, mixed and incubated for 10 minutes at room temperature. A 'Qiaquick' PCR purification kit was then used to purify the newly synthesised cDNA as described in Section 2.1.8. The cDNA was eluted from the 'Qiaquick' spin column with 32 µl of nuclease free water.

3.5.2 Amplification of murine BVR-A c-DNA

The putative murine biliverdin-IXα reductase was amplified from the first strand cDNA synthesis product described in Section 3.5.1. The thermo cycling conditions outlined in Table 3.3 were used to amplify murine BVR-A cDNA insert of the expected size 910 base pairs as shown in Figure 3.9. PCR products were cleaned and prepared for digestion with the 'QIAquick PCR clean up kit' as described in Section 2.1.8.

3.5.3 Digestion and ligation of Murine cDNA into ppMAL and pGEX-KG

The ppMAL plasmid (Appendix II, Figure 1), was transformed into *E.coli* XL1 Blue cells as described in Section 2.2.1, from which the plasmid was purified using the Qiagen Midi Kits detailed in Section 2.1.6. The amplified mouse BVR-A cDNA was digested at both ends using XbaI and HindIII in 'sure cut buffer B' (Roche). The ppMAL plasmid was digested with 20 units XbaI and HindIII using 1 X 'buffer B' in a total volume of 50 µl, containing 1 µg plasmid DNA. The digest was incubated for 6 hours at 37°C. Following this 6 hour incubation, 2 units of bacterial alkaline phosphatase (Takara) was added to the plasmid digests and incubated between 60-65°C for 1 hour. The digests were cleaned and prepared for ligation with the 'Qiagen PCR clean up kit' as described in Section 2.1.8.

The digested ppMAL and amplified murine BVR-A cDNA were ligated using the Takara DNA Ligation Kit Version 2.1. A series of ligation reactions containing a molar excess of insert contained in 10 µl was set up. These reactions contained 100 ng vector with incremental insert concentrations from 20 ng to 100 ng. To each reaction 10 µl of 'Takara ligation kit solution 2' was added, mixed and then incubated at 16°C overnight. As described in Section 2.2.1, aliquots (200 µl) of competent XL1 Blue cells were transformed with the ligation mix and plated onto ampicillin plates which were incubated overnight at 37 °C.

3.5.4 Screening for the presence of murine BVR-A insert in transformed cells.

The antibiotic resistant colonies from the transformation plates were streaked onto fresh ampicillin plates and incubated overnight at 37 °C. A single colony of each population was

Expression Vector	Primer Name	Direction	Sequence
ppMAL	MusFXbaI	Forward	CCTCTAGAATGAGTACTGAGCCAA
ppMAL	MusRHindIII	Reverse	CCAAGCTTCCTCCTCACTGCTTCC

(a)

Nuclease free water	39 µl
10X pfu reaction buffer	5 µl
Forward primer (MusFXbaI 10pmol/µl)	1 µl
Reverse primer (MusRHindIII 10pmol/µl)	1 µl
dNTPs (10mM each nucleotide)	2 µl
Murine BVRA cDNA from RTPCR	1 µl
Pfu DNA polymerase	1 µl

(b)

Step Number	Temperature	Time
1	95 °C	1 minute
2	95 °C	1 minute
3	60 °C	1 minute
4	68 °C	1.5 minutes
5	Go to step 2	28 more times
6	68 °C	5 minutes
7	4 °C	Hold

(c)

Table 3.3 The PCR components and cycling parameters used to amplify the *Murine* BVR-A cDNA.

Presented above are (a) the primers used in the amplification of *Murine* BVR-A. The components of the successful PCR reaction are shown (b), and also the thermo cycling conditions used to amplify the murine cDNA insert of the expected size ~890 base pairs as shown in Figure 3.9.

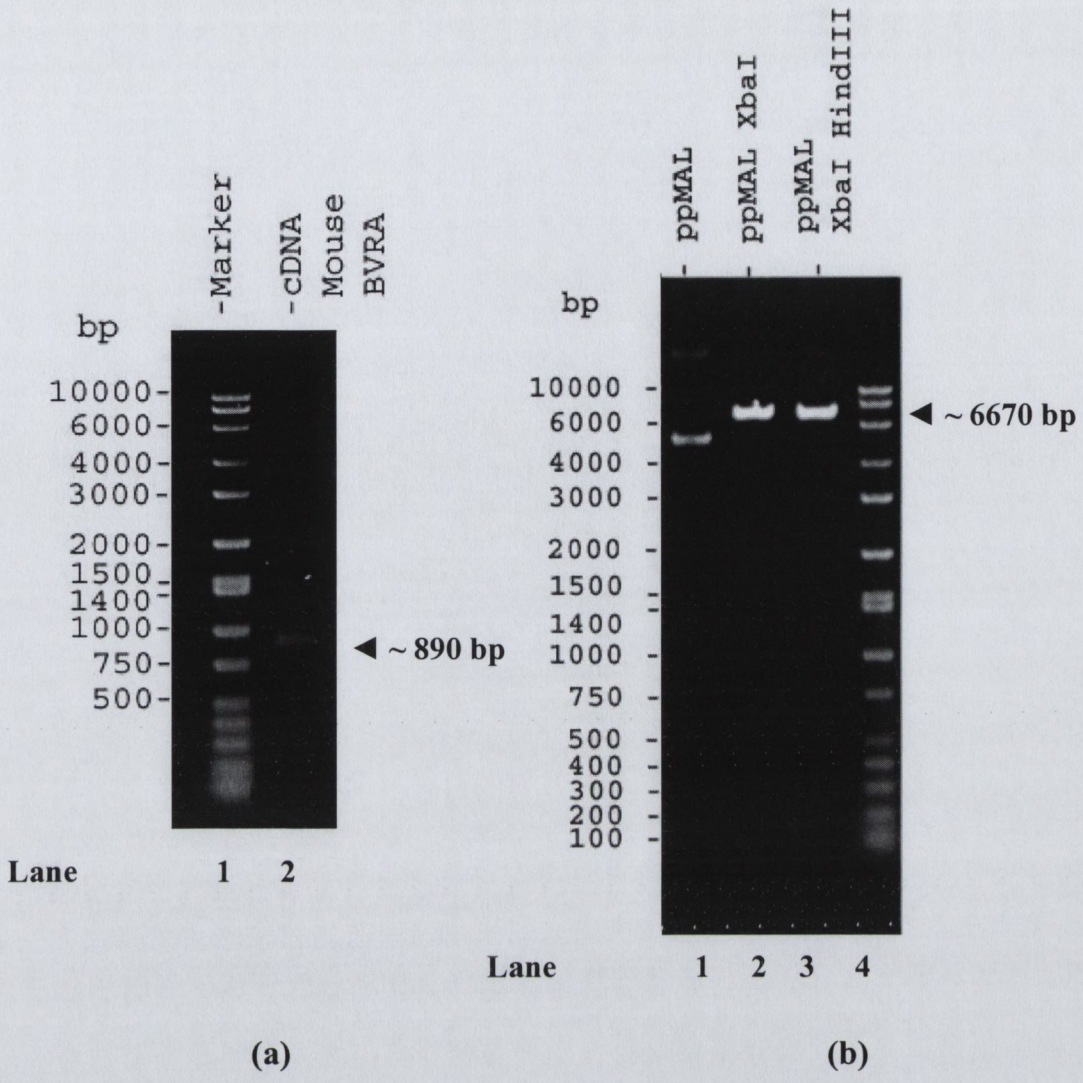

Figure 3.9 The cloning of murine BVR-A into the ppMAL expression vector.

(a) The amplification and digestion of murine BVR-A cDNA

Lane 1 contains 'Sigma (D7058)' molecular markers (5 µl). Lane 2 contains a 5 µl aliquot of the HindIII and XbaI digested 890 bp murine BVR-A cDNA insert. Conditions outlining the amplification of murine BVR-A cDNA are described in Section 3.5.2.

(b) The digestion of ppMAL expression vector

The ppMAL expression vector was prepared for the insertion of amplified murine BVRA cDNA by digestion with XbaI and HindIII as described in Section 3.5.3. Lane 1 contains undigested ppMAL, lane 2 contains ppMAL digested with XbaI only, and lane 3 contains pp MAL cut with XbaI and HindIII. Lane 4 contains 'Sigma (D7058)' molecular weight markers.

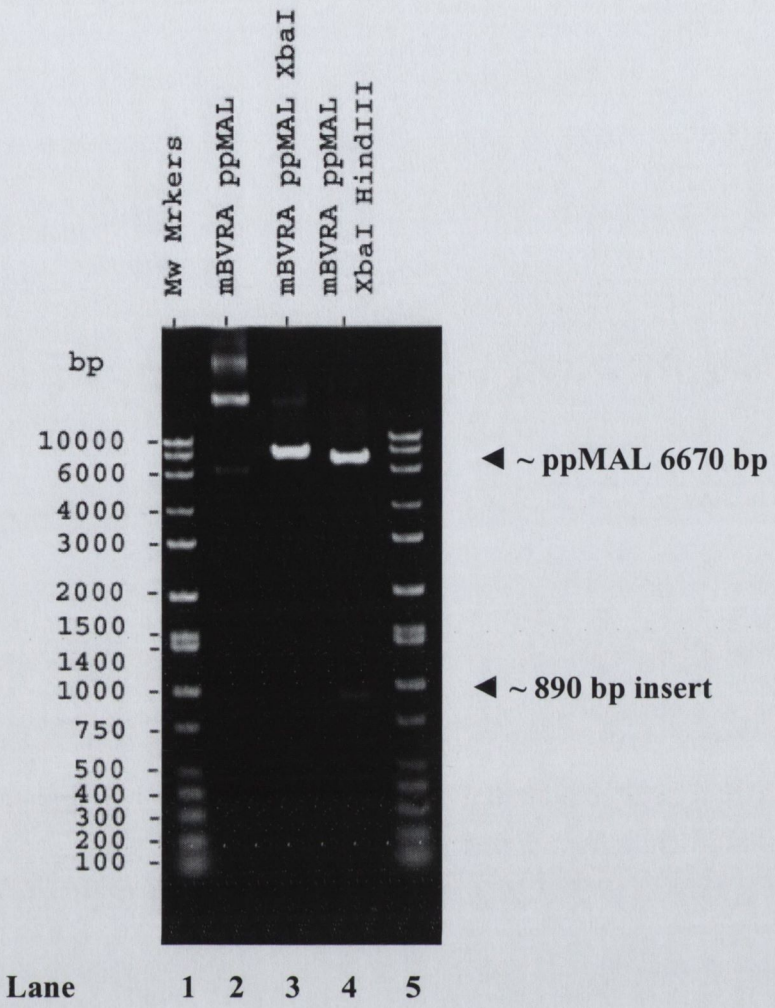

Figure 3.10 Screening for the successful ligation of the murine BVR-A cDNA insert into ppMAL.

Following the ligation of murine biliverdin-IXα reductase into the ppMAL expression vector, positive transformants were selected and subjected to restriction digest analysis. One such digest is shown above. Lanes 1 and 5 contain 'Sigma D7058' molecular markers (5 μl). Lane 2 contains undigested ppMAL-mBVR-A clone. Lane 3 contains ppMAL-mBVR-A digested with XbaI. Lane 4; ppMAL-mBVR-A digested with XbaI and Hind III, showing the excised 890 bp mBVRA insert. All digestion and ligation conditions for murine biliverdin reductase are detailed in section 3.3.2.

used to inoculate individual 5 ml cultures containing ampicillin, and these were grown for 16 hours at 37 °C with shaking at 270 rpm. DNA was isolated from these cultures using the 'Wizard Plus SV Miniprep DNA purification system' as described in Section 2.1.7. Each clone was screened for the presence of murine cDNA insert with a restriction digest using XbaI and HindIII. DNA (~500 ng) was digested in a final volume of 50 µl using '1X Sure Cut buffer B'. Screening of colonies containing the murine BVR-A ppMAL plasmid is shown in Figure 3.10.

3.5.6 Sequence analysis of murine BVR-A cDNA ppMAL construct.

DNA sequencing of the murine BVR-A cDNA construct was carried out as described in Section 2.1.9. The results are shown in Figure 3.11 and Appendix III Figure 2. The alignments in Appendix III Figure 2 show a comparison of the murine BVR-A ppMAL construct with four other EST sequences. The cDNA sequence of EST number 1 (Accession Number AK002231.1) appears to have its stop codon 21 base pairs after the stop codon of all other cDNA sequences aligned including that of the cloned product. Another point of difference occurs in the codon (TTG) which codes for leucine 27. In three of these sequences (numbered 2, 3 and 5) which includes the murine BVR-A ppMAL construct, the codon is as expected, however in EST's numbered 1 and 3, the codon reads (TCG) which encodes for lysine at this position.

3.7 The tissue and gender distribution of *Murine* Biliverdin-IXα reductase.

Tissue cytosols of 2 balb/c mice, male and female, were prepared as described in Section 2.4.7. Following the elucidation of the protein content of each cytosolic tissue fraction as described in Section 2.4.11a, the biliverdin-IX α reductase of each sample was then determined. These measurements were undertaken using the methods detailed in Section 2.5.1. A small blank rate was observed on addition of NADPH, and cytosolic in 100 mM Tris-HCl pH 8, however this tapered off after 30 seconds after which time the reaction was started with the addition of biliverdin-IXα. The results of these experiments are presented in Figure 3.9. Higher levels of biliverdin-IXα reductase activity are evident in all tissues of the male mice when compared with females. The kidney and spleen are the tissues with the highest levels of activity in both male and female mice examined.

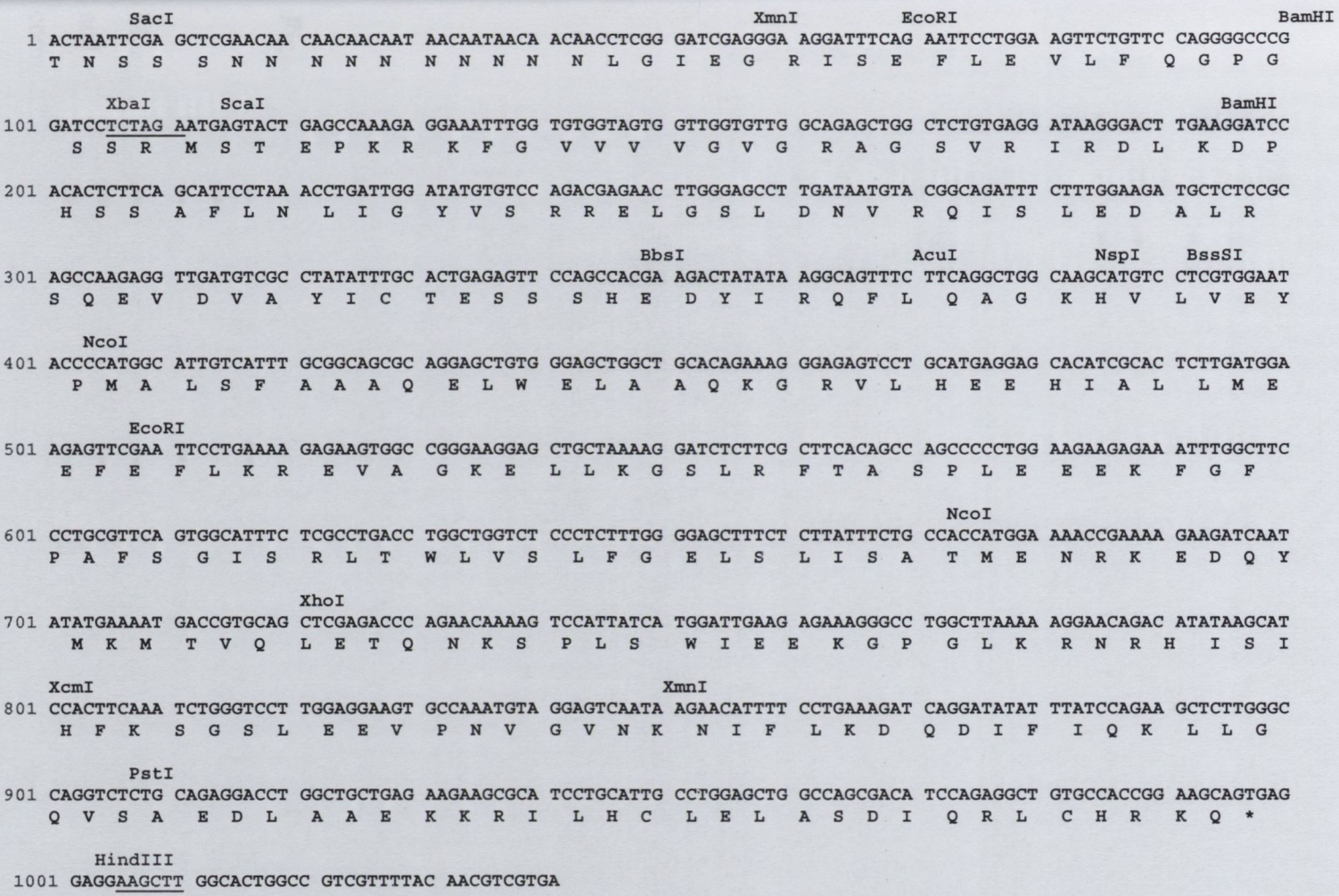

Figure 3.11 The *Murine* BVR-A ppMAL construct.

Shown above is the sequencing result for the recombinant ppMAL/murine BVR-A construct. The restriction sites (XbaI and HindIII) highlighted in red were used to insert the amplified murine cDNA.

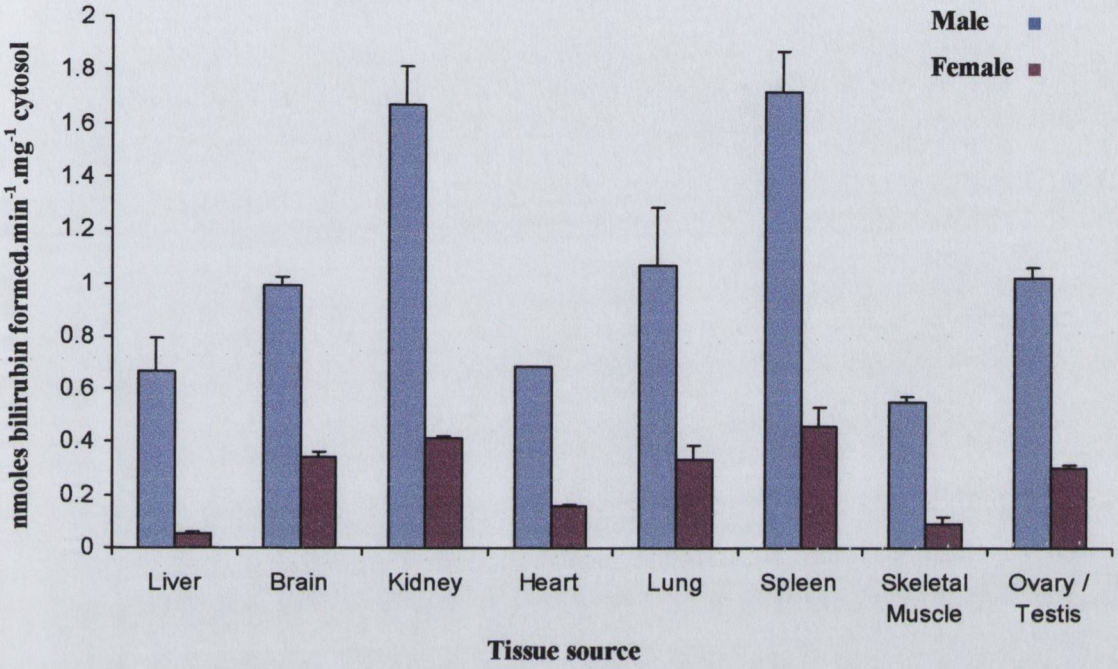

Figure 3.12 Differences in the tissue and gender distribution of *Murine* biliverdin-IXα reductase.

Measurements of the BVR-A activity in male tissue is represented by blue bars (■), and BVR-A activity in female tissue is represented by purple bars (■). Assay components consisted of 50 μg cytosolic fractions, 10 μM biliverdin-IXα, 37 μM BSA, 100 μM NADPH in 100 mM Tris pH 8 as described in Section 3.8.

3.8 Cloning of human biliverdin- IXα reductase.

3.8.1 Amplification of human BVR-A c-DNA

Although a pGEX-KG human BVR-A expression clone had been made previously by Dunne (2000), expression levels from this construct dramatically decreased over time. It was established that the induction of the GST-human was very low. Attempts to establish why this construct had low levels of induction proved inconclusive as the sequencing of the promoter region and the open reading frame for GST/human BVR-A provided little explanation. It was decided to reclone this protein and the pET41a-Mod expression was used, as it has the added advantage of a fusion of a his-tagged GST to the human BVR-A. This provides a very convenient way of separating the BVR-A from the GST moiety once cleaved. Human biliverdin-IXα reductase was amplified from a human spleen cDNA library kindly provided by Prof. Luke O'Neill, School of Biochemistry and Immunology, Trinity College, Dublin. The primers and thermo cycling conditions outlined in Table 3.4 were used to amplify the human cDNA insert of the expected size (~897 base pairs) as shown in Figure 3.13(a). PCR products were cleaned and prepared for digestion with the 'QIAquick PCR clean up kit' as described in Section 2.1.8.

3.8.2 Digestion and ligation of human cDNA into pET41a-Mod

The pET41a-Mod shown in Appendix II Figure 4, was used in the cloning of the human cDNA insert. The restriction buffer incompatibility of BamHI and SalI in 'sure cut buffer B' (Roche) does not allow for the digestion of both insert and plasmid in a single step. As a result the digests containing 1 μg plasmid DNA was performed sequentially, initially with 20 units BamHI in 'Sure Cut Buffer B' followed by digestion with 20 units SalI in 'Buffer H' (Roche) in a total volume of 50 μl. The digests were incubated for 6 hours at 37°C. DNA was purified using the 'QIAquick PCR purification kit' as described in Section 2.1.8. Following the sequential digests, 2 units of bacterial alkaline phosphatase (Takara) was added to the digested plasmid and incubated between 60-65°C for 1 hour. The amplified human BVR-A cDNA was digested in similar fashion but without BAP treatment.

The digested and purified inserts were ligated into pET41aMod plasmid using the Takara DNA Ligation Kit Version 2.1, as described in Section 3.5.3. Chemically competent XL1

Expression Vector	Primer Name	Direction	Sequence
pET41aMod	HumForBamHI	Forward	CTGGATCCATGAATGCAGAGCCCGA
pET41aMod	HumRevSalI	Reverse	CTTGTCGACTTACTTCCTTGAACA

(a)

Nuclease free water	38.5 µl
10 X pfu reaction buffer	5 µl
Forward primer (HumFor BamHI 10pmol/µl)	1 µl
Reverse primer (HumRev SalI 10pmol/µl)	1 µl
dNTPs (10mM each nucleotide)	2 µl
Human BVRA cDNA library (50ng)	1.5 µl
Pfu DNA polymerase	1 µl

(b)

Step Number	Temperature	Time
1	95 °C	1 minutes
2	95 °C	1 minutes
3	58.5 °C	1 minutes
4	68 °C	1.5 minutes
5	Go to step 2	28 more times
6	68 °C	5 minutes
7	4 °C	Hold

(c)

Table 3.4 The PCR components and cycling parameters used to amplify human BVR-A from a human spleen cDNA library.

Details of the primers used to successfully amplify human BVR-A are detailed in (a) above, while the components and cycling parameters are presented in (b) and (c) respectively. The amplification of the human cDNA insert with the expected size of 895 base pairs shown in Figure 3.13 was achieved using these conditions.

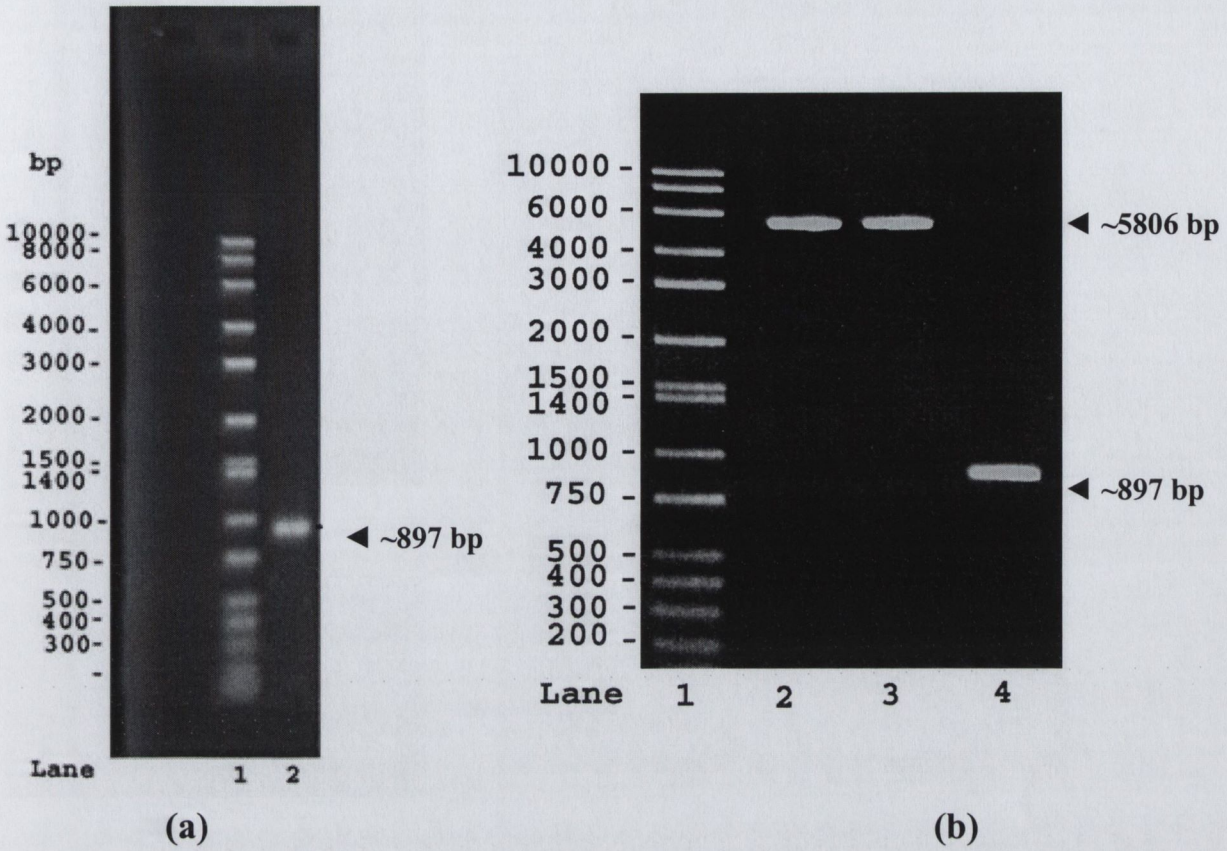

Figure 3.13 The cloning of human biliverdin-IXα reductase from a human spleen cDNA library.

(a) The amplification of the human BVR-A cDNA.

Lane 1 contains molecular weight markers (Sigma D-7058). Lane 2 contains 10 µl of the human BVR-A cDNA amplification reaction (Section 3.8). The 897 bp human BVR-A cDNA PCR product is visible. Details of the reaction components and thermocycler parameters used for the amplification of this product are presented in Table 3.4.

(b) The digestion and purification of amplified human BVR-A cDNA and pET41a-Mod expression plasmid.

Lane 1 contains 5µl of Sigma (D-7058) markers, lane 2 contains BamHI digested pET41aMod, lane3 contains the BamHI and SalI digested pET41a-Mod plasmid (~5806 bp) and lane 4 contains purified BamHI and SalI digested human BVR-A cDNA.

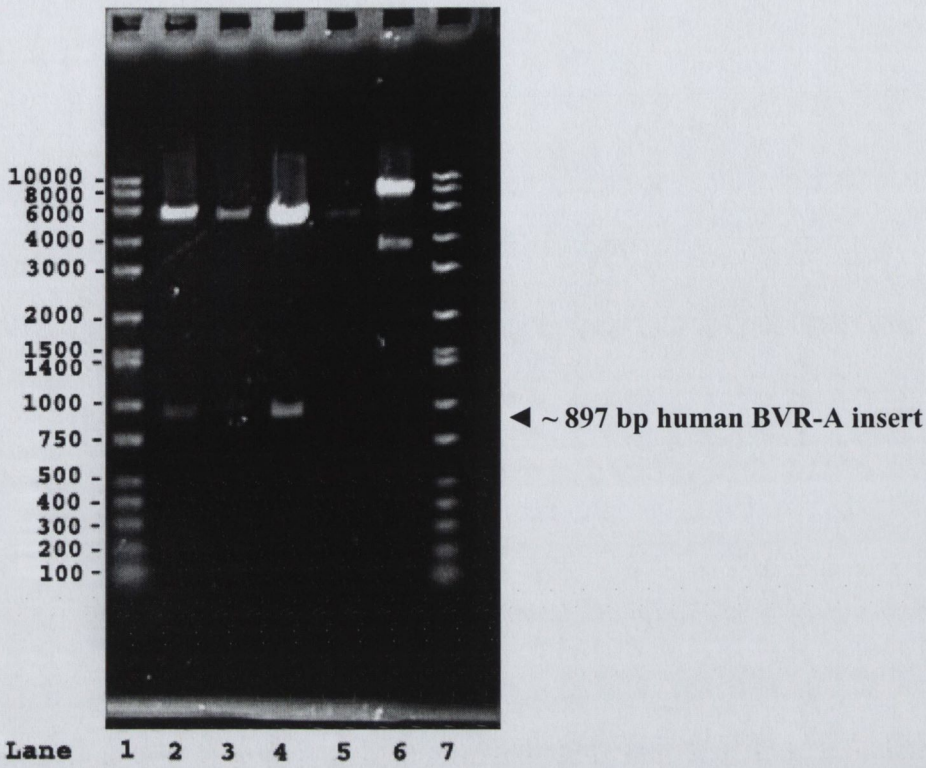

Figure 3.14 Screening for the presence of a human BVR-A insert from human BVR-A/pET41aMod transformed XL-1 blue *E.coli*.

Positive transformants were screened using restriction digest analysis with BamHI and SalI. The appearance of an 897 bp fragment indicates the successful ligation of human BVR-A cDNA insert into pET41a-Mod plasmid. Lanes1 and 7 contain 5µl of Sigma (D-7058) markers. Lanes 2, 3 and 4 contain purified plasmid from various colonies with an insert ~ 897 bp being cut from the pET41a-Mod (~5760 base pair) plasmid. Lane 6 contains undigested pET41a-Mod.

Blue cells were then transformed with the ligation mix and plated onto kanamycin plates which were incubated overnight at 37 °C.

3.8.3 Screening for the presence of human BVR-A insert in transformed cells.

A single colony from the overnight ligation plates was used to inoculate individual 5 ml cultures containing ampicillin, and these were grown for 16 hours at 37 °C with shaking at 270 rpm. DNA was isolated from these cultures using the 'Wizard Plus SV Miniprep DNA purification system' (see Section 2.1.7). Each clone was screened for the presence of human cDNA insert with a restriction digest using BamHI and SalI. DNA (~500 ng) was sequentially digested in a final volume of 50 µl using '1X sure cut buffers B and H'. Screening of a colony with containing the human BVR-A pET41a-Mod plasmid is shown in Figure 3.14.

3.8.4 Sequence analysis of human cDNA in the plasmid pET-41aMod.

DNA sequencing was carried out as described in Section 2.1.9. The results are shown in Appendix III Figure 2 and from these alignments it is evident that there are no nucleotide sequence changes with reference to the other sequences aligned.

3.9 Investigation of a putative avian biliverdin- IXα reductase.

3.9.1 The *Gallus gallus* genomic sequence

During blast searches using other biliverdin reductases as query sequences, a chicken nucleotide sequence sharing a high degree of similarity with the other BVR-A proteins was apparent. The gene (geneID: 420776) is present at locus (LOC420776) on *Gallus gallus* chromosome 2. Analysing the genomic sequence around this locus using the genomic shotgun sequence accession number NW_060265.1 Gga2_WGA74_1:20391605-20406900), the gene seems to consist of 6 exons, distributed over 10,363 bases. Exon 1 encodes for the first 40 amino acids of the predicted protein which includes the N-terminal nucleotide binding domain. Exon 3 contains the active centre of these enzymes which contains the consensus sequence AGKHVLVEYPM. Exon 6 is the longest coding for 89

amino acids before the 3' terminal stop codon. Details of this gene are depicted in Appendix III Figure 3. It is interesting to note that some EST evidence has been found (clone ChEST458f9) in cDNA prepared from RNA extracted from 16 day old White Leghorn chicks brain tissue.

3.9.2 Preparation of erythrocyte lysate from packed turkey red blood cells

100 ml packed erythrocytes were lysed by adding 700 ml ice cold deionised water. The solution was left for 30 minutes at 4°C with continuous stirring and then centrifuged for 30 minutes at 4°C to pellet the cellular debris. The supernatant was then subjected to a 40% ammonium sulphate precipitation step. The solution was left stirring at 4°C for 30minutes and centrifuged at 8000 rpm for 10 minutes. The supernatant was then removed and subjected to an 80% ammonium sulphate precipitation step. The solution was again left stirring and centrifuged at 8000 rpm for 10 minutes. Both the 40% and the 80% pellets were resuspended in 10 ml 20mM sodium phosphate pH 7.2. The solution was then dialysed 5 times against 5L of 20 mM sodium phosphate pH 7.2 at 4°C, and allowing each dialysis step at least 3 hours to equilibrate. Ion exchange chromatography on DEAE-cellulose equilibrated in 10 mM sodium phosphate pH 7.2 was used as a further purification step in the isolation of the reductase activity. The dialysed sample was loaded onto the column and washed with 10 mM sodium phosphate pH 7.2. A gradient (2 X 500 ml) of 10-300 mM sodium chloride 10 mM sodium phosphate pH 7.2 was run through the column and the eluate collected and monitored for biliverdin reductase activity. Figure 3.15(a) shows the NADPH dependent BVR-A activity in turkey cytosol dialysed against 20 mM sodium phosphate pH 7.2. Increasing volumes of cytosol showed the expected linear relationship between v_0 versus [E], as shown in Figure 3.15(b). Partial purification on DEAE-cellulose was monitored using a plate assay presented in Figure 3.15(c).

3.10 Protein expression and purification

The human, rat, murine and synechocystis BVR-A enzymes were successfully expressed and purified to homogeneity and are detailed below. Expression of the *Xenopus* BVR-A as a GST fusion protein has been achieved and some preliminary activity measurements have been taken (see Figure 4.4b). However efforts to purify both the *Xenopus* BVR-A and the *Danio rerio* BVR-A to homogeneity are ongoing.

Figure 3.15 Detection of a biliverdin-IXα reductase activity in crude turkey cytosol.

(a) The apparent biliverdin reductase activity from the hypotonic cell lysate was monitored at 460 nm. Each individual reaction mix contained 10 μM biliverdin-IXα, 100 μM NADPH and increasing volumes of cell lysate in 100 mM sodium phosphate buffer pH 7.2. The reaction rate at 460 nm was shown to be dependent on addition of nucleotide and biliverdin.

(b) The effect of enzyme concentration on the initial rate. Data points shown are an average of duplicate rate values obtained on assay of cell lysates.

(c) A crude plate assay for BVR-A activity in fractions eluted from DEAE cellulose as described in Section 3.9.2. Row A: Protein fractions taken from the salt gradient were incubated with 12-ethyl-mesobiliverdin-XIIIα and 100 μM NADPH in 100mM sodium phosphate pH 7.5. Row B: The 12-ethyl-mesobiliverdin-XIIIα reaction without the addition of protein.

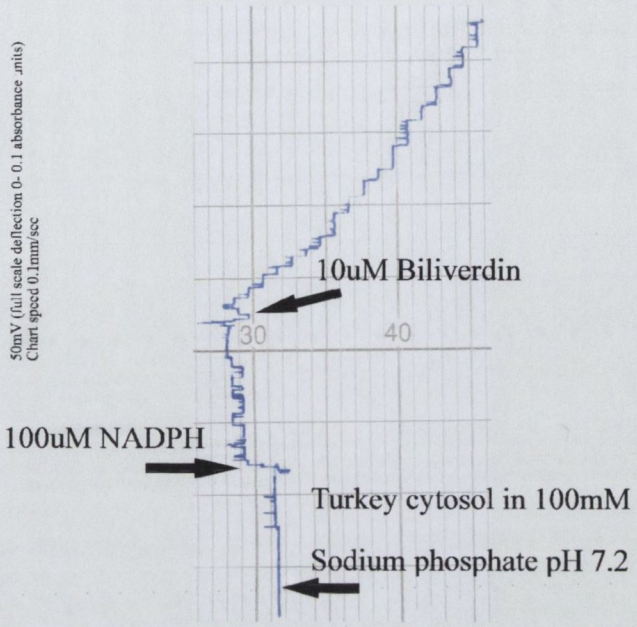
50mV (full scale deflection 0- 0.1 absorbance units)
Chart speed 0.1mm/sec
10uM Biliverdin
30
40
100uM NADPH
Turkey cytosol in 100mM
Sodium phosphate pH 7.2

(a)

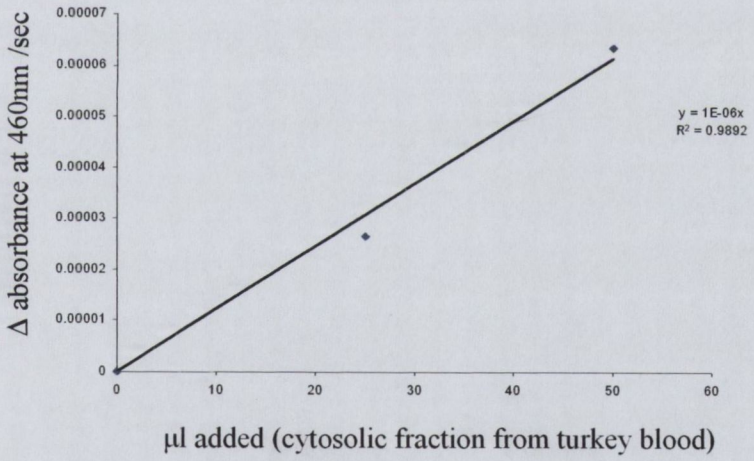
Δ absorbance at 460nm /sec
0.00007
0.00006
0.00005
0.00004
0.00003
0.00002
0.00001
0
y = 1E-06x
R² = 0.9892
0
10
20
30
40
50
60
µl added (cytosolic fraction from turkey blood)

(b)

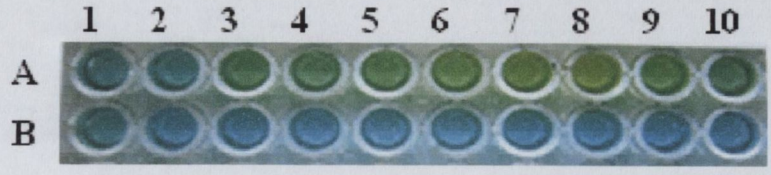
1 2 3 4 5 6 7 8 9 10
A
B

(c)

3.10.1 Purification of recombinant human BVR-A

Recombinant human BVR-A was purified according to the method outlined in Section 2.4.4. In brief, 2L cultures of LB containing (100 μg / ml) kanamycin and (50 μg / ml) chloramphenicol, were inoculated with overnight cultures of human BVR-A/pET-41aMod transformed *E.coli BL21 DE3 RIL* cells. These cultures were induced with a final concentration of 0.2 mm IPTG when the culture reached an optical density of 0.6 at 600 nm. The cells were then induced for 10 hours at 20°C. Following the cell harvesting and lysis, fusion protein purification was achieved using *S*-hexyl glutathione sepharose column chromatography. The glutathione column was eluted with 200 ml of 5 mM *S*-hexyl glutathione in 100 mM sodium chloride, 1% glycerol, 20mM sodium phosphate pH 7.8. Eluted protein fractions were pooled, followed by cleavage of human BVR-A from the GST moiety using thrombin (1 unit/mg fusion protein) while dialysing against 20 mM sodium phosphate, 100 mM sodium chloride 1% glycerol pH 7.8 at 4°. The sample was then passed through a Ni^{2+} agarose affinity resin column which removed the cleaved His-tagged GST from the human BVR-A. The results of this purification are detailed in Figure 3.16. This purification routinely yielded up to 40 mg fusion protein /L culture media, which was substantially higher than the levels produced in the original human BVR-A pGEX clone (usually 3 - 5 mg fusion / L culture media). Human BVR-A was purified to homogeneity on passing through the Ni^{2+} agarose affinity resin which bound any uncleaved fusion protein and cleaved GST. The purified human BVR-A was used in the production of antibodies (Section 2.3.4), all kinetic studies and in crystallisation attempts (Section 2.7). It was found that the concentration of human BVR-A over concentrations of 6 mg/ml resulted in the precipitation of the protein, and for crystal growth concentrations of 4-5 mg/ml have been used in the hope of obtaining micro crystals which could be used as seeding material. Attempts are ongoing in this regard.

3.10.2 Purification of recombinant murine BVR-A

Recombinant murine BVR-A was purified according to the method outlined in Section 2.4.5. An overnight incubation with 'PreScission™ Protease' (Amersham Biosciences) cleaved the ppMAL moiety from the murine BVR-A using the recommended protease buffer (50mM Tris-HCl, 150mM NaCl, 1mM EDTA, 1mM DTT, pH 7.0). Digestion of

Figure 3.16 SDS PAGE analysis of the purification of recombinant human biliverdin-IXα reductase.

(a) Purification of the His tagged GST human BVR-A fusion protein using a *S-hexyl* glutathione affinity chromatography. Lane 1 contained 10 μl of molecular weight markers (Sigma M3913). Lanes 2 and 3 contained 10μl cytosolic fraction. Lane 4 contained 5 μl of the pooled peak protein fractions after elution of the *S-hexyl* glutathione column with 5 mM *S-hexyl* glutathione. Lane 5 contained 10 μl of the thrombin cleaved fractions.

(b) Removal of the cleaved His-tagged GST from human BVR-A was facilitated by passing the thrombin treated His-tagged GST human BVR-A mixture through a Ni^{2+} agarose affinity column as described in Section 2.4.4. Lane 1 contains 10 μl 'Sigma molecular weight standards' (M3913), and lanes 2 to 12 contain the peak flow through samples from the Ni^{2+} agarose column.

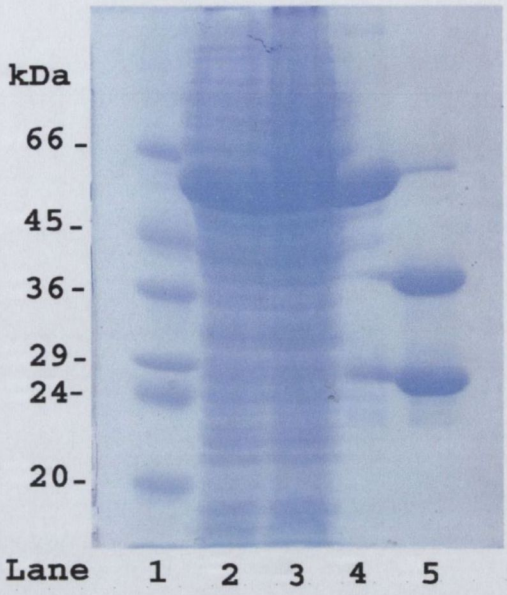
kDa
66
45
36
29
24
20
Lane 1 2 3 4 5

(a)

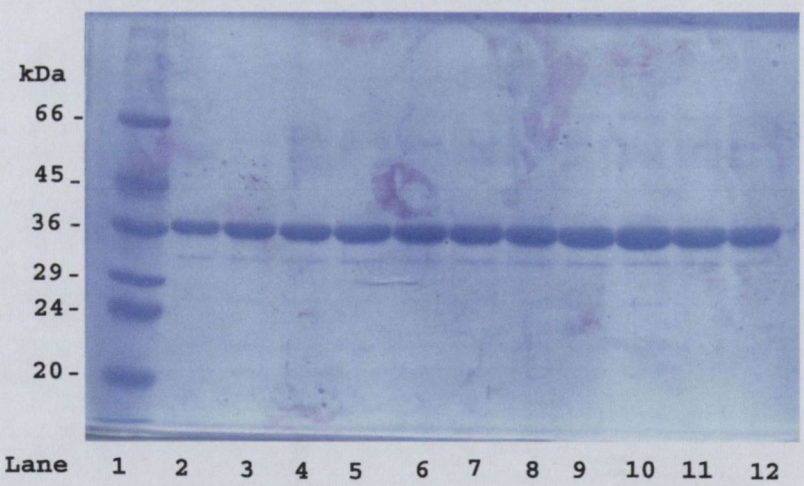
kDa
66
45
36
29
24
20
Lane 1 2 3 4 5 6 7 8 9 10 11 12

(b)

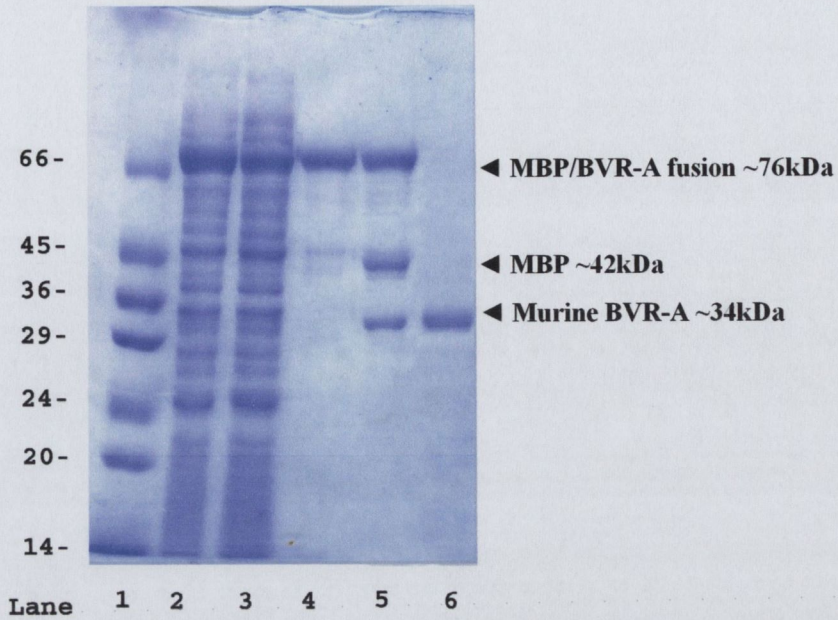

Figure 3.17 SDS-Page analysis of the purification of murine biliverdin reductase.

Lane 1 contains molecular weight markers (Sigma M3913). Lanes 2 and 3 contain 19000 g supernatant. Lane 4 contains a 10 μg sample of the pooled fractions eluted from the amylose resin. Lane 5 is the MBP-*Murine* BVR-A fusion protein after treatment of precision protease (cleaved for 12 hours at 4°C in precision protease buffer). Lane 6 is purified *Murine* BVR-A (10 μg) which was separated from the MBP tag and un-cleaved fusion protein using ion exchange chromatography as described in Section 3.10.2.

approximately 50% of the MBP fusion protein was achieved after overnight incubations at 4°C. Attempts to increase the cleavage efficiency by incubating the murine BVR-A/MBP fusion protein and the protease at room temperature were counterproductive due to the levels of protein precipitation experienced during the incubation period. Following cleavage the MBP moiety and uncleaved MBP/BVR-A were separated from murine BVR-A by ion exchange chromatography as described in Section 2.4.5. Samples were taken throughout the purification procedure and analysed on SDS PAGE as described in Section 2.3.1. The results of this purification are detailed in Figure 3.17. Murine BVR-A was purified to homogeneity in quantities of 20-30 mg/L original culture volume. The enzyme was also used for the production of antibodies as described in Section 2.3.4. Results of the chromatofocusing of murine BVR-A are presented in 3.20. It is interesting to note that two protein peaks are eluted, one at pH 6.8 and the other at pH 7. The latter although having lower protein content has higher proportional activity than the first. This phenomenon was not investigated further. The results of the chromatofocusing experiment confirm how separation of the protein on DEAE is possible as MBP has a pI of 5.07 and elutes between 100 and 150 mM NaCl on the salt gradient. Murine BVR-A binds to DEAE anion exchange resin as expected from a pI of ~7 but elutes at lower concentrations of salt 50 mM.

3.10.3 Purification of recombinant *Synechocystis* and rat BVR-A

Recombinant *Synechocystis* BVR-A was purified according to the method outlined in Section 2.4.5, the results of which are presented in Figure 3.19. The *Synechocystis* enzyme is larger (328 amino acids) than the mammalian enzymes (approximately 296 amino acids) respectively. Yields of this protein using this method were very high, typically 40-50 mg purified protein / L culture media. Recombinant rat BVR-A was purified according to the method outlined in Section 2.4.6, and again yields of this protein were high and purified in quantities similar to the recombinant *Synechocystis* BVR-A. Results of the purification of recombinant 6 x His tagged rat BVR-A are presented in Figure 3.18.

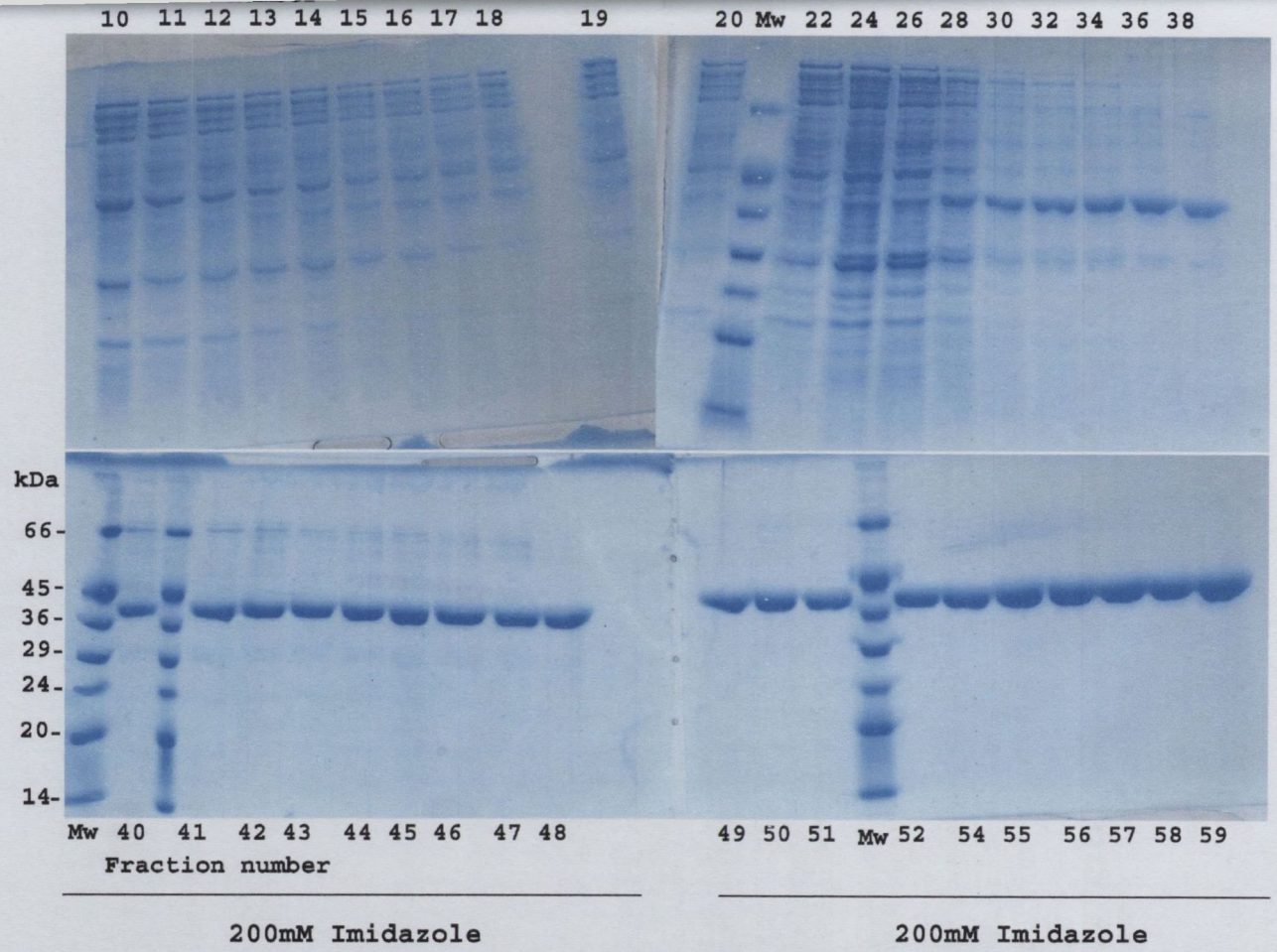

Figure 3.18 The purification of recombinant 6X His tagged rat biliverdin-IXα reductase on Ni^{2+} charged agarose.

His tagged rat BVR-A was purified according to the methods described in Section 2.4.6. Aliquots (20 µl) of each 2 ml fraction eluted from the Ni^{2+} agarose column were analysed using SDS PAGE. The column was washed with 100 and 150 mM imidazole to elute non specifically bound contaminant proteins. Purified rat BVR-A eluted in the 200 mM imidazole.

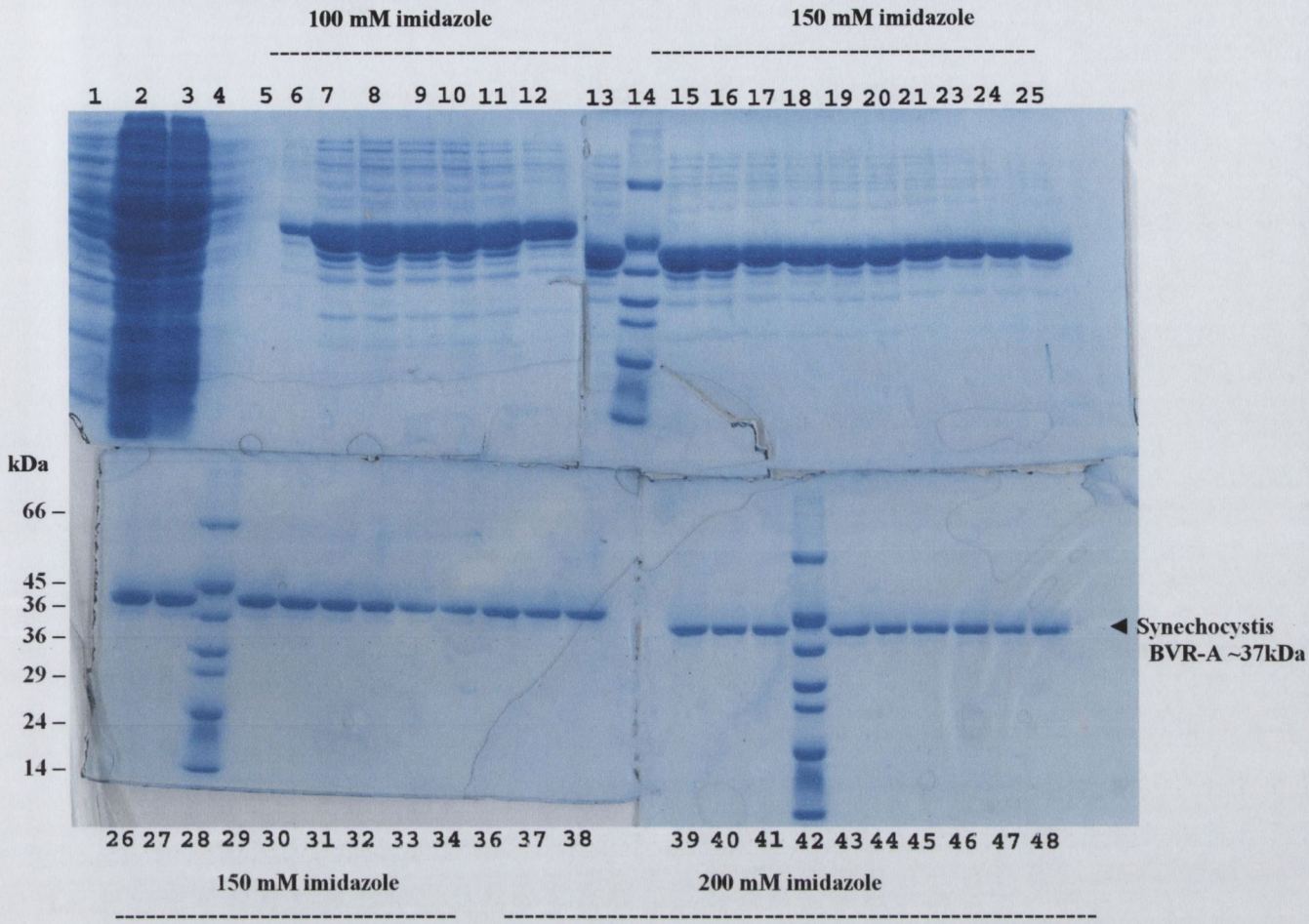

Figure 3.19 The purification of recombinant 6X His tagged synechocystis BVR-A.

His tagged synechocystis BVR-A was purified according to the methods described in Section 2.4.3. Lane 2 contains 5 µl cytosolic fraction before loading on the Ni^{2+} agarose column, Lane 3 contains 5 µl of the non bound cytosolic fraction collected after loading the Ni^{2+} agarose column. Lanes 14, 28 and 42 contain Sigma molecular weight standards' (M3913). The column was washed with 100 and then 150 mM imidazole in 100mM NaCl, 20mM Tris pH 8 to elute non specifically bound contaminant proteins. Purified synechocystis BVR-A eluted in the 200 mM imidazole wash. Aliquots (20 µl) of each 2 ml fraction eluted from the Ni^{2+} agarose column were analysed using SDS PAGE.

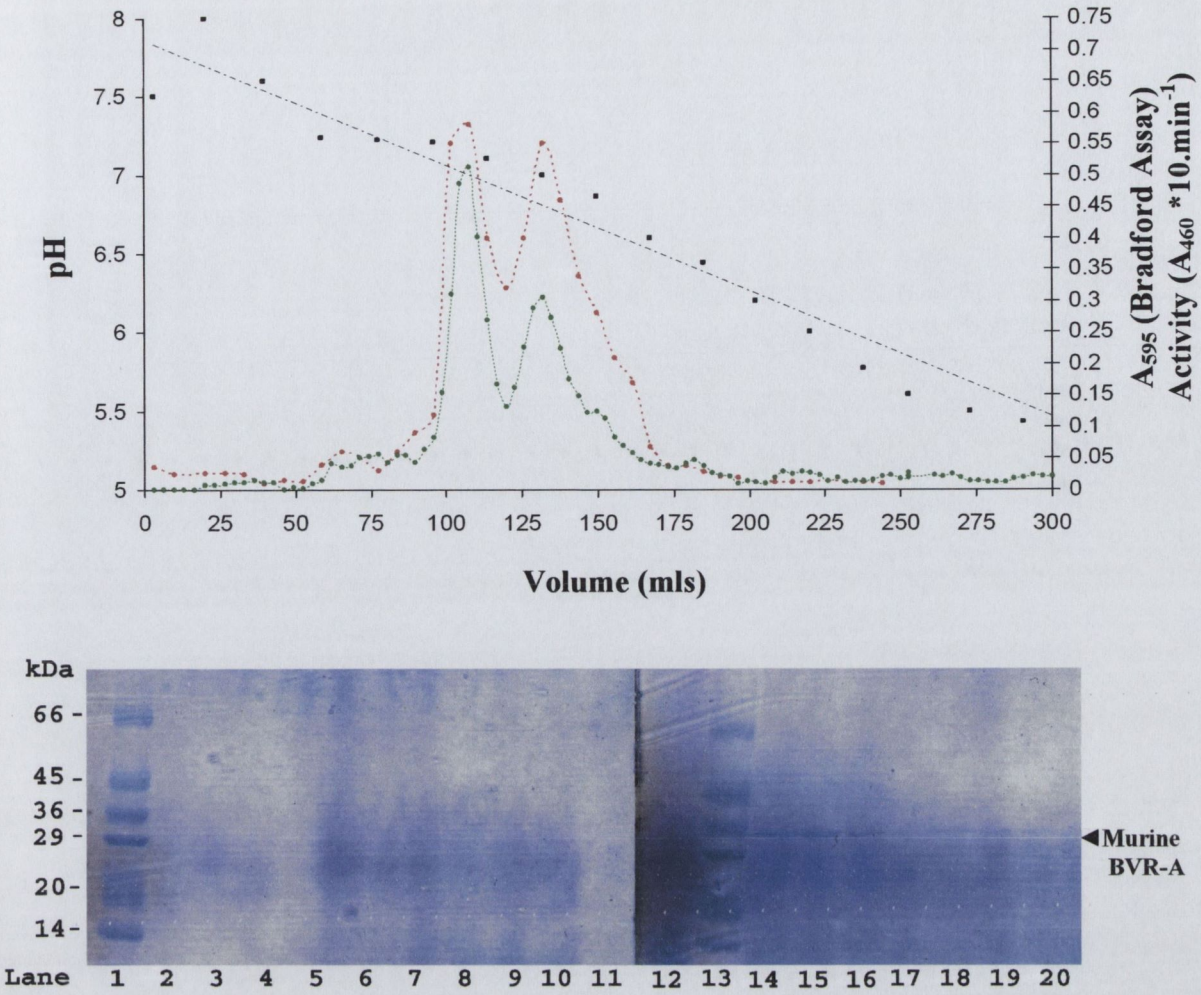

Figure 3.20 Chromatofocusing of purified murine BVR-A on Polybuffer Exchanger 9-4.

(a) The PBE94 column was prepared as described in Section 2.4.9. Purified murine BVR-A (10mgs) were applied in start buffer (25mM imidazole/HCl pH 7.4) and eluted with a 1/8 dilution of Polybuffer 74 pH4. Protein elution was monitored using the Bradford plate assay (A_{595}) as described in Section 2.4.11, while activity measurements were also taken using the standard assay described in Section 2.5.1. The pH of each fraction was also monitored to establish the pH gradient across the elution profile.

(b) The coomassie blue-stained SDS-PAGE gels are of eluted column fractions: Lanes 14, 15 and 16 contain murine BVR-A and correspond to the Polybuffer peak fractions. Samples were taken over every 3rd fraction (approx 7.5 ml volume intervals) Gel lanes corresponding to peak fractions are indicated below the chromatograms.

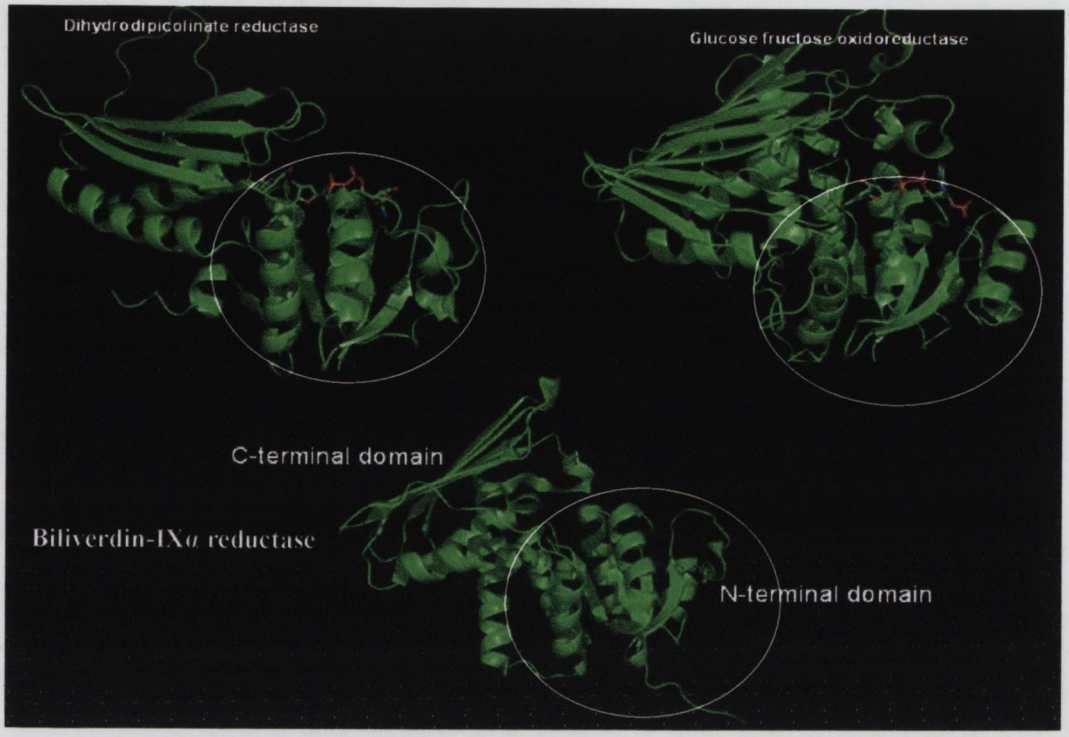


```
GFOR          ATLPAGASQVPTTPAGRPMPYAIRPMPEDRRFGYAIVGLGKYALNQILPGFAGCQHSRIE 60
rBVR-A        ----------------------MDAEPK-RKFGVVVVGVGR-AGSVRLRDLKDPRSAAFL 36
                :       :         :   : . *: *:** .:**:*: * .  * .: . : : :

GFOR          ALVSGNAEKAKIVAAEYGVDPRKIYDYSNFDKIAKDPKIDAVYIILPNSLHAEFAIRAFK 120
rBVR-A        NLIG--------FVSRRELGSLDEVRQISLEDALRSQEIDVAYICSESSSHEDYIRQFLQ 88
               *:.        :..:.  :.. .     .::.  :. :**..**   .* * ::  : ::

GFOR          AGKHVMCEKPMATSVADCQRMIDAAKAANKKLMIGYRCHYDPMNRAAVKLIRENQLGKLG 180
rBVR-A        AGKHVLVEYPMTLSFAAAQELWELAAQKGRVLHEEH----VELLMEEFEFLRREVLGKEL 144
              *****: * **: *.* .*.: : *   .: *   :       :    .:::*.: ***

GFOR          MVTTDNSDVMDQNDPAQQWRLRRELAGGGSLMDIGIYGLNGTRYLLGEEPIEVRAYTYSD 240
rBVR-A        LKGS----LRFTASPLEEERFGFPAFSG-------ISRLTWLVSLFG--ELSLISATLEE 191
              :  :    :    .* :: *:     .*  :: : *  *.    *:*   :.: : * .:

GFOR          PNDERFVEVEDRIIWQMRFRSGALSHGASSYSTTTTSRFSVQGDKAVLLMDPATGYYQNL 300
rBVR-A        RKEDQYMKMTVQLETQN---KGLLSWIEEKGPGLKRNRYVN--------FQFTSGSLEEV 240
               :::::::: :: *  : .* **   .. .  . .*:       ::::: ::*  :::

GFOR          ISVQTPGHANQSMMPQFIMPANNQFSAQLDHLAEAVINNKPVRSPGEEGMQDVRLIQAIY 360
rBVR-A        PSVGVN---------------KNIFLKDQDIFVQKLLGQVSAEDLAAE---KKRIMHCLG 282
               ** .       ::  :::  :* *  : * :.: ::.: .... . * : . *:::.:

GFOR          EAARTGRPVNTDWGYVRQGGY 381
rBVR-A        LASDIQKLCHQKK-------- 295
               *:   : : .   :
```

Figure 3.21 The 3-dimentional structures of proteins with a similar fold to biliverdin reductase.

Members of the GFO/IDH/MOCA protein family have similar overall structures, with very distinct N and C terminal domains. The most conserved regions within these proteins are the nucleotide binding domains with their characteristic Rossmann folds. A sequence alignment between the glucose-fructose oxidoreductase (GFOR) from *Zymomonas mobilis* and rat biliverdin-IXα reductase is also shown.

3.11 DISCUSSION

Before discussing the results of the various cloning experiments it will be helpful to 'look' at the structure of BVR-A so that the importance of various structural elements that help to distinguish BVR-A within a super family (GFO/IDH/MOCA) can be addressed. This also helps to provide background information for the kinetic studies in Chapter 4. The availability of high resolution X-ray structures Kikuchi *et al.*, 2001; Whitby *et al.*, 2002, for rat BVR-A has opened new avenues in our understanding of the enzyme. BVR-A has been shown to have two well defined domains, the N-terminal domain which consists of the first 123 amino acids, and the larger C-terminal domain which consists of the remaining 168 amino acids. The N-terminal domain encompasses the nucleotide binding domain with a very characteristic α/β dinucleotide binding motif known as the Rossmann fold (Bellamacina 1996). It consists of one antiparallel β3 core surrounded by six parallel (β1- β2 and β4-β7) strands flanked on both sides by five α-helices (αA- αE). This type of structure has been seen in a number of other oxidoreductases such as glucose fructose oxidoreductase (GFOR), glucose-6-phosphate dehydrogenase (G6PD) and dihydrodipicolinate reductase as shown in Figure 3.21. Despite having such similar structural folds these enzymes have very low sequence identity and very different functions. The diversity of the reactions catalysed by dinucleotide binding proteins is explained by the modular nature of their structures. Members of this family may have very different substrates, but it is clear that the nicotinamide moiety of the co-factor, and the second substrate are always positioned at the interface of the N-terminal and C-terminal domains.

In order to better identify the conserved elements within members of the biliverdin reductase protein family, it was thought that a detailed look at the amino acid sequences and their equivalent positioning within the rat crystal structure may prove informative. Until now sequence alignments have only been performed with the human, rat, mouse and *Synechocystis* enzymes (Whitby *et al.*, 2002 & Kikuchi *et al.*, 2001). The analysis of a greater number of biliverdin reductases including all the putative BVR-A enzymes suggested within this study (17 in all) helps to focus our attention on a more defined group of conserved residues, over and above those which have been traditionally examined. The other significant benefit of such sequence analysis is the establishment

of a number of specific sequence criteria which could be used to define a biliverdin reductase subgroup from the larger population of putative dehydrogenases found in the protein databases. Swiss-Prot have categorised BVR-A into a super family of enzymes which utilise NADP(H) or NAD(H), the so called GFO/IDH/MOCA super family because of its N-terminal NAD-binding Rossmann fold as mentioned above. It gets its name from exemplary members of this group such as GFO which is a glucose-fructose oxidoreductase and MOCA an enzyme involved in rhizopine catabolism (rhizopines are inositol derivatives synthesised in legume nodules).

The GFO/IDH/MOCA family consensus sequences are outlined in Appendix III Figure 5, and it is evident that many proteins display good sequence similarity within this region. Indeed, 'blast' searches of protein databases using the GFO/IDH/MOCA family consensus sequence produces a long list of proteins containing elements of this motif which becomes somewhat problematic when performing Blast searches. Blast searches using any mammalian BVR-A produces significant hits which include 4-carboxy-2-hydroxymuconate-6-semialdehyde dehydrogenase, lipopolysaccharide biosynthesis protein, trans-1,2-dihydrobenzene-1,2-diol dehydrogenase, NDP-hexose 3-ketoreductase, glucose-fructose oxidoreductase, myo-inositol dehydrogenase and many dehydrogenases which as yet remain uncharacterised. The question arises whether or not we define a subset within this GFO/IDH/MOCA family which would be characteristic only for biliverdin-IXα reductases. The amino acid sequences of the reductases were aligned using the 'CLUSTAL W' program. As we can see in Figure 3.2, BVR-A sequences display a very low sequence identity for instance between the cyanobacterial and mammalian enzymes. However there are a number of conserved amino acids which are of great interest, since they represent functionally important sites retained through the evolution of the protein from cyanobacterial through to the higher species. One thing is clear and that is that there is substantial conservation of the amino acids in the heart of the interface between the N and C terminal domains, which is in agreement with the observation made by Bellamacina (1996) for other dehydrogenases. In the alignments of BVR-A shown in Figure 3.2 the emergence of a set of 5 highly conserved motifs is evident, three of which are in the GFO/IDH/MOCA region as defined in Appendix III Figure 5. These motifs have been 'deconstructed' in Figure 3.22 for clarity. I propose that these regions should be used to identify biliverdin reductases

1. **The Rossmann fold which is one of the sequence motifs common to all members of the GFO/IDH/MOCA family.**

The nucleotide binding domain between β1 and αA in the rat structure.

V14 G20

VGVGRAG

2. **The GFO/IDH/MOCA consensus sequence.**

Within this motif there are a number of highly conserved residues common to all biliverdin-IXα reductases which are positioned at the end of β6 in the rat structure.

H79 L87 H92 Y97

LEDALRSQEIDVAYICSESSSHEDYIRQFLQAGKHVLVEYPMT

3. **The consensus sequence positioned between β7 sheet and 3_{10} helix F.**

L120 E126

LHEEHVELL

4. **The consensus sequence positioned from αI through αJ.**

F161 P164 R171 F179

FGFPAFSGISRLTWLVSLFG

5. **The consensus sequence positioned at the start of αL.**

F250 D253

IFLKD

Figure 3.22 Evolutionary conservation of amino acid residues in biliverdin-IXα reductase.

Five highly conserved motifs have been identified on sequence analysis of biliverdin reductases. Motifs 1, 2 and 3 are in the MOCA region as defined in Appendix III Figure 5, while Motifs 4 and 5 are outside the MOCA region. The rat BVR-A sequence is shown while residues common to all BVR-A enzymes are in larger font.

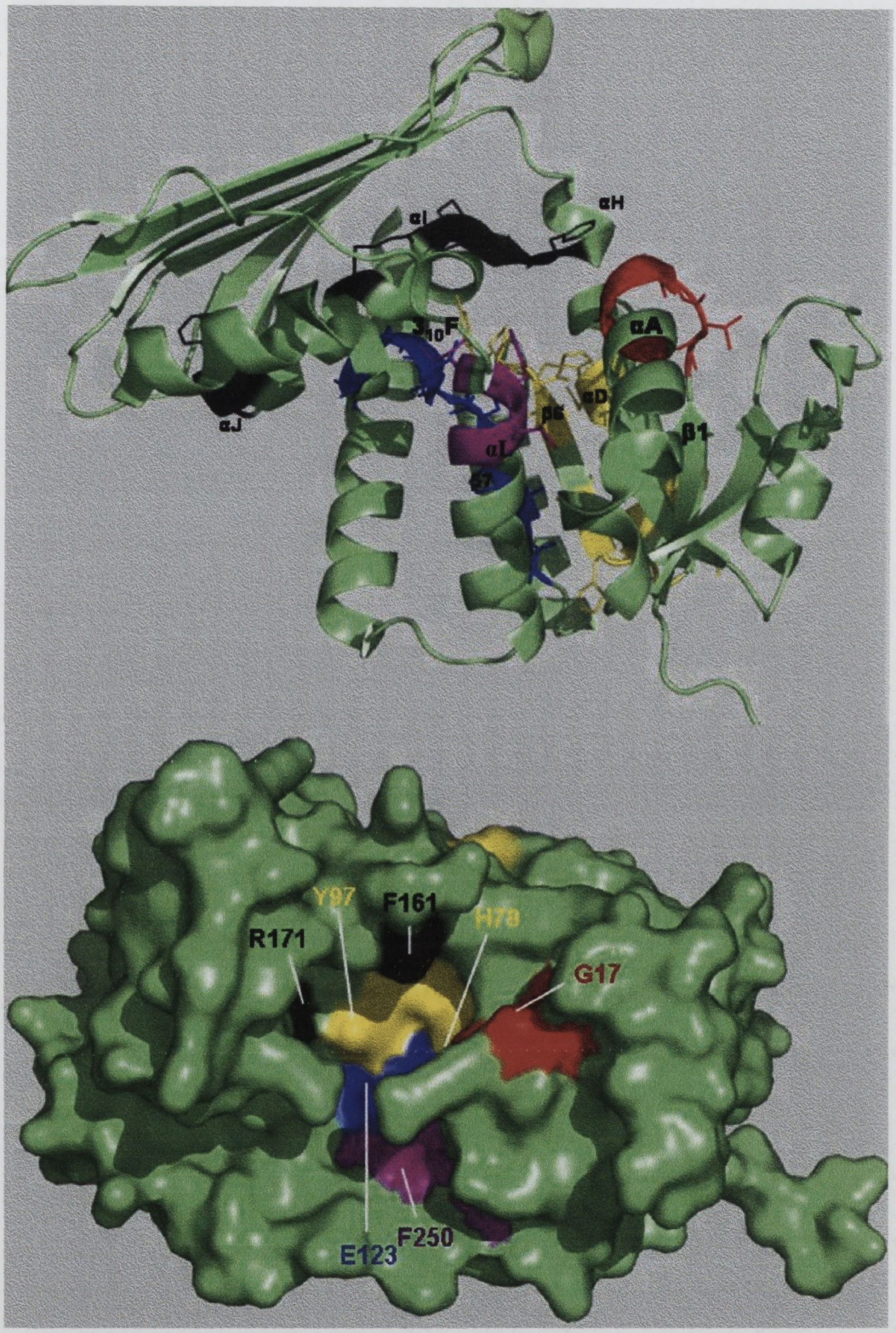

Figure 3.23 The most conserved residues of BVR-A.

The 5 highly conserved motifs have been colour coded red, yellow, blue, grey and purple. Similar colouring was used in the alignments of Figure 3.2. The ribbon diagram (top) shows the extent of conservation with many residues conserved deep at the core of the protein. The surface diagram (bottom) highlights the most conserved amino acids which are positioned around the active site and which are exposed at the surface.

within the GFO/IDH/MOCA family, and this is of importance for reasons which will be explained. Let us first look at the three conserved 'BVR-A' motifs within the greater GFO/IDH/MOCA region.

The first region of importance is the loop between sheet β1 and the helix αA which can be seen in the alignments of Figure 3.2 and is colour coded in red. The functioning of this region is relatively well understood, and the sequence G15 V16 G17 R18 A19 G20 which is found in the loop between β1 and αA is typical of the Rossmann fold sequence VGXGXXA where X is any residue (Figure 3.22). Hydrogen bonding between the phosphate moieties and sugar hydroxyl groups of the cofactor with the enzymes amide backbone groups are thought to hold the nucleotide in place (Kikuchi 2001, Whitby 2002 & Kleiger 2002).

The second important region encompasses the GFO/IDH/MOCA consensus sequence spanning the αD helix and the β6 sheet. Alignment analysis would lead to the conclusion that biliverdin-IXα reductases have a more specific consensus sequence within this greater GFO/IDH/MOCA protein family and the sequence is outlined as follows:

H X X X X X X L X X G K H V X X E Y P

This sequence begins with His 79 which positioned in αD of the rat structure, and it is seen to interact with the hydroxyl group of S74 (or possibly the threonine substitute in the non mammalian enzymes). This presumably helps to stabilise the loop between αD and the β5. It is also worth noting that H79 is exposed on part of the surface of the substrate binding pocket as highlighted in Figure 3.23. It's central positioning and high conservation in different species is worth stressing, and it remains to be seen whether this residue can take part in substrate binding, or if it is involved in the catalytic mechanism of the enzyme. It most likely forms the site of interaction with the cofactors nicotinimide ribose hydroxyl group shown in Figure 3.24 (c). The most conserved part of this motif within BVR-A however is the β6 sheet and the loop bridging the αE helix. Kikuchi *et al.,* 2001, has highlighted some similarities between E96 of BVR-A and E 128 of GFOR (shown in the alignments below).

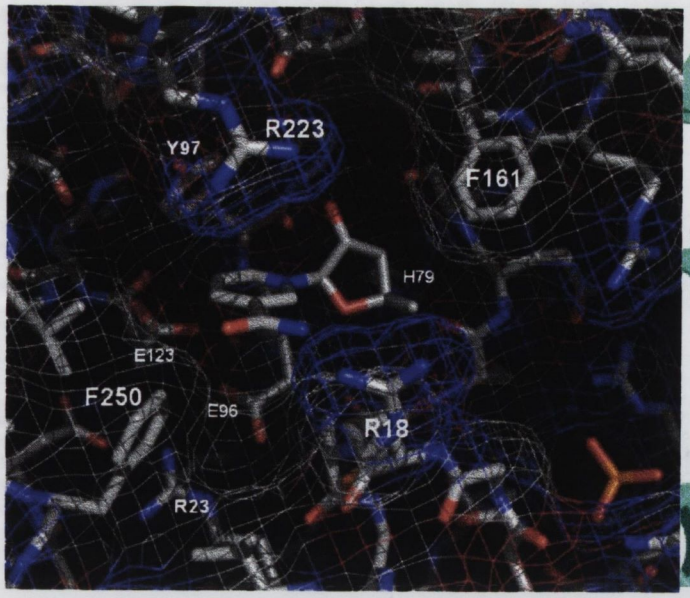

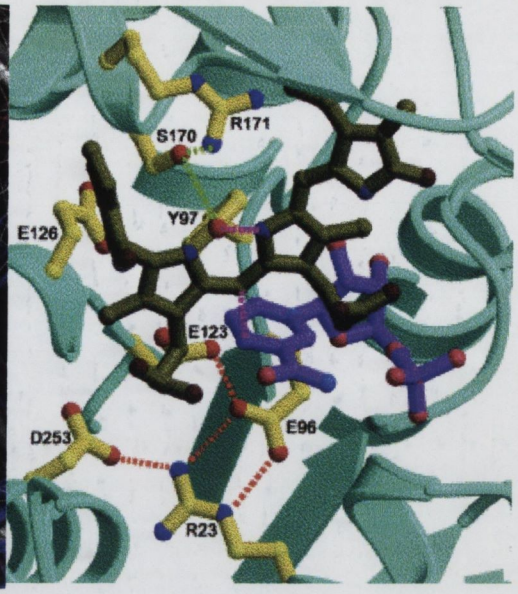

(a) (b)

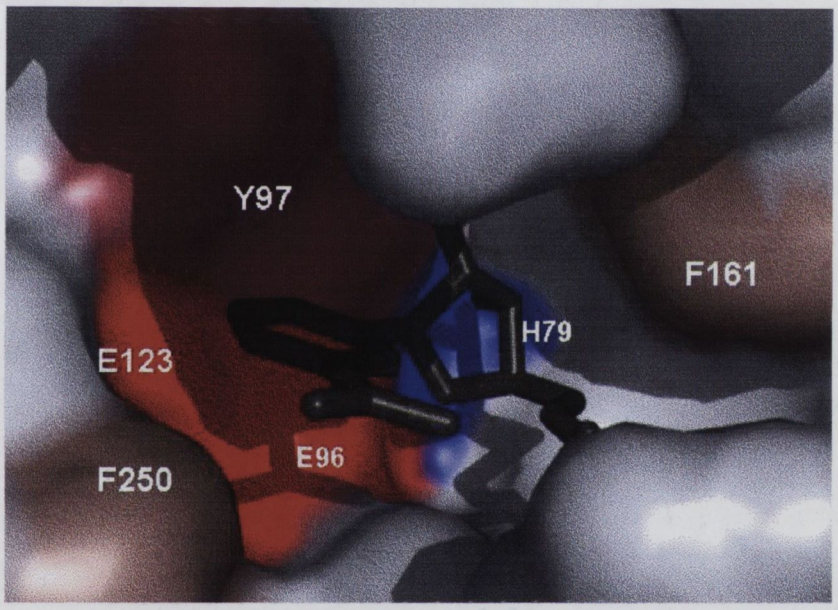

(c)

Figure 3.24 The substrate binding site of rat biliverdin-IXα reductase.

Pictures (a) and (c), show wire frame and surface representations of the active site respectively (pictures were generated using Pymol). The ribbon model of (b) shows the proposed position of substrates within the active site of rat BVR-A (taken from Whitby *et al.*, 2002). The conserved active site residues R23, E96, Y97, E123, E126, S170, R171, and D253 side-chains are shown as a ball-and-stick model. NADH is shown in purple and biliverdin in olive-green (the adenine half of the cofactor is omitted for clarity). The pink dashed lines represent Y97 donating a proton to the pyrrole nitrogen and the nicotinamide C4 carbon donating a hydride to the central carbon of the methene bridge.

```
GFOR        DPKIDAVYIILPNSLHAEFAIRAFKAGKHVMCEKPMATSVADCQRMIDAA
BVRA        SQEIDVAYICSESSSHEDYIRQFLQAGKHVLVEYPMTLSFAAAQELWELA
            . :**..**   .* * ::  : ::*****: * **: *.* .*.: : *
```

In the GFOR enzyme this residue hydrogen bonds to the amide group of the nicotinamide ring, and site directed mutagenesis by Kikuchi *et al.*, (2001) revealed that the E97A BVR-A mutant completely lost activity which supports this idea. Adjacent to E 96 in the rat structure are Y 97 and P 98 which form a loop between β6 and αE. Although the GFO/IDH/MOCA sequence is present in many oxidoreductases, it has become evident that biliverdin reductases are unique in that they are the only dehydrogenases to date containing the EYP motif at the centre of their active site. Many dehydrogenases have a lysine at this position (such as the 'EKP' motif in glucose fructose oxidoreductases, glucose-6-phosphate dehydrogenases and semialdehyde dehydrogenases). Other variations are 4-carboxy-2-hydroxymuconate-6-semialdehyde dehydrogenase having 'EIP', myo-inositol 2-dehydrogenase has 'EDP', while the predicted dehydrogenase protein product of the MviM gene in *Zymomonas mobilis* has 'DKP'. One could propose that the appearance of 'EYP' in a common ancestral reductase and its stringent conservation was a key step in the evolution of BVR-A as we know it.

The third area of conservation in BVR-A has the consensus sequence **L H x E H x E L** which extends from β7 through to the 3_{10}F helix. The residues within this sequence form a network of ionic interactions between H120 and D253 which helps to hold β7 and αL in position. H123 in embedded below the proposed catalytic residue Y97, and is seen to interact with E121. The β7 helix is packed between αE, αL and β6 through to the 3_{10}F helix. The negatively charged E96, E123 and E126 are all situated at the proposed binding site of the nicotinamide ring and this may play a part in the promotion of hydride transfer by stabilisation of $NADP^+$ (Whitby *et al.,* 2002). The hydrogen bonding between R171, S170, and Y97 may also serve to lower the pK_a of Y97. So the conservation in the β7 / 3_{10}F helix is vitally important and not only backs the 'catalytic' loop between β6 αE but it also forms part of the substrate pocket surface (Figures 3.27 and 3.28). For these reasons it is expected that this region would be highly conserved among all biliverdin reductases.

The last two regions of interest are the **FGFPXXXXXXRXXXXXXLFG** region positioned from αI to αJ (F161 to F169), and secondly the $^{I}/_{L}$ **F X X D** motif located between I 249 to D 253 located at the start of αL. These are both outside the GFO/IDH/MOCA region defined in Appendix III Figure 5. One interesting observation here is of the presence of two phenylalanines (F161 and F260), which protrude out of the active site surface. The position of these hydrophobic residues is somewhat curious as they are found directly opposite each other straddling the charges of Y97, E123, H79 and R171. It may be reasonable to suggest that F161 is positioned close to the biliverdin-IXα 'C pyrrole ring' and may 'insulate' it from other charged residues, which could interfere with proton transfer to the pyrrole nitrogen (see Figure 3.24). In a similar way F250 is positioned directly under the nicotinimide C4 adjacent to acidic region comprising of E96, E123 and E126. Again the high conservation of phenylalanine at this site would suggest that it may have a pivotal role in protecting the negative charges around the nicotinimide C4.

Looking at all the conserved residues mentioned it is important to note that these motifs are not widely dispersed through the structure, but are in immediate proximity to one another and combine to form a single conserved region around the active centre in the protein. Perhaps a good analogy of the functioning of many of the residues would be that of a 'knot' in a ribbon tie, which is at the heart of the structure holding all the functional catalytic elements in place.

Using the theory that all BVR-As have the conserved sequences mentioned, searches of the database identified a protein from the cyanobacteria *Anabaena variabilis* ATCC 29413 (accession number gi|75906978|ref|YP_321274.1|). It has been predicted to be a homoserine dehydrogenase type enzyme in the database. Analysis of the amino acid sequence indicates that this protein has a higher degree of similarity to the biliverdin reductase enzymes especially the cyanobacterial BVR-As than to the homoserine dehydrogenases as presented in Appendix II Figure IV. Also Suits *et al.*, (2005) reported the crystal structure of a novel *E.coli* haem oxygenase. In this study they make reference to a protein (the YhhX open reading frame in *E.coli* K12, O157:H7) which could be an *E.coli* biliverdin-IXα reductase and point out that it shares 19% sequence identity to the human biliverdin reductase. Looking at the sequence of this proposed

YhhX gene product we see that it does not fulfil the 5 criteria outlined for it to be a biliverdin reductase, the most important being that it has a lysine at the position of Y97 in the rat corresponds to lysine residue in YkkX protein. In fact this protein shares similar sequence homology to myo-inositol 2-dehydrogenases and 1-carboxy-3-chloro-3,4-dihydroxycyclo hexa-1,5-diene dehydrogenase. So in effect sequence homologies up to 20% can be expected between any members of the GFO/IDH/MOCA family upon alignments with different members of this family including BVR-A proteins. As a result the characterisation of a sub family encompassing all biliverdin-IXα reductases within the GFO/IDH/MOCA family is advantageous.

From Figures 3.1b and 3.1c it is evident that BVR-A is present in two very different lineages the archaeic cyanobacteria and vertebrates. It seems likely that these enzymes initially evolved in ancient bacteria like the cyanobacteria which used them in the regulation of phycobilin synthesis. As shown in Figure 3.1c, DNA encoding BVR-A is detected in members from 3 of the 5 classified groups of cyanobacteria. This would imply that biliverdin-IXα reductase emerged early in the development of cyanobacteria, and has been highly conserved since its ancient origins. The question arises why this enzyme is reported to be absent in many organisms. For example free living worms (*Caenorhabditis elegans*) and the parasitic helminths are unable to synthesise haem as they lack the necessary enzymes in the biosynthesis pathway (Rao *et al.*, 2005). As a consequence they are highly dependent on the acquisition of haem from the host for their survival.

As discussed in the introduction for many years it was assumed that biliverdin reductase was absent in birds, reptiles and amphibia. Bilirubin has been found albeit in low quantities in the bile of frogs chickens turkeys, alligators and turtles and in chicken bruises (Dolphin, 1979).

The great increases in genetic information and availability of gene sequence results is helping to clarify this age old confusion. To answer why BVR-A exists in some species but is reported to be absent in others, we must pose two questions. Firstly do these animals have the ability to express biliverdin reductase, that is has the gene been lost in the evolution of that particular species, and secondly, if the gene is present does the

protein encoded have activity. The characterisation of some of the predicted biliverdin-IXα proteins from representative species of birds, amphibia, and fish were initiated during this study.

Blast searches of the database reveal that the chicken (*Gallus gallus*) has a gene which encodes for a biliverdin reductase like protein. The gene is divided into 6 exons which are detailed in Appendix III Figures 3.1 and 3.2. The protein product is predicted to be 272 amino acids in length, and has all the characteristic motifs typical of the biliverdin-IXα reductases which are aligned in Figure 3.2. The strong degree of similarity to other biliverdin reductase sequences especially in the key catalytic sites suggests that the gene is strongly conserved. The EST (ChEST458f9) also spans much of exons I, II, III, and IV and its detection implies that mRNA is being transcribed. So from a genetic level, the chicken seems to have the ability to produce an intact functional BVR-A like protein. With the availability of turkey blood during this study it was thought that an examination of biliverdin-IXα reductase activity would prove informative. As can be seen in Figure 3.15 biliverdin-IXα reductase activity was detected in turkey cytosol. This activity was shown to be protein dependent as increased volumes of cytosol showed the expected linear relationship between the initial rate and enzyme activity. This provides good evidence of a biliverdin reductase activity in turkey and future work involving a full purification of this protein is anticipated. Amplification attempts on a chicken cDNA library may also prove productive.

The full length cDNAs encoding human, *Danio Rerio*, murine, and *Xenopus* BVR-A were successfully amplified and subsequently cloned into various expression vectors (pET4a-Mod for human and *Danio Rerio*, ppMAL for the murine and pGEX-KG for the *Xenopus* enzyme). To date human BVR-A pET41a-Mod, murine BVR-A ppMAL, and *Xenopus* BVR-A pGEX-KG transformed cultures have been induced with IPTG resulting in the expression of recombinant proteins which display the appropriate molecular weights. The human and murine enzymes have been purified to homogeneity and are catalytically active. The Xenopus BVR-A protein is active as a GST fusion however during incubations to cleave the GST tag with thrombin stability problems have been encountered. Further work is necessary to obtain a homogenous *Xenopus* BVR-A fraction. The rat human and *Synechocystis* BVR-A enzymes were all induced

at 30°C with 200 μM IPTG. In fact with all these proteins the induction temperatures and incubation times, rather than the IPTG concentration, were the most influential parameters affecting protein yields. The conditions outlined in Section 2.4, produced maximum soluble yields. One exception was the murine enzyme as it was necessary to induce the murine enzyme at 27°C as higher temperatures resulted in diminished yields with much of the protein being expressed in inclusion bodies. Sequence analysis of the recombinant human BVR-A pET41a-Mod plasmid, and the murine BVR-A ppMAL plasmid reveal that the cDNA inserts are intact and in frame as discussed in Sections 3.8.4 and 3.5.6. Attempts to solve the three dimensional structure of the human and murine BVR-A enzymes are ongoing and in collaboration with Dr. Amir Khan, School of Biochemistry and Immunology, Trinity College, Dublin.

In a preliminary survey of the tissue distribution of the mouse enzyme it was noted that higher activity was always found in tissues from male mice. This was particularly noticeable in liver (Figure 3.12). It is interesting that bovine and lapine liver have been reported previously to have very low levels of BVR activity. In the case of bovine liver it is unclear as to the sex of the animals.

Chapter Four

The nature of the dual pH-cofactor specificity of BVR-A

The most unusual feature associated with the kinetics of BVR-A is the fact that it is said to have two distinct pH optima. NADH is preferentially used between pH 6 and 7 while NADPH is the preferred cofactor between pH 8.5 to 8.7. Both native and recombinant human and rat BVR-A enzymes (Maines *et al.*, 1983, Yamaguchi *et al.*, 1994, Maines *et al.*, 1996, and Kutty & Maines 1981) the ox kidney enzyme, (Rigney *et al.*, 1986) and the pig spleen enzymes (Noguchi *et al.*, 1979) all share this interesting pH dependent behaviour (pH profiles for human and rat BVR-A are presented in Figures 4.1a and 4.1b). Of the non mammalian enzymes studied the salmon liver has a slightly lower pH optimum between 5.5 and 6.2, while its NADPH dependent activity displayed increasing activity at the extremes of the pH ranges studied, and showed minimal activity at physiological pH (Figure 4.1c). BVR-A from the liver of the eel (*Anguilla japonica*) also displays this behaviour (Fang & Lai, 1987). Interestingly one notable exception to this dual pH behaviour is the cyanobacterial BVR-A (Figure 4.1d). It displays maximal activity at pH 5.8 when using either NADPH or NADH as cofactor (Schluchter & Glazer 1997). NADPH however is the cofactor which provides maximal activity at this pH. Although all the enzymes mentioned can use both cofactors to catalyse the reduction of biliverdin-IXα, it is important to note that of the biliverdin-IXα reductases examined from various species NADPH is the preferred cofactor with apparent K_M values close to two orders of magnitude below that for NADH. It must be noted that the approximate concentrations of pyridine nucleotides in the liver of rat have been reported as 120 μM for NADPH, 35 μM for NADP, 70 μM for NADH, and 500 μM for NAD (Llorente *et al.*, 1970, Marco *et al.*, 1974). With the apparent K_M for NADPH of biliverdin reductases being in the low micro molar range, typically 1-10μM, the enzyme itself is most likely saturated with NADPH in vivo. In contrast, the apparent K_M for NADH is generally reported between 300 and 500mM, and with cytosolic concentrations of NADH generally around 70 μM this is unlikely to be a physiologically significant substrate.

Despite having such similar structural characteristics, NADH and NADPH generally participate in very different enzymatic processes. NADPH is generally the cofactor of choice for reductive biosynthesis, whereas NAD^+ is used mainly in oxidative degradations that ultimately yield ATP. Enzymes that utilize pyridine nucleotides as cofactor transfer a

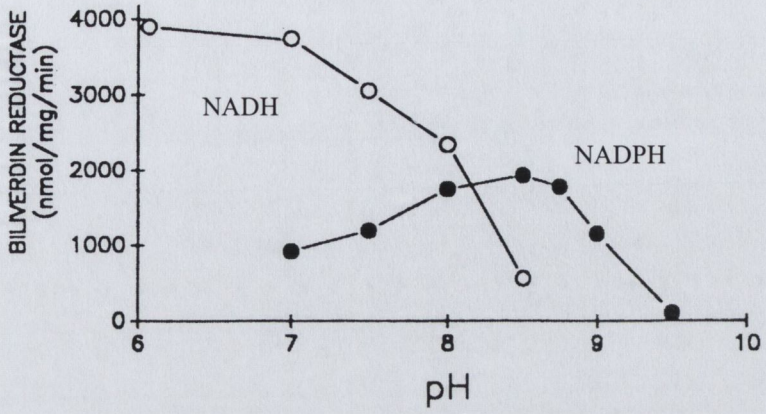

Figure 4.1a The effect of pH on the activity of human biliverdin-IXα reductase activity (Maines & Trakshel, 1993).

Enzyme activity with NADH was measured using phosphate buffer at the indicated pH range, whereas activity with NADPH was assayed using Tris-HCl buffer. NADH dependent (○) activity, NADPH dependent (●) activity.

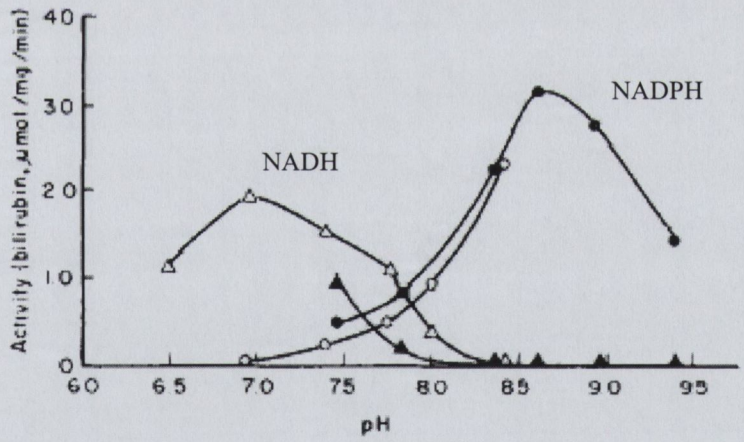

Figure 4.1b The effect of pH on the activity of rat biliverdin-IXα reductase activity (taken from Kutty & Maines, 1981).

The effect of pH on the activity of rat liver biliverdin-IXα reductase (Kutty and Maines, 1981). Enzyme activity with 1 mM NADH as cofactor in Tris buffer (▲), activity with 100 μM NADPH in Tris buffer (●), activity with 100 μM NADPH in phosphate (○), and activity with 1mM NADH in phosphate buffer (Δ).

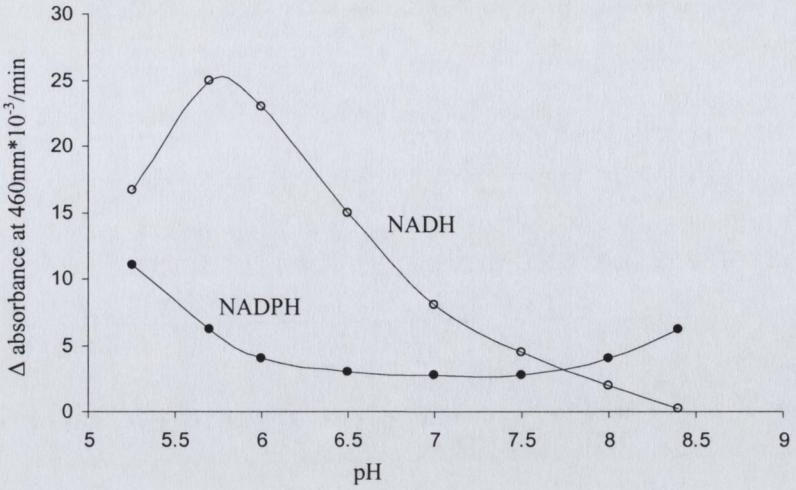

Figure 4.1c The effect of pH on salmon liver biliverdin-IXα reductase activity (taken from Elliott, 1996).

In summary the optimal activity of salmon liver BVR-A when using NADH as cofactor is pH 6, whereas the NADPH dependent activity displays a broad activity which is maximal at either end of the pH range studied. 100mM sodium phosphate was used from pH 5.3 to 7.5, and glycine used from pH 7.5 to 8.4.

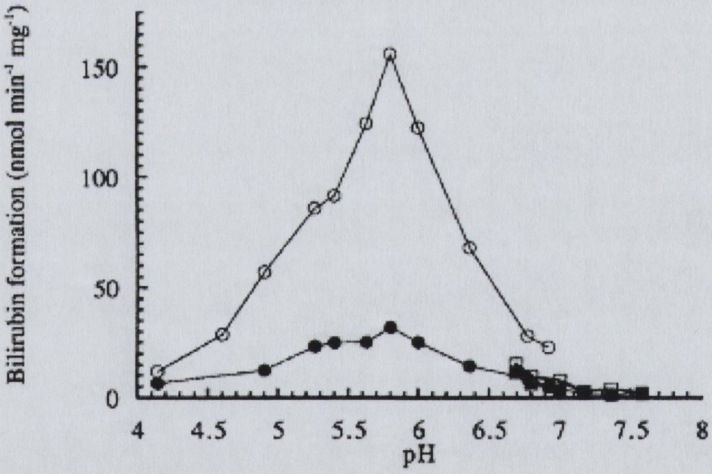

Figure 4.1d The effect of pH on the activity of synechocystis biliverdin-IXα reductase activity (taken from Schluchter, 1997).

The effect of pH on NADH (●) and NADPH (o) dependent activities are shown in Figures 4.1a and 4.1b. The synechocystis enzyme however Figure 4.1b displays a pH optimum of 5.8 for both NADH and NADPH dependent activity. NADPH dependent activity was measured in 100mM sodium citrate (○), and 100mM potassium phosphate (□). NADH dependent activity was measured in citrate (●) and 100mM potassium phosphate (■).

hydride ion from position C4 of the nicotinamide ring in a stereospecific way. Biliverdin-IXα reductase from rat (Ennis *et al,* 1996) and human (Dunne, 2000) have both been shown to transfer the hydride from the B-face position of the nicotine ring. With the only difference between NADPH and NADH being at the 2' phosphate position, the presence (NADPH) or absence (NADH) of this phosphoester provides a discriminatory method which ultimately governs the nucleotide preference of the enzyme itself (Argos & Carugo 1997, Didierjean *et al.*, 1997 and Elmore *et al.*, 2002). The cofactor-enzyme interactions which allow successful binding of either NADH or NADPH occurs mainly through hydrogen bonds of the phosphate moieties and the ribose hydroxyl groups of each cofactor, with the back bone amide groups of the protein.

Generally an acidic residue Asp or Glu is present at the C-terminal edge of the β-2 strand in proteins that use NADH as cofactor. Such negatively-charged residues can interact productively with the 2'OH group of the adenosine ribose of NADH but preclude the 2'phosphate anion. In contrast where NADPH is the preferred residue this site is occupied by small hydrophobic residues. Meanwhile positively charged residues are present around the pocket which interacts with the negatively charged 2' phosphate of the adenosine ribose of NADPH. Site directed mutagenesis studies of positively charged amino acids such as lysine and arginine, and their replacement with uncharged amino acids (Bocanegra *et al.*, 1993; Shen *et al.*, 1999; Dohr *et al.*, 2001) significantly increases the Km for NADPH without affecting the Km for NADH in some enzymes.

The crystal structures resolved by Kikuchi *et al.*, (2001) and Whitby *et al.*, (2002), show that there is only one nucleotide binding site in BVR-A, which is defined by the Rossmann fold the sequence of which encompasses residues Gly 15, Val 16, Gly 17, Arg 18, Ala 19 and Gly 20. These residues are found spanning the loop between β1 and αA. The nicotinamide moieties of both NADH and NADPH are proposed to extend into the active site of BVR-A in a well defined position and orientation (Kikuchi *et al.*, 2001). If there is only one binding site for both the nucleotides, and the C4 carbon positioning of the NADH and NADPH nicotinamide rings are identical, one must question why there is such a difference in activity when using each nucleotide as cofactor over the pH ranges studied. The mechanism of hydride transfer at any given pH using each nucleotide is expected to be

identical, and therefore it is rational that the differences in activities is most likely as result of different modes of binding NADH and NADPH.

Of the two crystal structures for rat BVR-A only one (Whitby *et al*, 2002) has bound pyridine nucleotide (NAD). This is bound in an unusual conformation with the adenine ring stacking over the nicotinamide. This precludes productive binding of biliverdin and the authors suggest that packing in the crystal has produced a conformation of NAD that is unlikely to be adopted in solution. It is also possible to model an extended conformation and to predict that both NADH and NADPH can occupy this site. Kikuchi *et al* (2001) have tentatively identified Arg 44 and Arg 45 as residues important in binding the 2'-phosphate of NADPH. It is intriguing therefore that closer examination of the structure reported by Whitby *et al.,* (2002) reveals three phosphate anions bound to rat BVR-A with one in the putative 2'-phosphate pocket (Figure 4.1e).

4.1 Effect of pH on the stability, activity and cofactor selectivity of biliverdin-IXα reductases from various species

4.1.1 The effects of pH on the stability of various BVR-As.

To determine the stability of the rat, murine and human recombinant BVR-A, the enzymes were pre-incubated in various buffers over the pH range 5 – 9. BVR-A was diluted 10 fold to a concentration of 0.1 mg/ml in 100 mM buffer at each pH. The diluted mixtures were incubated at 30°C for 10 minutes in the buffers indicated, after which time 10μl aliquots were assayed in 100mM Tris-HCl pH 8 (final volume 2ml), with a final concentration of 100 μM NADPH and 10μM biliverdin. The human enzyme (Figure 4.1a) loses no more than 5 – 10% of its activity even at the extremes of pH tested (5 – 9). Under the conditions examined the enzyme was relatively dilute (0.1mg/ml) and was pre-incubated for 10 minutes at the various pH values. In kinetic studies the reaction was generally initiated by the addition of enzyme and the initial rate measured from the initial 10 – 20 seconds of the reaction. It is unlikely therefore that any significant inactivation due to pH occurred in these initial rate experiments. The rat enzyme exhibited a similar tolerance to pH but was marginally less stable at alkaline values, losing 25% of its activity at pH 9 after a 10 minute pre-incubation (Figure 4.1b). The mouse enzyme is considerably less stable at both

Figure 4.1e The nucleotide binding site of BVR-A and its interaction with inorganic phosphate.

Panel A; A cartoon diagram of BVR-A displaying the three phosphates in red which co-crystallised with the enzyme.

Panel B; A space-fill model of the enzyme showing the inorganic phosphate anion (PO_4^{-3}) which is bound to the proposed NADPH 2' phosphate binding site. The active site Y97, above which the nicotinimide and biliverdin sit, is also highlighted.

Panel C and D; Space-filled models which show the nucleotide binding pocket with and without a bound phosphate anion.

Panel E and F; The residues which are involved in binding the 2' phosphate of NADPH and (PO_4^{-3}) anions. The binding pocket consists of positively charged residues S43, R44 and R45 which co-ordinate with the phosphate anion.

Panel G and H; The nucleotide binding domain of BVR-A (Panel G), is compared to the corresponding domain of glucose–fructose oxidoreductase (GFOR) from *Zymomonas mobilis* (Panel H). The Rossmann fold shown in red is located between the end of β1 and the start of α1 of BVR-A. The binding pocket consists of positively charged residues namely S43, R44 and R45 which in conjunction with the Rossmann fold co-ordinate with NADPH and also with phosphate anions. A similar fold and the distribution of positively charged residues facilitating the interaction of the phosphate moiety of NADPH exist in the GFOR structure.

All pictures were constructed using pymol (http://pymol.sourceforge.net/) from the crystal structure 1LC3.pdb of Whitby *et al.*, (2002), coordinates of which are accessible through the protein bank (Bermann *et al.*, 2003).

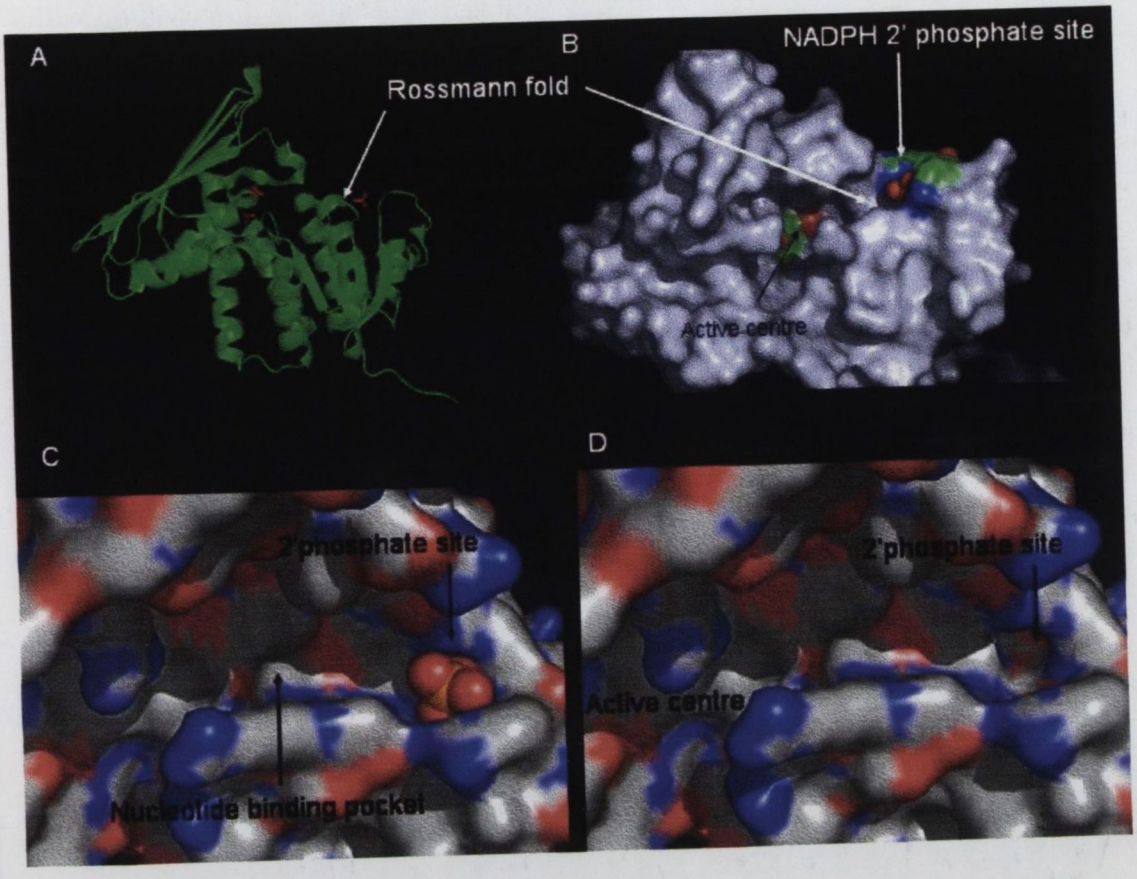
A
Rossmann fold
B
NADPH 2' phosphate site
Active centre
C
2'phosphate site
Nucleotide binding pocket
D
2'phosphate site
Active centre


E
Arg 44
Arg 45
Ser 43
F
G
H

acid and alkaline pH values and even at pH values between 6 and 8 loses 10 – 20% activity after 10 minutes incubation at 30°C (Figure 4.1f). The relative instability of murine BVR-A at acid pH values prompted a further investigation to determine the kinetics of inactivation at pH 4 and 4.5. After 10 minutes pre-incubation at pH 4.5, only 10% of the activity remained (Figure 4.2a) in agreement with the data in Figure 4.1f. However 50% activity remains after 2 minutes pre-incubation at pH 4.5 (Figure 4.2a) and extrapolation suggests that measurements up to 30 seconds at pH 4.5 will yield 90% of the original activity. It is not possible to extend this level of confidence to pH 4 where only 50% activity remains after 30 seconds pre-incubation (Figure 4.2b). The degradation of NADH and NADPH under acid conditions has been reported in numerous studies (Wu *et al.*, 1986 and Lowry *et al.*, 1961). It is clear from these studies that both temperature and pH affect the rate of NADPH and NADH degradation substantially. Wu *et al.*, (1986) found that at 30°C, the half life of NADPH was just 38 minutes at pH 5. As a result it was necessary to clarify the extent of nucleotide breakdown in the assay buffers and pH range used during the present study. The absorbance of 150 μM NADH and 150 μM NADPH was monitored over the pH range 5-9 at 30°C, the results of which are shown in Figure 4.3. There is a marked increase in the breakdown of NADPH (2.6 $\mu M.min^{-1}$) and NADH (1 $\mu M.min^{-1}$) at pH 5, with NADPH being the most unstable. Resulting from the information obtained in these experiments, it was decided that stock solutions of each nucleotide were to be prepared freshly on the day of use in 100mM Tris-HCl pH 8 and stored on ice to minimise degradation. The reduction of biliverdin-IXα to bilirubin-IXα over the pH range was shown to be enzyme dependent. All BVR-A assays were measured at 460nm and the initial rates were calculated over the earliest time points (the first 30 seconds of the reaction) to avoid the added complexity of significant nucleotide breakdown.

4.1.2 The effect of pH on the activity of BVR-A

As mentioned in Chapter 1, BVR-A can use either NADH or NADPH as cofactor. Maines and co-workers have stressed an apparently unique property of BVR-A, namely that it has a different pH optimum for each nucleotide (Figure 4.1a). It is important to note that of all the BVR-A enzymes characterised to date the *Synechocystis PCC6803* enzyme is the only form where activity has been surveyed over the entire pH range using both nucleotides (Schluchter & Glazer, 1997). All published work regarding the human and rat enzymes has

Figure 4.1f Stability of BVR-A upon 10 minute pre-incubation at various pHs.

The stability of BVR-A from various sources was assessed over the pH range 4 to 9. The enzyme was pre incubated for 10 minutes in various buffers at 30°C before being assayed for BVR activity in 100mM Tris/HCl buffer at pH 8 using 100μM NADPH and 10μM biliverdin-IXα as substrate.

(i) Stability of the human enzyme.

(ii) Stability of the rat enzyme.

(iii) Stability of the murine enzyme.

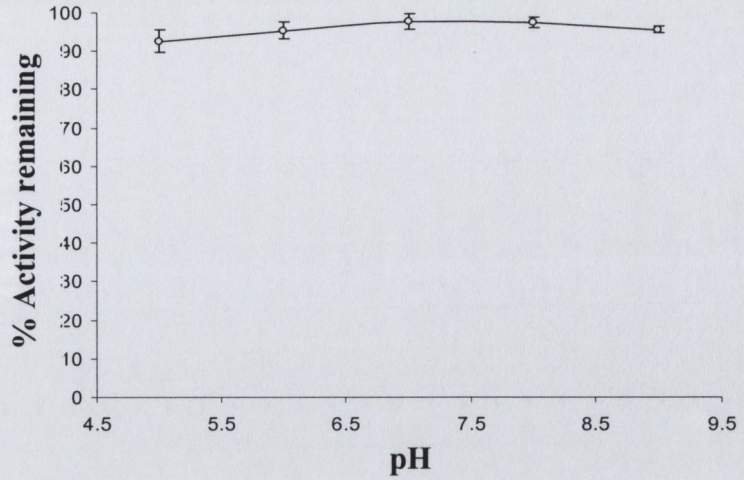
% Activity remaining
100
90
80
70
60
50
40
30
20
10
0
4.5
5.5
6.5
7.5
8.5
9.5
pH

(a)

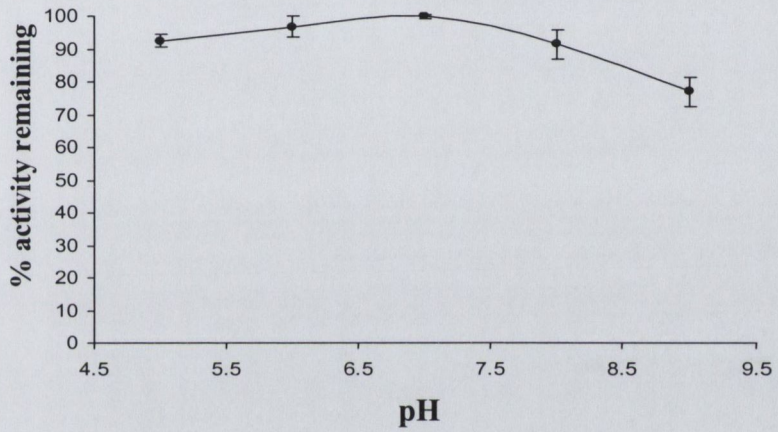
% activity remaining
100
90
80
70
60
50
40
30
20
10
0
4.5
5.5
6.5
7.5
8.5
9.5
pH

(b)

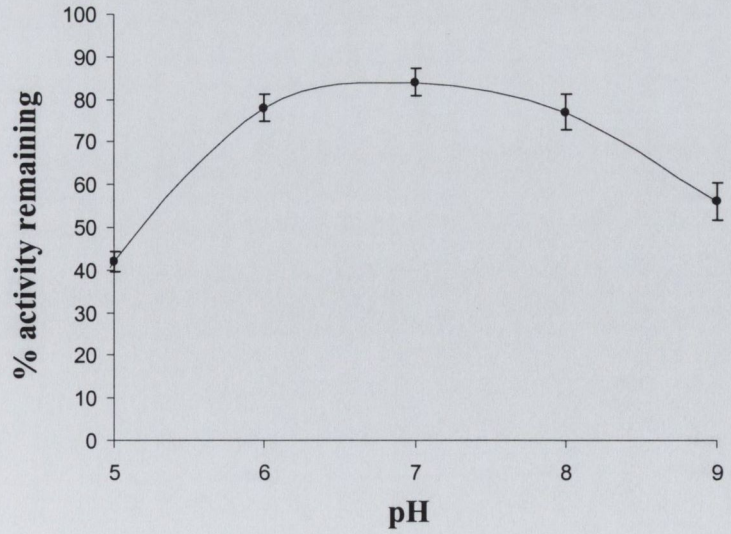
% activity remaining
100
90
80
70
60
50
40
30
20
10
0
5
6
7
8
9
pH

(c)

Figure 4.2 The activity of murine BVR-A after pre-incubation at pH 4 and pH 4.5 over different time points.

The time dependence of pH inactivation of murine BVR-A at pH 4 (a), and pH 4.5 (b) was determined. The enzymes was pre incubated over various time points (0 - 10 minutes) in 100mM Sodium Citrate pH 4 and pH 4.5, at 30°C as described in Section 4.1 before being assayed for BVR activity in 100mM Tris/HCl buffer at pH 8 using 100μM NADPH and 10μM biliverdin-IXα as substrate.

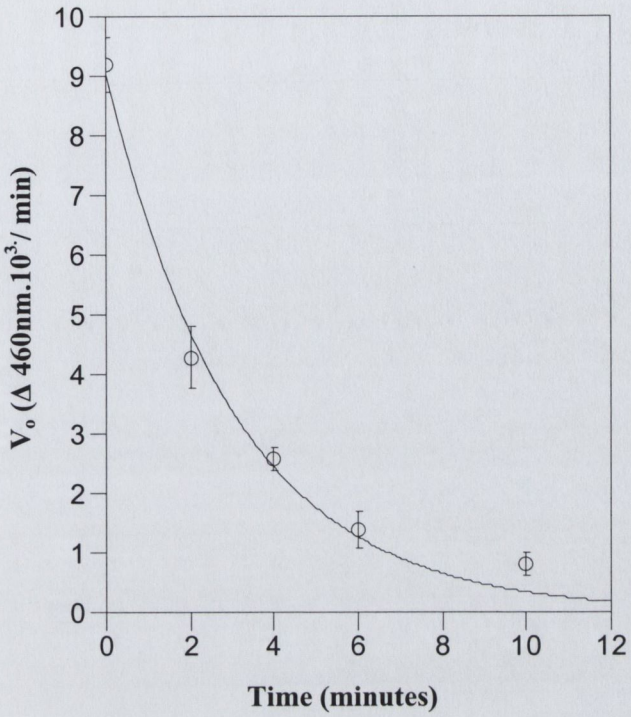
10
9
8
7
6
5
4
3
2
1
0
0
2
4
6
8
10
12
V₀ (Δ 460nm.10³⁻/ min)
Time (minutes)

(a)

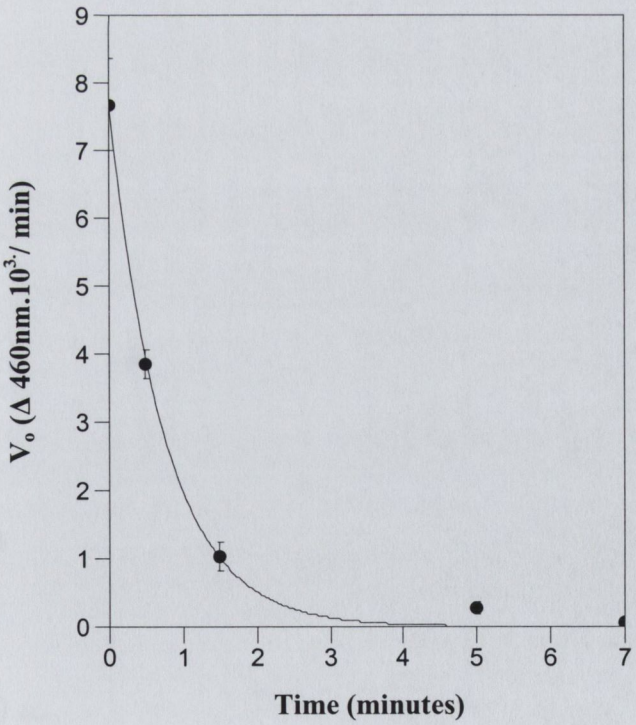
9
8
7
6
5
4
3
2
1
0
0
1
2
3
4
5
6
7
V₀ (Δ 460nm.10³⁻/ min)
Time (minutes)

(b)

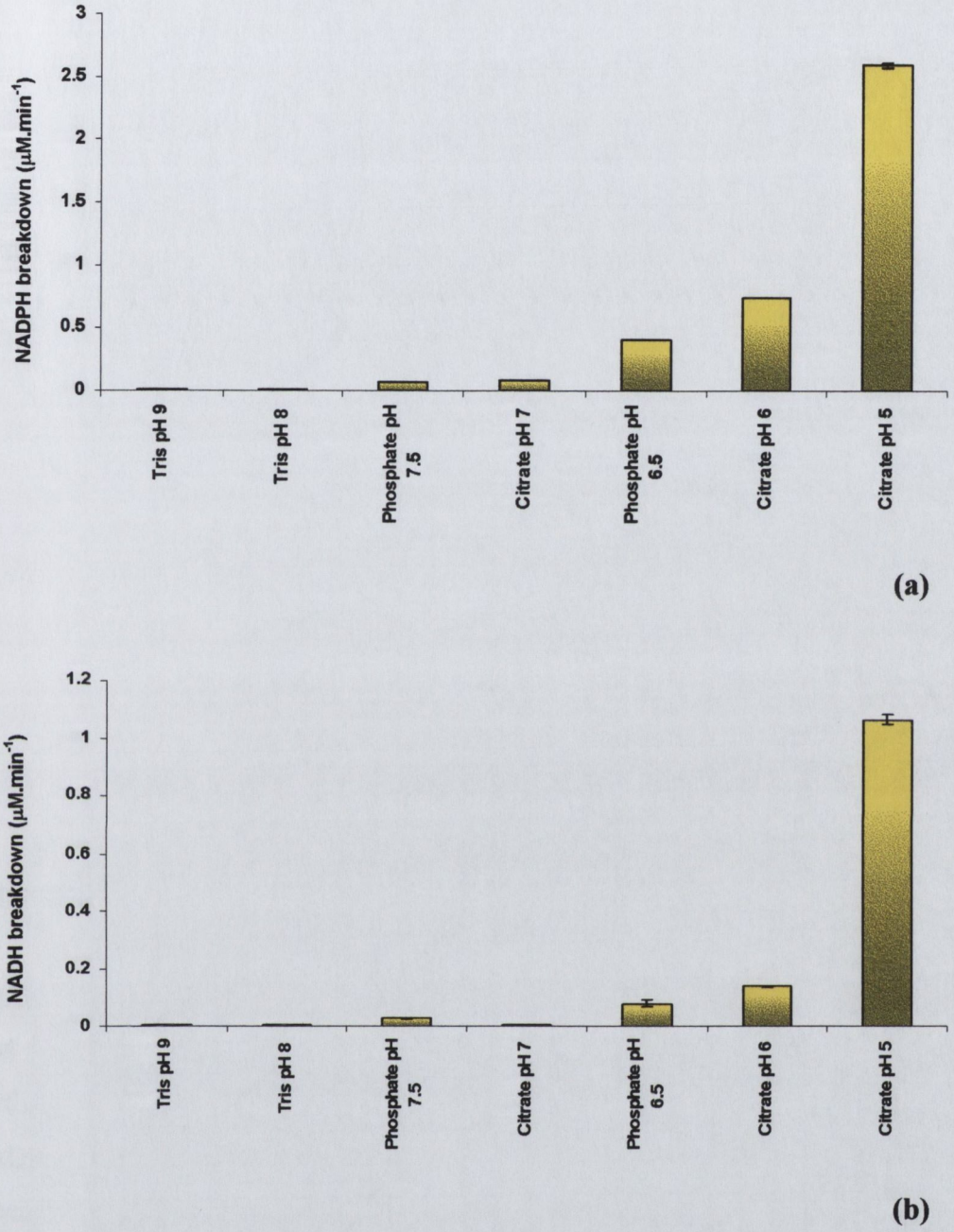

Figure 4.3 Determining the stability of NADH and NADPH over the pH range 5 - 9.

Figures (a) and (b) show the rate of breakdown of NADPH and NADH respectively. Rates of breakdown were determined by monitoring the decrease in absorbance (at 340nm) of 150μM of each nucleotide in 100mM buffered solution over the pH range 5 – 9.

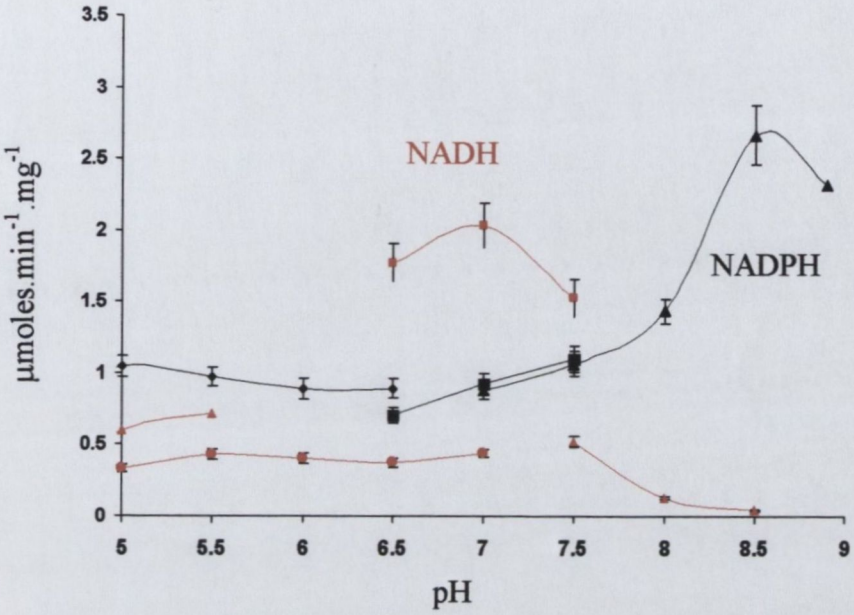

Figure 4.4a **Effect of pH on the activity of rat biliverdin-IXα reductase.**

Buffers used were 100 mM sodium citrate (♦), 100 mM sodium phosphate (■), 100 mM Tris (▲) and also with sodium acetate in the acidic region (▲). Assays were performed using 10 µM biliverdin as substrate and either 700 µM NADH or 100 µM NADPH as cofactor. NADH dependent activity is presented in red while NADPH dependent activity is presented in black.

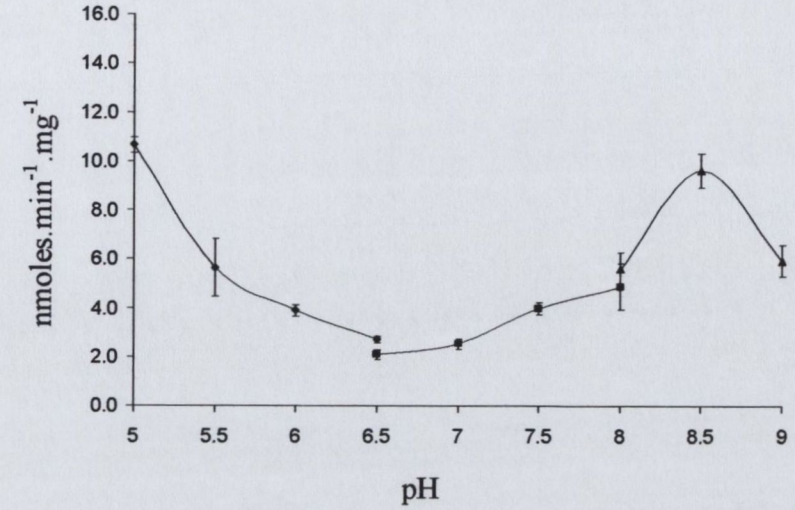

(a)

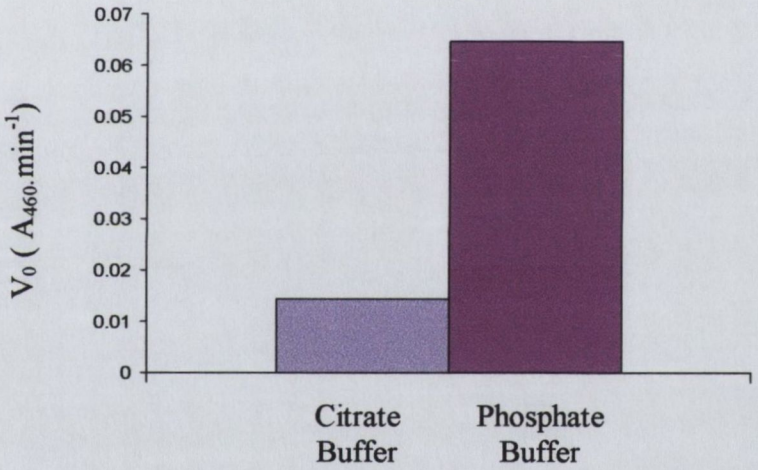

(b)

Figure 4.4b **Effect of pH on the activity of *Xenopus* biliverdin-IXα reductase.**

(a) Buffers used were 100 mM sodium citrate (♦), 100 mM sodium phosphate (■), and 100 mM Tris (▲). Assays were performed using 10 μM biliverdin as substrate and 100 μM NADPH as cofactor.

(b) The effect of sodium phosphate buffer on *Xenopus* BVR-A at pH 7 using 700μM NADH as cofactor and 10μM biliverdin as substrate.

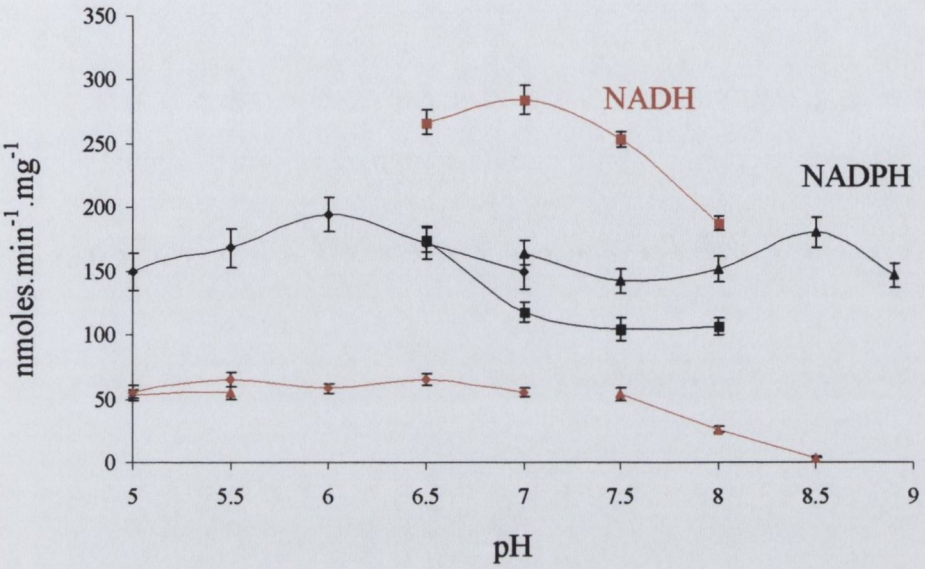

Figure 4.4c **Effect of pH on the activity of human biliverdin-IXα reductase.**

Buffers used were 100 mM sodium citrate (♦), 100 mM sodium phosphate (■), 100 mM Tris (▲) and also with sodium acetate in the acidic region (▲). Assays were performed using 10 μM biliverdin as substrate and either 700 μM NADH (in red) or 100 μM NADPH (in black) as cofactor in the buffers indicated.

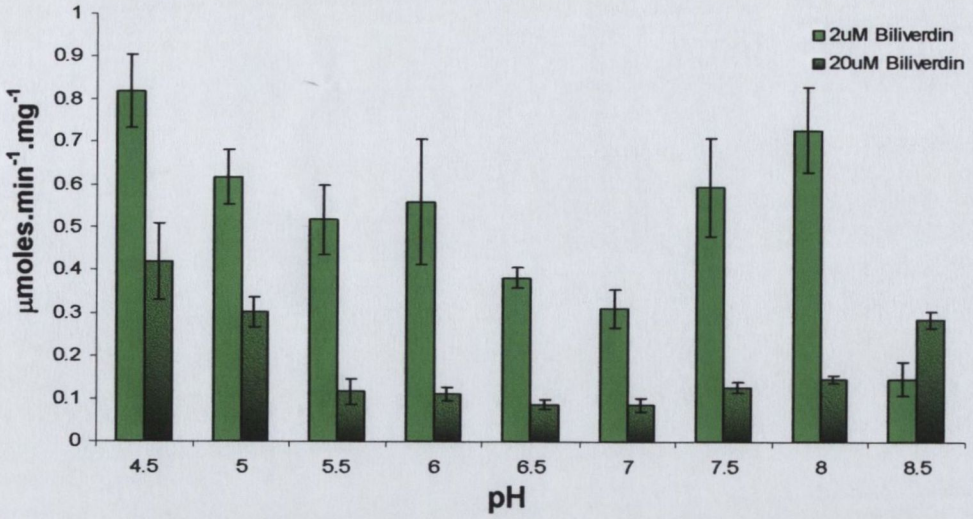

(a)

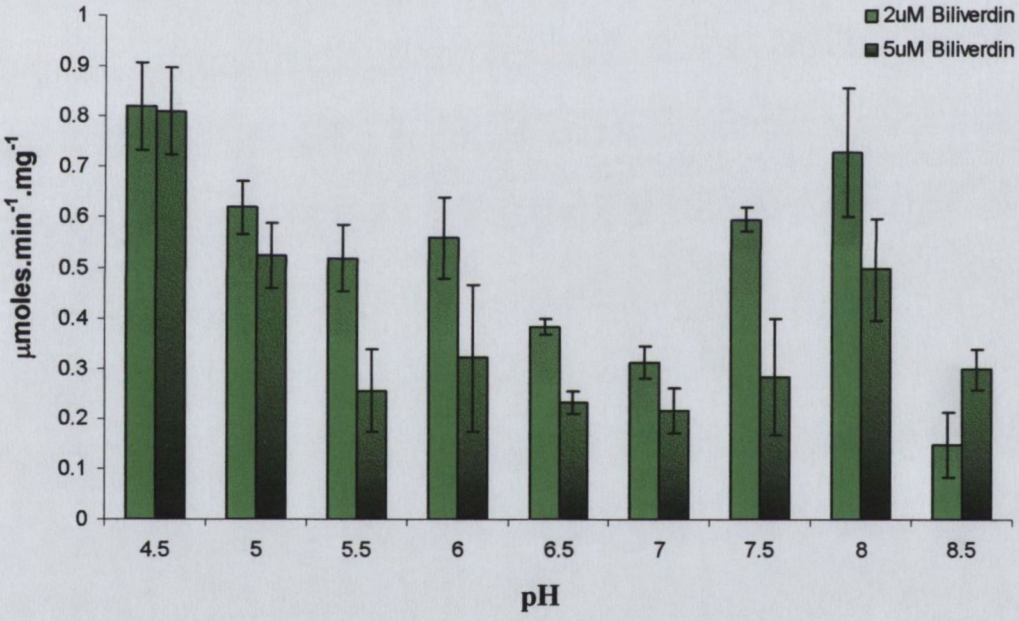

(b)

Figure 4.5 The effect of pH and biliverdin-IXα concentrations on the initial rate of human BVR-A using NADPH as cofactor.

Bilirubin production was monitored at 460nm and individual reactions contained a final concentration of 100µM NADPH with Figure 4.1xx (a) showing the results for 2 and 20µM biliverdin-IXα and Figure 4.1x (b) showing the results for 2 and 5 µM biliverdin-IXα over the pH range 4.5-8.5. The reaction temperature was maintained at 30°C throughout these experiments.

failed to examine the NADPH dependent activity below pH 7. There is a lack of knowledge regarding NADPH dependent activity below pH 7 which is very curious especially considering that NADPH is the preferred cofactor for the *Salmo salar* and *Synechocystis* BVR-A enzymes at pH 6. Having conducted preliminary pH stability experiments it was felt that a more in depth examination of the effect of pH on the activity of BVR-A was warranted.

A series of reactions were set up to determine the effects of pH on the activity of human, rat and xenopus BVR-A. Bilirubin production was monitored at 460nm at 30°C. Nucleotide concentrations of 100 μM NADPH and 700 μM NADH were used in 100 mM buffer at the desired pH. Buffers used were sodium acetate (pH 5-6), sodium citrate (pH 5-6.5), sodium phosphate (pH 6.5-8) and Tris-HCl (pH 8-9). Each assay was started by the addition of enzyme. The pH profiles obtained are presented in Figures 4.4a, b, and c.

During the course of these experiments three interesting observations were made. The first is that the use of phosphate buffers substantially increased the rate for the NADH-dependent reaction over the pH range (from pH 6-8) used in these experiments. The second point worth noting is that the NADPH-dependent activity of the human, rat and mouse enzymes is clearly not just limited to the pH range of 7.5 to 9. Thirdly, the concentration of biliverdin used in these studies is a very influential parameter with respect to the pH profile observed (see Figure 4.5). It was decided to investigate these observations in some detail.

4.2 Studies on phosphate activation of human BVR-A

4.2.1 The effects of various anions on the activity of human BVR-A

Figure 4.6 shows the effect of increasing concentrations of phosphate buffer (pH 7) on the activity of human BVR-A with NADH as the cofactor. The data fits well to the Hill equation, as illustrated, however there are probably effects due to ionic strength and additional specific activation by phosphate. The activity in 5mM phosphate is 0.04 $\mu moles.min^{-1}.mg^{-1}$ and in 200mM phosphate this increases 37.5 fold to 1.5 $\mu moles.min^{-1}.mg^{-1}$ (Figure 4.6). To determine whether this effect was specific to phosphate a range of concentrations of various buffers at pH 7 was tested. Assays were performed with 20μM

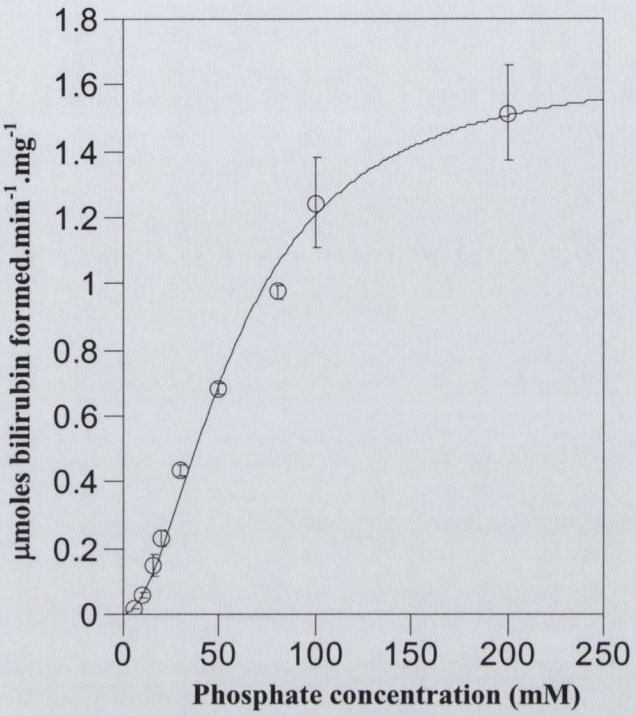

Figure 4.6 The effect of phosphate on the activity of human BVR-A.

Assays were performed with 20µM biliverdin and 700µM NADH at 30°C with increasing sodium phosphate, at pH 7.0 (○). The reaction was started on addition of enzyme. Experimental data obtained from the effect of phosphate on the activity of human BVR-A is fitted to the Hill equation, the results of which are presented in Appendix IV Figure 1.

biliverdin and 700 μM NADH at 30°C in incremental concentrations of sodium phosphate (2, 5, 10, 25, 50, 75, 100 and 200 mM) and sodium carbonate, Tris-HCl and sodium citrate (all at 10, 50, 100 and 200 mM) at pH 7.0. The reaction was started by the addition of enzyme. The pH of each assay were tested before and after the assay to ensure that pH did not alter through the course of the assay especially when using salts at the limits of their buffering capacity (see Appendix III for a full list of buffer ionisation constants). The results of the experiment detailed in Figure 4.7 clearly demonstrate that phosphate is a powerful activator using NADH as cofactor. There is a modest ionic strength effect as shown by the increase in initial rates seen with increasing concentrations of sodium citrate, Tris-HCl and sodium carbonate up to the 200 mM. The effect of phosphate on enzyme activity is particularly noticeable however. Following this observation it was decided to look at the effects of pyrophosphate. Although pyrophosphate has similar properties to phosphate the size differences between the two anions might impede the ability of pyrophosphate to activate the enzyme. The results of this are shown in Figure 4.8. Interestingly pyrophosphate also displayed an activatory effect, indeed the potency observed was greater than that obtained with phosphate. It is also clear from Figure 4.8 that the anion activation seen with both phosphate and pyrophosphate is specific for NADH as cofactor as only a very modest increase in activity was seen with NADPH as cofactor over the same range. The basis for the activation however was unclear from these results. Phosphate may allow substrates to bind more productively to the enzyme or enhance turnover. At this point it was felt that an analysis of the effect of phosphate on the Michaelis constant for NADH may prove informative.

4.2.2 The effects of phosphate on the NADH dependent activity of human BVR-A

A series of saturation curves were generated with NADH as the variable substrate (20 μM to 3.2 mM) in 10, 50, 100, and 200mM sodium phosphate pH 7. Biliverdin-IXα at a final concentration of 20 μM was used as substrate and the reaction was performed at 30°C. As shown in Figure 4.9, phosphate has a potent effect on the apparent K_m for NADH. Data points were fitted to the Michaelis equation as outlined in Section 2.5.1 (Equation 2.1). The rectangular hyperbolas generated by these fits were used to obtain the apparent K_m and V_{max} (Table 4.1). Increasing phosphate from 10mM to 200mM causes over a 150-fold

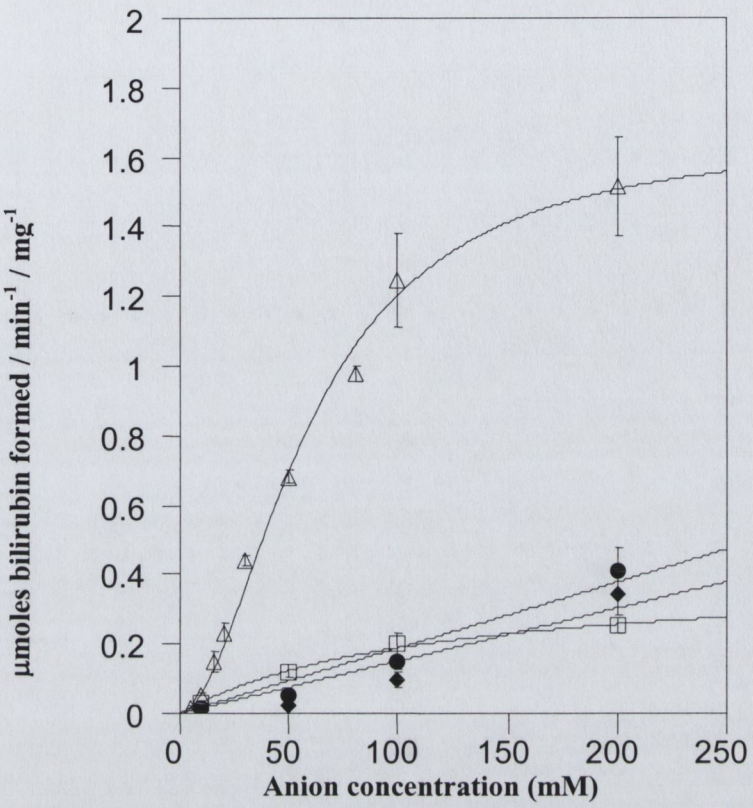

Figure 4.7 The effect of various anions on the activity of human BVR-A.

Assays were performed with 20µM biliverdin and 700µM NADH at 30°C in various buffer concentrations (Δ sodium phosphate, ♦ sodium carbonate, ● Tris, □ sodium citrate) at pH 7.0.The reaction was started on addition of enzyme.

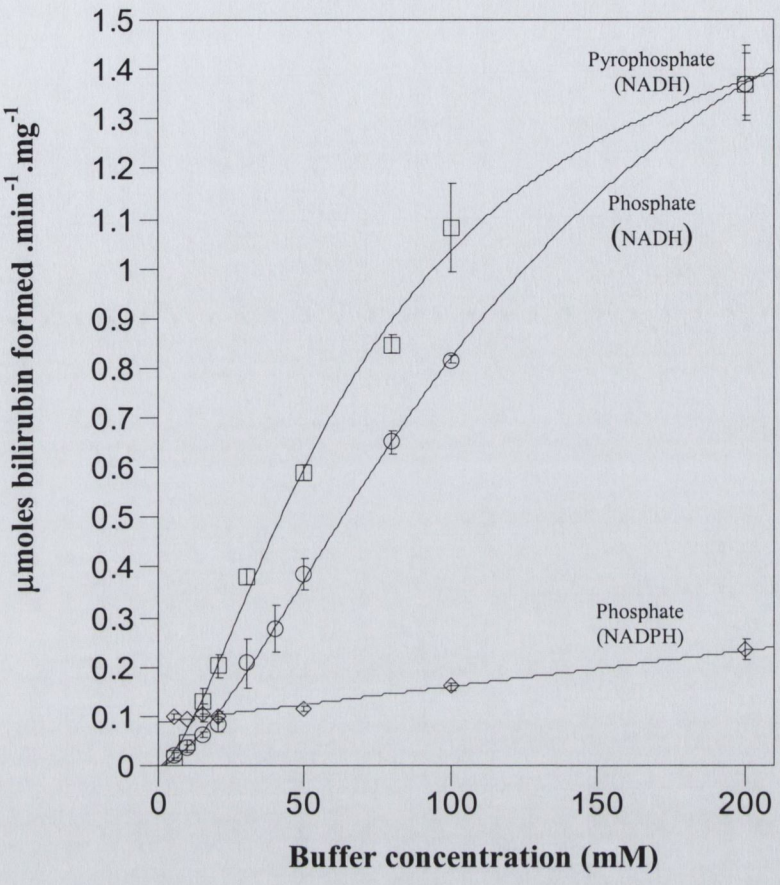

Figure 4.8 The effects of sodium phosphate and sodium pyrophosphate on the activity of human biliverdin IX-α reductase.

Data points represent human BVR-A activity measured with increasing concentrations of sodium pyrophosphate pH 7 (□), and increasing sodium phosphate pH 7 (○). These reactions contained a final concentration of 700µM NADH as cofactor, and 20µM biliverdin-IXα as substrate. Also presented with this dataset is the activity of human BVR-A with increasing concentrations of sodium phosphate at pH 7. In this case however 100µM NADPH was used as cofactor (◊). Bilirubin production was measured at 460nm and assays were performed at 30°C.

decrease in the $appK_m^{NADH}$. It is important to note however that the ability to obtain reliable values for the $appK_m^{NADH}$ and $appV_{max}^{NADH}$ in 10mM phosphate is hampered by the lack of experimental data where NADH is saturating. Although the square of residuals (R^2 0.99758) for the fit is acceptable the ability to predict robust values for saturation and apparent $appV_{max}^{NADH}$ is limited. The data obtained would suggest that a concentration of greater than 100mM NADH would be necessary to approach saturation in 10mM sodium phosphate. Further analysis of the $appK_M$ and $appV_{max}$ obtained from the NADH saturation curves presented in Figures 4.10(a) and 4.10(b) reveal that there is an as asymptotic decrease in the $appK_M$ with increasing phosphate concentrations, while the $appV_{max}$ remains constant. Figure 4.10(c) shows the effect of phosphate on the $appV_{max}$ / K_m for human BVR-A.

4.2.3 The effect of phosphate on the burst rate constant of human BVR-A.

The effect of phosphate on the pre-steady state kinetics was determined by monitoring the increase in absorbance at 460nm at 23°C as described in Section 2.5.4. Human BVR-A (1.6 μM) in 100mM sodium citrate pH 7.2 was rapidly mixed with 1.4 mM NADH, 14 μM biliverdin-IXα in varying concentrations of sodium phosphate pH 7.2 (Figure 4.11). The concentration of phosphate in the substrate syringe was varied to give final concentrations of 5, 10, 20, 50, 100 and 200 mM. The results of these stopped flow experiments were fitted to a curve of single exponential with slope (see Section 2.5.4). The steady state rate showed that at 23°C there is a pronounced activation by phosphate anion (8-fold compared with the rate in Tris-Cl) and the burst rate constants (k_b) obtained from these experiments are shown in Figure 4.12. All the kinetic constants and statistical evaluation for this experiment are shown in Appendix IV Table 3. There is a modest effect of phosphate concentration on the burst rate constant which essentially doubles between 0 and 50mM phosphate from 0.15 s^{-1} to 0.28s^{-1}.

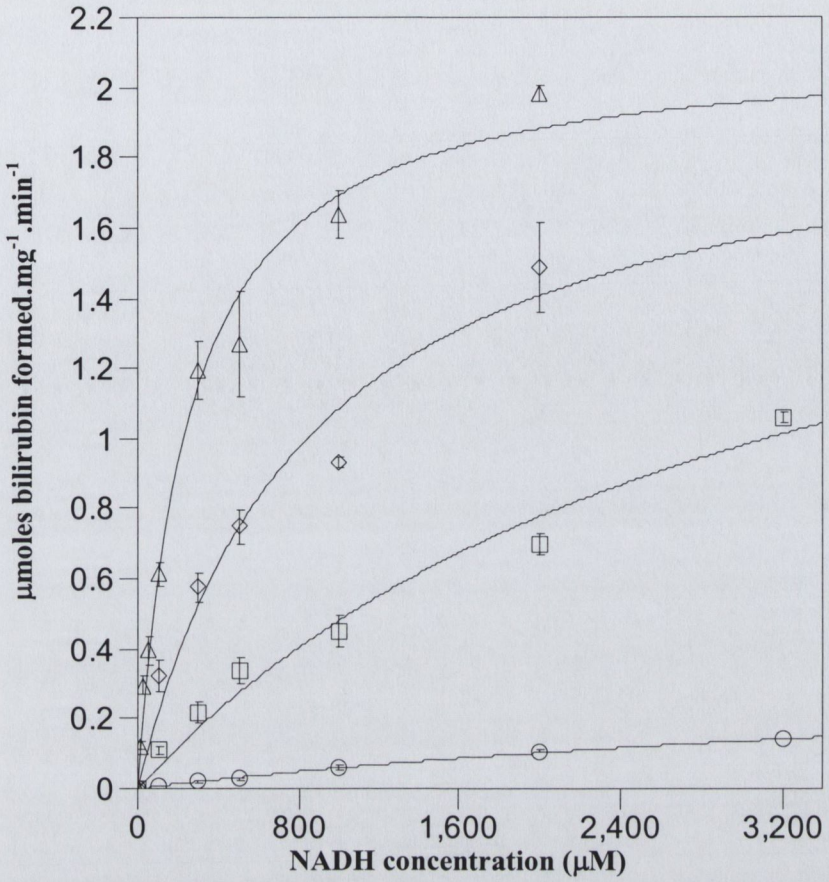

Figure 4.9 Determination of human BVR-As apparent Michaelis constant for NADH at various concentrations of sodium phosphate.

Data points represent activity with 20µM biliverdin as substrate in (○) 10mM sodium phosphate pH 7, (□) 50mM sodium phosphate pH 7, (◊) 100mM sodium phosphate pH 7 and (Δ) 200mM sodium phosphate as buffer.

[Phosphate] (mM)	appKm^{NADH} (mM)	appVmax	appVmax/Km^{NADH} v/k	Fold increase
10	39.2	2	5.10E-05	1
50	3.2	2.0316	6.30E-04	12.4
100	0.84	2.00058	2.37E-03	46.5
200	0.25	2.12166	8.35E-03	164

Table 4.1 **Determination of the apparent K_M and V_{max} of human BVR-A for NADH with increasing concentrations of sodium phosphate.**

Figure 4.10 The effect of phosphate on the apparent kinetic constants of V_{max} and K_M for NADH of human BVR-A

(a) The appK_M for NADH of human BVR-A as a function of phosphate concentration. Data points represent the appK_M values obtained from the NADH saturation curves of Figure 4.4. Refer to Table 4.2 for the analysis of the curve fitting data. A final concentration of 20μM was biliverdin-IXα was used in these assays.

(b) The appV_{max} of human BVR-A as a function of phosphate concentration. Data points represent the appV_{max} values obtained from the NADH saturation curves in Figure 4.4. Refer also to Table 4.2 for the analysis of the curve fitting data.

(c) The appK_m of human BVR-A as a function of phosphate concentration. Data points represent the appV_{max} / K_m values presented in Table 4.1.

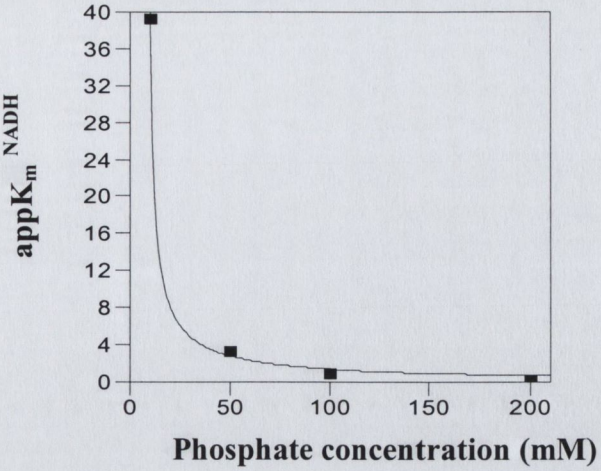
40
36
32
28
24
20
16
12
8
4
0
0
50
100
150
200
appK$_m$ NADH
Phosphate concentration (mM)

(a)

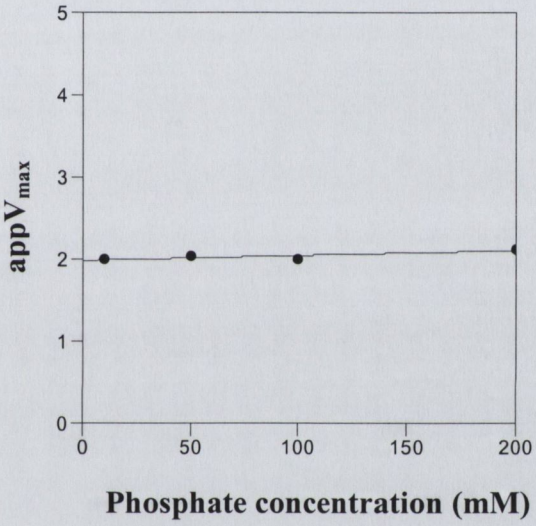
5
4
3
2
1
0
0
50
100
150
200
appV$_{max}$
Phosphate concentration (mM)

(b)

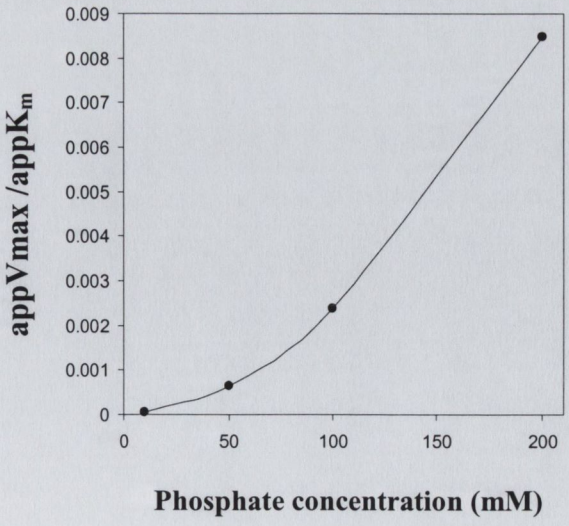
0.009
0.008
0.007
0.006
0.005
0.004
0.003
0.002
0.001
0
0
50
100
150
200
appVmax /appK$_m$
Phosphate concentration (mM)

(c)

Figure 4.11 The effect of phosphate on the pre-steady state kinetics of human biliverdin-IXα reductase.

(a) Measurements of the pre-steady state kinetics were carried out using an 'Applied Photophysics π*-180' spectrophotometer fitted with the kinetic sample handling unit as described in Section 2.5.4. An initial burst of bilirubin was observed while monitoring the absorbance at 460nm. The final reaction mix contained 700μM NADH, 7μM biliverdin-IXα over increasing concentrations of (5, 10, 50, 100mM and 200mM) phosphate at pH 7.2. The data set shown shows the effects of 50mM phosphate. Best fits were obtained on fitting the results to a single exponential curve with slope as discussed in Section 4.4.

(b) The reaction chemistry was divided into two separate syringes. The first contained 1.6μM hBVR-A in 100mM sodium citrate pH 7.2 while the second contained NADH (1.4mM), biliverdin (14μM) sodium phosphate pH 7.2.

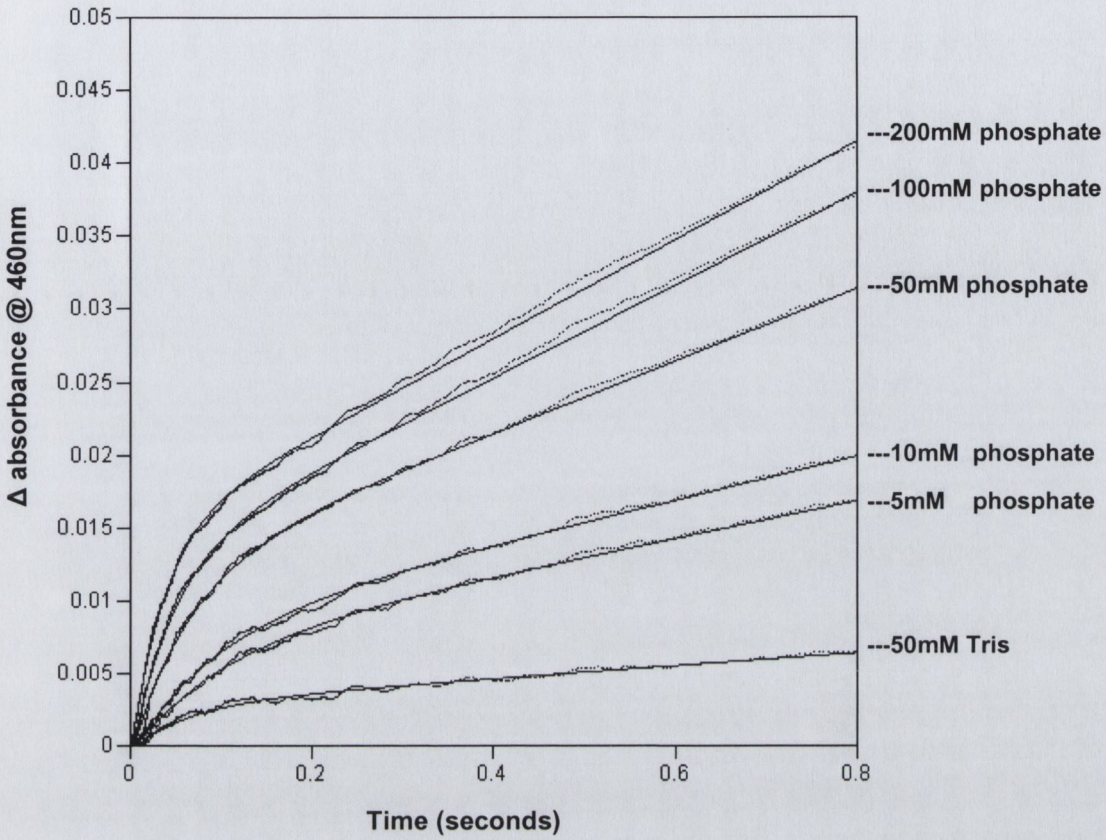
0.05
0.045
0.04
0.035
0.03
0.025
0.02
0.015
0.01
0.005
0
Δ absorbance @ 460nm
0
0.2
0.4
0.6
0.8
Time (seconds)
---200mM phosphate
---100mM phosphate
---50mM phosphate
---10mM phosphate
---5mM phosphate
---50mM Tris

(a)

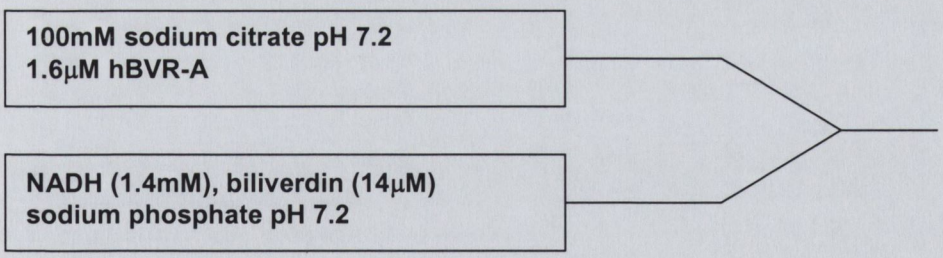
100mM sodium citrate pH 7.2
1.6μM hBVR-A
NADH (1.4mM), biliverdin (14μM)
sodium phosphate pH 7.2

(b)

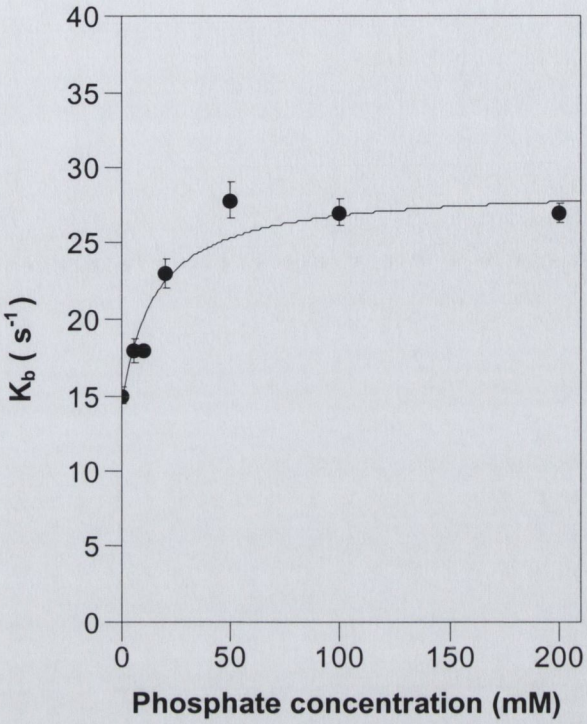

Figure 4.12 The effects of phosphate concentration on the burst rate constant of human biliverdin reductase in 50mM sodium citrate pH 7.2.

Values for the apparent burst constant (k_b) were obtained from curve fits to the data presented in Figure 4.11 and presented in detail in the Appendix II Table 3. The reactions were carried out with 700 μM NADH and 7 μM biliverdin-IXα in 50 mM sodium citrate pH 7.2. Phosphate concentrations were varied from 0 – 200 mM.

4.2.4 The effect of pH on the anion activation of human BVR-A using NADH as cofactor.

The effect of pH on the activity of human BVR-A with increasing phosphate concentrations was also investigated. The activity was measured in 100 mM sodium citrate over the pH range 5-7 with 7 μm biliverdin-IXα and 100 μM NADH as substrates. Phosphate concentrations were increased (0, 5, 10, 15, 20, 40, 60, 80, 100 mM) in 100 mM sodium citrate over the pH range 5 -7. From Figure 4.13(a), it is clear that at pH 5 the activation by phosphate anion is less potent than that seen at neutral pH. By plotting A_{50} (concentration of activator giving 50% activation) against pH an apparent pK of approximately 4.9 can be identified (Figure 4.13(b)). Deprotonation of this residue increases the affinity for phosphate anion 6-fold. This is tentatively identified as glutamate 75.

4.3 Studies on phosphate activation of rat BVR-A

4.3.1 Identification of a putative 2'-phosphate binding site

In an effort to further understand the nature of the activation of the NADH-dependent activity of human BVR-A by phosphate and related anions it was decided to analyse the only BVR-A structures available, those reported by Kikuchi *et al* (2001) and Whitby *et al.* (2002) for the rat enzyme.

As discussed in the introduction, rat BVR-A (Whitby *et al.*, 2002) co-crystallised with three inorganic phosphate molecules. Interestingly, one of these phosphates occupies a site which is the proposed binding pocket for the 2'-phospho ester of NADPH. In light of this information it was decided to look at the residues involved in phosphate binding in more detail. As shown in Figure 4.14, serine-43, arginine-44 and arginine-45 form an intricate lattice of ionic interactions with inorganic phosphate. It was decided to mutate these residues to alanine to further analyse their role if any, during NADH dependent phosphate activation.

4.3.2 Site-directed mutagenesis of residues in the 2'-phosphate pocket

This method, described in Section 2.1.11, involves the site-directed mutagenesis of the plasmid containing the target gene by PCR (Fisher *et al.*, 1997). Complementary forward

Figure 4.13 The effect of pH on the activation of human BVR-A using NADH as cofactor.

(a) The activity of human BVR-A was measured in 100mM sodium citrate over the pH range 5-7 (● pH 5, ○ pH 5.5, □ pH 6, ■ pH 6.5, and ◊ pH 7) with 7 μm biliverdin-IXα and 100 μM NADH as substrate. Phosphate concentrations were increased from 0 to 100mM phosphate at each pH measured.

(b) A plot of the activation constant (K_A), extrapolated from the curves presented in (a) yields the dataset shown in (b). When fitted to the equation for a sigmoidal curve (a+(b*10^(x-c)))/((10^(x-c))+1), the equation yields a pKa of ~ 4.9

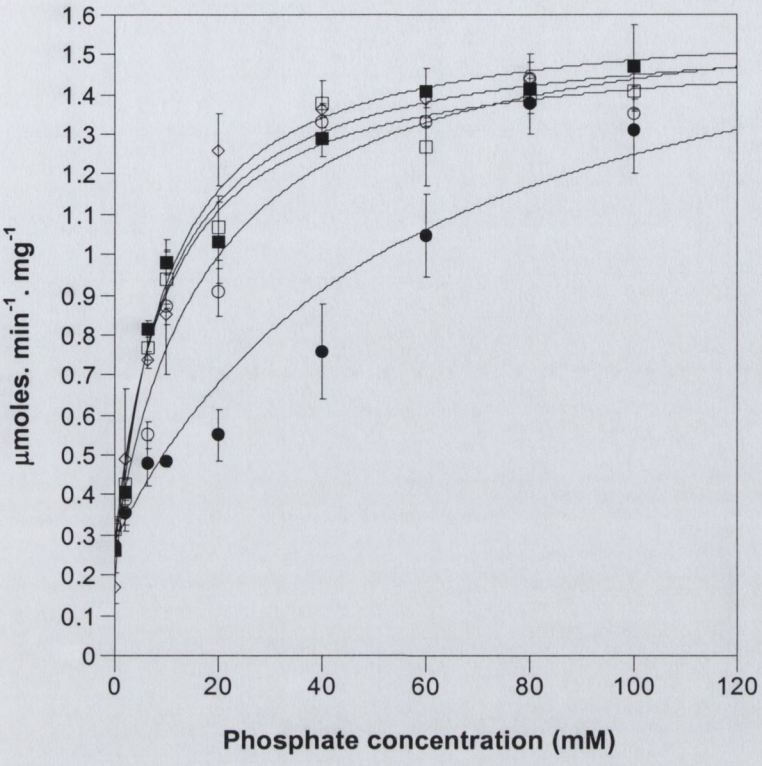
µmoles. min-1. mg-1
Phosphate concentration (mM)
0
0.1
0.2
0.3
0.4
0.5
0.6
0.7
0.8
0.9
1
1.1
1.2
1.3
1.4
1.5
1.6
0
20
40
60
80
100
120

(a)

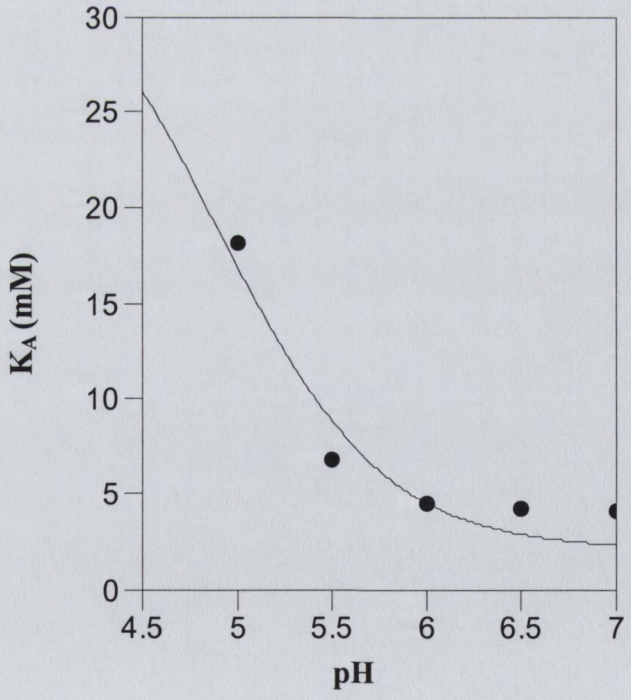
KA (mM)
pH
0
5
10
15
20
25
30
4.5
5
5.5
6
6.5
7

(b)

Figure 4.14 The phosphate binding site of rat BVR-A

(a) The residues which interact with the inorganic phosphate in rat BVR-A. Ionic contacts are represented by dotted lines (yellow). The numbers also in yellow correspond to the distances between interacting atoms. Red dots represent water molecules.

(b) A surface diagram of the residues shown in (a). The phosphate pocket is clearly defined. There is a large distribution of positively charged residues along the walls of this pocket which co-ordinate with the phosphate anion.

(c) Interactions of various residues within the phosphate binding pocket are highlighted. It is interesting to note that R44 and E75 form a salt bridge which connects the loop between B-sheets $\beta 2$ and $\beta 3$ with the αD helix in the rat crystal structure. Residues S43, R44 and R45 were target for mutation, in an attempt to determine their effects on NADH dependent phosphate activation.

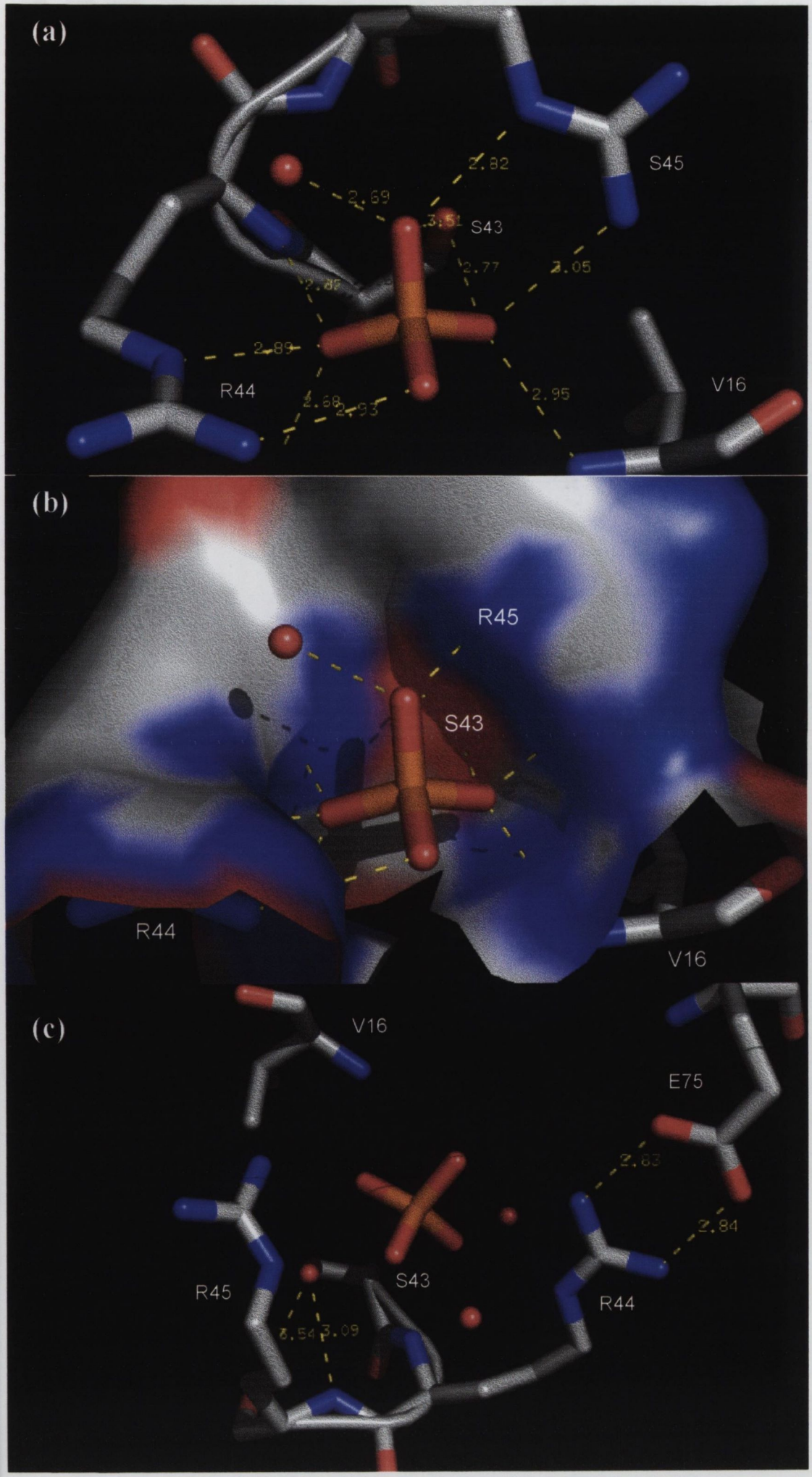
(a)
2.82
S45
2.69
S43
2.77
2.05
2.89
R44
2.68
2.93
2.95
V16
(b)
R45
S43
R44
V16
(c)
V16
E75
2.83
2.84
S43
R45
R44
3.09

and reverse primers (~30 base pairs long) were designed which contained the required mutations in the middle of the primers. Primer sequences are outlined in Figure 4.15 and optimised PCR conditions are presented in the Appendix IV Table 2. Single bands of the predicted size (6.5 kb) were obtained as PCR products and were analysed by 1% agarose gel electrophoresis (Figure 4.16). After digestion with DpnI (see Section 2.1.11) a 1μl aliquot of the PCR reaction was transformed into *E.coli* XL1 Blue super competent cells. Individual colonies of successful transformants were streaked on agar plates and grown at 37°C overnight. These plates were used to inoculate overnight cultures from which the pHis-Parallel 1 rat BVR-A mutant plasmids were purified. The plasmids used in the sequencing reactions are shown in Figure 4.17. Alignments of sequencing results are presented in Figure 4.18. The plasmids containing the cDNA for the rat BVR-A mutants were transformed into *E.coli* BL21 DE3 cells and BVR-A mutants was expressed using the protocol described in Section 2.4.6. A 5μg sample of each of the purified mutants were analysed on a 12% acrylamide gel as shown in Figure 4.19. The purification of the R45A mutant proved problematic due to the precipitation of protein throughout the purification procedure.

4.3.3 Effect of phosphate concentration on the activity of wild type and "2'-phosphate pocket" mutants of rat BVR-A

Figure 4.20 shows the effect of phosphate concentration on the activity of the rat enzyme (wild type) in Tris-HCl buffer. As with the human enzyme there is a marked activation by phosphate with an A_{50} value of 20 mM. Although all three of the desired mutants were created only the S43A and the R44A mutants were sufficiently stable to examine kinetically. The A_{50} for the S43 mutant increases significantly (Figure 4.21) to 100mM indicating that significant binding energy results from the interaction between serine 43 and the phosphate anion.

4.3.4 Comparision of the kinetic parameters for NADH and NADPH with the wild type and S43A mutants and R44A mutants of rat BVR-A

The R44A mutant equalises the apparent K_m for NAD and NADPH (Figure 4.22). The wild type enzyme has been reported to have an apparent K_m for NADH of 100 μM and for

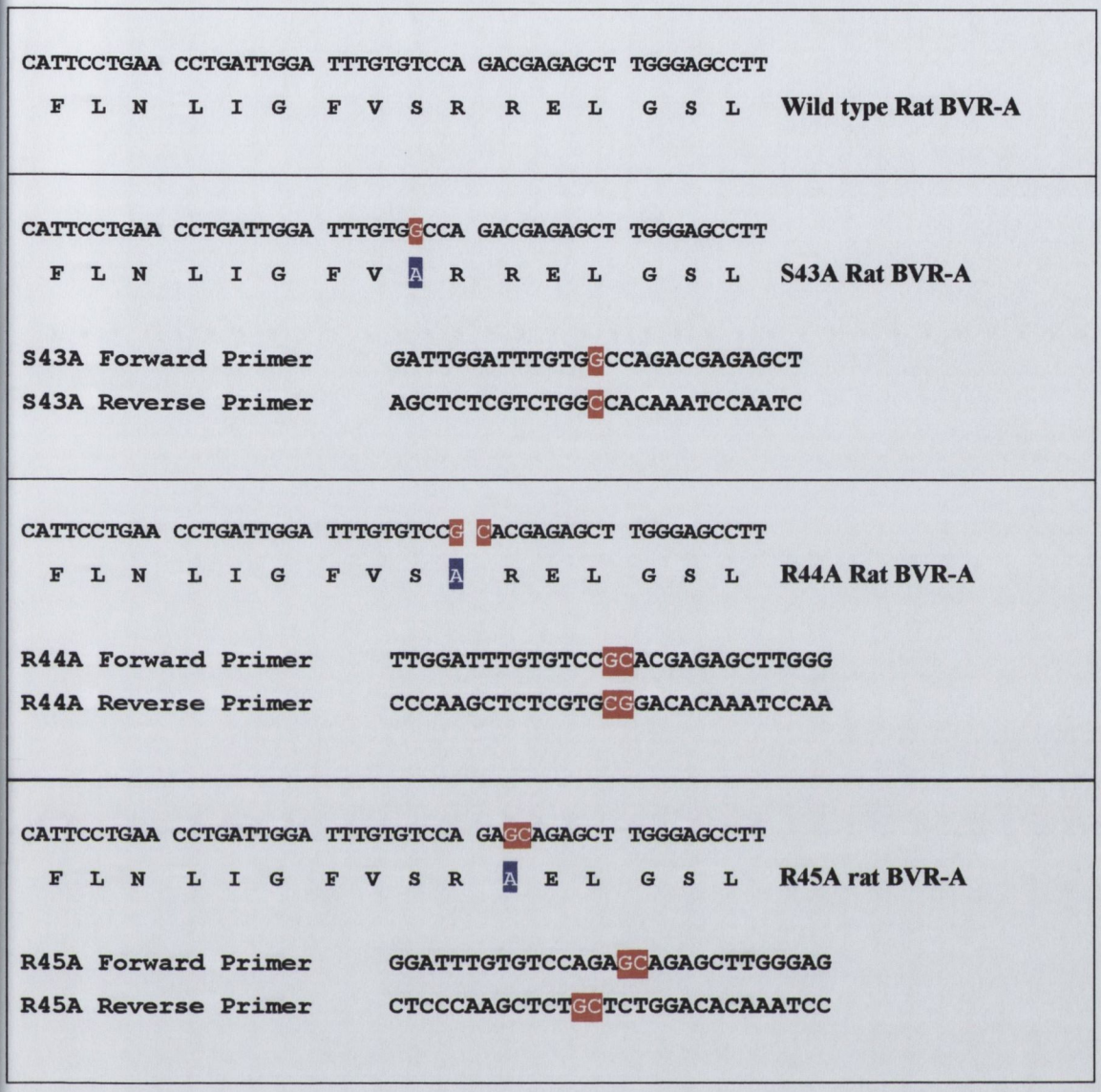

Figure 4.15 Sequences of the oligonucleotides used in the site directed mutagenesis of rat BVR-A

The base pairs highlighted in red were changed producing the necessary alanine mutations. The nucleotide sequences of the complementary primers used in the PCR reactions are also shown in 5'-3' direction.



(a)

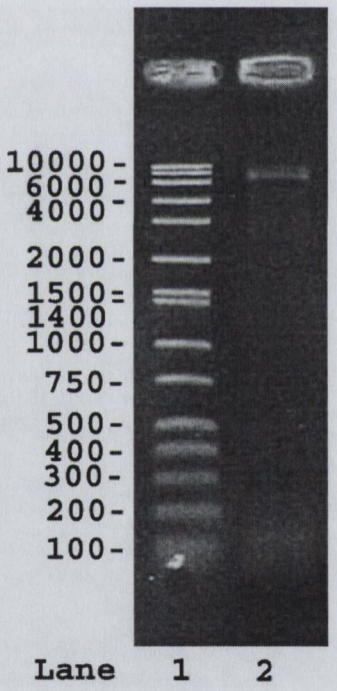

(b)

Figure 4.16 Agarose gel analysis of the site directed mutagenesis PCR products.

PCR reactions were carried out as described in section 4.6. Lane 1 of both (a) and (b) contain molecular weight standards (Sigma D-7058) with the sizes labelled in base pairs. **(a)** The PCR products of the S43A and R44A mutagenic reaction are presented in lanes 1 and 2 respectively. **(b)** The PCR product of the R45A is shown in lane 2. 10µl aliquots of the individual PCR reactions were loaded on each gel.

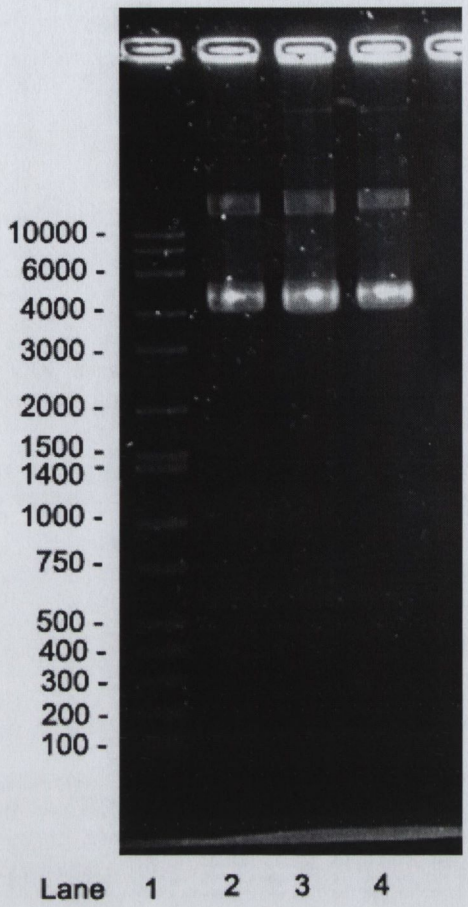

Figure 4.17 Agarose gel electrophoresis of the undigested pHis-Parallel 1 rat BVR-A mutant plasmids used as template in the sequencing reactions.

Lane 1: Molecular weight markers (Sigma D-7058) with the number of base pairs in each marker indicated.

Lane 2: A 2µl aliquot of pHis-Parallel 1 rat BVR-A S43A mutant purified plasmid.

Lane 3: A 2µl aliquot of pHis-Parallel 1 rat BVR-A R44A mutant purified plasmid.

Lane 4: A 2µl aliquot of pHis-Parallel 1 rat BVR-A R45A mutant purified plasmid.

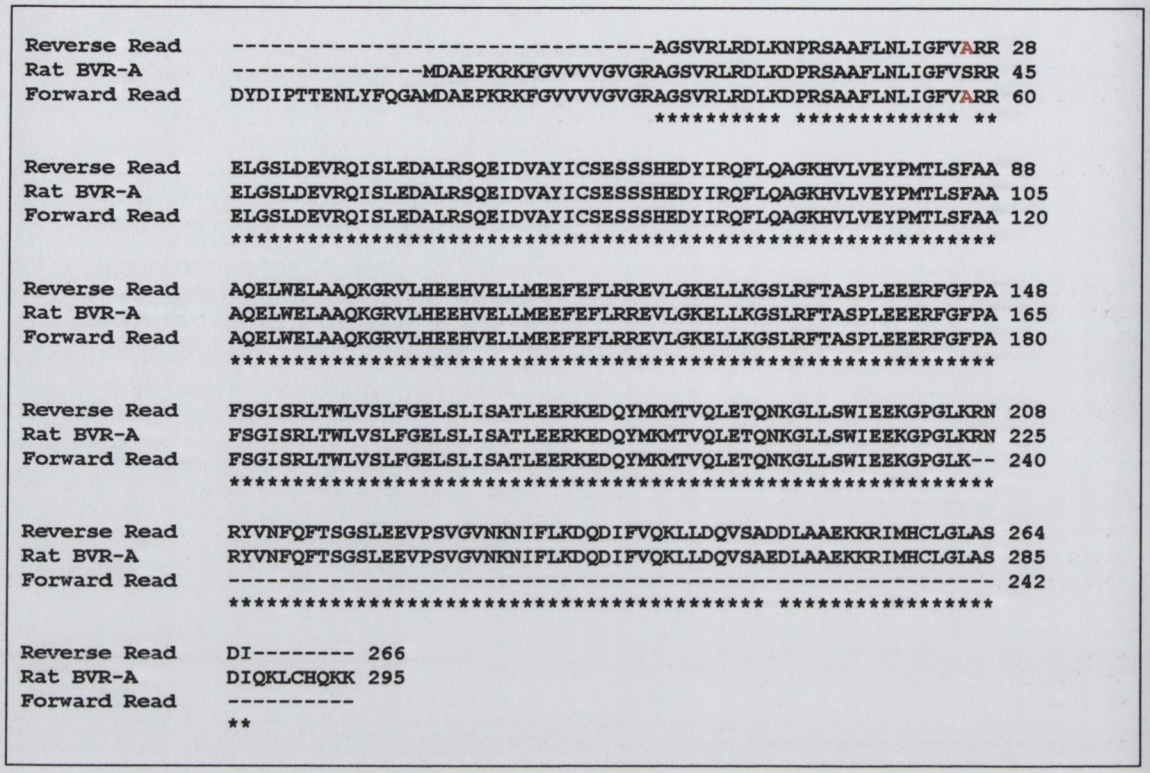
Reverse Read ----------AGSVRLRDLKNPRSAAFLNLIGFVARR 28
Rat BVR-A ----------MDAEPKRKFGVVVVGVGRAGSVRLRDLKDPRSAAFLNLIGFVSRR 45
Forward Read DYDIPTTENLYFQGAMDAEPKRKFGVVVVGVGRAGSVRLRDLKDPRSAAFLNLIGFVARR 60
Reverse Read ELGSLDEVRQISLEDALRSQEIDVAYICSESSSHEDYIRQFLQAGKHVLVEYPMTLSFAA 88
Rat BVR-A ELGSLDEVRQISLEDALRSQEIDVAYICSESSSHEDYIRQFLQAGKHVLVEYPMTLSFAA 105
Forward Read ELGSLDEVRQISLEDALRSQEIDVAYICSESSSHEDYIRQFLQAGKHVLVEYPMTLSFAA 120
Reverse Read AQELWELAAQKGRVLHEEHVELLMEEFEFLRREVLGKELLKGSLRFTASPLEEERFGFPA 148
Rat BVR-A AQELWELAAQKGRVLHEEHVELLMEEFEFLRREVLGKELLKGSLRFTASPLEEERFGFPA 165
Forward Read AQELWELAAQKGRVLHEEHVELLMEEFEFLRREVLGKELLKGSLRFTASPLEEERFGFPA 180
Reverse Read FSGISRLTWLVSLFGELSLISATLEERKEDQYMKMTVQLETQNKGLLSWIEEKGPGLKRN 208
Rat BVR-A FSGISRLTWLVSLFGELSLISATLEERKEDQYMKMTVQLETQNKGLLSWIEEKGPGLKRN 225
Forward Read FSGISRLTWLVSLFGELSLISATLEERKEDQYMKMTVQLETQNKGLLSWIEEKGPGLK-- 240
Reverse Read RYVNFQFTSGSLEEVPSVGVNKNIFLKDQDIFVQKLLDQVSADDLAAEKKRIMHCLGLAS 264
Rat BVR-A RYVNFQFTSGSLEEVPSVGVNKNIFLKDQDIFVQKLLDQVSAEDLAAEKKRIMHCLGLAS 285
Forward Read ---------- 242
Reverse Read DI-------- 266
Rat BVR-A DIQKLCHQKK 295
Forward Read ----------

(i)

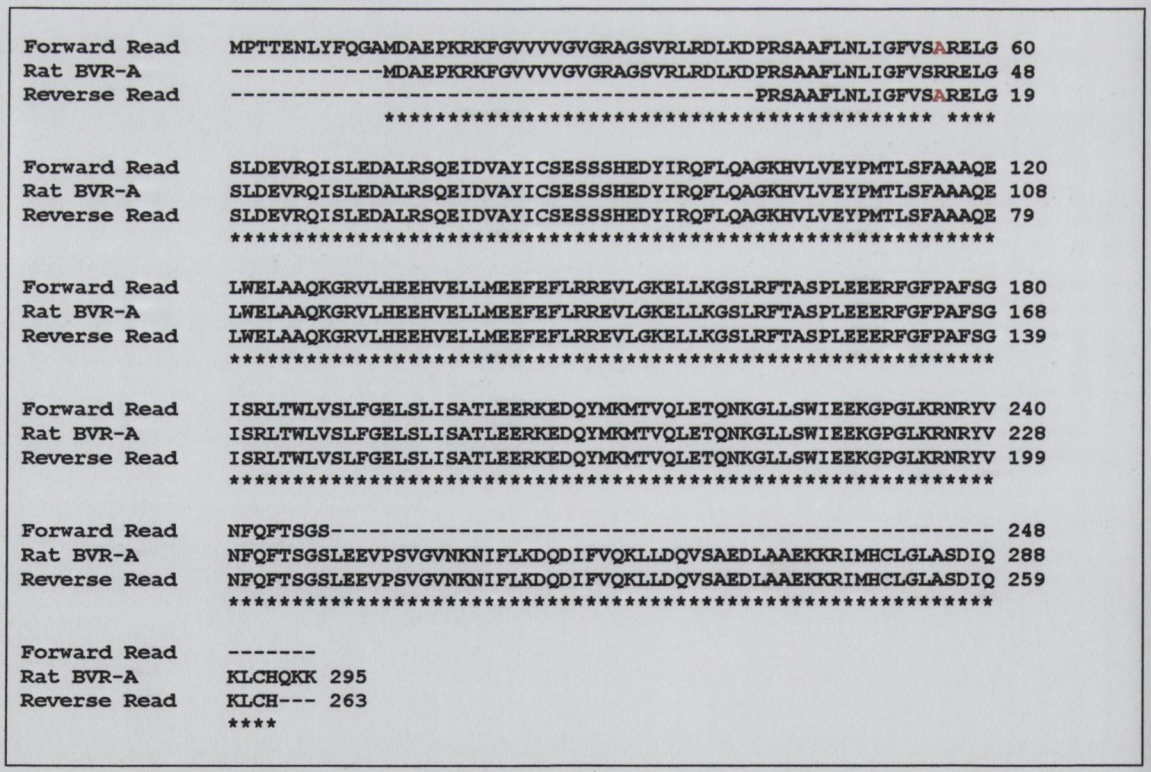
Forward Read MPTTENLYFQGAMDAEPKRKFGVVVVGVGRAGSVRLRDLKDPRSAAFLNLIGFVSARELG 60
Rat BVR-A ----------MDAEPKRKFGVVVVGVGRAGSVRLRDLKDPRSAAFLNLIGFVSRRELG 48
Reverse Read ----------PRSAAFLNLIGFVSARELG 19
Forward Read SLDEVRQISLEDALRSQEIDVAYICSESSSHEDYIRQFLQAGKHVLVEYPMTLSFAAAQE 120
Rat BVR-A SLDEVRQISLEDALRSQEIDVAYICSESSSHEDYIRQFLQAGKHVLVEYPMTLSFAAAQE 108
Reverse Read SLDEVRQISLEDALRSQEIDVAYICSESSSHEDYIRQFLQAGKHVLVEYPMTLSFAAAQE 79
Forward Read LWELAAQKGRVLHEEHVELLMEEFEFLRREVLGKELLKGSLRFTASPLEEERFGFPAFSG 180
Rat BVR-A LWELAAQKGRVLHEEHVELLMEEFEFLRREVLGKELLKGSLRFTASPLEEERFGFPAFSG 168
Reverse Read LWELAAQKGRVLHEEHVELLMEEFEFLRREVLGKELLKGSLRFTASPLEEERFGFPAFSG 139
Forward Read ISRLTWLVSLFGELSLISATLEERKEDQYMKMTVQLETQNKGLLSWIEEKGPGLKRNRYV 240
Rat BVR-A ISRLTWLVSLFGELSLISATLEERKEDQYMKMTVQLETQNKGLLSWIEEKGPGLKRNRYV 228
Reverse Read ISRLTWLVSLFGELSLISATLEERKEDQYMKMTVQLETQNKGLLSWIEEKGPGLKRNRYV 199
Forward Read NFQFTSGS---------- 248
Rat BVR-A NFQFTSGSLEEVPSVGVNKNIFLKDQDIFVQKLLDQVSAEDLAAEKKRIMHCLGLASDIQ 288
Reverse Read NFQFTSGSLEEVPSVGVNKNIFLKDQDIFVQKLLDQVSAEDLAAEKKRIMHCLGLASDIQ 259
Forward Read -------
Rat BVR-A KLCHQKK 295
Reverse Read KLCH--- 263

(ii)

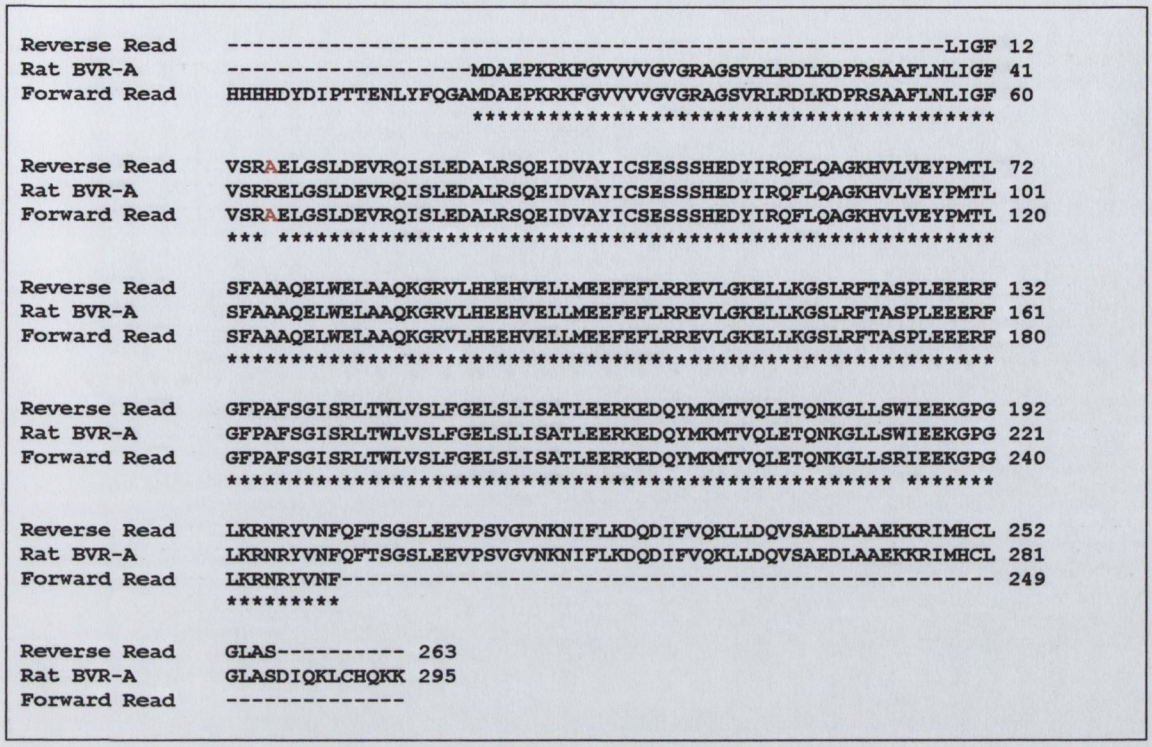

(iii)

Figure 4.18 Protein sequence alignments of the pHis-Parallel 1 rat BVR-A mutants.

The multiple sequence alignments of the nucleotide translated rat BVR-A S43A, R44A, and R45A sequencing results. The sequences were aligned with the rat protein sequence (Accession number: NP_446302 from the National Centre of Biotechnology Information databases at http://www.ncbi.nlm.nih.gov/)

(i) Deduced amino acid sequence of the pHis-Parallel 1 S43A rat mutant.

(ii) Deduced amino acid sequence of the pHis-Parallel 1 R44A rat mutant.

(iii) Deduced amino acid sequence of the pHis-Parallel 1 R45A rat mutant.

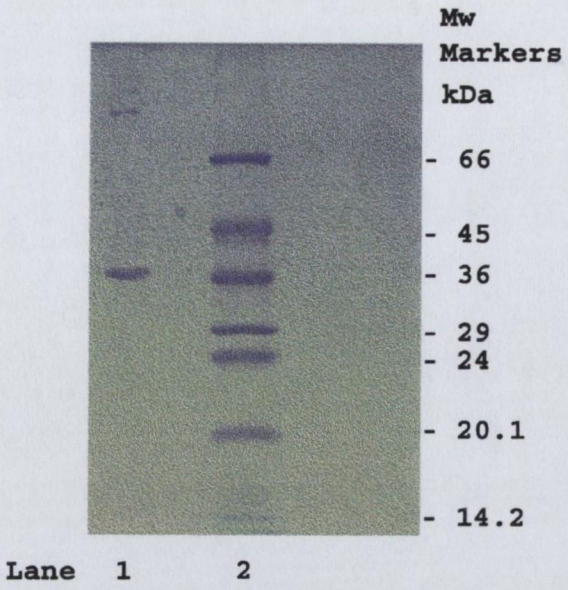

(a)

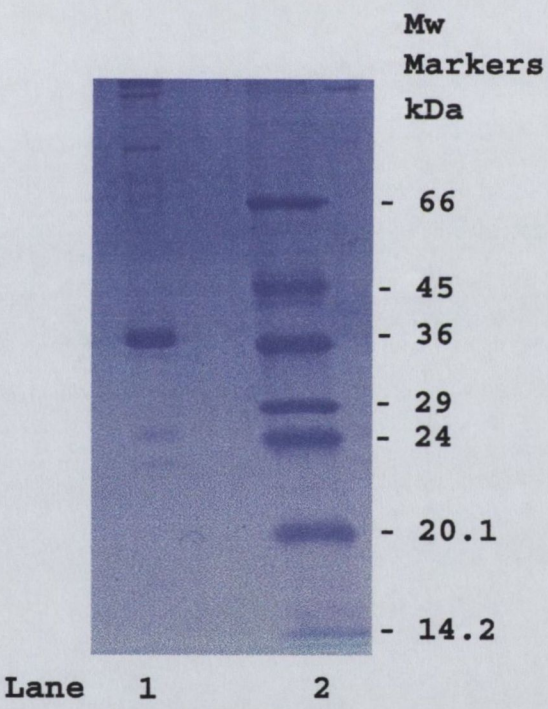

(b)

Figure 4.19 Analysis of purified rat BVR-A mutants on SDS-polyacrylamide gels

Rat BVR-A mutants were purified as described in Section 2.4.6

(a) Purified rat BVR-A S43A mutant. Lane 1: 5μg rat S43A mutant. Lane 2: Sigma molecular weight markers (sizes are indicated as kDa).

(b) Purified rat BVR-A R44A mutant. Lane 1: 5μg rat S43A mutant. Lane 2: Sigma molecular weight markers.

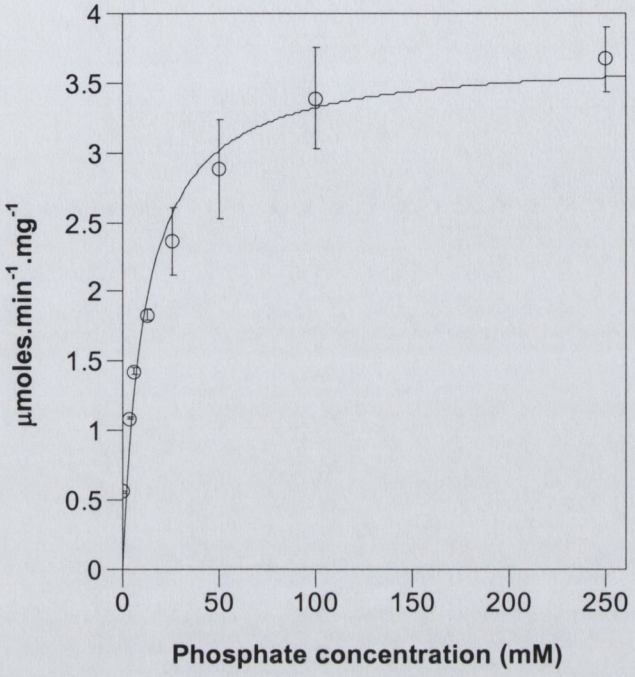

Figure 4.20 The effect of phosphate on the activity of rat BVR-A.

Rat BVR-A was assayed using 700µM NADH and 10µM BV as substrate in 50 mM Tris pH 7.2 at 30°C with increasing concentrations of phosphate (0, 3.125, 6.25, 12.5, 25, 50, 100, 250mM). Data points were fitted to the Michaelis equation f(x)=((a*x)/(x +b))+c, the results of which are presented in Appendix IV Table 6.

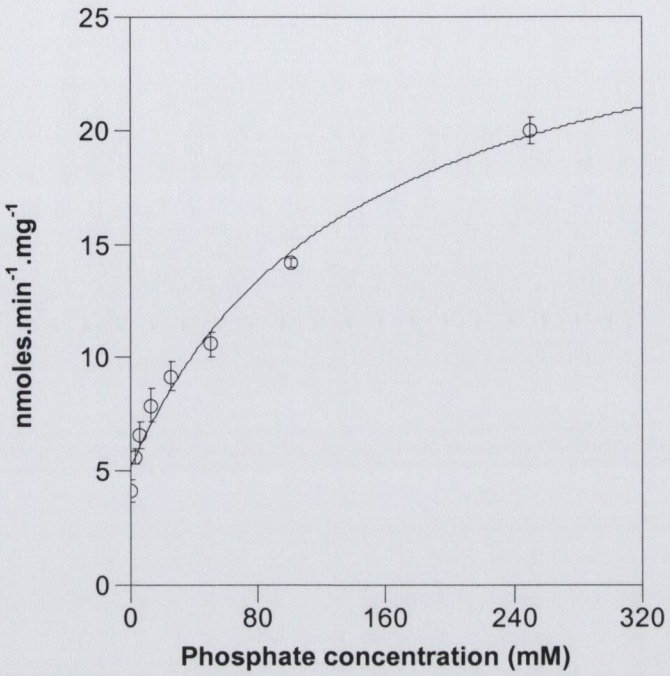

Figure 4.21 The effects of phosphate on the activity of the rat BVR-A S43A mutant.

Rat BVR-A was assayed using 700 μM NADH and 10 μM biliverdin as substrate in 50 mM Tris pH 7.2 at 30°C with increasing concentrations of phosphate (0, 2, 5, 10, 25, 50, 100, 250 mM). Data points were fitted to the Michaelis equation f(x)=(a*x)/(x +b)+c.

Figure 4.22 The effect of increasing NADH and NADPH concentrations on activity of the rat BVR-A R44A mutant.

(a) The activity was measured by monitoring bilirubin production at 460nm using various NADH concentrations (5, 10, 25, 50 100, 200 and 400μM) in 50mM Tris pH 8.7.

(b) NADPH was varied over the concentrations 2, 5, 10, 15, 25, 50 100 and 200 μM in 50mM Tris pH 8.7.

Data points for both (a) and (b) were fitted to the Michaelis equation f(x)=(a*x)/(x +b) and estimates for the Km (b) and Vmax of both experiments are presented in Appendix IV Table 5.

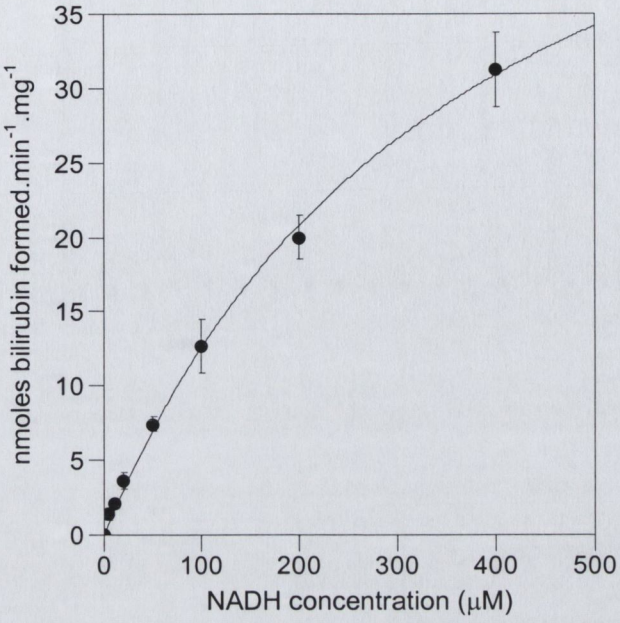
nmoles bilirubin formed.min-1.mg-1
0
5
10
15
20
25
30
35
0
100
200
300
400
500
NADH concentration (μM)

(a)

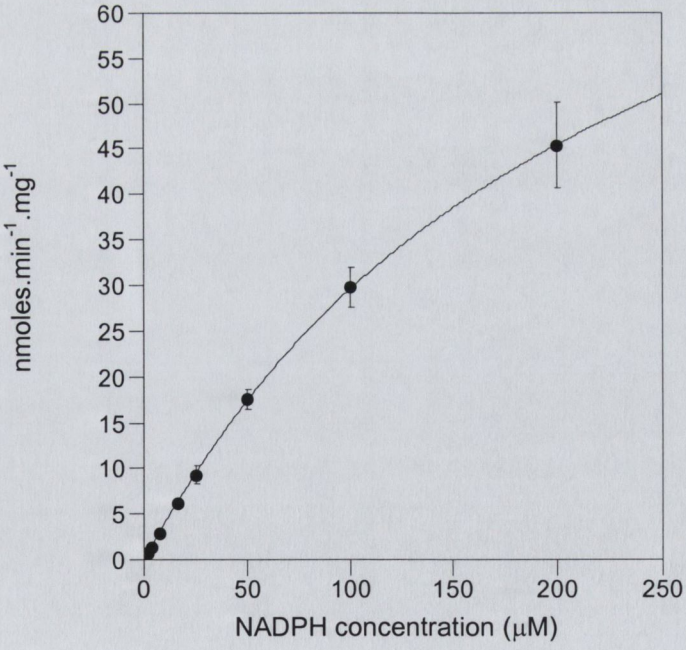
nmoles.min-1.mg-1
0
5
10
15
20
25
30
35
40
45
50
55
60
0
50
100
150
200
250
NADPH concentration (μM)

(b)

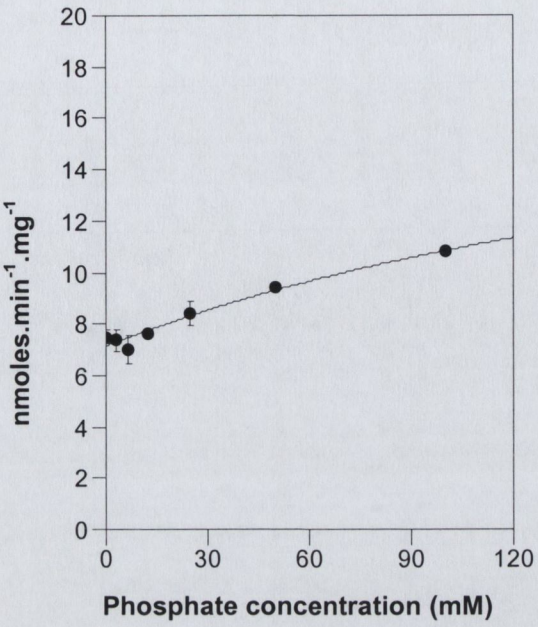

Figure 4.23 The effects of phosphate on the activity of the rat BVR-A R44A mutant using NADH as cofactor.

Rat BVR-A was assayed using 700μM NADH and 10μM BV as substrate in 50 mM Tris pH 7.2 at 30°C with increasing concentrations of phosphate (0, 2, 5, 10, 25, 50, 100, 250mM). Data points were fitted to the Michaelis equation plus constant f(x)=(a*x)/(x +b)+c.

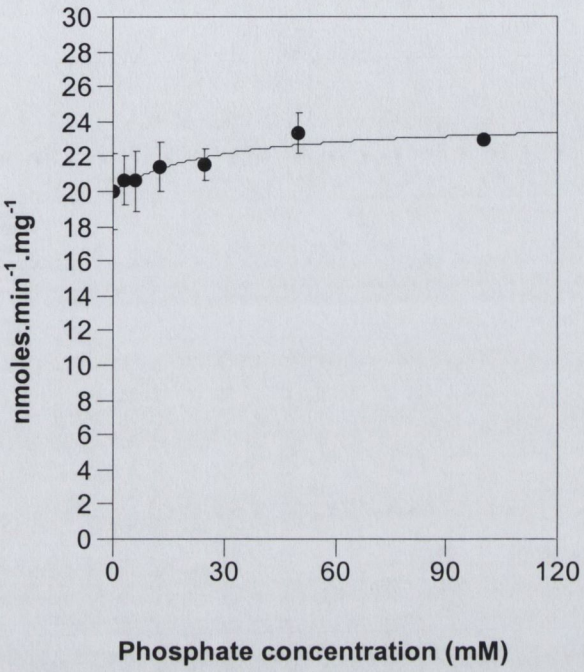

Figure 4.24 The effects of phosphate on the activity of the rat BVR-A R44A mutant using NADPH as cofactor.

Rat BVR-A was assayed using 100μM NADPH and 10μM Biliverdin as substrate in 50 mM Tris pH 7.2 at 30°C with increasing concentrations of phosphate (0, 2, 5, 10, 25, 50, 100, 250mM). Data points were fitted to the Michaelis equation plus constant f(x)=(a*x)/(x +b)+c.

NADPH of 2.6 μM (Kikuchi *et al.*, 2001). These workers also constructed S43, R44 and R45 mutants, but unfortunately the instability of the arginine mutant R45A in this study prevented any reliable kinetic measurements. Kikuchi *et al.*, 2001, found that the NADPH dependent activity of both arginine mutants was low in comparison to the wild type, and proposed that both these residues were important in binding the 2' phosphate. Both studies show clearly that R44 plays a significant role in stabilising a tighter binding of NADPH over NADH, implicating R44's importance in binding the 2'-phosphate moiety. The present study also shows that the R44A mutant is not activated by increasing phosphate when using NADH as cofactor.

4.3.5 The effect of phosphate on the dissociation constant of NAD^+ with BVR-A

The effects of phosphate on the dissociation constant (K_D) for NAD^+ was also determined. Sequential additions of NAD^+ (from a 20 mM stock) and $NADP^+$ (from a 2mM stock) were made to a cuvette containing rat BVR-A (2 μM) with increasing concentrations of sodium phosphate (0, 5, 10, 50 and 50 mM) in 50 mM Tris-HCl pH 7.2. Results are presented in Table 4.2. The fluorescence intensity was measured at 340nm (excitation wavelength 295nm) after each addition of nucleotide. The measured fluorescence intensities were corrected for the 'inner filter effect' to yield the corrected fluorescence F_{corr} which is represented as Delta F (described in Section 2.5.5). Changes in the apparent K_D for NAD^+ with respect to phosphate concentration are displayed in Figure 4.25. This reveals the apparent biphasic response of the enzyme to increases in phosphate in the presence of NAD^+. At low concentration of phosphate (5 and 10mM) the K_D^{NAD+} decreases from 113 μM to 46 μM but at higher concentrations of phosphate the K_D^{NAD+} returns to the values obtained in 50 mM Tris-HCl. Table 4.2 summarises the effects of phosphate and pH (Appendix IV Figures 1-4) on $appK_D^{NAD+}$ and $appK_D^{NADP+}$. Interestingly it is the buffering solution pH which has greatest effect on the apparent dissociation constant of NADH. In 50mM Tris-HCl and 50mM phosphate pH 7.2, both the $appK_D^{NADP+}$ and $appK_D^{NAD+}$ remain constant at 8.64 μM - 6.39μM and 112-113 μM respectively. In Tris-HCl pH 8.7 however the values increases to 11.2 μM for $appK_D^{NADP+}$ and 654 μM for $appK_D^{NAD+}$.

	$NADP^+$ $appK_D$ (μM)	NAD^+ $appK_D$ (μM)
In 50 mM sodium phosphate pH 7.2	**8.64 +/-0.6**	**112 +/- 4.1**
In 50 mM Tris 7.2	**6.39 +/- 0.6**	**113 +/- 8**
In 50 mM Tris 8.7	**11.2 +/-1.4**	**654 +/- 106**

Table 4.2 The apparent dissociation constant ($appK_D$) of both NAD^+ and $NADP^+$ with rat BVR-A in 50mM Tris pH 7.2 and at pH 8.7, and also in 50mM sodium phosphate pH 7.2.

Sequential additions of each nucleotide were made to 2mls of the buffers outlined. The fluorescence intensity was measured at 340nm (excitation wavelength 295nm) after each addition of nucleotide. The measured fluorescence intensities were corrected for the 'inner filter effect' to yield the corrected fluorescence F_{corr} which is represented as Delta F in the data presented (see section 2.5.5). Data points were fitted to the Michaelis equation $F(x) = a*x/(b+x)$ where b represents the $appK_D$ value for nucleotide on the enzyme.

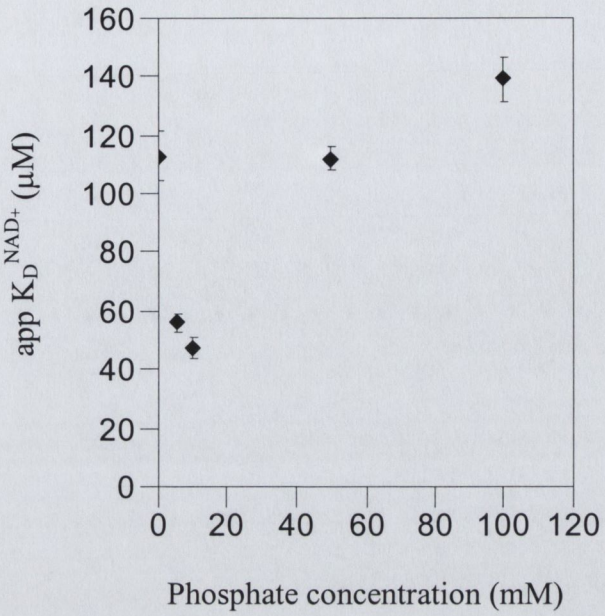

Figure 4.25 The effect of increasing sodium phosphate concentrations on the apparent dissociation constant of NAD^+ ($appK_D^{NAD+}$) on rat biliverdin-IXα reductase.

Sequential additions the nucleotide were made to 2mls of 50mM Tris pH 7.2 containing increasing concentrations of phosphate as outlined in Appendix IV **Figures 3 - 6.** The fluorescence intensity was measured at 340nm (excitation wavelength 295nm) after each addition of nucleotide. The measured fluorescence intensities were corrected for the 'inner filter effect' to yield the corrected fluorescence F_{corr} which is represented as Delta F. Data points were fitted to the Michaelis equation F(x) = a*x/(x+b) with b representing the $appK_D$ values.

4.4 The effect of pH and biliverdin-IXα concentrations on the initial rate using NADPH as cofactor.

During the course of these experiments it was noticed that the concentration of biliverdin-IXα used in the determination of the pH optima for biliverdin reductase activity is an important factor which needs clarification. A series of reactions were set up to determine the effects of different biliverdin-IXα concentrations on the activity of human BVR-A over the pH range 4.5-8.5. Bilirubin production was monitored at 460 nm and individual reactions contained a final concentration of 100 μM NADPH and between 2 and 25μM biliverdin-IXα at each pH.

The assay temperature was maintained at 30°C. In a second series of experiments the effects of the substrate inhibition associated with 2 μM, 5 μM and 20 μM biliverdin-IXα over the pH range 4.5-8.5 was determined and the activities presented in Figure 4.5. It is worth noting the shift in the apparent pH optima for NADPH dependent activity as the biliverdin-IXα concentrations increase. At 2 μM biliverdin-IXα the enzyme is active over all pH range 4.5 – 6 and also at pH 7.5 to 8. As the substrate concentration is increased to 5 μM maximal activity is at pH 4.5 to 5 and at pH 8 and by 20 μM the activity is limited to the extremes of the pH range studied. Further evidence showing the effects of pH and substrate inhibition is presented in the time course of the *Xenopus tropicalis* enzyme where an increase in rate is observed as the substrate concentration decreases over the course of the reaction at neutral pH values (Figure 4.26). However at the acid and alkaline limbs this behaviour disappears and more normal P(t) curves are observed From this it becomes increasingly evident that the substrate concentration used in the pH kinetics for BVR-A is an important factor for consideration.

Figure 4.26 The effects of pH on the substrate inhibition of *Xenopus* BVR-A.

The final reaction mixture contained NADPH (100μM), biliverdin (5μM) and the buffers (100mM) as indicated on each time course. The reaction was started on addition of 1μg *Xenopus* BVR-A Each reaction was monitored at 460nm at 30°C until the reaction neared completion. The horizontal plane represents the change in absorbance at 460nm observed with the vertical plane representing time.

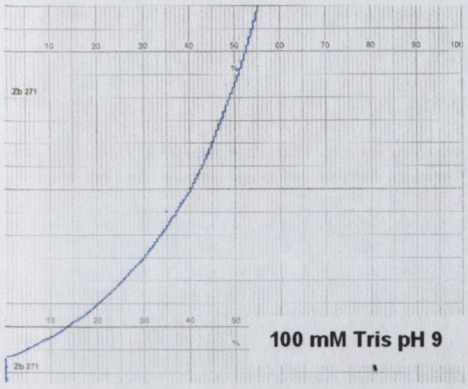

100 mM Tris pH 9

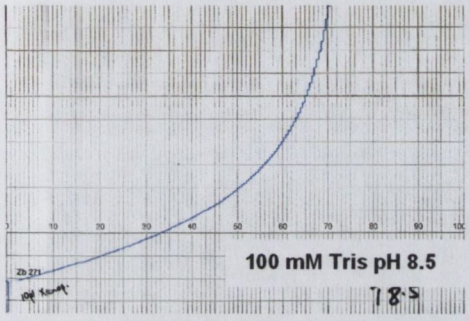

100 mM Tris pH 8.5

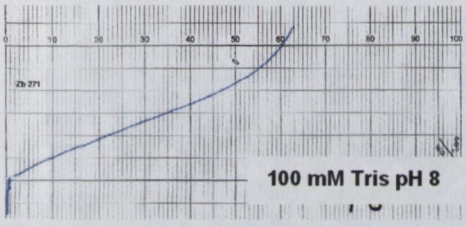

100 mM Tris pH 8

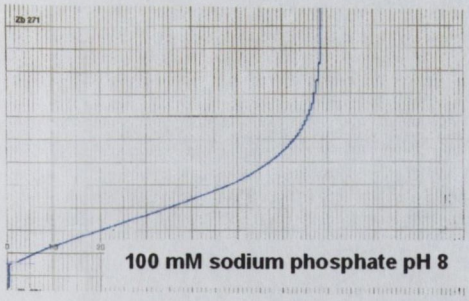

100 mM sodium phosphate pH 8

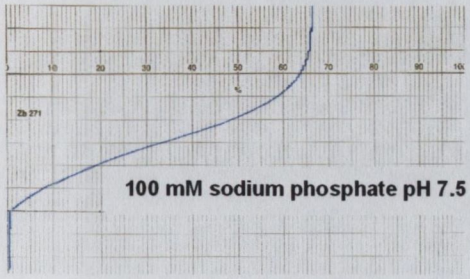

100 mM sodium phosphate pH 7.5

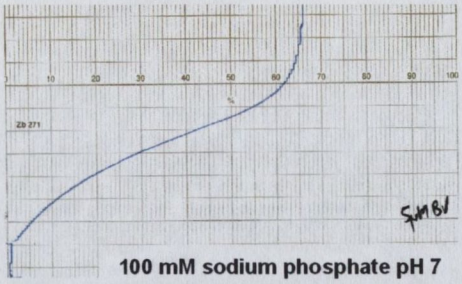

100 mM sodium phosphate pH 7

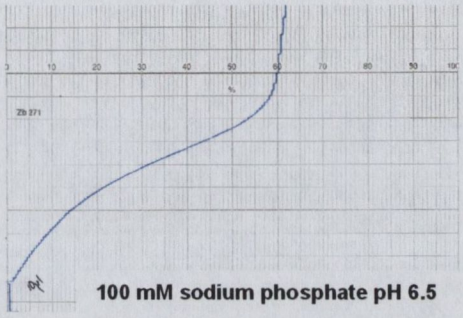

100 mM sodium phosphate pH 6.5

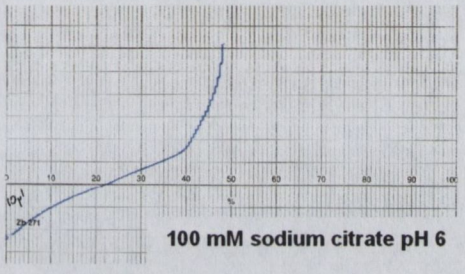

100 mM sodium citrate pH 6

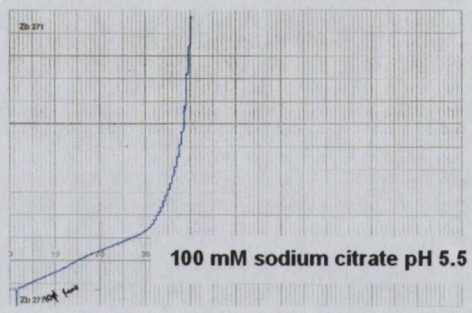

100 mM sodium citrate pH 5.5

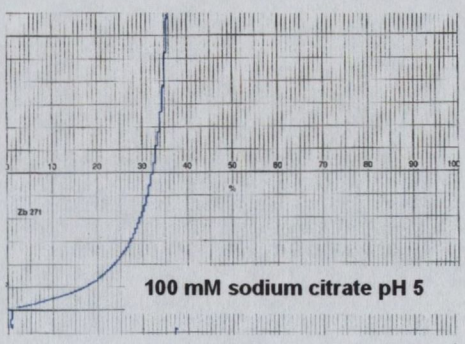

100 mM sodium citrate pH 5

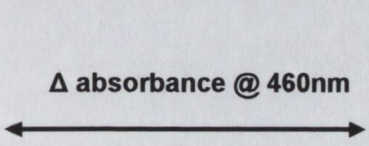

Δ absorbance @ 460nm

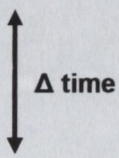

Δ time

It is clear that previous examinations on the effect of pH on BVR-A activity have not provided an adequate kinetic explanation for the disparate pH optima observed depending on whether the pyridine nucleotide used is NADH or NADPH. A major result from the present study is that the activity of the "vertebrate" BVR-As with NADH as cofactor is markedly activated in the presence of phosphate and related anions. As phosphate buffer is often used in kinetic studies over the pH range 6 to 8 the apparent optimum at 7 to 7.5 with NADH simply reflects this phenomenon, which will be discussed further below. A second observation is that activity with both NADH and NADPH is high at acid pH values (5 to 6) and tends to decrease around neutrality in all buffers (with the exception of the activity with NADH in the presence of phosphate). The decrease at neutral pH values is sensitive to the concentration of biliverdin as substrate inhibition is pronounced at neutral pH values but not evident at the acid or alkaline extremes. This was particularly evident in the time course of the *Xenopus tropicalis* enzyme which shows the classical increase in rate as the substrate concentration is depleted at neutral values of pH (where substrate inhibition is potent), but which reverts to the more normal P(t) curve – with a steady decline in rate (after the linear initial rate period) at the acid and alkaline extremes (Figure 4.26). It is still not clear why NADPH supports a significant rate at pH 8.5 to 9 but that NADH in unable to achieve this.

The activation of NADH-dependent activity by phosphate and related anions is common to the human, rat, mouse and *Xenopus* enzymes but the *Synechocystis* enzyme is refractory in this respect. For the human enzyme it is clear that the effect of phosphate is to enhance NADH binding as the apparent K_m for NADH is decreased over a 100-fold with no change in the apparent V_{max} (Refer to Figure 4.9 and Table 4.1). An intriguing possible interpretation of this observation comes from a careful examination of the structure of rat BVR-A where three phosphate anions are bound to the enzyme. Two of these sites are identifiable as candidates for the nucleotide pyrophosphate moiety and the 2'-phosphate of NADPH respectively. In the present study I have focussed on the putative "2'-phosphate pocket" as a possible candidate for the activation site. Kinetic analysis of the S43A rat mutant revealed that the A_{50} for phosphate activation was increased 5-fold in accord with a role for this residue in providing efficient binding for the activating phosphate anion. Figures 4.23 and 4.24 show the effects of phosphate on the rat BVR-A R44A mutant. Both

the NADH and NADPH dependent activities show only modest increases in the rate over the phosphate concentration 0-100mM phosphate. These increases could be attributed to an 'ionic effect' with increasing ion concentrations typical of those also observed with the human enzyme (Figure 4.7). It is important to note that the R44A mutant essentially abolished the kinetic discrimination between NADH and NADPH, which is also in accord with the correct identification of this residue as forming part of the "2'-phosphate pocket". The pH dependence of the activation of the human enzyme by phosphate has identified a residue, tentatively identified as glutamate 75 which needs to be ionized to afford tight binding of the phosphate anion. In the rat structure this residue forms a salt bridge with arginine 44. The hypothesis that NADH binding can be augmented by inorganic phosphate "mimicking" the 2'-phosphate of NADPH is not entirely novel as a similar conclusion had recently been reached by Christensen *et al.,* (2005) for the Mg-dependent methylenetetrahydrofolate dehydrogenase-cyclohydrolase (NMDMC). This follows from the initial observations by Kauffman & Matthews (1980) who were the first to report that phosphate buffer had a marked effect on the NADH associated dihydropterin reductase activity of pig liver methylenetetrahydrofolate reductase. MacKenzie *et al.*, (2005) points out that the cofactor binding site of NMDMC more closely resembles an NADP binding site, yet the role of phosphate ions in the NADH dependent activity is to compensate for the lack of the covalently bound phosphate group of the co-factor. They have shown that phosphate ions mediate multiple hydrogen bonding interactions which adapt the NMDMC site to bind NAD, which is very similar to the effects observed with biliverdin reductase. These results also predict that the 2'phosphate binding pocket of biliverdin reductase is the single most important site of interaction between the cofactor and the Rossmann fold of biliverdin reductase, providing cofactor selectivity and a higher binding affinity. It is now clear that changes in substrate inhibition curves over the pH range 5 – 9, as observed for BVR-A, complicate our understanding of the pH dependent activity of this enzyme. It is also clear that the use of phosphate buffer in light of our knowledge of the effects of phosphate activation has caused further complications when interpreting pH/activity profiles. It now seems likely that the nature of the dual pH-cofactor specificity, initially reported by Kutty & Maines (1981), is due to the effect of substrate inhibition and also phosphate activation which manifests in two apparent associated pH optima, with each nucleotide.

Chapter Five

Spectral and kinetic studies on biliverdin-IXα reductase

5.1 Introduction

As mentioned in the introduction, detailed kinetic studies on BVR-A have been difficult mainly because the enzyme suffers from very potent substrate inhibition (even at low micromolar concentrations of biliverdin). Attempts to fit curves to initial rate data exhibiting substrate inhibition at low concentrations of biliverdin are thwarted by the lack of data on the ascending limb of saturation curves. Consequently, the conventional spectrophotometric assay precludes reliable estimation of parameters such as the Michaelis constant for biliverdin. The ability to monitor the BVR-A catalysed reaction using nanomolar biliverdin-IXα would not only help with the enzymatic determination of biliverdin levels (which are probably sub micromolar) in tissues, but should also provide a robust data set allowing the determination of the enzyme's kinetic parameters with greater confidence.

Over the course of this work the development of an alternative assay using radio-labelled NADPH was initiated. Both [^{14}C] and [^{3}H]-labelled tetrapyrroles have been widely used in metabolic studies (Manitto *et al.*, 1975; Plieninger *et al.*, 1972; Howe *et al.*, 1970; Lester & Klein, 1966 b; Grodsky *et al.*, 1962 and Menken *et al.*, 1966). Labelled tetrapyrroles are generally prepared biosynthetically in rats and dogs from labelled [^{14}C]-δ-aminolevulinic acid (ALA). Although the ALA is incorporated very well into the hepatic haem and further metabolised to conjugated bilirubin within 10 hours, the conjugates need to undergo hydrolysis to yield bilirubin-IXα which is then purified by TLC. Purified bilirubin-IXα is then oxidised to biliverdin with 2,3-dichloro-5,6-dicyanobenzoquinone. The main methods of preparing [^{3}H]-bilirubin-IXα are through the Wilzbach method which simply consists of exposing the compound to tritium gas (Steinberg 1957). [^{3}H]-bilirubin-IXα has been produced using this method but the yields obtained were quite low. Not only is the synthesis of these compounds difficult but the production of large quantities of [^{14}C] or [^{3}H]-labelled waste during their synthesis and also during the assay of BVR-A would also be of concern due to the half lives involved (5730 years for [^{14}C] and 12.3 years for [^{3}H]).

It was decided to develop a new [^{32}P]-based assay system for BVR-A activity which would have a number of advantages over a [^{14}C] or [^{3}H] based assay, especially since [^{32}P]-

NADPH and [^{32}P]-NADH provide a far more flexible and sensitive assay method which would be applicable to other pyridine nucleotide utilising enzymes.

Unfortunately [^{32}P]-NADPH and [^{32}P]-NADH are not commercially available, and as a result a method for their production was needed. There are a number of ways which would theoretically allow the enzymatic synthesis of [^{32}P]-NADPH. These are presented in Figure 5.1. Both nicotinamide adenine [adenylate-^{32}P] dinucleotide (^{32}P-NAD^{+}) with a specific radioactivity of 1000 Ci/mmol and adenosine 5'-[γ-^{32}P] triphosphate with a specific radioactivity of 3000 Ci/mmol are available from 'GE Healthcare' life science division (formerly Amersham). The '[adenylate-^{32}P] NAD^{+}, (Figure 5.1) is so named, as it has the [^{32}P] label positioned at the adenine ribose phosphate. In Sections 5.2.4 and 5.2.5 the synthesis of [^{32}P]-NADH and [^{32}P]-NADPH are discussed.

Additional kinetic studies on human biliverdin-IXα reductase were carried out in the hope of gaining further insight into the nature of the substrate binding pocket. As discussed in the introduction the crystal structure of BVR-A from the rat has been resolved by two independent groups (Kikuchi *et al.*, 2001 and Whitby *et al.*, 2002). As a result our understanding of the nucleotide binding domain is substantial. However it should be noted that the rBVR-A-NAD^{+} complex reported by Whitby *et al.*, (2002) has the adenine moiety stacked over the nicotinamide ring. As will be discussed later, there is compelling evidence that this may be an artefact of crystallisation and that in solution a more linear extended structure of the pyridine nucleotide is probably adopted. From the experiments of Cunningham *et al.* (2000), we do know that at least one bridging propionate is required for optimal binding in the biliverdin binding pocket although two are preferred. The crystal structure with both cofactor and substrate bound however has not yet been determined, and as a result the nature of the biliverdin binding is less clear.

It was decided to further probe the nature of the biliverdin pocket using two initiatives. Firstly, similar to the methods of Cunningham *et al.* (2000) a range of synthetic biliverdins was used to further our knowledge and establish some of the 'general rules' associated with the kind of substrates which the enzyme can reduce.

Secondly, some CD spectral studies were also performed to examine whether or not a single conformer of biliverdin is adopted on binding to BVR-A. The interaction of bilirubin with serum albumin has been extensively studied (Lightner *et al.*, 1988, Lightner *et al.*, 1986, Petersen *et al* 2000 Blauer *et al* 1970, Honoré 1988 and the references cited therein). Many of these studies have utilised a very interesting property associated with bilirubin, and that is the optical rotatory dispersion (ORD) which arises when bilirubin interacts with a number of proteins. The most extensive studies have been with BSA which is now known to have a high affinity for bilirubin with at least one high affinity site $K_A \sim 10^8\ M^{-1}$, and two less specific secondary sites to which bilirubin may bind with $K_A \sim 10^5\ M^{-1}$ (McDonagh 1979 and Brodersen 1982). The optical activity of (4Z, 15Z)-bilirubin-IXα (Figure 5.23), arises from the 'ridge tile' type structure which the molecule adopts. This phenomenon is caused by extensive intramolecular hydrogen bonds which link the polar carboxylic acids with the terminal lactams and causes the molecule to twist over onto itself. Many groups have shown experimentally that bilirubin adopts such a conformation and it has been detected in crystals, in non polar solvents, and also as the predominant species present in polar solvents (all cited in Lightner *et al.*, 1988). Bilirubin-IXα (and biliverdin-IXα) is optically inactive in aqueous solutions due to the racemic nature of the solution as both enantiomeric forms are present in equimolar amounts. Again looking at the structures presented in Figure 5.23 we can see the two intramoleculy hydrogen bonded isomers have helicity designated P- (Plus) and M- (Minus) respectively (Nogales & Lightner 1995). When bilirubin binds to ligandin and albumin it adopts a specific conformation with either P helicity or M-helicity and the solution becomes optically active (Woolley *et al.*, 1976).

With little structural information available on the nature of biliverdin interactions with BVR-A it was considered that the optical rotatory dispersion of biliverdin-IXα and bilirubin-IXα may provide some insight into the nature of the enzyme-substrate complex and also the substrate binding pocket.

5.2 Separation of nucleotides

The development of an alternative assay for biliverdin reductase activity is highly dependent on the ability to detect and separate the various components of the radiolabelled

nucleotide synthesis reactions and also during the assay of human BVR-A. The most common methods for the separation of mixtures of nucleotides have been liquid chromatography on columns of anion exchange resins Silverstein (1970) and thin layer chromatography on polyethyleneimine cellulose (Randerath & Randerath 1967). Numerous techniques involving HPLC separations are also available. It was decided to look at some of these methods and determine the most reproducible and applicable methods for this assay.

5.2.1 Separation of nucleotides using DEAE column chromatography

One of the methods examined which could facilitate the separation of various nucleotides was ion exchange chromatography using DEAE mini-columns. Experimental procedures are outlined in Section 2.5.9a. Solutions, 1mM of NAD^+, NADH, $NADP^+$ and ATP were made in 10mM Tris-HCl pH 7.2. Samples (200µl) were loaded onto the column and washed with 10mM Tris pH 7.2 (18ml) followed by elution with a 2 x 50ml gradient (50mM KCl to 400mM KCl in 10mM Tris pH 7.2). Results of these experiments are presented in Figure 5.2. It is evident that NAD^+ elutes with good resolution between 60 – 70 mM KCl. The resolution of ATP, NADPH and $NADP^+$ is less effective however. Elution peaks of each nucleotide have been shown to overlap. Dilution of the samples loaded is also quite extensive with NADPH elution occurring over 20ml. It is interesting to note the appearance of a peak corresponding to that of NAD^+ when samples of freshly prepared NADH were run. This implies that significant quantities of NAD^+ are present in the NADH commercially available from Sigma. Although this system would have some merit with its ability to purify NAD^+ prior to its phosphorylation by NAD^+ kinase, its use as a method for the separation of ATP and $NADP^+$ during the synthesis of 2' [^{32}P]-$NADP^+$ would not be useful due to large sample dilution and lack of clear resolution between nucleotides.

5.2.2 Separation of nucleotides using PEI cellulose TLC

The chromatographic mobility of $NADP^+$, NADPH, NADH and NAD^+ on PEI-cellulose were determined. Samples (2µl of a 2mM solution of each nucleotide) were spotted onto PEI-cellulose TLC plates (Sigma Cat N0; Z12,288-2) and developed in an enclosed glass

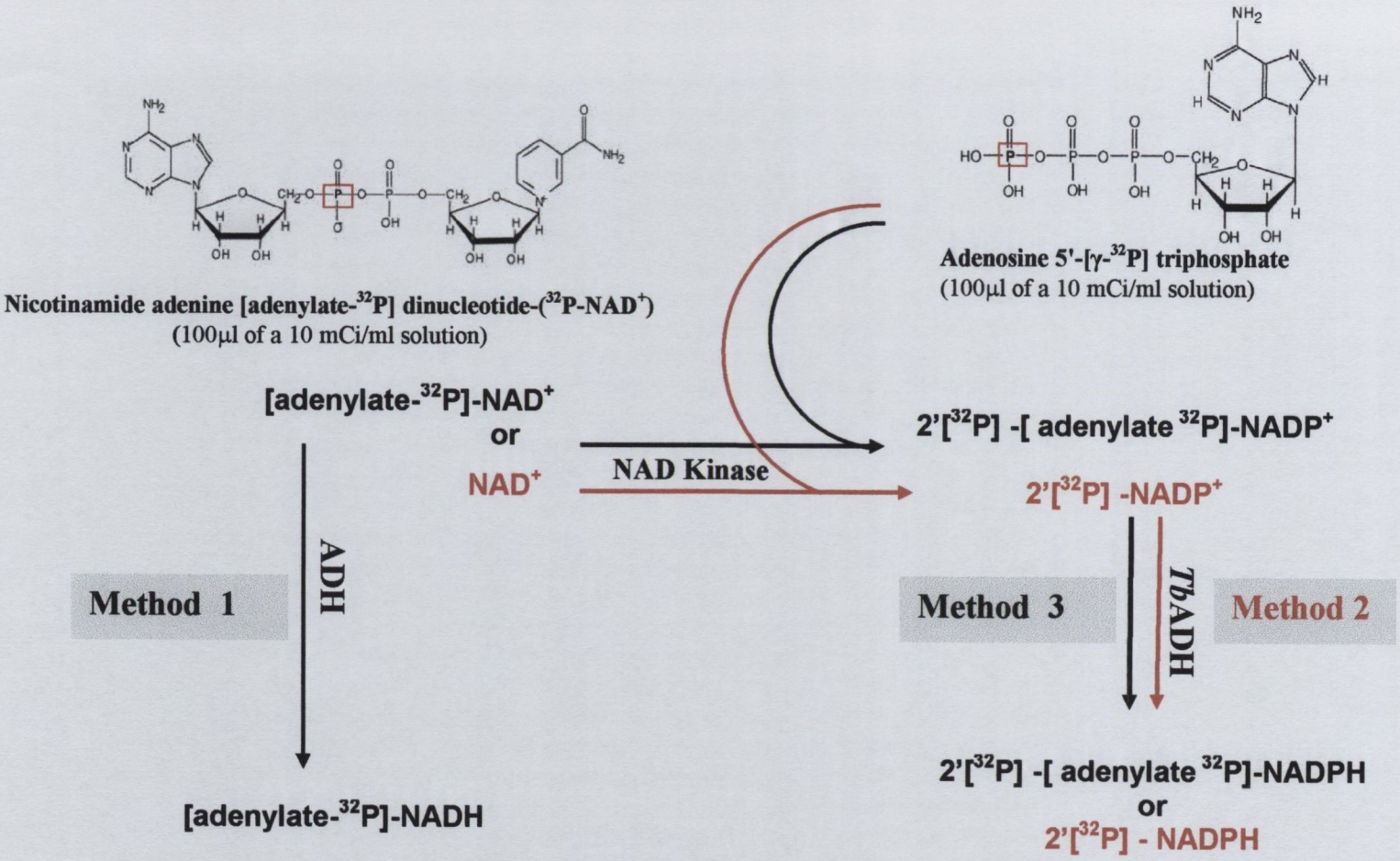

Figure 5.1 The various methods which would allow the production of ^{32}P labelled NADPH and NADH are shown.

The synthesis of three different labelled nucleotides are possible with the methods described. It is possible to produce NADPH with a double [^{32}P] label incorporated [adenylate-^{32}P]-NADPH, 2'[^{32}P] [adenylate-^{32}P]-NADPH and [adenylate-^{32}P]-NADH. The [^{32}P] is highlighted in red in the structures shown.

container using the solvents outlined in Table 5.1. Also presented in this Table are the relative mobilities of the nucleotides in each solvent. Since over time it can be difficult to keep experimental conditions constant the relative R_f values were calculated. "Relative R_f" means that the values are reported relative to a standard, and in this case LiCl (0.8M) was used for the calculation of relative mobilities during each of the separations. Visualisation of 'cold' nucleotide was achieved by exposing the dried plates to UV light at 254nm, and observing the fluorescence using a UVP bioimaging system attached to an Epi Chemi II Darkroom with a UVP ultraviolet products camera.

It was found that both oxidised nucleotides ($NADP^+$ and NAD^+) had greater mobilities than the reduced forms (NADH and NADPH) in the solvents used during these separations. It is also clear that divalent cations such as Ca^{2+} increase the mobility over monovalent cations in solution. One plausible explanation could be that divalent cations causes an increased rate of desorption of the ribose phosphates (and the 2'phosphate of NADPH and $NADP^+$) from the poly ethyleneimine cellulose particles

Presented in Figure 5.3 (a) is the separation of 'cold' $NADP^+$ and NADPH using PEI cellulose TLC. The solvent used was 200mM $CaCl_2$ 50mM Tris-HCl pH 7.2. Figure 5.3b shows the separation of 'cold' NAD^+ and NADH, using 50mM $CaCl_2$ 50mM Tris-HCl pH 7.2 as solvent. One could ideally visualise the separated labelled nucleotides by exposing the plate on a phosphoimager screen and the amount of $NADP^+$ and NADPH quantified using this system. Unfortunately this equipment was unavailable during the course of this work. As a result the most convenient method of visualising the labelled reactions was using autoradiography as presented in Figure 5.3 (c). Here a 5µl aliquot of the heat-inactivated BVR-A assay using 2'-[^{32}P]-NADPH as cofactor was loaded onto a PEI-cellulose TLC plate. After the nucleotides were separated by TLC, the plate was dried, and over-laid with X-ray film and exposed for 8 hours. Shown in lane 1 is a control experiment without human BVR-A in the assay mix. Lane 2 contains all components of the reaction using 2µM biliverdin as substrate and in lane 3, 5µM biliverdin was used as substrate. The production of $NADP^+$ by BVR–A can be calculated using densitometry or alternatively, the plates can be scraped and nucleotide extracted from the PEI cellulose with solvent and counted by liquid scintillation counting.

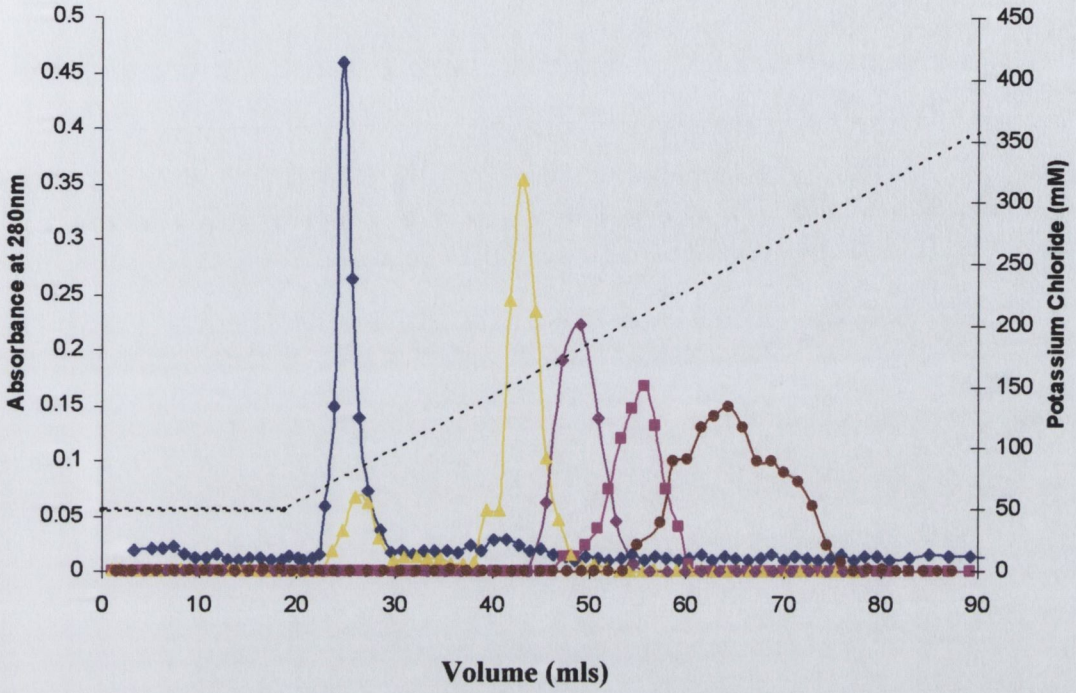

Figure 5.2 The separation of various nucleotides on DEAE cellulose anion exchange chromatography.

Separation of various pyridine nucleotides (♦ NAD^+ , ■ ATP, ● NADPH, ▲ NADH, ♦ $NADP^+$) on DEAE cellulose as described in Section 2.5.9a. Elution was achieved using (-.-.-.-)a potassium chloride gradient (50 to 400mM).

Figure 5.3 TLC separation of NADH NAD^+ $NADP^+$ and NADPH using PEI-cellulose.

(a) The separation of cold $NADP^+$ and NADPH was achieved using PEI cellulose TLC plates. The separation of 2µl of 2mM solutions of each nucleotide is presented. The solvent used was 200mM $CaCl_2$ 50mM Tris pH 7.2. After separation the plates were air dried and visualised with an overhead UV light source (254nm).

(b) For the separation of NAD^+ and NADH, 50mM $CaCl_2$ Tris pH 7.2 was used as solvent. Again the separation of 2µl of 2mM solutions of each nucleotide is presented. Detailed descriptions of the methods used are described in Section 2.5.9c.

(c) TLC analysis of a BVR-A reaction using 2'-[^{32}P]-NADPH as cofactor. A 5µl of volume of the heat-inactivated BVR-A assay was loaded onto a PEI-cellulose TLC plate. After nucleotides were separated by TLC, the plate was dried, and over-laid with x-ray film and allowed to expose for 8 hours. The $NADP^+$ and NADPH The production of $NADP^+$ by BVR–A can be calculated using densitometry or alternatively, the plates can be scrapped and nucleotide extracted from the PEI cellulose with solvent before being counted. Shown in lane 1 is a control experiment without human BVR-A in the assay mix. Lane 2 contains all components of the reaction using 2µM biliverdin as substrate and in lane 3, 5µM biliverdin was used as substrate.

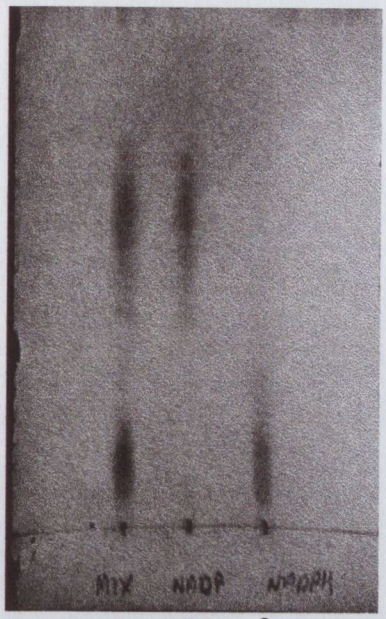

Lane 1 2 3

(a)

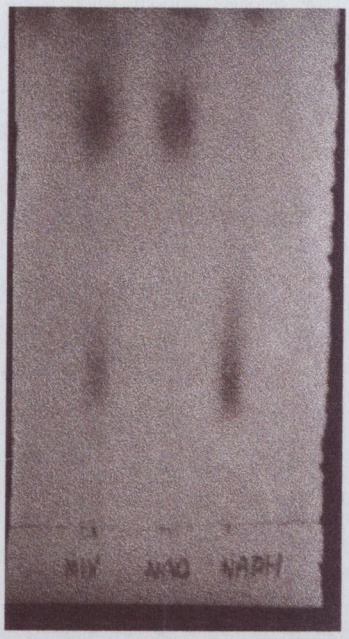

Lane 1 2 3

(b)

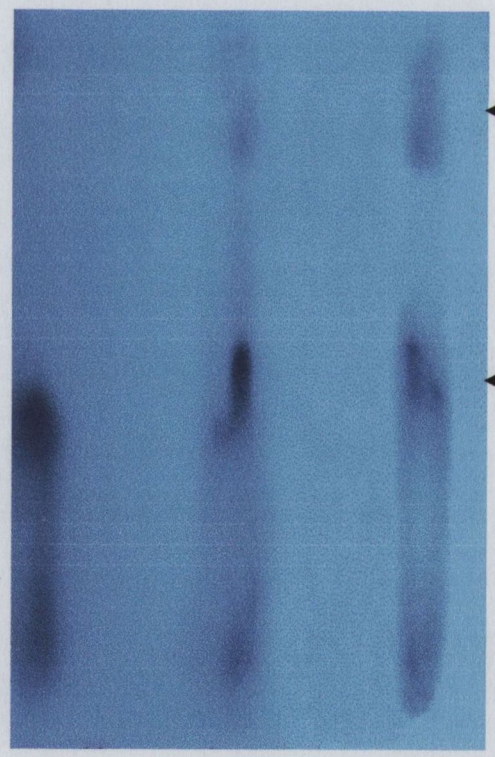

Lane 1 2 3

(c)

Solvent	Relative retention factor		
	$NADP^+$	**NADPH**	**R_f $NADP^+$ - R_f NADPH**
75mM Tris-HCl pH7.2	0.05	0.03	0.02
200mM NaCl 75mM Tris-HCl pH7.2	0.074	0.037	0.037
180mM $CaCl_2$ 75mM Tris-HCl pH7.2	0.54	0.13	0.41
200mM $CaCl_2$ 75mM Tris-HCl pH7.2	0.754	0.377	0.377
200mM $CaCl_2$ 75mM Tris-HCl pH 6	0.616	0.09	0.526
0.8M $LiCl_2$	0.615	0.29	0.325
1M $LiCl_2$	0.95	0.6	0.35
1.2M $LiCl_2$	0.98	0.87	0.11
0.8M $LiCl_2$ 20% Methanol	0.526	0.122	0.404
0.6M KCl	0.53	0.18	0.35
0.8M KCl	0.7	0.26	0.44
20% methanol 200mM $CaCl_2$ 10mM Tris-HCl pH7.2	0.636	0.181	0.455
20% methanol 250mM $CaCl_2$ 75mM Tris-HCl pH7.2	0.672	0.19	0.482
20% methanol 300mM $CaCl_2$ 75mM Tris-HCl pH7.2	0.69	0.272	0.418
200mM $MgCl_2$ 10mM Tris-HCl pH7.2	0.532	0.193	0.339
	NAD^+	**NADH**	**R_f NAD^+ - R_f NADH**
50mM $CaCl_2$ 50mM Tris-HCl pH 7.2	0.76	0.29	0.47

Table 5.1 Determination of the R_f values for $NADP^+$ NADPH NADH and NAD^+ in various solvents on PEI-cellulose TLC.

5.2.3 Separation of nucleotides using HPLC

The method of Markham *et al.* (2004) was selected as the method of choice to allow for the separation of a mixture of ATP, $NADP^+$, NADPH, NAD^+ and NADPH. The HPLC system used was a Shimadzu LC-10AL with a Discovery C-18 HPLC column (25cm x 4mm) attached via 500µl loop. Elution profiles were recorded using the Shimadzu C-R8A chromatopack. The presence of nucleotide was detected by monitoring the absorbance at 254 nm using the Shimadzu LC-10AL UV/VIS detector. Three buffers were used during the separations. Buffer A comprised of 100mM potassium phosphate pH 6.0, Buffer B comprised of a mixture of 60% Buffer A with 40% MeOH and Buffer C comprised of 100% MeOH. Elution from the column was achieved using the following program 0 – 9 minutes 100% buffer A, 10-15 minutes 98.5% Buffer A 1.5% Buffer B, 15-20 minutes 96.5% Buffer A, 3.5% Buffer B, 20-28 minutes 75% Buffer A and 25% Buffer B, and finally between 29 - 40 minutes the column was washed with 100% Buffer C (methanol). The flow rate was maintained at 0.8ml/min for the first 29 min of the program after which it was increased to 1ml/min during the methanol wash. Presented in Figure 5.4 is the HPLC separation of a mixture of 250 µM solutions of ATP, $NADP^+$, NADPH, NAD^+ and NADPH in a total volume of 500µl. Using this method all nucleotides in the mixture resolved into well define peaks with sufficient differences in retention times. ATP elutes at t_R =5.1 mins, $NADP^+$ at t_R =12.1 mins, NAD^+ at t_R= 23.4 mins, NADPH at t_R = 27.1 mins, and finally NADH at t_R = 29.5 mins. This technique was chosen as the method of choice for all separations during the synthesis of labelled nucleotides.

5.2.4 Synthesis of [adenylate-^{32}P] NADH

There are a number of methods which one could use to synthesise both [^{32}P] NADPH and [^{32}P] NADH using the commercially available isotopically labelled nucleotides and these are detailed in Fig. 5.1. The first involves the enzymatic reduction of [adenylate-^{32}P] NAD^+ to [adenylate-^{32}P] NADH using alcohol dehydrogenase from *Saccharomyces cerevisiae*.

Ethanol + [^{32}P-adenylate]-NAD^+ $\overset{\text{ADH}}{\rightleftharpoons}$ Acetaldehyde + [^{32}P-adenylate]-NADH

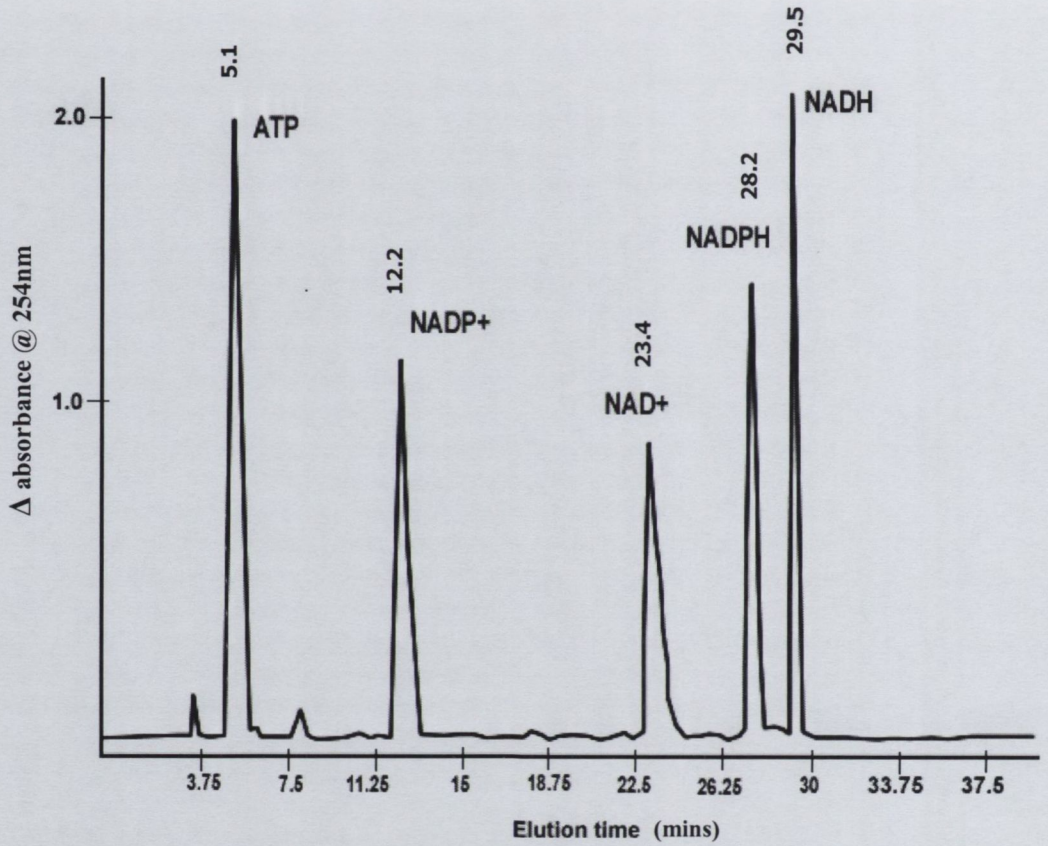

Figure 5.4 HPLC separation of a mixture of ATP, $NADP^+$, NADPH, NAD^+ and NADPH

The separation of a 500 µl sample containing ATP, $NADP^+$, NADPH, NAD^+ and NADPH, all at a final concentration of 250 µM as described in section 5.2.3.

The equilibrium of this reaction lies in favour of ethanol and NAD^+, however under alkaline conditions (pH 8.6) and with a large excess of ethanol (500 mM) equilibrium shifts to the right producing conversion yields of up to 80% NADH. The ADH reaction was performed at 30°C and the extent of conversion was measured by monitoring the increase in absorbance at 340 nm due to the reduction of NAD^+ by the enzyme using ethanol as substrate. The final concentrations of reactants in the conversion assay is 500mM ethanol, 2.5 mM [^{32}P-adenylate] NAD^+, and 100mM Tris-HC1, pH 8.6 in a total volume of 500µl. The reaction was started by the addition of 0.1 units of enzyme. The percentage conversion to NADH was calculated from the increase in absorbance observed at 340nm. The conversion of the [adenylate-^{32}P] NAD^+ to the reduced form proved problematic however. Although up to 80% yields of 'cold' NADH were routinely produced, the assay using [^{32}P-adenylate] NAD^+ produced yields with less than 20% conversion. One possibility is that the stabilisation solution used in the shipment of this nucleotide, which included β-mercaptoethanol and various salts, may interfere with the ADH reaction. Furthermore attempts to perform multiple rounds of purification in the hope of producing sufficient reduced nucleotide were hindered by its instability and subsequent breakdown as determined by A_{260}/A_{340} ratio. Although [adenylate-^{32}P] NADH was successfully produced, further work is required to determine what factors cause a reduction in yields and the deterioration of nucleotide.

5.2.5 Synthesis of 2'-[^{32}P]-NADPH

[^{32}P]-$NADP^+$ was formed enzymatically by phosphorylation of the NAD^+ adenosine ribosyl residue's C(2')-OH group using NAD^+ kinase and adenosine 5'-[γ-^{32}P] triphosphate as [^{32}P] donor. This was made feasible by utilising recombinant *E.coli* NAD^+ kinase which was cloned, expressed and kindly provided by Dr. Seamus Browne of the Biochemistry Department in Trinity College, Dublin. The conversion of NAD^+ to $NADP^+$ was carried out essentially according to the method of Kawai (2001) as described in Section 2.5.10.

Radiolabelled 2'-[^{32}P]-$NADP^+$ purified from the NAD^+ kinase reaction was reduced to 2'-[^{32}P]-NADPH using the $NADP^+$ dependent alcohol dehydrogenase from *Thermoanaerobium brockii (TbADH)*. The final concentration of each of the components of the ADH reaction used in the synthesis of 2'-[^{32}P]-NADPH were propan-2-ol 500µM,

Figure 5.5 HPLC analysis of the ADH reactions used to synthesise 2'-[^{32}P]-NADPH.

(a) The components of the alcohol dehydrogenase reaction shown in Table 5.2, with the exception of ADH, were incubated at 40°C for 30mins before loading on the column as described in section 5.3. Elution of the nucleotide (designated peak 1) is the $NADP^+$ component of the reaction which was detected at 254nm.

(b) Following a 30 minute incubation at 40°C, the components of the entire ADH reaction shown in Table 5.X15 were separated by HPLC and (Section 5.3). Again nucleotides in the eluate were detected at 254nm. The emergence of an additional peak (designated peak 2) was the 2'-[^{32}P]-NADPH produced when propan-2-ol is oxidised to acetone by the TbADH.

(c) The elution profile of the total radioactivity/sample for a "hot" ADH reaction. Samples of fractions collected following the ADH reaction were adequately diluted to maintain counting efficiency and counted in scintillation fluid (1ml). Peak 1 is 2'-[^{32}P]-$NADP^+$. Peak 2 is 2'-[^{32}P]-NADPH.. Peak 3 is most likely a breakdown product of 2' -[^{32}P]-NADPH .

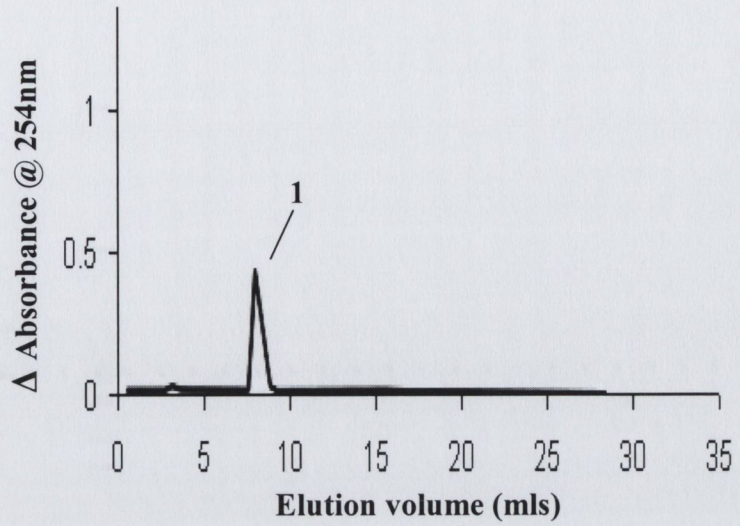
Δ Absorbance @ 254nm
1
0.5
0
1
0 5 10 15 20 25 30 35
Elution volume (mls)

(a)

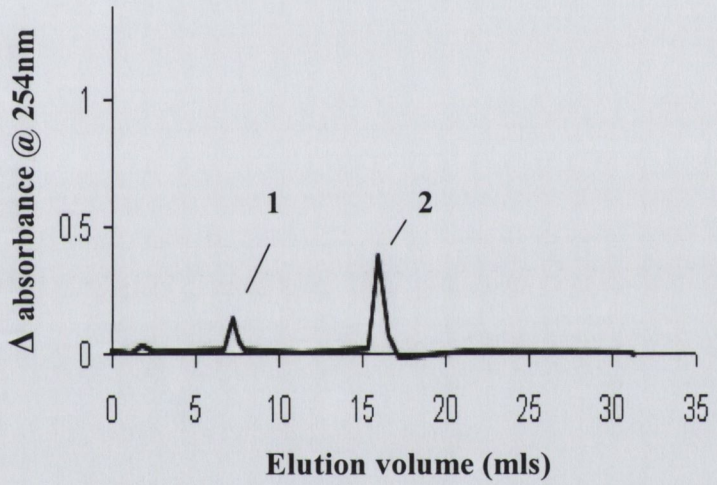
Δ absorbance @ 254nm
1
0.5
0
1
2
0 5 10 15 20 25 30 35
Elution volume (mls)

(b)

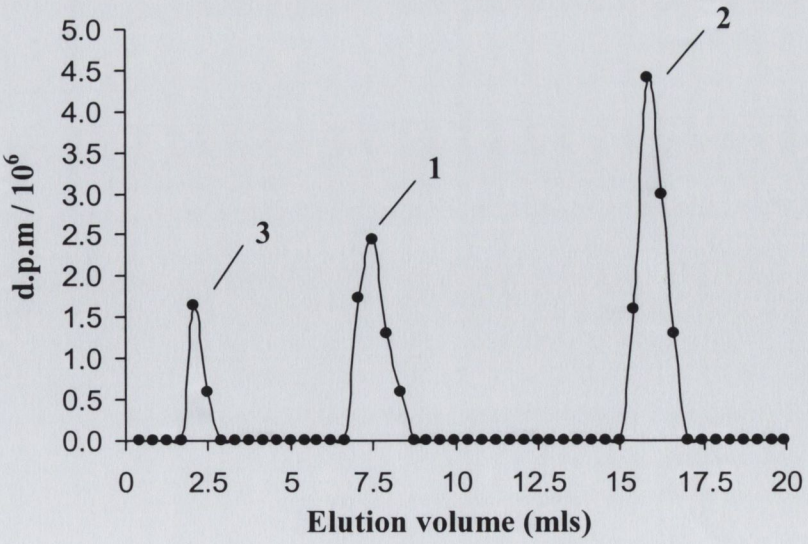
d.p.m / 10^6
5.0
4.5
4.0
3.5
3.0
2.5
2.0
1.5
1.0
0.5
0.0
3
1
2
0 2.5 5 7.5 10 12.5 15 17.5 20
Elution volume (mls)

(c)

Figure 5.6 HPLC analysis of the newly synthesised 2'-[^{32}P]-NADPH

(a) A_{254} elution profile from C-18 column when 20µl of the newly synthesised 2'-[^{32}P]-NADPH (243mCi/mmol) was mixed with 500µl of ~500µM of NADPH and analysed as described in Section 2.22.4.

(b) DPM elution profile when 20ul of the newly synthesised 2'-[^{32}P]-NADPH (2.7Ci/mmol) with 500µl of ~500µM of NADPH analysed as described in Section 2.22.4. Radioactivity was detected by counting 100µl of each of the elution fractions in scintillation fluid (1ml). This plot represents the radioactivity present per 100µl of sample.

(c) A_{340} elution profile from C-18 column when 20µl of the newly synthesised 2'-[^{32}P]-NADPH (243mCi/mmol) is mixed with 500µl of ~500µM of NADPH and analysed as described in Section 2.22.4

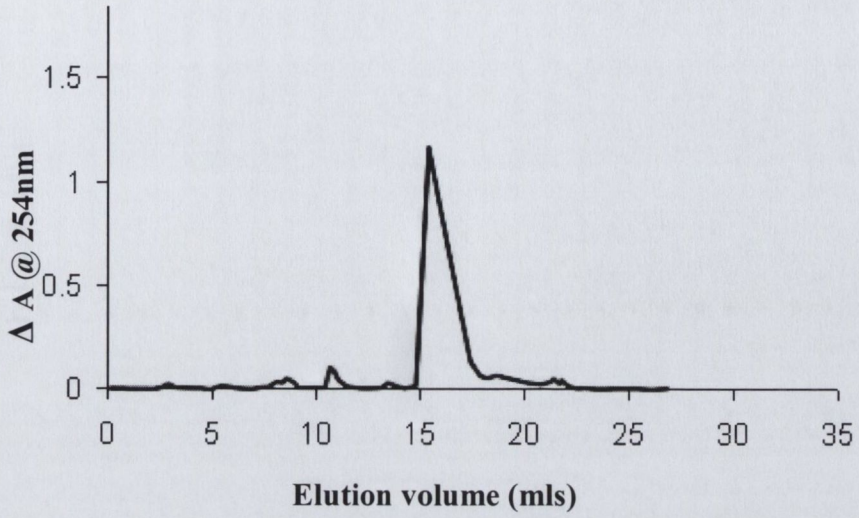
Δ A @ 254nm
1.5
1
0.5
0
0
5
10
15
20
25
30
35
Elution volume (mls)

(a)

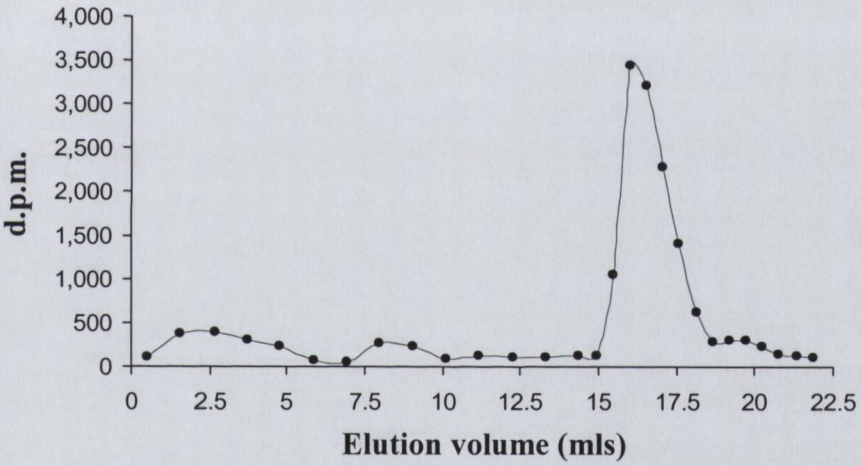
d.p.m.
4,000
3,500
3,000
2,500
2,000
1,500
1,000
500
0
0
2.5
5
7.5
10
12.5
15
17.5
20
22.5
Elution volume (mls)

(b)

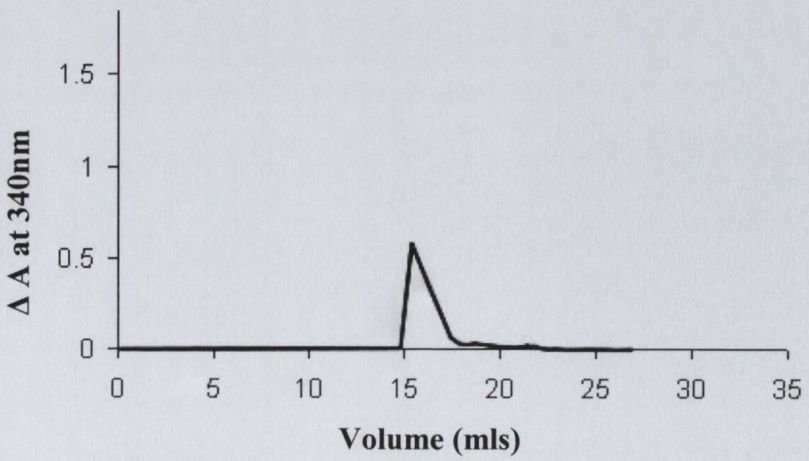
Δ A at 340nm
1.5
1
0.5
0
0
5
10
15
20
25
30
35
Volume (mls)

(c)

Component	Stock concentration	Volume	Final concentration
Propan-2-ol	50mM	5µl	500µM
2'-[^{32}P]-NADP$^+$ (2.7Ci/mmol)	8.25µM	500µl	~7.5µM
***Tb*ADH**	100U / ml	2ul	0.1U
NADP$^+$	2mM	5µl	20µM
Reaction buffer	10 X	50µl	1 X

(a)

Compound	Concentration	Volume	Solvent	Total d.p.m.	d.p.m./µl	% Yield	Specific Activity
2'-[^{32}P]-NADP$^+$	8.25µM	2ml	100mM sodium phosphate pH 7.0	1.05×10^8	52500	18.4	2.7Ci/mmol
2'-[^{32}P]-NADPH	14.6µM	1.6ml	30% MeOH : 70% 100mM sodium phosphate pH 7.0 (v/v)	1.257×10^7	7856	2.2	243mCi/mmol

(b)

Table 5.2 Synthesis of 2'-[^{32}P]-NADPH.

(a) Components of ADH reaction used to synthesis 2'-[^{32}P]-NADPH

The (10X) reaction buffer was 1M sodium phosphate, pH 7.8 while the propan-2-ol stock was made from HPLC grade propan-2-ol (0.78g/ml). With the exception of the 2'-[^{32}P]-NADP$^+$, all reactants were made up in 100mM sodium phosphate, pH 7.8. 2'-[^{32}P]-NADP$^+$ was in 100mM potassium phosphate, pH 7. The reaction was allowed to take place at 40°C for 30min.

(b) Purification of 2'-[^{32}P]-NADP$^+$ and 2'-[^{32}P]-NADPH.

2'-[^{32}P]-NADP$^+$ 7.5μM, *Tb*ADH 0.1units, NADP$^+$ 20μM in 100mM sodium phosphate, pH 7.8 (see Table 5.2). The HPLC method of Markham *et al.* (2004), described in Section 2.5.9b allowed the purification of 2'-[^{32}P]-NADPH from the ADH reaction. The components of the ADH reaction listed in Table 5.2, with the exception that ADH was not added, were incubated at 40°C for 30 minutes. This mixture was then analysed by HPLC the results of which are presented in Figure 5.5 (a). As one would expect, in the absence of enzyme the main nucleotide component of the reaction mixture is NADP$^+$ (designated as Peak 1). Figure 5.5 (b) shows the A_{254} elution profile for a 'hot' ADH reaction containing all of the components necessary for the conversion of [^{32}P]-NADP$^+$ to [^{32}P]-NADPH following 40 minute incubation at 40°C. The appearance of a second peak 'Peak 2' is the [^{32}P]-NADPH produced when propan-2-ol is oxidised to acetone by *Tb*ADH. Analysis of the peak areas of Figures 5.5 (a) and Figure 5.5 (b), revealed that ~75% of the NADP$^+$ had been converted to NADPH. Samples of each of the 0.4ml fractions collected following the HPLC purification of the ADH reaction were counted in 1 ml of 'Ecoscint'. Multiple dilutions of the samples were taken and counted to ensure that the detection range of the counter was not exceeded thereby affecting the counting efficiency. The total radioactivity per sample was then measured and is presented in Figure 5.5 (c). The appearance of a third radioactive peak is evident when comparing Figures 5.5 (c) and 5.5 (b). The only reasonable explanation for the emergence of this peak would be the conclusion that this peak is most likely a breakdown product of the 2'-[^{32}P]-NADP$^+$ used in the ADH reaction. Further identification of this contaminant was not pursued. To maximise the yield of 2'-[^{32}P]-NADPH the ADH reaction was performed twice. The concentration of 2'-[^{32}P]-NADPH was determined by measuring the absorbance at 260 nm and 340 nm. Its purity was also confirmed by calculating the ratio of these two values (i.e. from the extinction coefficients the A_{260} / A_{340} of ~2.26 is ~100% pure). A total of 1.6 ml of a ~14.6 μM of 2'-[^{32}P]-NADPH (243 mCi/mmol) was made and purified from 1 ml of 8.25 μM solution of 2'-[^{32}P]-NADP$^+$ (2.7 Ci/mmol). After the purification of the 2'-[^{32}P]-NADPH a 20μl aliquot was mixed with a 500 μM solution of NADPH (500 μl) in 100 mM potassium phosphate pH 7. Again this mixture was analysed using the HPLC methods described above. The radioactive peak co-eluted with a single peak detected at 254nm and 340nm, providing evidence that the synthesised 2'-[^{32}P]-NADPH was indeed homogenous and co-purified as expected as shown in Figure 5.6.

5.2.6 The temperature dependent inactivation of human BVR-A.

A stopped assay such as this requires inhibition of the enzyme or its denaturation at specific time points. It was concluded that the simplest method to achieve this was to heat inactivate the enzyme. A number of experiments were set up which involved heating the enzyme at 50°C, 60°C and 70°C in a water bath over 3 minutes. Following each incubation the enzyme was assayed in 100 mM Tris-HCl pH 8 containing 10 μM biliverdin-IXα and 100 μM NADPH. Rates were plotted with respect to enzyme incubated for similar periods at 30°C. The percent inactivation at each temperature is presented in Figure 5.7. It is apparent that incubation of human BVR-A at 70°C for 1 minute totally inactivates the enzyme. At 60°C the same levels of inactivation are achieved over a period of 90 seconds. A series of experiments were set up to determine the effects of exposing both NADPH and NADH to such temperatures. Figures 5.8 (a) and (b) show the rate of breakdown of NADPH and NADH respectively. NADPH is the most unstable with just over 1% of the total being broken down over 1 minute at 70°C. In contrast ~0.3% NADH was found to have broken down under similar conditions. It was concluded from this that the heat inactivation of the BVR-A reaction is a sensible option to denature the protein allowing a stopped assay.

5.2.7 The assay of human BVR-A using 2'-[^{32}P]-NADPH as cofactor

As discussed in Section 5.2.5, a total of 1.6 ml of a ~14.6 μM solution of 2'-[^{32}P]-NADPH (243 mCi/mmol) was made and purified from 1 ml of an 8.25 μM solution of 2'-[^{32}P]-$NADP^+$ (2.7 Ci/mmol). The apparent K_m for NADPH with human BVR-A is reported to be ~2μM. Unfortunately the quantity of nucleotide produced (14.6 μM) prevented any extensive studies on the kinetics of the enzyme. In the present study it has been shown that the assay of BVR-A activity is indeed possible using radiolabelled nucleotide as cofactor. Further work is required especially in the production of sufficient yields of radiolabelled nucleotide to facilitate the assay of BVR-A under saturation conditions with respect to nucleotide. Figure 5.9 details the methodology developed in its entirety. The purification of 1.6 ml of a ~14.6 μM of 2'-[^{32}P]-NADPH (243 mCi/mmol) has been detailed and the subsequent use of this nucleotide to assay BVR-A activity is possible as shown in Figure

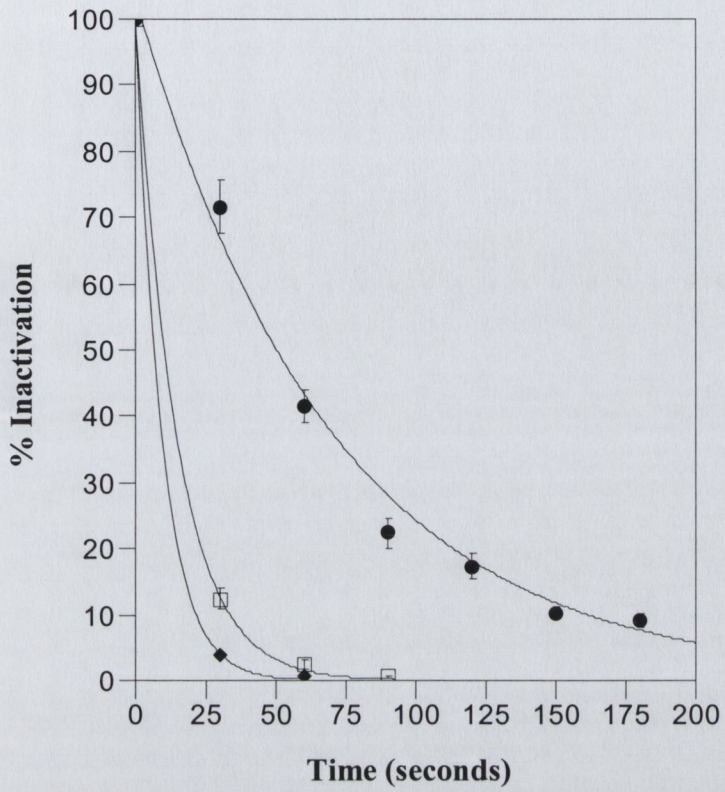

Figure 5.7 Heat inactivation of human biliverdin-IXα reductase.

Heat inactivation of human BVR-A was performed as described in Section 5.4. The enzyme was incubated at 50°C (●), 60°C (□), and 70°C (♦) and samples were assayed at various time points in 100mM Tris pH 8, containing 10μM biliverdin-IXα and 100μM NADPH.

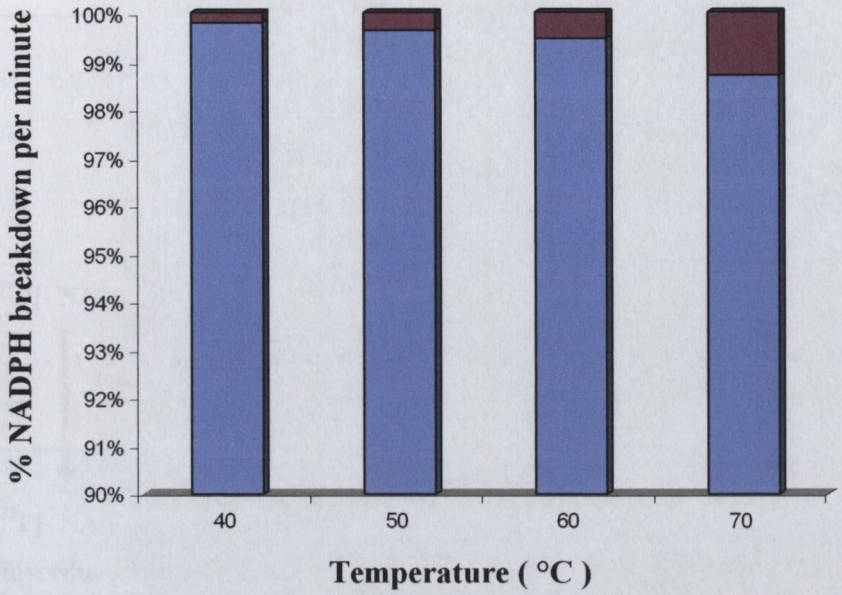

(a)

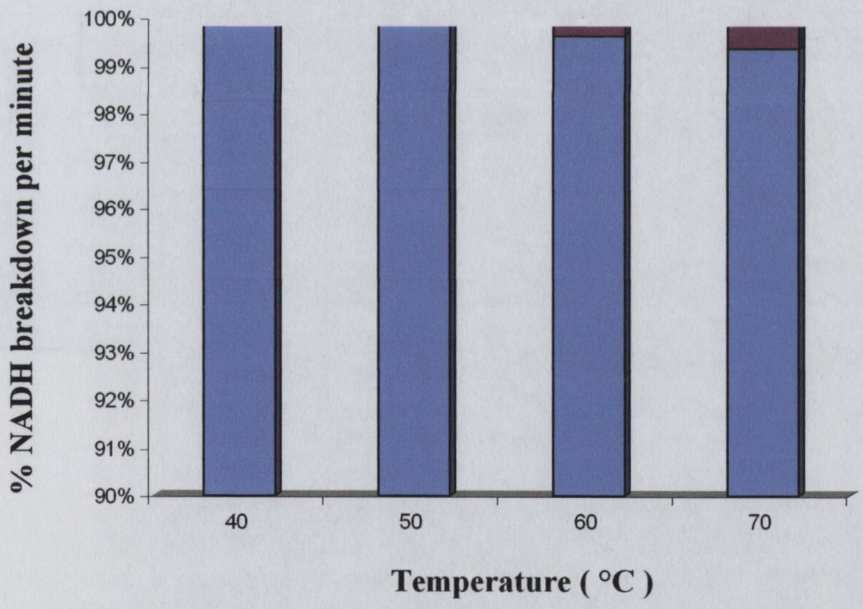

(b)

Figure 5.8 The heat stability of NADPH and NADH at various temperatures.

Figures (a) and (b) show the rate of breakdown of NADPH and NADH respectively. Rates of breakdown were determined by monitoring the decrease in absorbance at 340nm of 100μM solutions of each nucleotide in 100mM sodium phosphate pH 7.5.

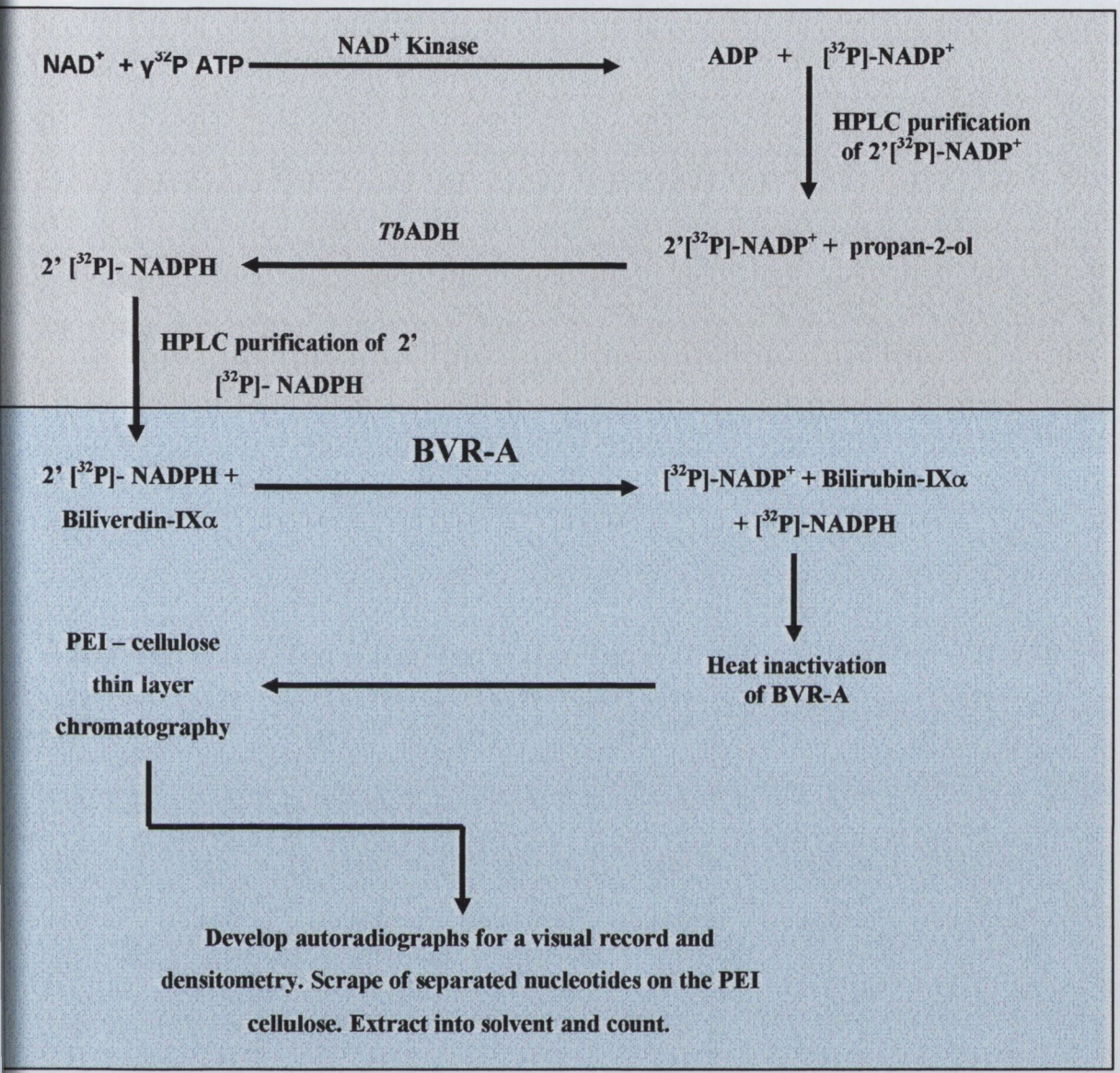

ure 5.9 **Flow chart representing the principle steps involved in the development of a new assay for biliverdin-IXα reductase.**

5.3(c) where 5µl of the heat-inactivated BVR-A assay was loaded onto a PEI-cellulose plate and the nucleotides separated by TLC using 200mM $CaCl_2$ 50 mM Tris-HCl pH 7.2. The plate was dried, and over-laid with x-ray film and allowed to expose for 8 hours. Shown in lane 1 is a control experiment without human BVR-A in the assay mix. Lane 2 and 3 contained 2 µM biliverdin and 5 µM biliverdin as substrate respectively with all other components of the reaction. The BVR-A dependent production of 2'-[^{32}P]-$NADP^+$ is clearly visible at 3 µM biliverdin.

5.3 Investigating the nature of the biliverdin binding pocket

5.3.1 Probing the nature of substrate specificity of human biliverdin-IXα reductase using conformationally locked biliverdin substrates.

The substrate specificity of human biliverdin-IXα reductase was examined using a range of synthetic biliverdins kindly provided by Prof. Katsuhiko Inomata, Division of Materials Sciences, Graduate School of Natural Science and Technology, Kanazawa, Ishikawa Japan. These biliverdin derivatives have their C and D rings sterically locked by cyclizing with an additional 2 or 3-carbon chain (Inomata *et al.*, 2005). These tetrapyrroles are termed 15ZZZ-anti 18ETBV, 15ZZZ-syn 18ETBV, 15ZZE-anti 18ETBV and 15ZZE-syn 18ETBV and the structures of each are shown in Figure 5.10a. The extinction coefficients of each of the locked isomers were determined and are presented in Figure 5.10b. Energy minimisation and structural comparisons were performed using the MOE program suite (MOE Molecular Operating Environment, Montreal, Chemical Computing Group Inc. 2001) in collaboration with Georgia Golfis, School of Biochemistry and Immunology, Trinity College, Dublin and the results of which are shown in Figure 5.11a, b and c.

The absorbance spectra of 17 µM 15 ZZZ-syn18ET biliverdin in 100mM Tris-HCl pH 8 with and without BSA were measured and the results are presented in Figure 5.13. The addition of 37 µM BSA causes λ_{max} shifts from 379 nm to 392 nm and from 660 nm to 680 nm (Figure 5.13a). During the course of this work it was noticed that the incubation of 15 ZZZ-syn 18ETBV with BSA (37 µM) resulted in a time-dependent change in the spectrum of this isomer which is suggestive of a reaction occurring on the surface of the albumin. This is clearly visible in Figure 5.15 (b). As shown there is a substantial increase in the

Figure 5.10a Biliverdin-IXα derivatives were used to investigate the substrate specificity of recombinant human BVR-A.

Structures 1 and 2 show biliverdin-IXα and (18ET biliverdin-IX α) 18,18'-dihydrobiliverdin-IXα respectively. Structures 3, 4, 5, and 6, depict the locked synthetic biliverdin isomers 15ZZZ-anti 18ET biliverdin-IX α, 15ZZZ-syn 18ET biliverdin-IX α, 15ZZE-anti 18ET biliverdin-IX α, 15ZZE-syn 18ET biliverdin-IX α.

These derivatives have fixed C and D rings through the addition of a carbon chain in either the Z-anti, Z-syn, E-anti, or E-syn conformations. The C15=C16 double bond is either in the Z or E conformation and the single bond in either the syn or anti position.

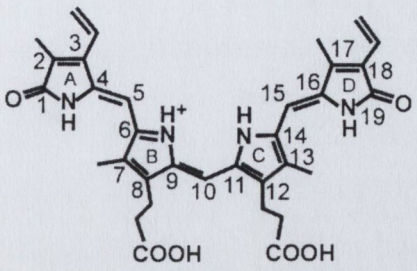

1. **Biliverdin-IX α**

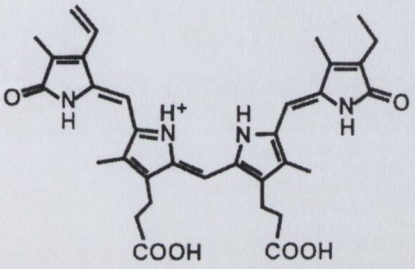

2. **18ET biliverdin-IX α**

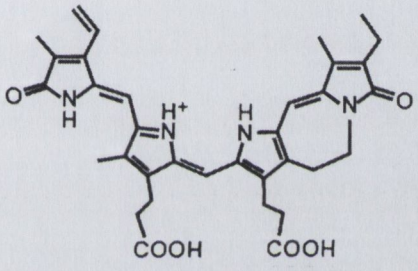

3. **15ZZZ-anti 18ET biliverdin-IX α**

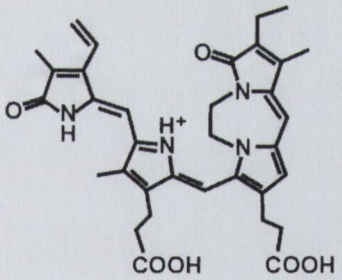

4. **15ZZZ-syn 18ET biliverdin-IX α**

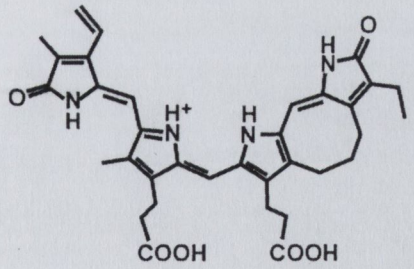

5. **15ZZE-anti 18ET biliverdin-IX α**

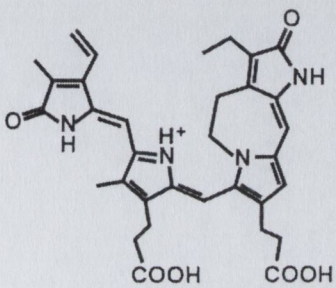

6. **15ZZE-syn 18ET biliverdin-IX α**

15ZZZ-anti 18ET biliverdin-IXα

15ZZZ-syn 18ET biliverdin-IXα

15ZZE-anti 18ET biliverdin-IXα

15ZZE-syn 18ET biliverdin-IXα

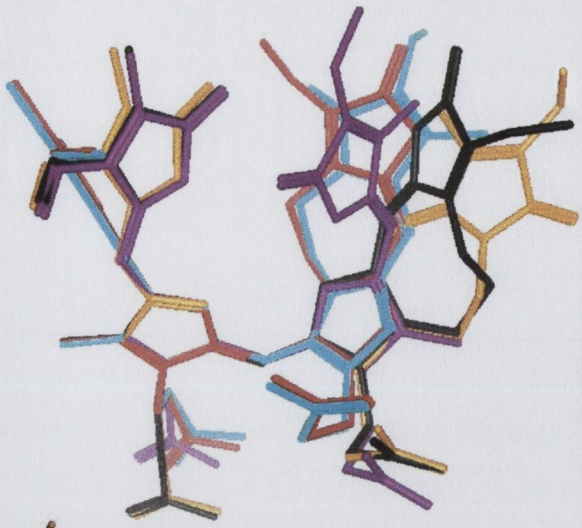

(a)

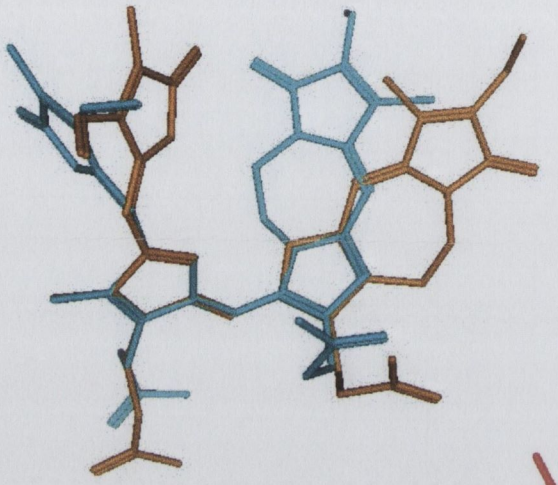

15ZZZ-anti 18ET biliverdin-IXα

15ZZZ-syn 18ET biliverdin-IXα

(b)

15ZZE-anti 18ET biliverdin-IXα

15ZZE-syn 18ET biliverdin-IXα

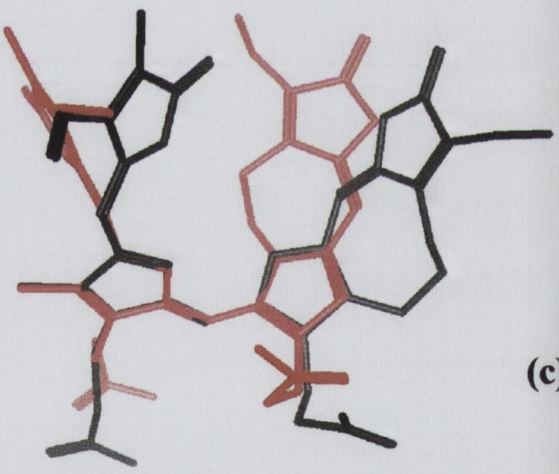

(c)

	Apparent Molar Extinction Coefficient (ε)		
Isomer \ Solvent	**MeOH**	**MeOH/HCl**	**100mM Tris pH 8**
	$M.cm^{-1}$	$M.cm^{-1}$	$M.cm^{-1}$
ZZE-anti 18ET biliverdin	40533 @ 380nm	38984 @ 368nm	29735 @ 379nm
ZZE-syn 18ET biliverdin	33000 @ 389nm	ND	ND
ZZZ-anti18ET biliverdin	23355 @ 385nm	24833 @ 370nm	24194 @ 379nm
ZZZ-syn 18ET biliverdin	39850 @ 382nm	31325 @ 376nm	31325 @ 376nm

(d)

Figure 5.10b Energy minimised structures of the locked biliverdins

Energy minimisation and structure comparisons were performed using the the MOE program suite (MOE Molecular Operating Environment, Montreal, Chemical Computing Group Inc. 2001).

(a) 15ZZZ-anti 18ET biliverdin-IXα, 15ZZZ-syn 18ET biliverdin-IXα, 15ZZE-anti 18ET biliverdin-IXα, 15ZZE-syn 18ET biliverdin-IXα, and 18ET biliverdin-IXα overlaid

(b) 15ZZZ-anti 18ET biliverdin-IXα, 15ZZZ-syn 18ET biliverdin-IXα, overlaid.

(c) 15ZZE-anti 18ET biliverdin-IXα, 15ZZE-syn 18ET biliverdin-IXα overlaid.

(d) Experimentally derived molar extinction coefficients of the locked biliverdins in various solvents.

These derivatives have fixed C and D rings through the addition of a carbon chain in the Z-anti, Z-syn, E-anti, or E-syn conformations. The C15=C16 double bond is either in the Z or E conformation and the single bond in either the syn or anti conformation.

absorbance at 425 nm with a corresponding decrease at 680 nm, which mimics the formation of bilirubin. Interestingly, Manitto and Monti (1979) reported the observation that sulphydryl groups add to the central methene bridge of biliverdin in organic solvents and that this addition reaction with organic thiols was also promoted in the presence of albumin. In this case there is an increase at 460 nm, however the 15ZZZ-syn 18ET isomer exhibits a slow increase at 425 nm coupled with a decrease at 680 nm. To determine the stability of this isomer in buffer and in the presence of NADPH kinetic scans from 300 nm to 750 nm were measured over a period of 10 minutes. Samples measured contained 17 μM 15 ZZZ-syn18ET biliverdin at 37°C in 100 mM Tris-HCl pH 8 and also with 120 μM NADPH included, the results of which are presented in Figure 5.13 (b). It is clear that there are no spectral changes observed over the time periods measured. On addition of 1.4μg human BVR-A there is a characteristic decrease in absorbance at 660nm and an increase in the absorbance at 460nm which is associated with bilirubin production. The effect of increasing concentrations of 15ZZZ-syn 18ET biliverdin (2, 5, 10 and 20μM) on the activity of human biliverdin IXα reductase was also examined. The production of bilirubin was measured by monitoring the increase in absorbance at 460nm. The reaction mixture contained 15ZZZ-syn 18ET biliverdin and 100μM NADPH in 100mM Tris-HCl pH 8 at 37°C, and the results are presented in Figure 5.14. As with biliverdin-IXα potent substrate inhibition was observed when using 15 ZZZ-syn 18ET biliverdin as substrate.

None of the other fixed isomers (15ZZZ-anti 18ET [Figure 5.11]; 15ZZE-anti 18ET [Figure 5.16] and 15ZZE-syn 18ET [Figure 5.18]) exhibited time-dependent spectral shifts simply on incubation with BSA. They were all substrates for human BVR-A and revealed the characteristic immediate blue shifts, on addition of BSA (for the "390" and "660" peaks), this being particularly marked for the 15ZZE-syn 18ET isomer (Fig. 5.18). Addition of NADPH (120μM) and human BVR-A produced the expected increase at 460nm coupled with a decrease at 660nm. When the initial rate was measured (Δ460) at a range of concentrations of the various locked isomers the characteristic substrate inhibition profile was evident (Figure 5.12; Figure 5.14 and Figure 5.17).

Figure 5.11 15 ZZZ-anti 18ET biliverdin as a substrate for human biliverdin IXα reductase

(a) The absorbance spectrum of 25μM 15 ZZZ-anti 18ET biliverdin in reaction buffer (100mM Tris pH 8) is represented by the blue line. On addition of 37uM BSA the spectrum shift observed is represented by the red line.

(b) The absorbance spectrum of 25μM 15 ZZZ-anti 18ET biliverdin and 37μM BSA in 100mM Tris pH 8 is represented in red. The addition of 120μM NADPH to the reaction mixture gives the spectrum shown in pink. This absorbance spectrum of this reaction mixture was monitored over a 10 minute period.

(c) The absorbance spectrum changes observed on the addition of 1.4μg human BVR-A to a reaction mixture containing of 25μM 15 ZZZ-anti 18ET biliverdin and 37μM BSA in 100mM Tris pH 8. The spectrum changes were monitored over 10 minutes at 37°C.

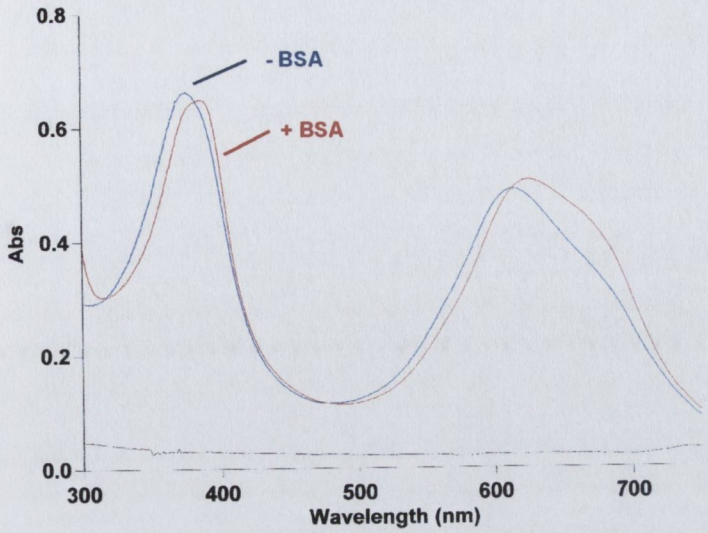
0.8
0.6
0.4
0.2
0.0
Abs
- BSA
+ BSA
300
400
500
600
700
Wavelength (nm)

(a)

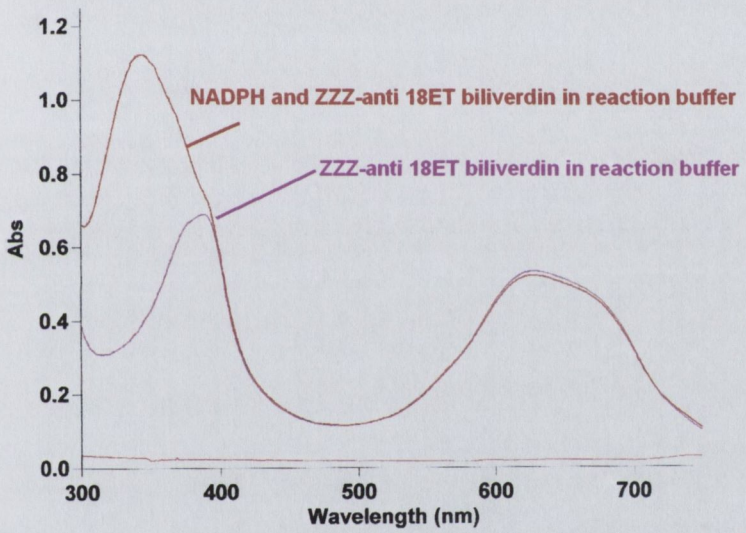
1.2
1.0
0.8
0.6
0.4
0.2
0.0
Abs
NADPH and ZZZ-anti 18ET biliverdin in reaction buffer
ZZZ-anti 18ET biliverdin in reaction buffer
300
400
500
600
700
Wavelength (nm)

(b)

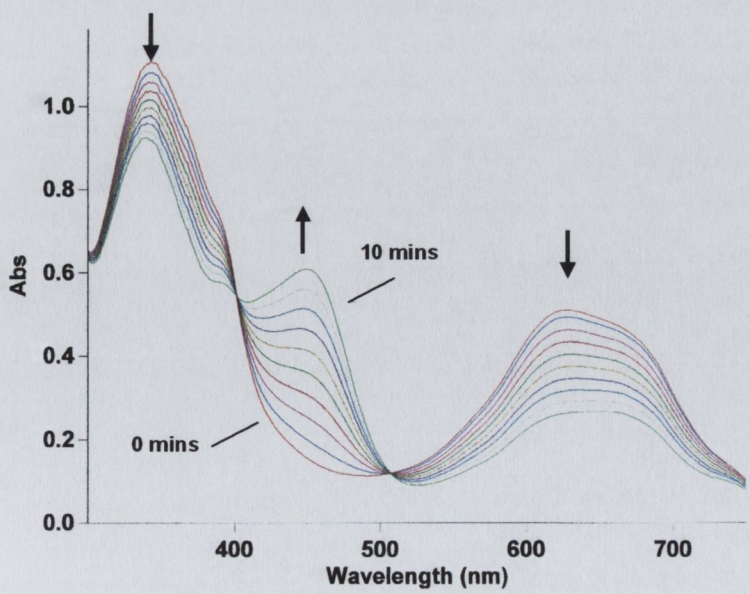
1.0
0.8
0.6
0.4
0.2
0.0
Abs
10 mins
0 mins
400
500
600
700
Wavelength (nm)

(c)

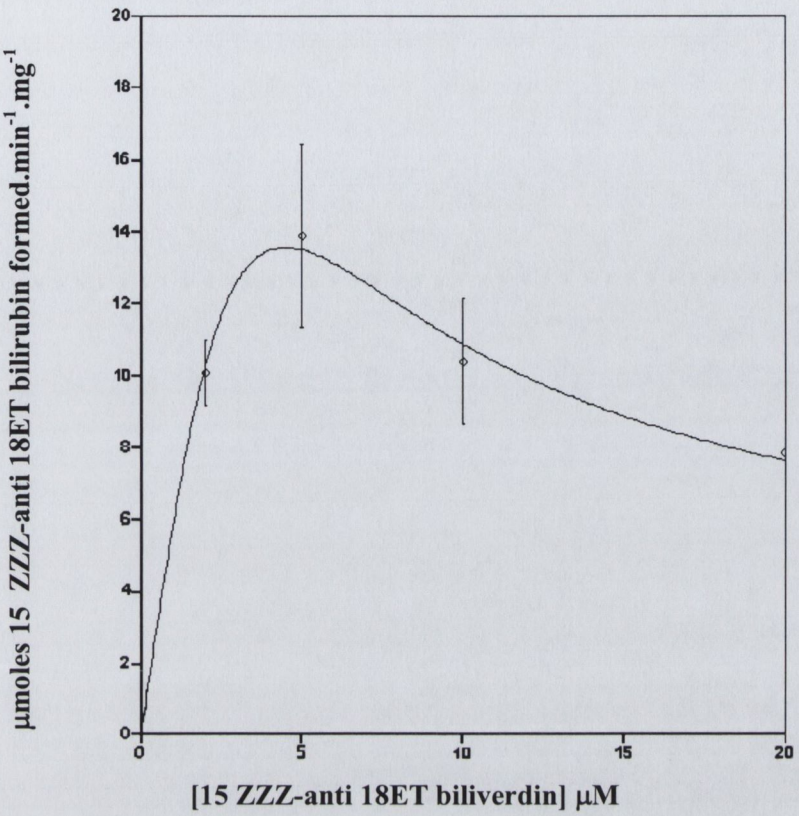

Figure 5.12 15 ZZZ-anti 18ET biliverdin as a substrate for human biliverdin-IXα reductase.

The effect of increasing concentrations of 15 ZZZ-anti 18ET biliverdin (2, 5, 10 and 20 µM) on the activity of human biliverdin IXα reductase. The activity was measured at 460nm and at 37°C. The reaction mixture contained 15 ZZZ-anti 18ET biliverdin and 100µM NADPH in 100mM Tris pH 8. The reaction was started on addition of enzyme. Data points represent triplicate datasets averaged. The data was fitted to the equation for partial substrate inhibition, the results of which are shown in Appendix V Figure 1.

Figure 5.13 15 ZZZ-syn 18ET biliverdin as a substrate for human biliverdin IXα reductase

(a) The absorbance spectrum of 17μM 15 ZZZ-syn18ET biliverdin in reaction buffer (100mM Tris pH 8) is represented by the blue line. On addition of 37uM BSA the spectrum shift observed is represented by the red line.

(b) The absorbance spectrum of 17μM 15 ZZZ-syn 18ET biliverdin in 100mM Tris pH 8 is represented in red. The addition of 120μM NADPH to the reaction mixture gives the spectrum detailed in blue. This absorbance spectrum of this reaction mixture was monitored over a 10 minute period. BSA was not added to this reaction.

(c) The absorbance spectrum changes observed on the addition of 1.4μg human BVR-A to a reaction mixture containing of 17μM 15 ZZZ-syn 18ET biliverdin in 100mM Tris pH 8. The spectrum changes were monitored over 12 minutes at 37°C. Again BSA was not added to this reaction.

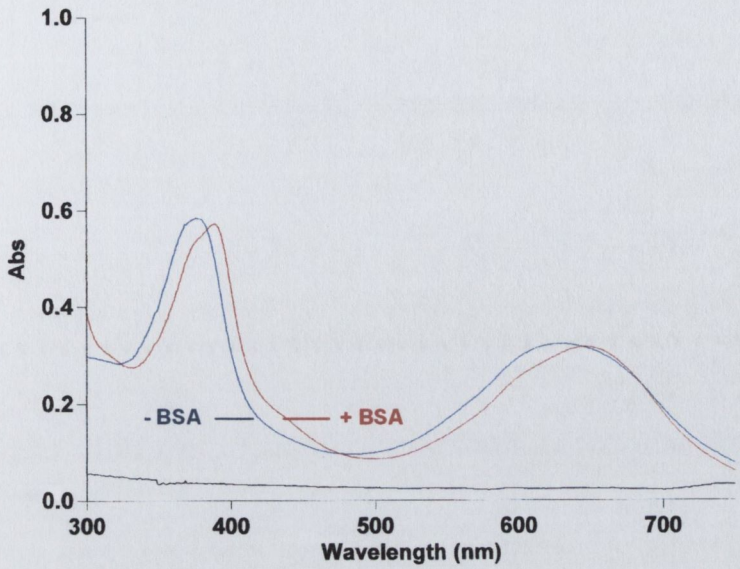
1.0
0.8
0.6
0.4
0.2
0.0
Abs
- BSA
+ BSA
300
400
500
600
700
Wavelength (nm)

(a)

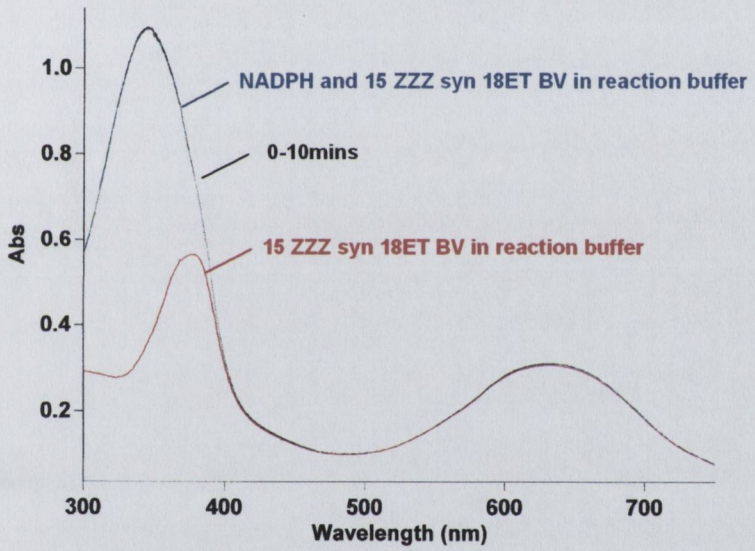
1.0
0.8
0.6
0.4
0.2
Abs
NADPH and 15 ZZZ syn 18ET BV in reaction buffer
0-10mins
15 ZZZ syn 18ET BV in reaction buffer
300
400
500
600
700
Wavelength (nm)

(b)

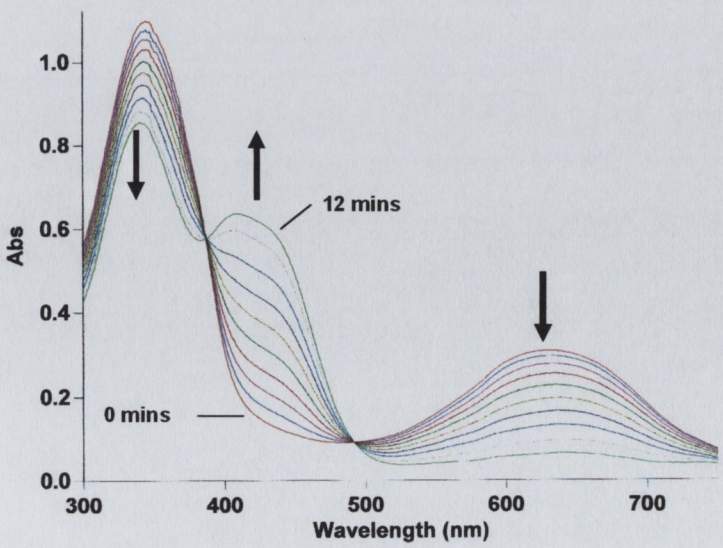
1.0
0.8
0.6
0.4
0.2
0.0
Abs
12 mins
0 mins
300
400
500
600
700
Wavelength (nm)

(c)

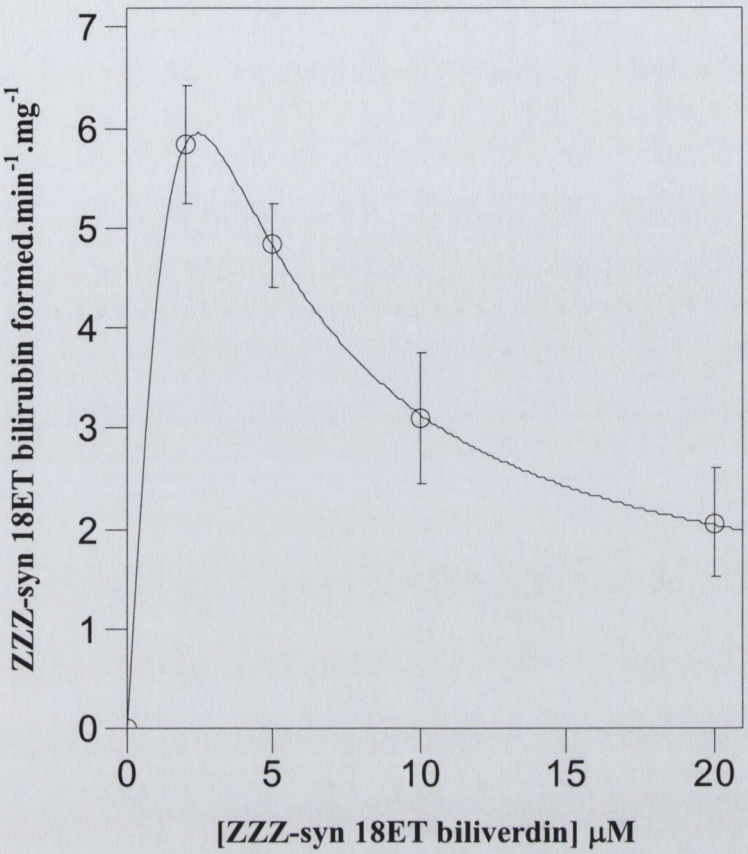

Figure 5.14 ZZZ-syn 18ET biliverdin as a substrate for human biliverdin IXα reductase.

The effect of increasing concentrations of ZZZ-syn 18ET biliverdin (2, 5 ,10 and 20μM) on the activity of human biliverdin IXα reductase. The activity was measured at 460nm and at 37°C. The reaction mixture contained ZZZ-syn 18ET biliverdin and 100μM NADPH in 100mM Tris pH 8. The reaction was started on addition of enzyme. Data points represent the averages of three datasets. The curve was fitted to the equation for partial substrate inhibition, the results of which are shown in Appendix V Figure 1.

Figure 5.15 The effects of BSA on the absorbance spectrum of 15 ZZZ-syn 18ET biliverdin.

(a) The absorbance spectrum of 15 ZZZ-syn 18ET biliverdin (17μM) in 100mM Tris pH 8 was monitored for 20 minutes at 37°C.

(b) The absorbance spectrum changes of 15 ZZZ-syn 18ET biliverdin (17μM) in 100mM Tris pH 8 on addition of BSA to a final concentration of 37μM. The mixture was monitored for 20 minutes at 37°C.

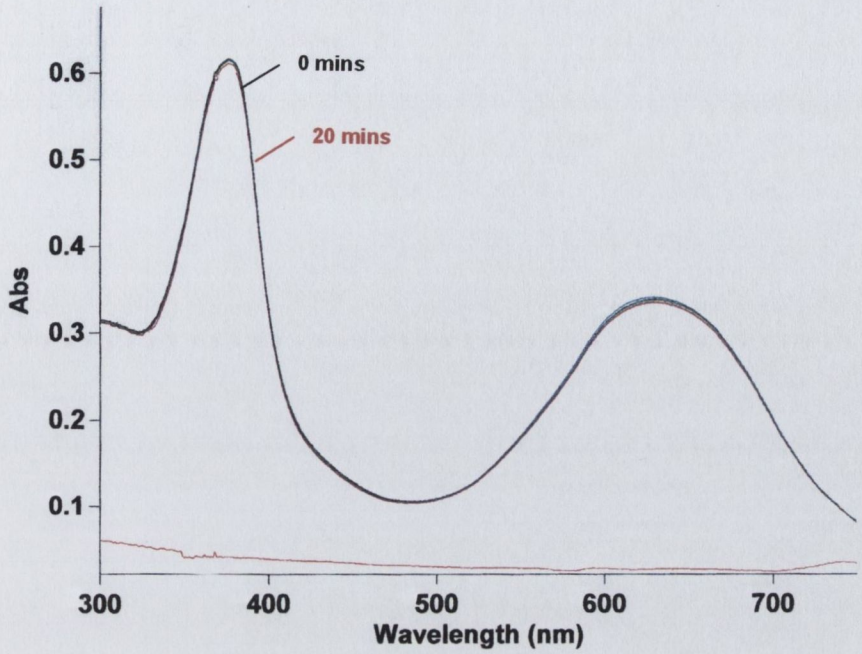
0 mins
20 mins
Abs
0.6
0.5
0.4
0.3
0.2
0.1
300
400
500
600
700
Wavelength (nm)

(a)

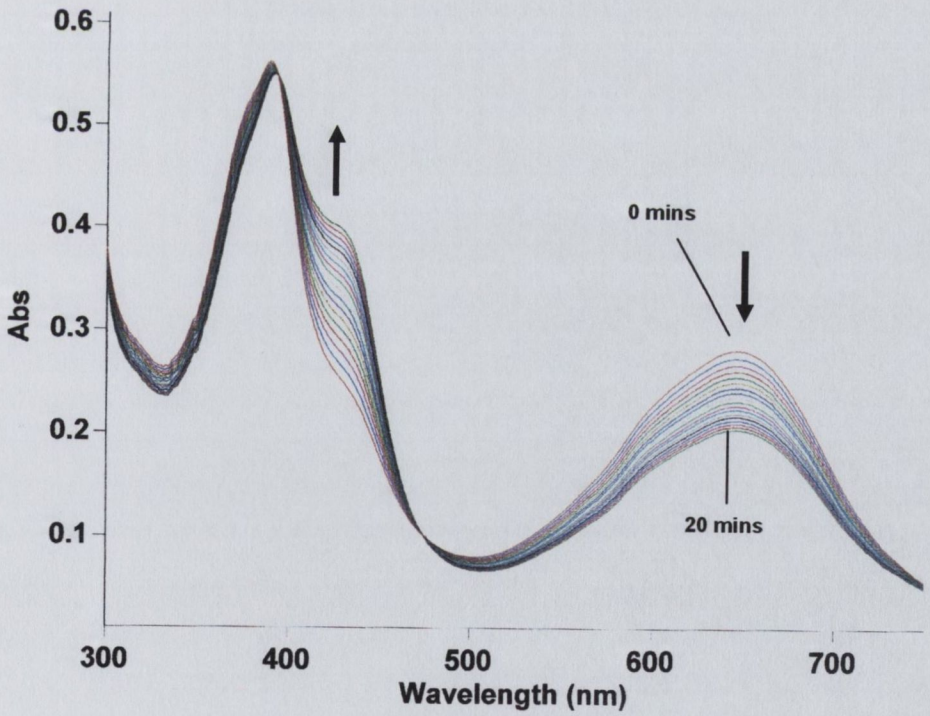
0 mins
20 mins
Abs
0.6
0.5
0.4
0.3
0.2
0.1
300
400
500
600
700
Wavelength (nm)

(b)

Figure 5.16 15ZZE-anti 18ET biliverdin as a substrate for human biliverdin IXα reductase

(a) The absorbance spectrum of 13μM 15ZZE-anti 18ET biliverdin in 100mM Tris pH 8 is represented by the blue line. On addition of 37uM BSA the spectrum shift observed is represented in red line.

(b) The absorbance spectrum of 13μM 15ZZE-anti 18ET biliverdin, 37uM BSA in 100mM Tris pH 8 is represented in black. The addition of 120μM to the mixture gives the spectrum observed in red.

(c) The absorbance spectrum changes observed on the addition of 0.28μg human BVRA to a reaction mixture containing of 13μM 15ZZE-anti 18ET biliverdin, 37uM BSA in 100mM Tris pH 8. The spectrum changes were monitored over 12 minutes at 37°C.

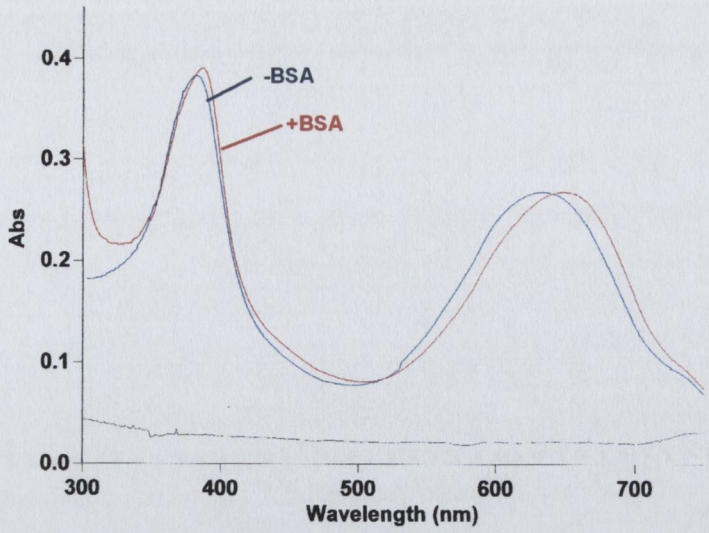
-BSA
+BSA
Abs
0.4
0.3
0.2
0.1
0.0
300
400
500
600
700
Wavelength (nm)

(a)

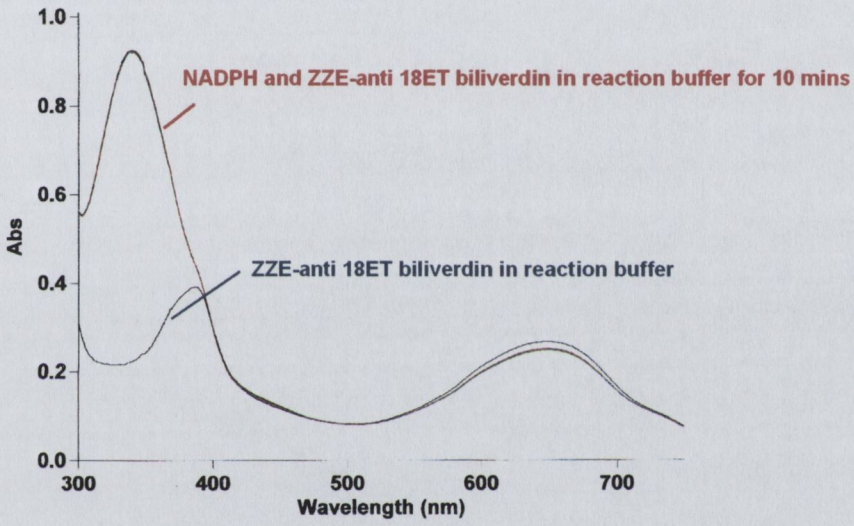
NADPH and ZZE-anti 18ET biliverdin in reaction buffer for 10 mins
ZZE-anti 18ET biliverdin in reaction buffer
Abs
1.0
0.8
0.6
0.4
0.2
0.0
300
400
500
600
700
Wavelength (nm)

(b)

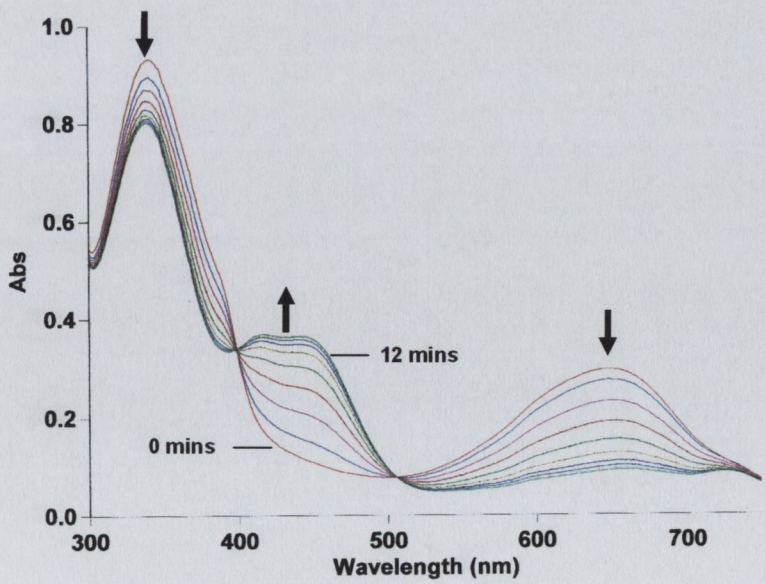
12 mins
0 mins
Abs
1.0
0.8
0.6
0.4
0.2
0.0
300
400
500
600
700
Wavelength (nm)

(c)

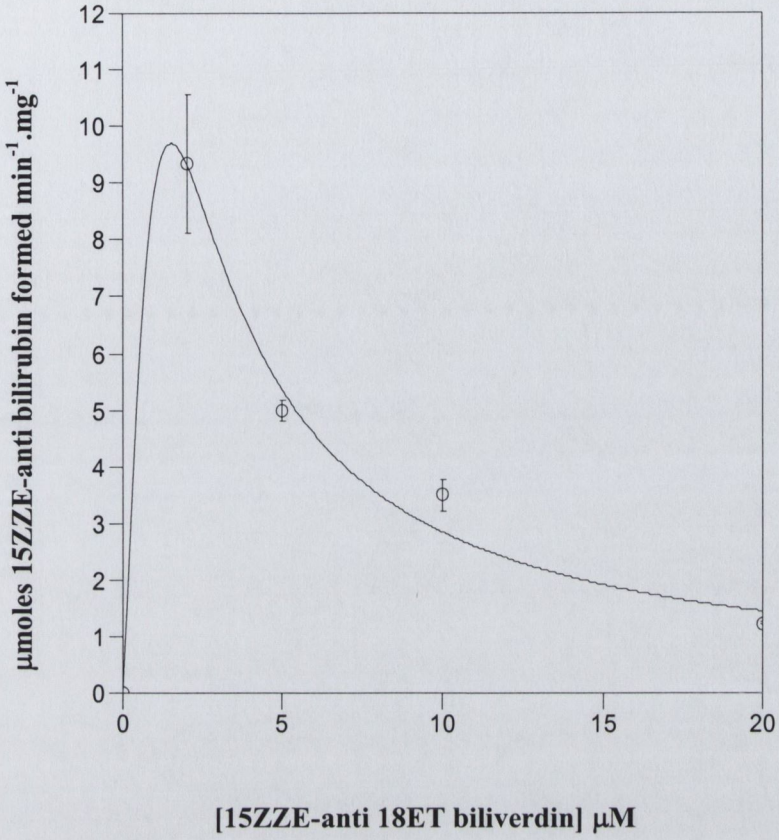

Figure 5.17 15ZZE-anti 18ET biliverdin as a substrate for human biliverdin IXα reductase.

The effect of increasing concentrations of 15ZZE-anti 18ET biliverdin (2, 5, 10 and 20 µM) on the activity of human biliverdin IXα reductase. The activity was measured at 460nm and at 37°C. The reaction mixture contained 15ZZE-anti 18ET biliverdin and 100µM NADPH in 100mM Tris pH 8. The reaction was started on addition of enzyme. Data points represent the average of three datasets. The curve was fitted to the equation for partial substrate inhibition, the results of which are shown in Appendix V Figure 1.

Figure 5.18 15 ZZE-syn 18ET biliverdin as a substrate for human biliverdin IXα reductase

(a) The absorbance spectrum of 17μM 15 ZZE-syn18ET biliverdin in reaction buffer (100mM Tris pH 8) is represented by the blue line. On addition of 37uM BSA the spectrum shift observed is represented by the red line.

(b) The absorbance spectrum of 17μM 15 ZZE-syn 18ET biliverdin in 100mM Tris pH 8 is represented in red. The addition of 120μM NADPH to the reaction mixture gives the spectrum detailed in blue. This absorbance spectrum of this reaction mixture was monitored over a 10 minute period.

(c) The absorbance spectrum changes observed on the addition of 1.4μg human BVR-A to a reaction mixture containing of 17μM 15 ZZE-syn 18ET biliverdin and 37μM BSA in 100mM Tris pH 8. The spectrum changes were monitored over 10 minutes at 37°C.

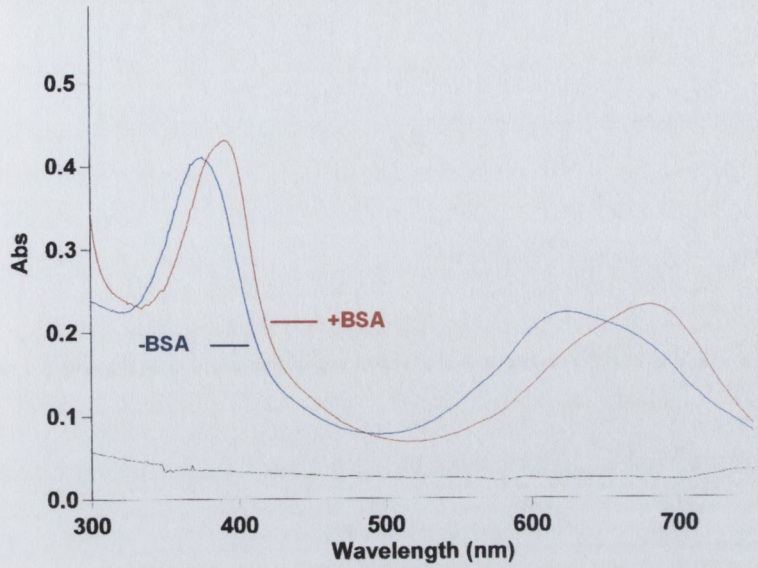
0.5
0.4
0.3
0.2
0.1
0.0
Abs
+BSA
-BSA
300
400
500
600
700
Wavelength (nm)

(a)

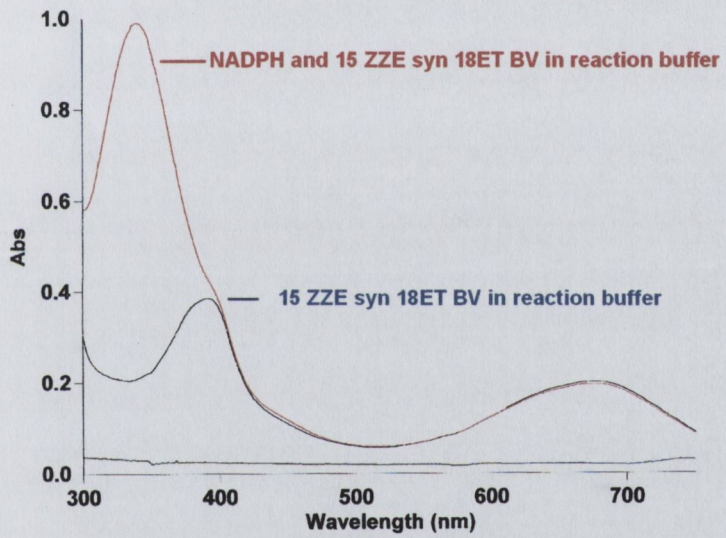
1.0
0.8
0.6
0.4
0.2
0.0
Abs
NADPH and 15 ZZE syn 18ET BV in reaction buffer
15 ZZE syn 18ET BV in reaction buffer
300
400
500
600
700
Wavelength (nm)

(b)

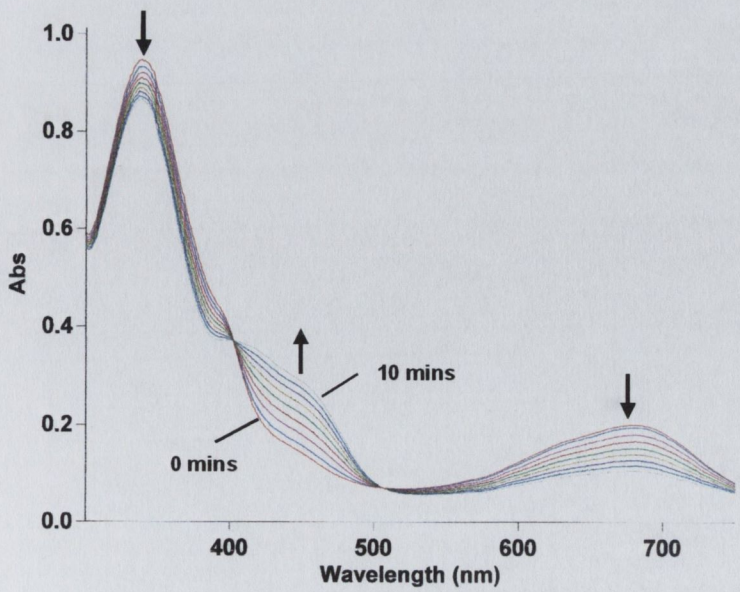
1.0
0.8
0.6
0.4
0.2
0.0
Abs
10 mins
0 mins
400
500
600
700
Wavelength (nm)

(c)

5.3.2 Initial rate studies with biliverdin sulphonate, biliverdin ditaurate and the dimethyl ester of biliverdin-IXα

Biliverdin- IXα sulphonate was a gift from Dr. David Lightner, University of Arizona, Reno. It is a good substrate (Figure 5.19) and the substrate inhibition is not as potent as that seen with biliverdin-IXα. The kinetic behaviour of biliverdin ditaurate is shown in Figure 5.20. The substrate inhibition with this sulphonate also exhibits less potent substrate inhibition than biliverdin-IXα. The dimethyl ester of biliverdin-IXα is clearly not a substrate for BVR-A (Fig 5.21), which supports previous findings reported by O'Carra & Colleran (1970).

5.3.3 The CD spectrum of biliverdin-IXα and bilirubin-IXα bound to BVR-A

Circular dichroism results shown in Figures 5.24, 5.25, 5.26 and 5.27, have been summarised in Figure 5.28. It is clear that human GST-π binds biliverdin with M helicity while all other protein examined (human serum albumin, rabbit serum albumin, bovine serum albumin and synechocystis BVR-A) bind biliverdin in the plus conformation. It is interesting that the synechocystis enzyme only binds biliverdin producing the characteristic CD spectrum in the presence of nucleotide. Also worth noting that human BVR-A binds bilirubin in the minus conformation in the presence of nucleotide while no CD spectrum was observed with the synechocystis enzyme in the presence of nucleotide.

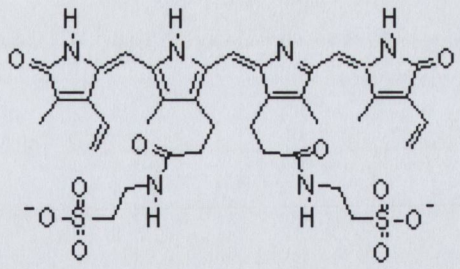

(a)

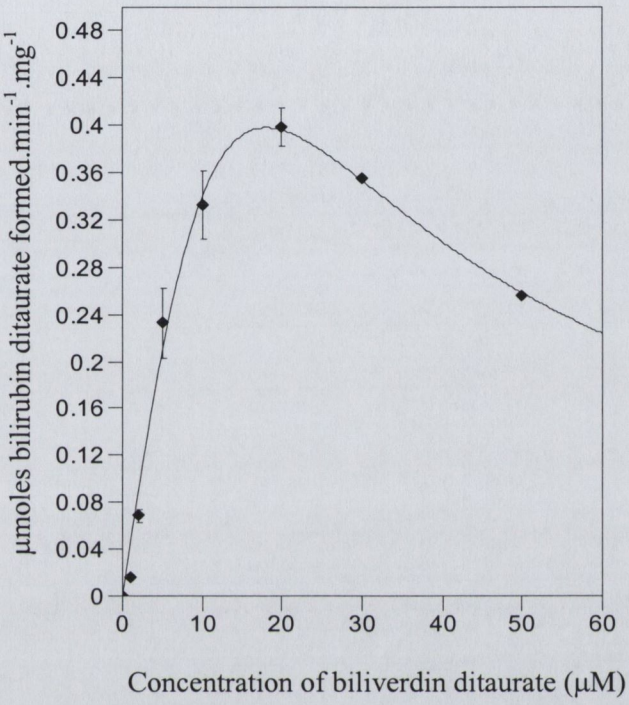

(b)

Total substrate inhibition			$V_0 = \frac{V_{max} S}{K_m + S + S^2/K_i}$
a	1.61E+01	1.06959E+02	SSE 0.00196
b	3.55E+02	2.39850E+02	R2 0.98888
c	9.14E-01	6.20260E+00	

(c)

Figure 5.19 **Biliverdin ditaurate as a substrate for human biliverdin-IXα reductase.**

(a) The structure of biliverdin ditaurate.

(b) The effect of increasing concentrations of biliverdin ditaurate (1, 2, 5, 10, 20, 30 and 50 µM) on the activity of human BVR-A was measured by monitoring the production of bilirubin ditaurate at 460nm. The reaction mixture also contained 100µM NADPH in 100mM Tris pH 8. The reaction was started by addition of enzyme and the temperature maintained at 30°C. The equation for total substrate inhibition (a*x) / (b+x+x^2/c) was used to curve fit to the data, the results of which are presented in (c).

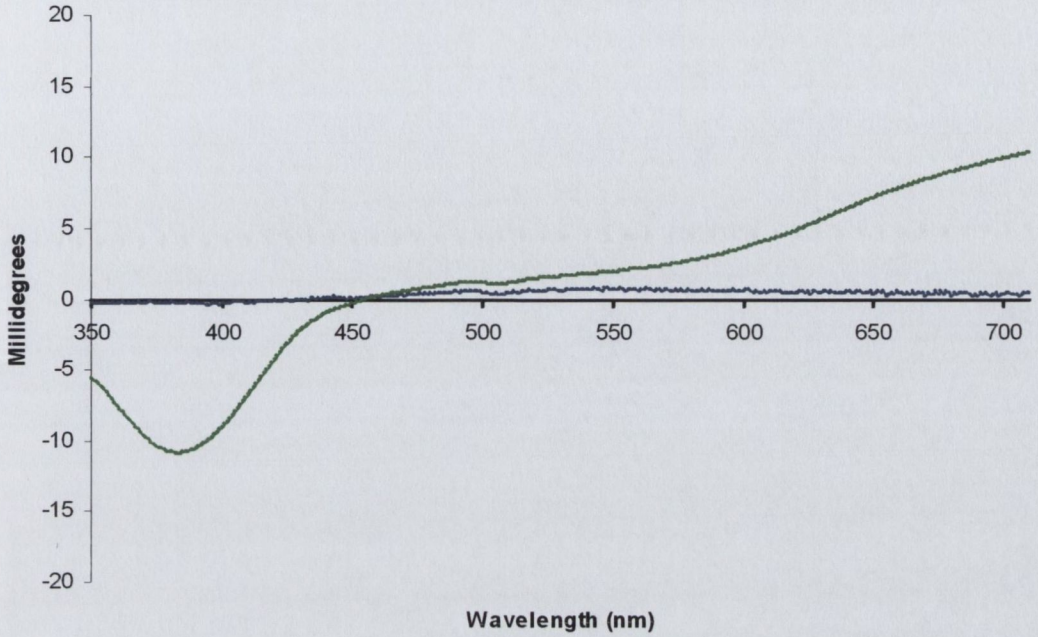

(b)

Figure 5.20 Circular Dichroism spectra of the complex of biliverdin ditaurate and bovine serum albumin.

Circular dichroism equilibrium spectra of 7.5μM biliverdin ditaurate in 10mM sodium phosphate pH 7 (●), and of 7.5μM biliverdin ditaurate and 37μM BSA in 10mM sodium phosphate pH7 (●).

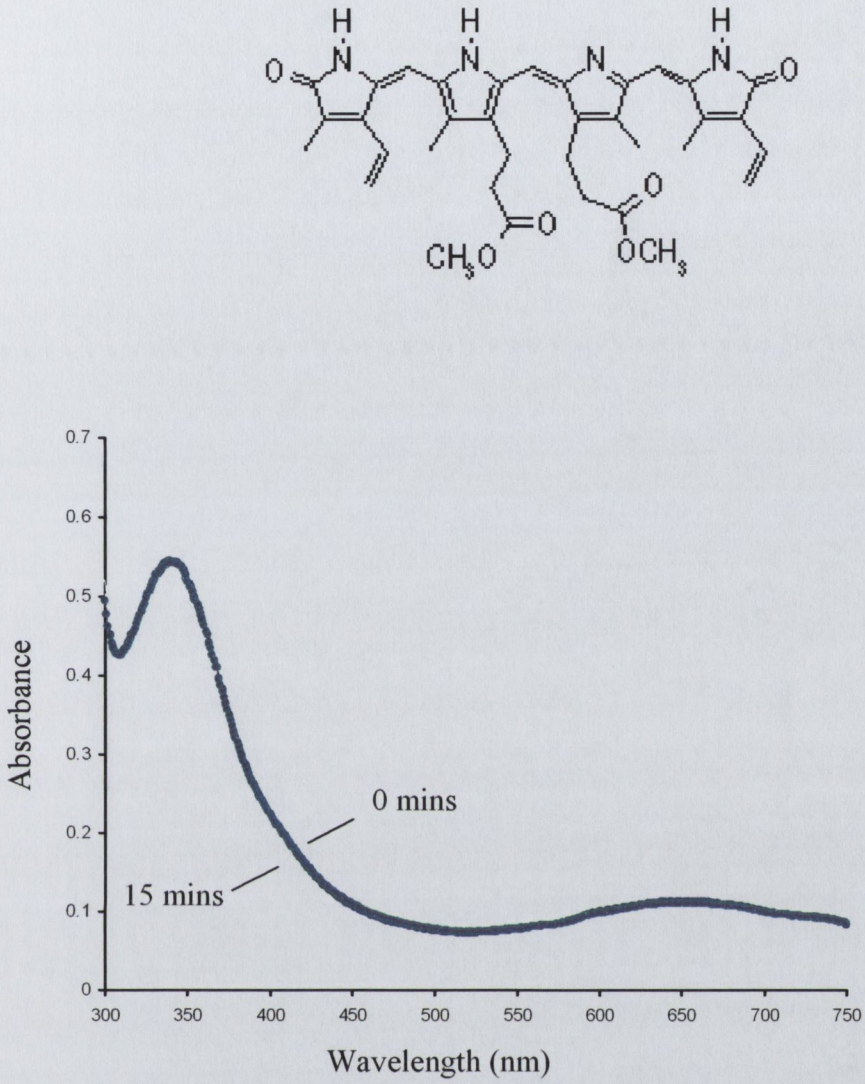

Figure 5.21 Biliverdin-IXα dimethylester is not a substrate for human BVR-A

Kinetic scan of a reaction mixture containing 10μM biliverdin-IXα dimethylester, 100μM NADPH and 37μM BSA, 5μg human BVR-A in 100mM Tris pH 8 at 30°C.

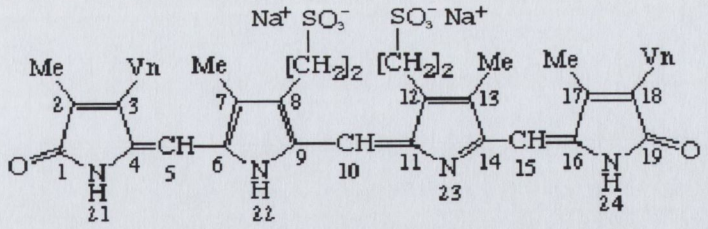

(a)

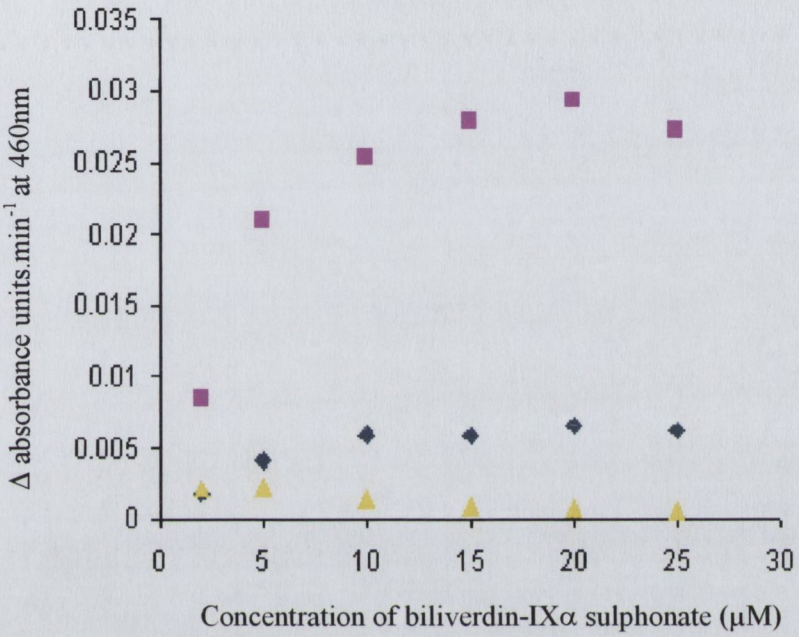

(b)

Figure 5.22 Biliverdin-IXα sulphonate as a substrate for human biliverdin-IXα reductase.

The effect of increasing concentrations (over the range 2, 5, 10, 15, 20, and 25 μM) of biliverdin-IXα sulphonate on the activity of human biliverdin-IXα reductase. The activity was measured by monitoring the increase in absorbance at 460nm and at 30°C. The reaction was started by the addition of 1.5 μg of human BVR-A. The rate of reaction using 700 μM NADH as co-factor and in the presence of 37 μM BSA is represented by (■), 700 μM NADH in the absence of BSA represented by (♦), and 100 μM NADPH as cofactor is represented by (▲).

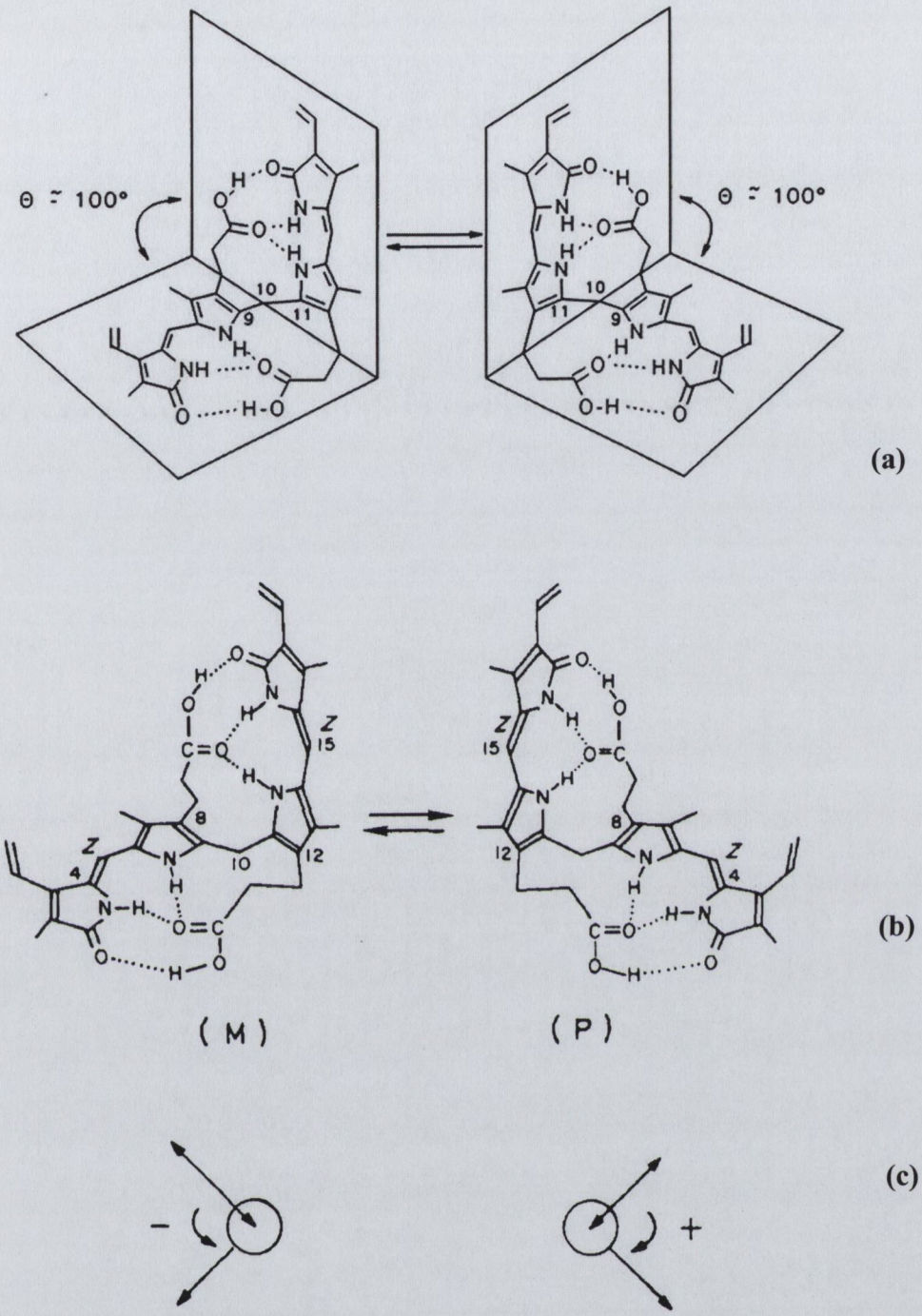

Figure 5.23 Diagramatic representations of the ridge tile structure and intramolecular hydrogen bonding of bilirubin-IXα

The ridge tile structure is shown in (a), which results from the intramolecular hydrogen bonding shown in (b). Two enantiomeric forms exist. The enantiomer on the left has M (minus) chirality while the enantiomer on the right has P (plus) chirality shown in (c).

Figure 5.24 Circular dichroism spectra of the complex of biliverdin-IXα and various proteins.

(a) Circular dichroism spectra of the complex of 7.5μM biliverdin-IXα and 37μM human serum albumin.

(b) Circular dichroism spectra of the complex of 7.5μM biliverdin-IXα and 37μM rabbit serum albumin.

(c) Circular dichroism spectra of the complex of 7.5μM biliverdin-IXα and 30μM human GST-Pi.

Measurements were taken at 30°C in 10mM sodium phosphate buffer pH 7.2. This buffer was also used in all baseline measurements for these experiments.

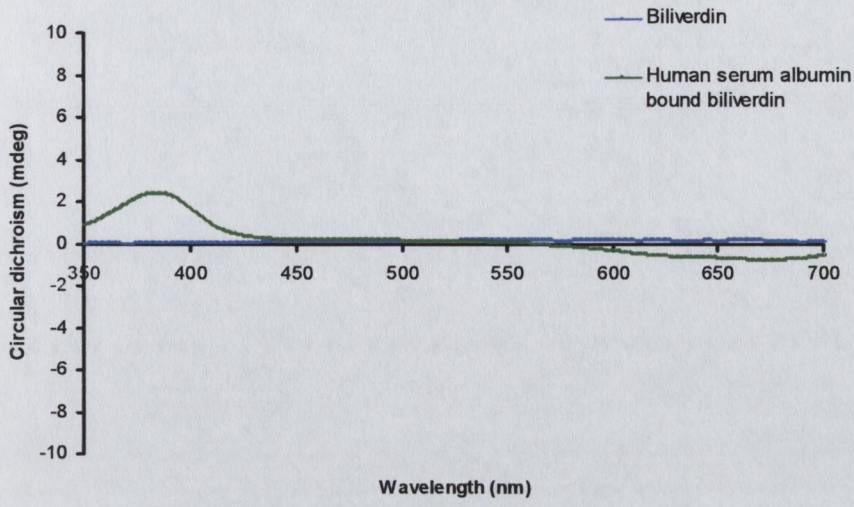
Biliverdin
Human serum albumin bound biliverdin
Circular dichroism (mdeg)
10
8
6
4
2
0
-2
-4
-6
-8
-10
350
400
450
500
550
600
650
700
Wavelength (nm)

(a)

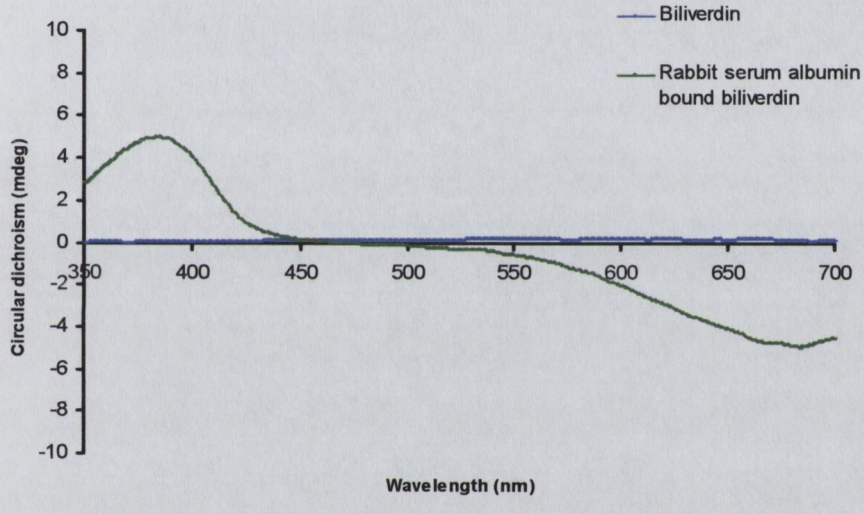
Biliverdin
Rabbit serum albumin bound biliverdin
Circular dichroism (mdeg)
10
8
6
4
2
0
-2
-4
-6
-8
-10
350
400
450
500
550
600
650
700
Wavelength (nm)

(b)

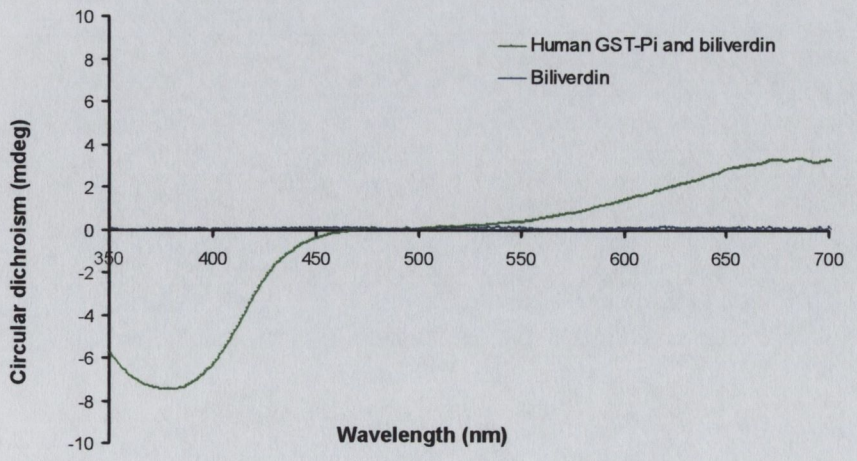
Human GST-Pi and biliverdin
Biliverdin
Circular dichroism (mdeg)
10
8
6
4
2
0
-2
-4
-6
-8
-10
350
400
450
500
550
600
650
700
Wavelength (nm)

(c)

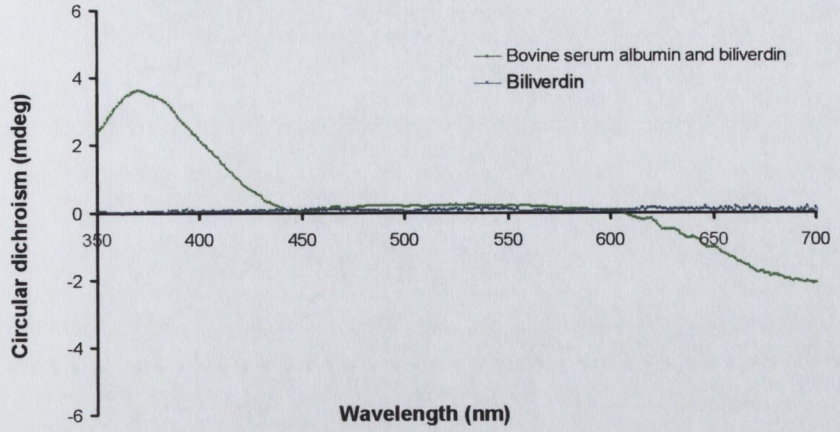

(a)

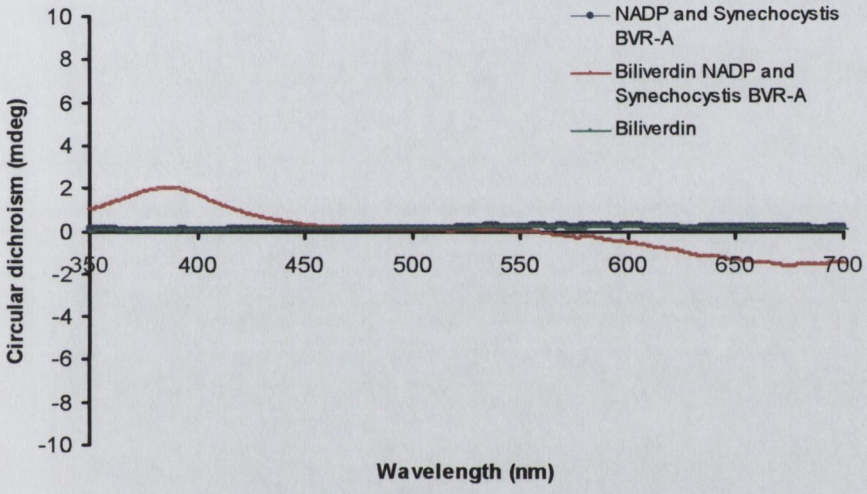

(b)

Figure 5.25 Circular dichroism spectra of the complex of biliverdin-IXα with BSA and with synechocystis biliverdin-IXα reductase.

(a) Circular dichroism spectra of the complex of 7.5μM biliverdin-IXα and 37μM bovine serum albumin in10mM sodium phosphate buffer pH 7.2 at 30°C.

(b) Circular dichroism spectra of the complex of 7.5μM biliverdin-IXα and 30μM synechocystis biliverdin-IXα reductase in 10mM sodium phosphate buffer pH 7.2 at 30°C.

Figure 5.26 Circular dichroism spectra of the complex of bilirubin-IXα with various proteins.

(a) Circular dichroism spectra of the complex of 7.5μM bilirubin-IXα and 37μM bovine serum albumin.

(b) Circular dichroism spectra of the complex of 7.5μM bilirubin-IXα and 30μM human π glutathione-*S*-transferase.

(c) Circular dichroism spectra of the complex of 7.5μM bilirubin-IXα and 30μM synechocystis bilirubin-IXα reductase.

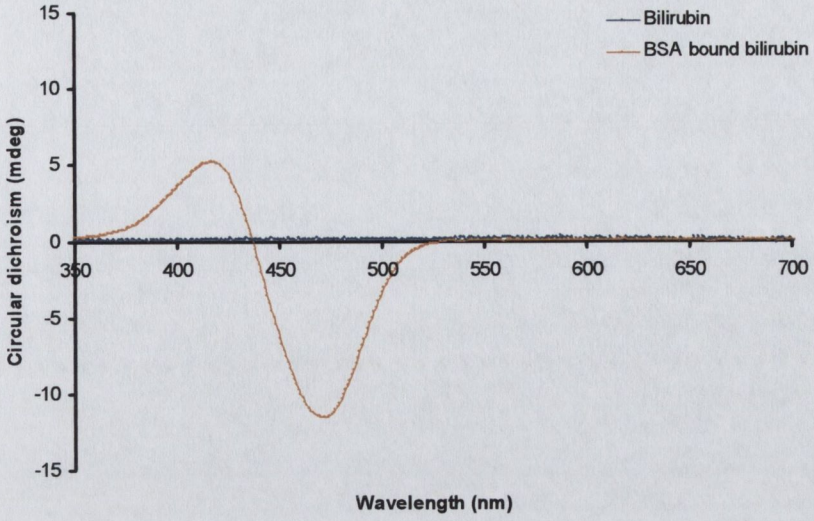
Bilirubin
BSA bound bilirubin
Circular dichroism (mdeg)
Wavelength (nm)

(a)

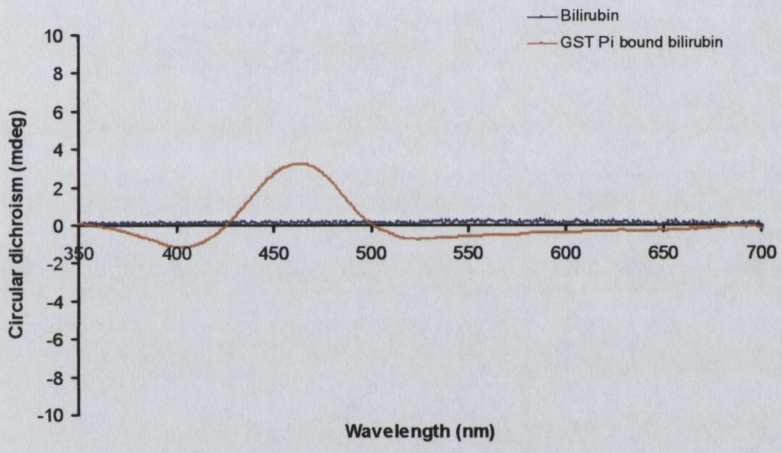
Bilirubin
GST Pi bound bilirubin
Circular dichroism (mdeg)
Wavelength (nm)

(b)

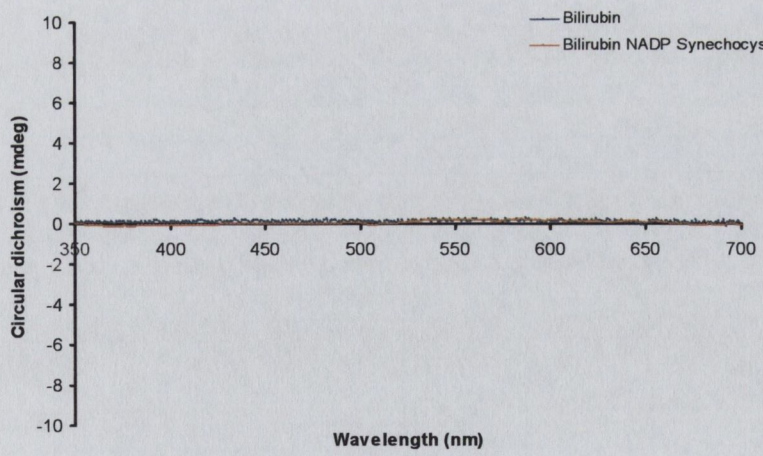
Bilirubin
Bilirubin NADP Synechocystis
Circular dichroism (mdeg)
Wavelength (nm)

(c)

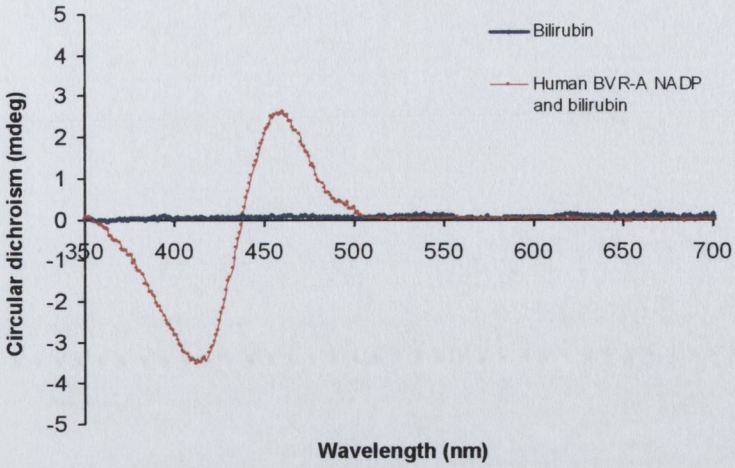

(a)

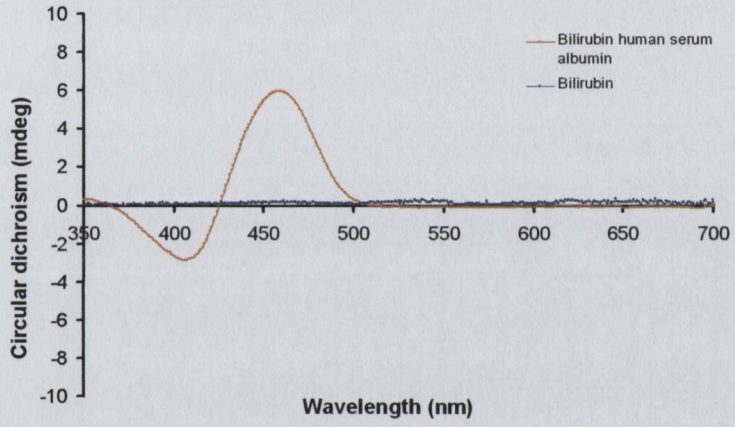

(b)

Figure 5.27 Circular dichroism spectra of the complex of bilirubin-IXα with various proteins.

(a) Circular dichroism spectra of the complex of 7.5 μM biliverdin-IXα with 20 μM human biliverdin IXα reductase and 100 μM $NADP^+$ in 10mM sodium phosphate pH 7.2

(b) Circular dichroism spectra of the complex of 7.5 μM biliverdin-IXα and 37 μM rabbit serum albumin.

Figure 5.28 The'ring-like' and 'open' structures of biliverdin-IXα.

The dihedral angles δ_1 - δ_6 govern the conformational structure of biliverdin-IXα. Studies by Wagnière & Blauer 1976 conclude that biliverdin adopts intermediate structures ranging from the conformations shown in (a) with a 'ring-like' structure to the 'open' structure shown in (b). The Fisher labelling system is used to identify individual atoms (see Chapter 1). The results of the CD experiments (Figure 5.24 to Figure 5.27) are summarised in (c).

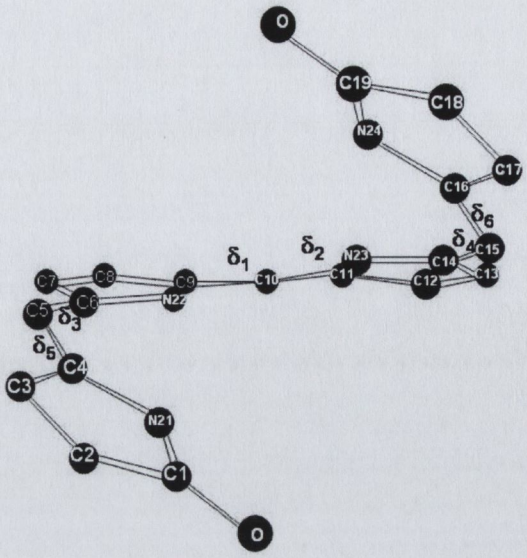

(a)

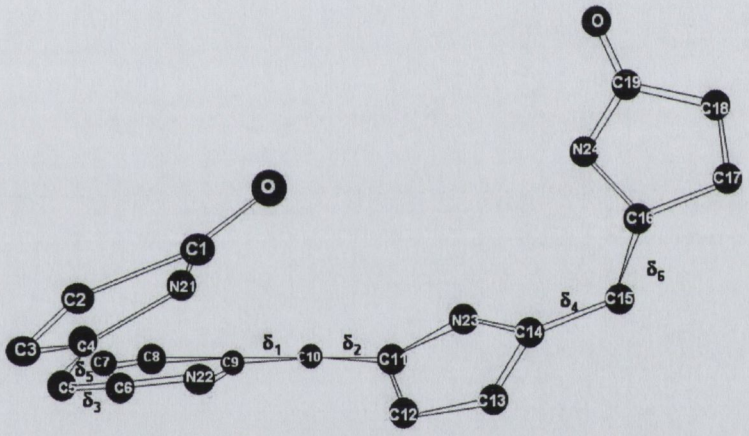

(b)

	Biliverdin	Bilirubin
HSA	Plus	Minus
RSA	Plus	
GST	Minus	Minus
BSA	Plus	Plus
Synechocystis	Plus	
Synechocystis NADP	Plus	No CD spectrum observed
Synechocystis hBVR-A NADP	No CD spectrum observed	No CD spectrum observed
		Minus

(c)

5.3.4 DISCUSSION

The very potent substrate inhibition and relative insolubility of the product bilirubin-IXα has hampered attempts to determine kinetic constants for biliverdin reductase. The problem arises when there are insufficient experimental data points on the ascending limb of the saturation curve to allow curve fitting routines to be used with confidence. The addition of BSA has been the traditional approach in reducing this problem however this introduces an additional complication. As mentioned in the introduction the addition of BSA increases the extinction coefficient of bilirubin from 27,000 M^{-1} cm^{-1} to 55,000 M^{-1} cm^{-1} (Phillips 1981). Although it is clear that a larger extinction coefficient provides increased sensitivity for the detection of bilirubin at 460nm the addition of BSA effectively decreases the concentration of free biliverdin. Previous studies (Phillips, 1981; Rigney, 1985) have tried to correct for both the increase in extinction coefficient for bilirubin and also the decrease in the concentration of free biliverdin as a fraction is bound to BSA. This is clearly not straightforward as Phillips (1981) could only fit her data if there was a large number of binding sites (N=10) on albumin with very low affinities for biliverdin binding with Kd values for biliverdin greater than 0.5M.

In the standard assay total conversion of a 1 μM solution of biliverdin-IXα to bilirubin-IXα will yield an absorbance increase of 0.027 in the absence of BSA. So measurement of initial rates during the conversion of the first 10% of substrate (that is before product inhibitory and substrate depletion effects are problematic) will result in an absorbance change of 0.0027. As a result measurements of initial rates with 1 μM biliverdin or less are inaccurate using the traditional assay with a 1cm light path. One possible solution to the problem would be to increase the light path of the assay to 10cm. Under the Beer Lambert law this would increase the sensitivity by tenfold giving an absorbance change of 0.027 for 10% conversion of 1μM biliverdin. Spectrophotometers such as the Beckman DU 650 Spectrophotometer which has a 10cm light path may provide the necessary experimental data allowing more accurate curve fits to be achieved. However this method would only be useful for measurement of concentrations of 0.25 μM biliverdin or above. The disadvantages of this method are obvious as the consumption of enzyme nucleotide and substrate would be tenfold. Other methods of increasing the sensitivity of the assay were examined. One of the standard tests for bilirubin involves the diazo reaction (reviewed in

Dolphin, 1979). Diazonium salts react with aromatic amines in bilirubin to give stable red/violet azo derivatives (Hutchinson *et al.*, 1972). Their use in a stopped assay as an extinction enhancement for bilirubin was considered but again the sensitivity would not be sufficient for this application. It was decided therefore that a method with most potential for the development of an alternate assay system for BVR-A was that of a radiolabelled assay using 2'-[^{32}P] NADPH. The production of 2'-[^{32}P] NADPH with sufficiently high specific activity would allow for the assay of this enzyme at nM concentrations. It would also provide the best method for the establishment of physiological concentrations of biliverdin-IXα in tissues. It is probable that the concentration of free biliverdin is so low the enzyme would not suffer from substrate inhibiton *in vivo*. In this study a number of methods to separate NADPH from $NADP^+$ and NADH from NAD^+ were examined. The separation of nucleotides on DEAE cellulose chromatography (Section 5.2.1) was deemed impractical for use in this study. The technique may have merits in processes whereby a single step purification of NAD^+ from NADH and $NADP^+$ from NADPH is necessary. The resolution of $NADP^+$ and NADPH peaks in the presence of ATP however is poor. Running a column for each assay sample would have proved very difficult due to the numbers of samples and the generation of large volumes of liquid wastes. For this reason the resolution of nucleotides was far superior using HPLC based separation. The synthesis of 2'-[^{32}P] NADPH is described in Sections 5.2.5. As shown in Table 5.5b the specific activity of the γ-[^{32}P] ATP in the NAD kinase reaction was 30 Ci/mmol and the 2'-[^{32}P] $NADP^+$ formed in the kinase reaction was 2.7 Ci/mmol which is approx 10% of the specific radioactivity of the starting ATP. If the starting material was of a higher specific radioactivity (γ-[^{32}P] ATP with a specific activity of 6000 Ci/mmol for instance) the reaction would facilitate the production of 2'-[^{32}P] $NADP^+$ with a specific activity close to 600 Ci/mmol which could in turn synthesise 2'-[^{32}P] NADPH with specific activity of 60 Ci/mmol. In the experiment described in Section 5.2.5, 14.6 μM 2'-[^{32}P] NADPH (1.6ml) was produced with 7856 dpm/μl. If this was used to assay BVR-A with a final reaction volume of 500μl, the volume of the labelled nucleotide which could have been added would have been 100μl. This results in a 1/5 dilution of the solvent (30% MeOH in 100mM sodium phosphate pH 7) used to elute the 2'-[^{32}P] NADPH. Concentrations of methanol diluted to this level were shown not to inhibit BVR-A activity. Addition of 100 μl nucleotide, to a final assay volume of 500 μl also means that the concentration of 2'-[^{32}P] NADPH is diluted from 14.6 μM to 2.9 μM, which is not saturating for the enzyme. Addition of nonradioactive

NADPH would be unproductive at this point as the specific activity would decrease. If the equivalent biliverdin concentration (2.9 μM) was used in the assay, and ~ 10% conversion of 2'-[^{32}P] NADPH to 2'-[^{32}P] $NADP^+$ obtained through the course of the reaction 0.29 μM of 2'-[^{32}P] $NADP^+$ would have been produced. Using the TLC method described to separate the 2'-[^{32}P] $NADP^+$ means that up to 5 μl of the assay would have been spotted onto each plate. The 2.9 μM 2'-[^{32}P] NADPH (785,620 dpm/500μl) used in the assay would have produced 0.29 μM 2'-[^{32}P] $NADP^+$ (78,562 dpm /500μl) in the assay assuming 10% conversion. A major problem arises with the TLC separation as the spotting of 5 μl of the assay at the origin means that of the total counts (7856 dpm) being spotted the oxidised nucleotide would account for 785 dpm. It was hoped to use this assay with biliverdin concentrations as low as of 0.1μM biliverdin which would produce 0.01μM oxidised nucleotide in the reaction. Using the 2'-[^{32}P] NADPH synthesised in this study this would not have been possible yielding just (~27 dpm) on the TLC separation. It must be said however that with access to a dedicated -[^{32}P] freeze drier or speedivac concentrator the 2'-[^{32}P] NADPH purified in this study could have been concentrated enough and used to perform BVR-A assays using low nM ranges of biliverdin-IXα as substrate. The synthesis of 2'-[^{32}P] NADPH at 60 Ci/mmol would also prove invaluable in the development of this radiolabelled assay for BVR-A. This protocol certainly supplies a novel and sensitive assay for BVR-A and other reductases that use NADPH.

Although the kinetic parameters for biliverdin-IXα are difficult to obtain, the study of the biliverdin binding pocket of BVR-A is still possible using synthetic isomers. Substrate specificity studies using various isomers help us to determine how restrictive this site is. Previous studies by Cunningham *et al.*, (2000) have shown that at least one bridging propionate is necessary for optimal binding of biliverdin isomers to BVR-A. They also showed that extending the propionate side chains to hexanoate resulted in a significant loss of activity whereas the butyrate derivatives retained high activity. The conclusions of that study was that a pair of positively charged amino acid side chains within the BVR-A structure were responsible for binding these propionates. Kikuchi *et al.* (2001) have suggested that the basic residues, Arg 171, Lys 218, Arg 224 and Arg 226, which are on the upper side of the putative NAD(P)H, binding pocket may be responsible for binding biliverdin through electrostatic interactions. In the present study biliverdin-IXα dimethylester was shown not to be a substrate for human BVR-A (Figure 5.21). Clearly

oblating the negative charge of the carboxylate by forming the methylester prevents interactions with the enzyme. In contrast biliverdin-IXα sulphonate (Figure 5.22) and biliverdin ditaurate (Figure 5.19) have been shown to be a good substrates. Further studies using isomers with conformational restraints were analysed (Figures 5.10a and 5.10b). All these isomers proved to be substrates. These results are very informative and show that conformationally restricted isomers around C-15 of biliverdin are accessible to the substrate binding pocket and are catalytically productive. Examination of Figure 5.10b shows that when the conformationally restricted isomers are overlaid that the enzyme requires the central dipyrrole and one, preferably two, anionic side chains but can accommodate a large variation in volume at the two outer pyrroles. This is reminiscent of the behaviour of BVR-B where the two reducible pyrroles are fixed in density but the two outer pyrroles appear far more flexible (Pereira *et al.*, 2001). This provides valuable information towards the development of an inhibitor for the enzyme. These substrate specificity studies show that the most important determining factors for substrate binding are the two charged propionate moieties and the central pyrrole rings. Modifications on the outer pyrroles do not impede binding and the enzyme's catalytic activity.

This study was extended to determine whether a particular "chiral" form of tetrapyrrole binds to the various BVR-As studied. The CD spectra of biliverdin-IXα and bilirubin-IXα arise for different reasons. The optical activity of bilirubin-IXα (Figure 5.23a), arises from the extensive intra-molecular hydrogen bonds which link the polar carboxylic acids with the terminal lactams producing a 'ridge tile' type structure. An exciton coupling then occurs between the two dipyrrinone chromophores of the molecule causing the characteristic CD spectrum, with two ORD maxima, the first between 400 and 440nm, and the second between 446 and 448 nm. The saturation of the C-10 position of bilirubin not only allows the molecule to adopt the ridge tile structure but it also divides the molecule into two adjoining dipyrrinone chromophores. As shown in Figure 5.23 the bilirubin isomers have helicity designated P- (Plus) and M- (Minus) helicity (Nogales & Lightner 1995). When bilirubin binds to ligandin and albumin it adopts a specific conformation with either P helicity or M-helicity and the solution becomes optically active (Lightner *et al.*, 1976).

In the case of biliverdin-IXα however, the whole molecule is considered a chromophore, and is not split into two chromophores as a result of methene C-10 bridging position. Biliverdin gives its characteristic CD when it 'twists' into an unsymmetrical chromophore, as it will on binding to certain proteins. In this case ORD maxima are evident at 380 nm and at 650 nm. The dihedral angles δ_1 - δ_6 govern the conformational structure of biliverdin-IXα. Studies by Wagnière & Blauer (1976) conclude that biliverdin adopts intermediate structures ranging from the conformations shown in Figure 5.28 (a) with a 'ring-like' structure to the 'open' structure shown in Figure 5.28 (b). From Figure 5.25 (b) it is clear that, in the presence of NADP, biliverdin binds to the enzyme in the plus configuration. No spectrum was detectable in the absence of nucleotide which would confirm that there is an ordered binding mechanism involved with this enzyme. All other purified biliverdin-IXα reductases will be examined using CD analysis and the conformation adopted will be considered in the design and screening for a specific and novel inhibitor for this enzyme. The physical basis for the binding of biliverdin in an optically active form will depend on the solution of a crystal structure of BVR-A with bound tetrapyrrole.

Chapter Six

Is biliverdin-IXα reductase a zinc metalloprotein and does it have a leucine zipper?

6.1 Introduction

Human biliverdin IXα reductase was shown to be a metalloprotein by Maines *et al.*, (1996). They performed both ^{65}Zn exchange and atomic absorption spectroscopy studies, the results of which indicate that both *E.coli* expressed and purified BVR-A from human liver contained zinc at a molar ratio of approximately 1:1. Maines *et al.*, (1996) also observed a loss in activity in human BVR-A when C280 and C291 were substituted with alanine and interestingly, found that exogenous zinc inhibited NADPH dependent, but not NADH dependent activity. Further experiments by Kikuchi *et al.*, (2001), during the successful crystallisation of rat BVR-A did not support the hypothesis that the rat enzyme is a zinc metalloprotein. These workers, supplemented the *E. coli* expression cultures with $ZnCl_2$ and, somewhat surprisingly, could not detect zinc in the purified protein. Later further efforts were made to introduce and co-crystallise rat BVR-A with zinc but this also proved refactory. Kikuchi *et al.*, (2001) also state that neither the NADH- nor the NADPH-dependent activity of rat BVR-A was altered on addition of $ZnCl_2$ (the concentration of which they have not specified). Site directed mutagenesis of cys 280 and cys 291 to alanine had little effect on activity. Kikuchi *et al.*, (2001) also point out that in the rat crystal structure the 'zinc finger like binding domain proposed by Maines *et al.*, is αM helix, which would not allow the tetrahedral coordination of Zn, and conclude that the structural and enzymatic observations strongly suggest that Zn is not essential for rat BVR-A activity.

It is interesting that rat and human enzymes share 83% amino acid sequence identity, and the proposed Zn binding site in the human corresponds to His 279-Cys 280-(X_{10})-Cys 291-His 292 of rat BVR which is shown in Figure 6.1. Looking at all the proposed BVR-A sequences in Figure 3.2, we can see that only the mammalian sequences have high sequence identity in this area. On alignment of the BVR-A sequences from various species from the cyanobacteria to the mammalian enzymes one can see that the presence of the proposed zinc binding motif is largely a mammalian phenomenon. It is interesting to note that in BVR-A the 'Rossmann fold' and proposed active site residues 'EYP' of all species are very highly conserved. If zinc played an important structural role in BVR-A one would expect to find a very high degree of sequence conservation at the C-terminus. It was

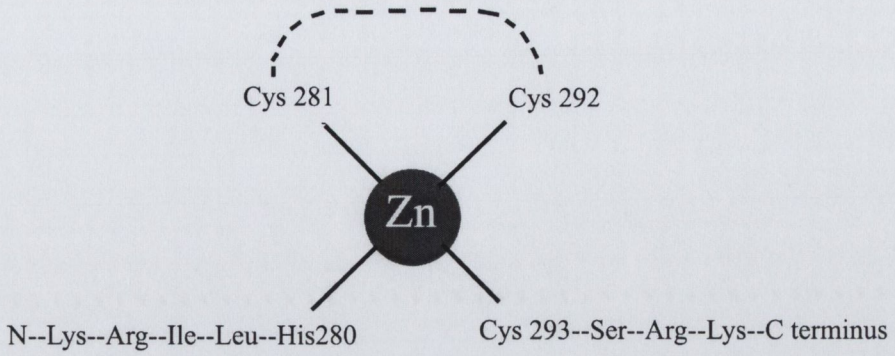

(a)

Gallus	LFMQDQNLFAKKLLGQVSKEELAAEKWRILRCLDLAGMIQQQCEQPEKICS	323
Xenopus	LFMQDQNLFAKKLLGQVTREELLAEKQRILKCIDLAEEIKKKCEH	290
Zebrafish	LFMQDRKLQGEVSAAELQAERNRILHCLELADRIQQITESTHA	292
Tetraodon	LFMQDMVLFSAKLLGQMQKEKLRVLHCLELADRIREL-C	287
Homo	QNIFVQKLLGQFSEKELAAEKKRILHCLGLAEEI-QKYCCSRK	296
Pan	QNIFVQKLLGQFSEKELAAEKKRILHCLGLAEEI-QKYCCSRK	296
Canis	QNIFVQKLLGQFSEKELAAEKKRILHCLWLAEEI-QKYCYSKK	296
Bos	QNIFVQKLLGQFSEEELAAEKKRILHCLWLAGEI-QKHCCSKQ	296
MOUSE	QDIFIQKLLGQVSAEDLAAEKKRILHCLELASDI-QRLCHRKQ	295
Rattus	QDIFVQKLLGQVSAEDLAAEKKRIMHCLGLASDI-QKLCHQKK	295
Nostoc_sp.PCC	TSMVLDHIFDGAPLYVTPEESLYTLRVADAAQRAAQMGITIFLT	318
Anabaena_variabilis	TSMVLDHLLDGTPLYVTPEESLYTLRVADAAQRAAQMGITIFLTDKLN	329
Nostoc punctiformePCC 73102	TAMVLDHLFDGTPLYVTPEQSLYTLKVADAAQRAAQTGFTMFMDKLN	322
Trichodesmium	TKMVIEYLLQGTPLYITPEASLYTLKVANLSQKSSHNSGKATKFK	335
Crocosphaera	TRMVLDHLFDSKPLYIKPESSIYALKVGETAHQSAISGKSVYL	341
Synechocystis	TEAVLDYLTTGKPLYVDLEASLYALEVADLCAQACGYKVEN	328
Gloeobacter	TRMVLDVLQGRGELYTTPERSLHILATAAACERSAALGRSEAVEVPALPIG	332

(b)

Figure 6.1 The proposed Zinc finger of BVR-A

(a) A graphical representation of the zinc finger motif of human BVR-A which has been proposed by Maines *et al.*, (1996). This is based on an amino acid sequence (His 280-Cys 281-(X_{10})-Cys 292-Cys 293) of human BVR-A.

(b) The position of the proposed zinc binding motif in BVR-A from various species.

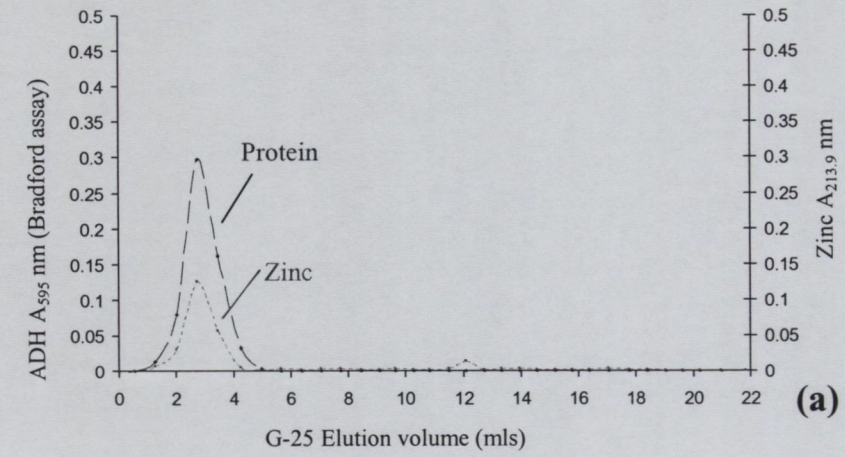
ADH A_{595} nm (Bradford assay)
Zinc $A_{213.9}$ nm
Protein
Zinc
G-25 Elution volume (mls)

(a)

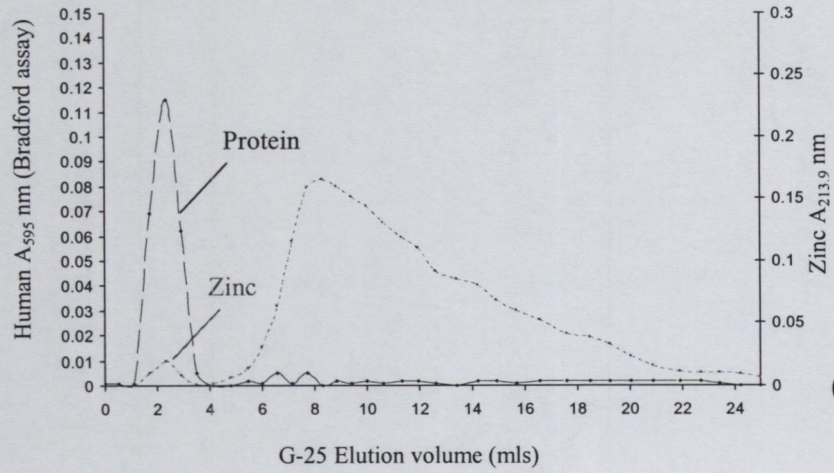
Human A_{595} nm (Bradford assay)
Zinc $A_{213.9}$ nm
Protein
Zinc
G-25 Elution volume (mls)

(b)

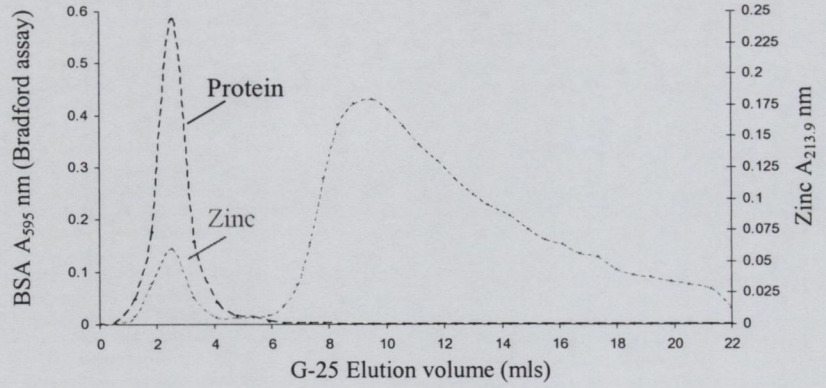
BSA A_{595} nm (Bradford assay)
Zinc $A_{213.9}$ nm
Protein
Zinc
G-25 Elution volume (mls)

(c)

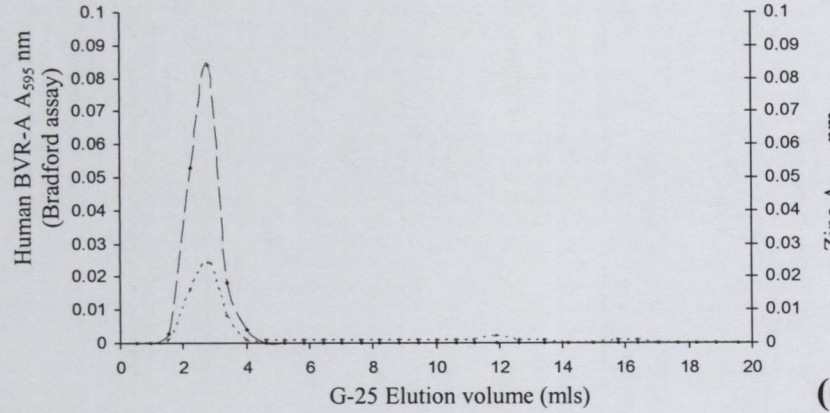
Human BVR-A A_{595} nm (Bradford assay)
Zinc $A_{213.9}$ nm
G-25 Elution volume (mls)

(d)

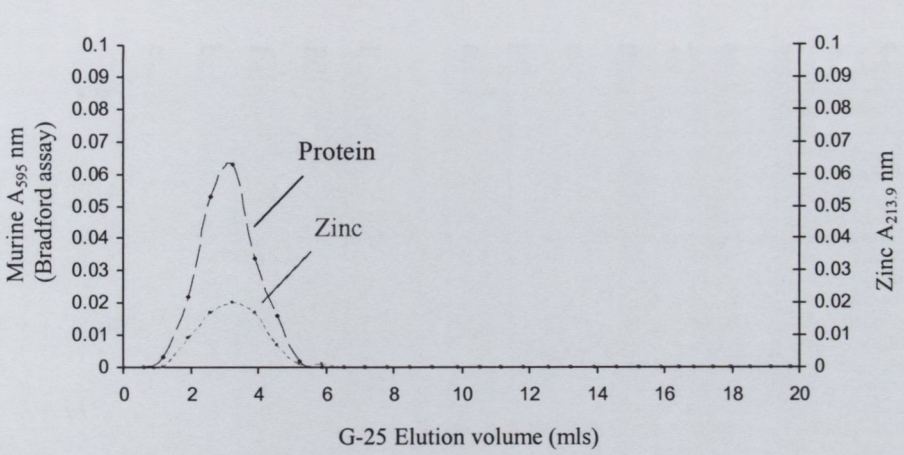

(e)

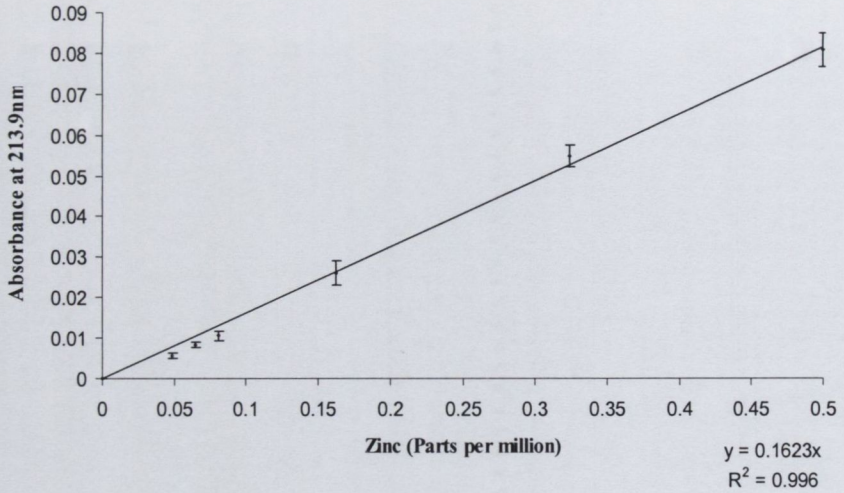

(f)

Figure 6.2 Detection of protein and zinc in the eluates of Hi-Trap G-25 gel filtration devices.

(a): Equine liver alcohol dehydrogenase, **(b):** Human BVR-A supplemented with zinc, **(c):** Bovine serum albumin supplemented with zinc, **(d):** Human BVR-A without zinc supplementation, **(e):** Murine BVR-A without supplementation, **(f):** The standard curve of absorbance at 213.9 nm versus parts per million zinc present.

decided to look at both the newly characterised mouse BVR-A as well as the human enzyme, to establish whether or not they have the ability to bind zinc.

6.2 Determination of protein bound zinc by atomic absorption spectrophotometry

Atomic absorption spectrophotometry was used to measure zinc levels. This technique has been widely used to determine metal concentrations in biological tissue samples (Hackley *et al.*, (1968). Sample preparation and zinc measurements were carried out according to the methods described in Section 2.5.6. The highest quality reagents available and distilled deionised water were used in the making of all solutions. $ZnCl_2$ was used to create a standard curve over the range 0-0.5 parts per million (ppm) which is presented in Figure 6.2 (f). The absorbance at 213.9 nm was linear with respect to zinc up to the maximum standard measured i.e. 0.5 ppm.

Bovine serum albumin, equine liver alcohol dehydrogenase, human and murine biliverdin IXα reductase were all analysed for the presence of zinc. In testing for protein bound zinc, both equine liver alcohol dehydrogenase (Sigma) and bovine serum albumin were used in control experiments. Equine liver ADH is known to contain two moles zinc per mole of enzyme (Drum *et al.*, 1967) while BSA contains one (Ohyoshi *et al.*, 1999). Human BVR-A was expressed in *E.coli* using LB supplemented with 100 μM $ZnCl_2$, and also in LB without zinc supplememtation. Expressed BVR-A was then purified to homogeneity. 1.5ml samples (0.5-1mg/ml) which had been supplemented with $ZnCl_2$ were dialysed against a 200 times volume of 100 μM $ZnCl_2$ in 100 mM Tris-HCl pH 7.2 for 3 hours. Aliquots of these (0.5ml) were then passed through a 5ml HiTrap™ Desalting Column (Amersham) equilibrated with 100mM Tris-HCl pH 7.2. Eluent fractions were collected and those with peak protein content were further analysed for the presence of zinc using atomic absorption spectroscopy.

Figures 6.2 (a) and (c) show the results of the gel filtration experiments using ADH and BSA (which was supplemented with 100μM $ZnCl_2$). Zinc co-elutes with BSA and on gel filtration as detected by the absorbance at 213.9nm, suggesting that BSA has a site which binds zinc with relatively high affinity. Figures 6.2 (b) and (d) represent the gel filtration experiments with human BVR-A [zinc supplemented and (b) and non supplemented (d)]

and Figure 6.2 (e) shows the results for murine BVR-A (non supplemented). Where zinc supplementation was performed the non free zinc is seen eluting after 5ml of 100mM Tris-HCl pH 7.2 had passed through. Analysis of the zinc detection results (Figure 6.3) taken from the peak protein fractions examined reveal that zinc is detectable in all proteins examined. As expected the levels in ADH are greatest with a molar ratio of 1.87 (zinc per protein). Interestingly, murine BVR-A seems to have substantially higher zinc bound than the other biliverdin reductases examined with 0.67 μM zinc present per μM enzyme. Human BVR-A both with and without supplementation contained between 0.2 and 0.3 μM zinc per 1μM enzyme, which is very similar to the levels found in BSA after supplementation. Even with the supplementation of zinc in the expression host growth media, and also through the purification process there is no significant increase in zinc levels. The 1:1 molar ratios reported by Maines *et al.*, (1996) present in human liver BVR-A were not detected in this study with the recombinant enzyme.

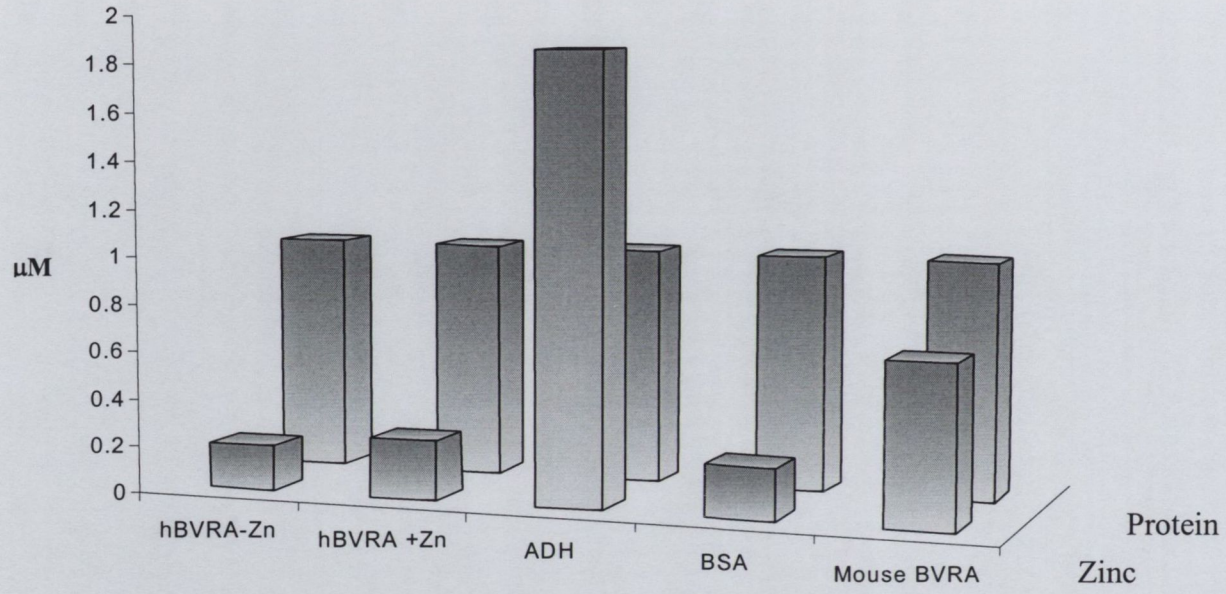

Sample	Protein Concentration	Zinc Concentration	Zinc to Protein Ratio
Human BVR-A	39.2 µM	7.5 µM	0.19
Human BVR-A (Zn supplemented)	13.4 µM	3.8 µM	0.28
Murine BVR-A	12.9 µM	8.7 µM	0.67
Equine Liver Alcohol Dehydrogenase	26.3 µM	49.2 µM	1.87
Bovine Serum Albumin	12.7 µM	2.7 µM	0.21

Figure 6.3 The detection of zinc in various protein samples subjected to desalting treatment on G-25.

6.3 Discussion

Based on the amino acid sequence similarities, Ahmad, Salim and Maines (2002) suggested that BVR-A is a basic leucine zipper-like (bZIP) DNA binding protein. They have indicated that certain key residues found in BVR-A are very similar to those conserved in the characteristic b-ZIP motifs of *Saccharomyces* GCN4 and YAP-1, human Shaker, c-myc, c-Jun, CREB, and c-Fos. b-ZIP motifs have been characterised in all of these transcription factors (Angel *et al.*, 1988). Generally such bZIP proteins dimerise to bind specifically recognised DNA target sequences which regulate gene expression. When bound to DNA each monomer retains a characteristic α-helical structure whose N-terminal half binds the major groove of DNA while the C terminal region facilitates dimerisation to form a parallel leucine zipper coiled coil.

There are three basic portions of the bZIP motif which are crucial to their ability to function as a transcriptional activator. The first region, the basic motif, is the DNA binding domain of the protein. The second region, is an alanine rich hinge region which separates the two structural motifs and allows for the transcription factor to bend. It is worth noting that some b-ZIP proteins (e.g., oct-1, oct-2, myc, myc-n and myc-l) are composed of two α-helical regions separated by a β-turn collectively known as helix-loop-helix zipper proteins. Both the alpha helices and loops section have been shown to stabilise the DNA-protein interaction. One good example of the helix loop helix proteins, is c-myc. Its 'hinge region' is replaced by a loop or 'turn', which allows the N terminal helix to bind the major groove of the target DNA (Figure 6.5) which is characteristic of the helix-turn-helix.

Finally, the third important point to note is the actual leucine zipper domain itself which causes stable dimerization of all the leucine zipper monomers (Busch *et al.*, 1990). The zipper domain contains four to five heptad amino acid repeats. Each heptad position is labelled a, b, c, d, e, f and g (John *et al.*, 1994). In Figure 6.7 the *Saccharomyces* GCN4 amino acid sequence is shown highlighting the key residues of this motif. As a general rule position A (typically valine), and position D (typically leucine), have hydrophobic requirements as they are positioned at the hydrophobic interface of the associated dimmers. In some cases the third heptad A position is an asparagine which can hydrogen bond with the asparagines of the A position of the second associating monomer as is the case with

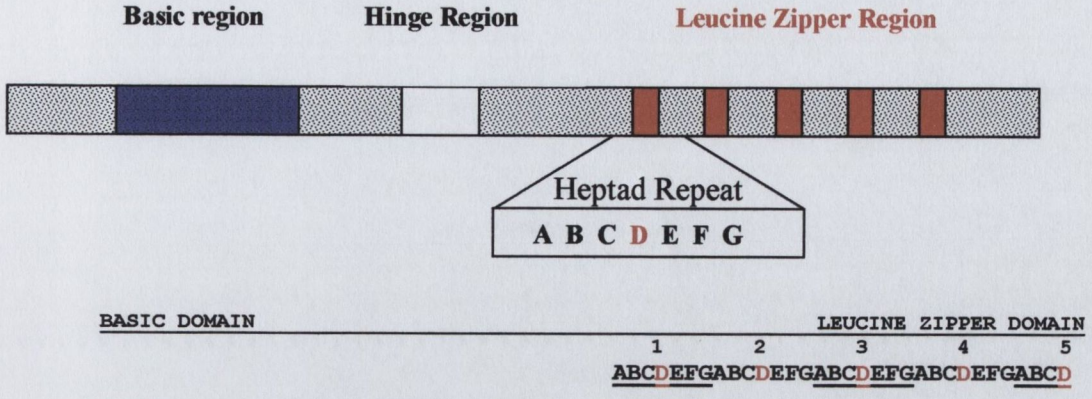

(a)

The complete Major Groove binding domain of hc-MYC

LOOP REGION

GHMNVKRRTHNVLERQRRNELKRSFFALRDQIPELENNEKAPKVVILKKATAYILSVQAEEQKLISEEDLLRKRREQLKHKLEQLG

hBVR-A	MTLSLAAAQELWELAEQKGKVLHEEHVELLMEEFAFLKKEVVGKDLLKGSLLFTSDPL
rBVR-A	MTLSFAAAQELWELAAQKGRVLHEEHVELLMEEFEFLRREVLGKELLKGSLRFTASPL
hSHAKER	GGGGQNGQQAMSLAILRVIRLVRVFRIFKLSRHSKGLQILGKTLQASMRELGLLIFFL
hc-MYC	LRDQIPELENNEKAPKVVILKKATAYILSVQAEEQKLISEEDLLRKRREQLKHKLEQL
sGCN4	SSDPAALKRARNTEAARRSRARKLQRMKQLEDKVEELLSKNYHLENEVARLKKLVGER
Hc-Jun	ERIKAERKRMRNRIAASKCRKRKLERIARLEEKVKTLKAQNSELASTANMLREQVAQL
hCREB	AARKREVRLMKNREAARECRRKKKEYVKCLENRVAVLENQNKTLIEELKALKDLYCHK
hC-FOS	EEEKRRIRRERNKMAAAKCRNRRRELTDTLQAETDQLEDEKSALQTEIANLLKEKEKL
sYAP-1	DPETKQKRTAQNRAAQRAFRERKERKMKELEKKVQSLESIQQQNEVEATFLRDQLITL

(b)

Figure 6.4 BVR-A as a putative b-ZIP protein.

(a) The bZIP monomer.

The typical bZIP monomer has a basic region which is the DNA binding domain of the protein, an alanine rich hinge region which separates the two structural motifs and allowing flexibility in the coil, and finally the leucine zipper motif with four to five heptad repeats with leucine invariably at position d.

(b) BVR-A as a b-ZIP transcription factor.

The similarities between BVR-A, and the b-ZIP transcription factor dimerisation domains are highlighted in the alignments above. The sequences shown represent 57 amino acids spanning the 'leucine zipper' domains and the 'basic domains'.

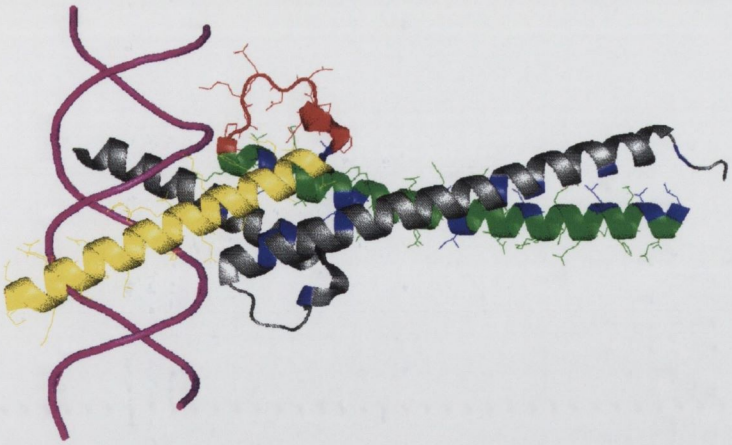

Figure 6.5 X-Ray Structure of c-Myc-Max heterodimer associated with target DNA.

c-Myc-Max heterodimer associated with target DNA (1NKP Protein Data Bank). The leucine repeats of the hydrophobic interface between the heterodimer coils of Max (grey) and c-myc (green). The basic loop region and DNA binding regions are displayed in red and yellow respectively.

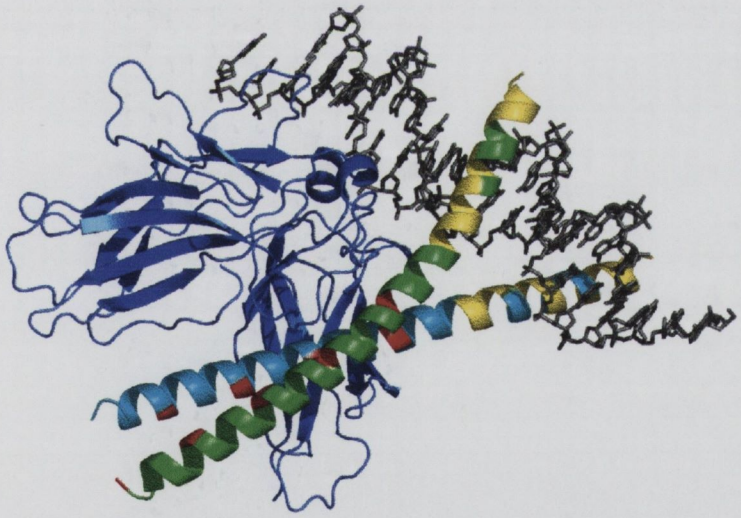

Figure: 6.6 Structure of the DNA binding domains of Nfat, Fos and Jun Bound to DNA.

The dimerisation of human c-fos, c-jun and Nfat proteins as they interact with DNA. Only 57 amino acids of the whole c-fos and c-jun proteins are shown for clarity. The side chains of the conserved leucine residues within the dimerisation domains are shown in red. The DNA binding helices (cyan hc-fos / green hc-jun) diverge from the base of the zipper motif and follow the major groove ot the target DNA. The conserved basic domains are coloured yellow. Nfat is coloured blue.

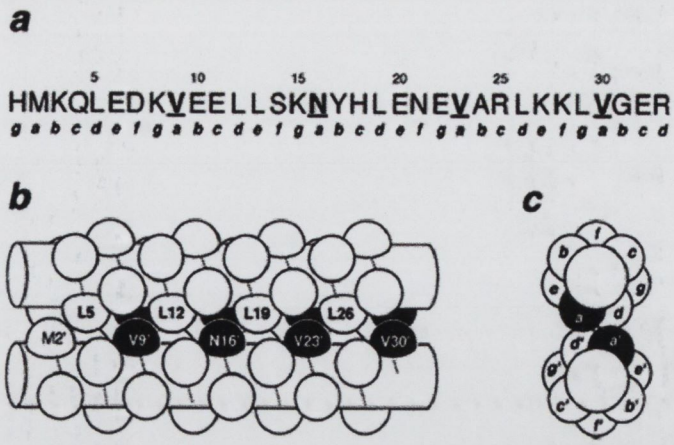

Figure 6.7 The parallel coiled coil of the leucine zipper of *Saccharomyces* GCN4.

(a) Heptad repeat positions are indicated by lower case letters.

(b) Side view of the homodimer. Amino acid backbones in helical conformation are represented by cylinders where the path of the polypeptide chain indicated by the dotted lines. Side chains are represented as knobs.

(c) End view showing how different heptad positions are arranged in the dimer. The side chains at the *a* positions are buried in the dimer interface (Zeng X. *et al.*, 1997).

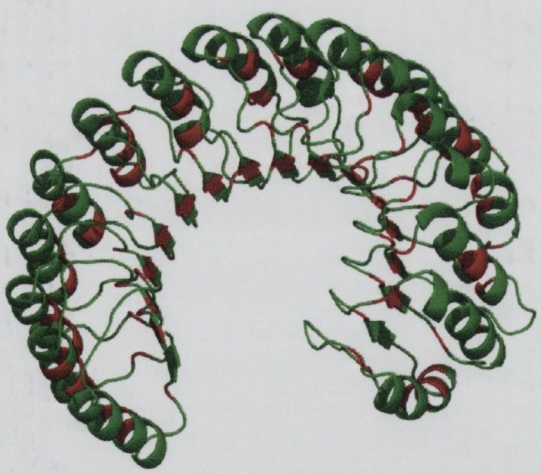

Figure 6.8 Structure of the horse shoe shaped leucine rich, α-helix-turn-β structure, present in porcine ribonuclease inhibitor.

Ribonuclease inhibitor is a cytoplasmic protein that tightly binds and inhibits ribonucleases of the pancreatic ribonuclease superfamily. The primary sequence of this inhibitor contains leucine-rich repeats which are highlighted in red. These motifs are present in many proteins that participate in protein-protein interactions and have different functions and cellular locations.

GCN4 and CREB and c-jun. The solvent-accessible e and g positions are frequently occupied by charged amino acids. The basic DNA binding region invariably contains lysine and arginine residues which interact with the negative phosphate groups of the DNA phosphodiester backbone, while hydrogen bonds and Van der Waals interactions between amino acid residues and specific DNA bases (Glover *et al*) allow recognition of specific DNA sequences.

The B-ZIP proteins Fos and Jun combine as a heterodimer to form activator protein-1 (AP-1). AP-1 is a heterodimeric leucine zipper transcription factor capable of binding the TPA (12-O-tetradecanoylphorbol 13 acetate) response element (TRE) with a consensus sequence 5' TGAGTCA 3'. The complex forms an extended interface between NFAT and the AP-1 site, which is facilitated by the bending of Fos and DNA. The tight association of the three proteins on DNA creates a continuous groove for the recognition of 15 base pairs. The AP-1 complex may often act in combination with other transcription factors. The crystal structure of the nuclear factor of activated T cells (NFAT)-Jun-Fos-DNA complex has been resolved (Figure 6.6). NFAT sites usually have an AP-1 like site downstream of the NFAT binding site and bind together with AP-1 binding fifteen nucleotides of the major groove to activate NFAT controlled genes in the T cell receptor (TCR) activation pathway. As is evident from Figures 6.5 and 6.6, the tertiary structure of the jun/fos heterodimer, and the c-myc/max heterodimer are continuous α-helices. These structures interact in the leucine zipper domain and each form an asymmetric coiled-coil in which the one subunit curls around the other. The subunits split at the flexible fork which allows them to bind the major groove of their specific target sequences such as the AP-1 binding site.

Salim and Maines (2002), compared the amino acid sequences for these b-ZIP transcription factors and BVR-A. They highlighted some striking similarities between BVR-A, and the dimerisation domains of these transcription factors, details of which are shown in the alignments below. The sequences shown represent 57 amino acids spanning the putative 'leucine zipper' domains and the 'basic domains'. The full amino acid sequence of c-myc which is depicted in the crystal structure of Figure 6.6 is shown in Figure 6.4 (b). For clarity the first 27 amino acids were not shown in the alignments. It is evident that in many of the recognised leucine zippers (with one notable exception, sYAP's

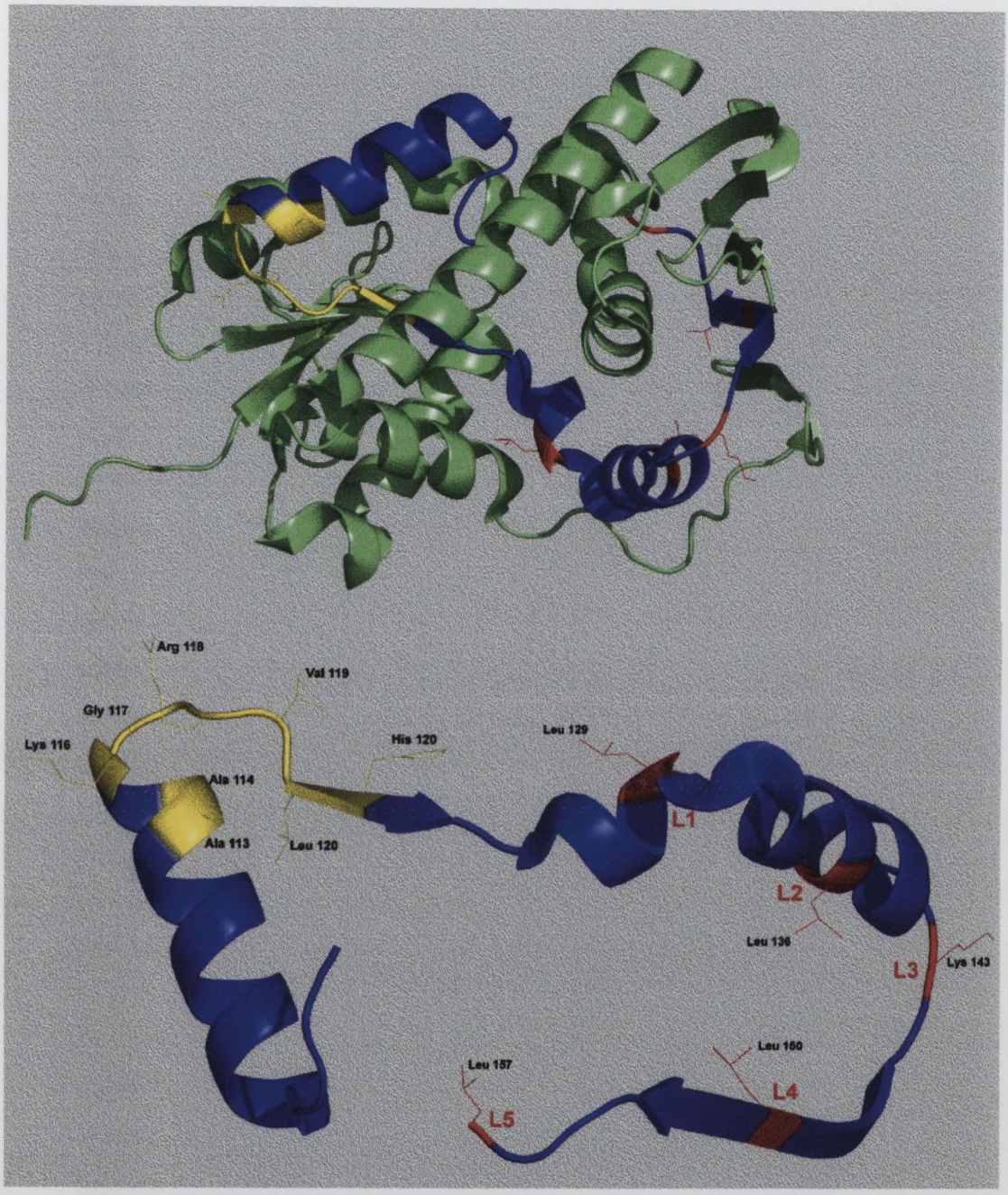

Figure 6.9 Crystal structure of rat BVR-A

A ribbon representation based on the crystal structure of rat BVR-A. Shown in red are the heptad D positions (L1-L5) and high-lighted in yellow is the basic DNA binding domain proposed by Ahmad Salim and Maines (2002).

asparagine), the D3 position is occupied by leucine residues. In both human and rat BVR-A, D3 positions are occupied by lysine. Both sGCN4 and hCREB have four leucine repeats with the D5 position being filled by arginine and lysine respectively. Ahmad Salim and Maines (2002), conclude that the lysine substitution at position D3 in BVR-A is acceptable on the basis that the D5 positions in sGCN4 and hCREB have arginine and lysine substitutions. One could suggest that since both lysine and arginine have positive charges at the ends of long, flexible hydrophobic element to produce a flat hydrophobic surface like that of isoleucine. From sequence analysis one could possibly conclude that BVR-A is a leucine zipper like protein as it seems to fulfil all the necessary criteria. However, Bornberg *et al.*, (1998) and Hirst *et al.*, (1996), have pointed out some of the problems of predicting leucine zippers from sequence information alone. Crystal structure data has provided a wealth of information on how these zippers function. Apart from the leucine repeats and the requirements of the other heptad positions the nature of the coil adopted by the zipper has proven to be very important for dimerisation and functionality. It is also worth noting that many sequences have the leucine repeat but do not adopt the leucine zipper structure Brendel (1989). Bornberg-Bauer (1998) developed the '2ZIP program', available from the Max Plank Institute for Molecular Genetics (http://cmb.molgen.mpg.de/), which combines a standard coiled coil prediction algorithm with searches for the characteristic leucine repeat. The GCN4, YAP-1, human Shaker, c-myc, c-Jun, CREB, and c-Fos sequences were all analysed using this program, the results of which are displayed in Appendix VI. Both rat and human BVR-A sequences failed to provide a positive result with 2ZIP.

The most convincing evidence that BVR-A is unlikely to be a b-ZIP or HLH-ZIP leucine zipper like protein comes from the crystal structure of rat BVR-A (Kikuchi *et al.*, (2001); Whitby *et al.*, (2002)). It is interesting to note that the sequence in question adopts an α-helix-turn-β-sheet fold which threads through the centre of the protein, and forms an internal bridge from the active centre to the characteristic beta sheet folds on the enzyme surface (Figure 6.9). Salim and Maines (2002) have curiously suggested that the 'α-helix-turn-β-sheet' fold may bind DNA in a fashion like that of the porcine ribonuclease inhibitor protein shown in Figure 6.8. This structure represents a class of alpha/beta protein fold where individual leucine repeats are integral constituents of the beta-alpha structural units. The interesting point here is that the leucine repeats help to achieve strong protein-

protein interactions. Looking closely at the interactions of the conserved BVR-A leucines, one could simply suggest that the high leucine content in this region functions structurally to form a hydrophobic core, which functions to anchor and provide packing stability to the (-helices of the Rosmann fold, and also on the inner surface of the β-sheets (Figure 6.10).

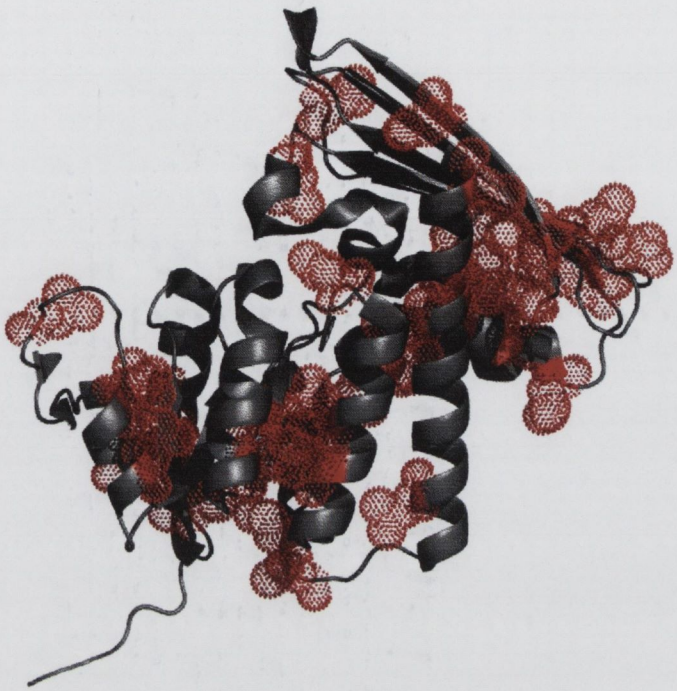

Figure 6.10 Crystal structure of rat BVR-A

A ribbon representation of the structure of rat BVR-A. Shown in red dots one can see the positioning of leucine residues. Note the concentration of these residues in core positions of the enzyme.

Chapter Seven

General Discussion

The species distribution of biliverdin-IXα reductase (both prokaryotic and eukaryotic) has been reinvestigated and the results of which are presented in Chapter 3. It seems increasingly likely that birds and amphibia have the potential to express an active biliverdin-IXα reductase. Searches of the database have revealed that the chicken (*Gallus gallus*) has a gene which encodes for a biliverdin reductase like protein. Furthermore biliverdin reductase activity has been detected in turkey erythrocyte cytosols. These findings should lead to a renewed interest in the detection and characterisation of putative avian biliverdin IX-α reductases. In tandem, the full length cDNAs encoding human, *Danio rerio*, murine, and *Xenopus* BVR-A were successfully amplified and cloned into various expression vectors (pET4a-Mod for human and *Danio rerio*, ppMAL for the murine and pGEX-KG for the *Xenopus* enzyme). To date human BVR-A pET41a-Mod, murine BVR-A ppMAL, and *Xenopus* BVR-A pGEX-KG transformed cultures have been induced with IPTG resulting in the expression of recombinant proteins which display the appropriate molecular weights. Antibodies against the murine, human and synechocystis enzymes have also been raised in this study. The cloning and expression of an active *Xenopus* BVR-A in this study extends the phylogenetic distribution of BVR-A to include amphibian and supports the idea that biliverdin-IXα reductase is not just present in some fish, mammals and in cyanobacteria. The study of this enzyme in different species may prove interesting and answer the question why bilirubin and bilirubin conjugates are found in these species even though biliverdin is seen as the major haem degradation product.

Phosphate has been shown to enhance NADH binding by human BVR-A as the apparent K_m for NADH is decreased over 100-fold with no change in the apparent V_{max}. Examination of the rat BVR-A crystal structure showed that three phosphate anions were bound to the enzyme. Of these phosphates two were interestingly positioned, one by the nucleotide pyrophosphate binding site and one at the NADPH 2'-phosphate binding site. Replacement of residues around the 2' phosphate binding pocket was used to further investigate the nature of phosphate activation. It was shown that the R44A mutant not only abolished the kinetic discrimination between NADH and NADPH, but also the activation by phosphate during the NADH dependent reaction. It is clear that NADH binding is augmented by inorganic phosphate "mimicking" the 2'-phosphate of NADPH.

The kinetics of the mammalian enzymes have been distorted by the effects of substrate inhibition and by the activation of NADH dependent activity by phosphate. It now seems likely that the nature of the dual pH-cofactor specificity initially reported by Kutty & Maines (1981), is due to the pH dependence of substrate inhibition which is additionally complicated by phosphate activation with NADH as cofactor.

In order to overcome the effects of substrate inhibition hampering the full characterisation of these enzymes it was decided to initiate the development of a radiolabelled assay for BVR-A using. This would allow the assay of BVR-A at sub-inhibitory biliverdin concentrations (nM range). It has been shown that recombinant *E.coli* NAD^+ kinase and *Thermoanaerobium brockii* alcohol dehydrogenase can be used to synthesise 14.6 μM 2'-[^{32}P] NADPH with a specific activity of 243mCi/mmol. It has also been shown that the TLC separation of $NADP^+$ from NADPH and NAD^+ from NADH on PEI cellulose allows for a convenient method to assay the activity of this enzyme.

The substrate specificity of BVR-A was further investigated with the hope of gaining an insight into factors determining substrate binding. These studies suggest that the most determining factors for substrate binding are the charged propionate moiety on two central pyrrole rings as biliverdin-IXα dimethylester was shown not to be a substrate for human BVR-A, while the reaction using biliverdin-IXα sulphonate as substrate was catalytically productive. Further studies using biliverdin isomers with conformational restraints were analysed and the results of these experiments suggest that significant modifications on the conformational volume occupied by the outer pyrroles of biliverdin do not impede substrate binding. This may be interpreted in a model where the outer prrroles are not intimately associated with the enzyme surface.

It has been suggested that BVR-A has functions, beyond its recognised catalytic activity. One such function is based on the enzymes ability to associate with zinc and as a result it has been suggested that BVR-A may play a role in either Zn^{2+} storage, or in the regulation of gene expression as suggested by Maines (1996), who proposed that there is a Zn^{2+} co-ordination site at the carboxy-terminal region which is similar to a zinc finger like motif. Atomic absorbance spectroscopy measurements show that Zn^{2+} can indeed associate with

hBVR-A, however the molar ratio of zinc to protein of 0.28:1 is of the same order as that seen with a control protein (BSA) not normally considered to be a zinc protein. Under the same conditions alcohol dehydrogenase was shown to have a zinc to protein ratio of 1.8 to 1 in agreement with its known zinc stoichiometry (2:1). The mouse enzyme is 'sticker' for zinc with a molar ratio of 0.67 to 1. Based on the crystal structure data for the rat enzyme there is no evidence for bound zinc and the residues proposed to co-ordinate a hypothetical zinc ion are not appropriately found in space. The suggestion that BVR-A is a zinc finger protein is therefore unlikely. Later the Maines group proposed that the enzyme functioned as a leucine zipper like protein based on amino acid sequence homologies to other leucine zipper proteins (Ahmad *et al.*, 2002). As outlined in this study an analysis of the crystal structure of the rat enzyme suggests otherwise.

Appendix I

Appendix I **Materials**

Biochemical reagents and chemicals were of analytical grade, where possible, and were obtained from BDH, Rieded-de Haen and Sigma.

Ambion Inc. 2130 Woodward Street Austin, TX 78744, USA

Amicon Corporation, Scientific Systems Division, Danvers, MA 01923, USA.

Amersham Biosciences UK Limited, Little Chalfont, Buckinghamshire, England HP7 9NA.

Bio-Rad Laboratories Ltd., Export Division, Bio-Rad House, Marylands Avenue, Hemel Hempstead, Herts., HP2 7TD, England.

Bio-Sciences, 3 Charlemont Tce., Crofton Road, Dun Laoghaire, Co. Dublin
BDH Laboratory supplies, Poole, BH15 ITD, England

Calbiochem, *biosciences inc*, La Jolla, CA 92039-2087 and Merck Biosciences GmbH Ober der Roth 4, 65824 Schwalbach/Ts, Germany

Greiner GmBH, Maybachstrasse 2, D-7443, Frickenhausen, Germany

Kodak Ltd., Acornfield road, Kirkby, Liverpool 546 2101, England

Lennox Laboratory Supplies Ltd., John F Kennedy Drive, Naas Road, Dublin 12

Naglene Company, Subsidary of Sybron Corporation, Rochester, New York 14602-0365, USA

National Diagnostics, 305 Patton Drive, Atlanta, Georgia 30336, USA

Promega Biosciences Inc., Promega Corporation San Luis Obispo, California

Roche Diagnostics GmbH, Mannheim, Germany
Takara Bio Inc, Seta 3-4-1, Otsu, Shiga 520-2193, Japan

Sigma-Aldrich Chemie Gmbh P.O 1120 89552 Steinheim, Germany 4-7329-970

Starstedt, Sinnetstown Lane, Drinagh, Wexford / Aktiengesellschaft & Co., D-51588 Numbrecht, Germany.

Appendix II

Appendix II

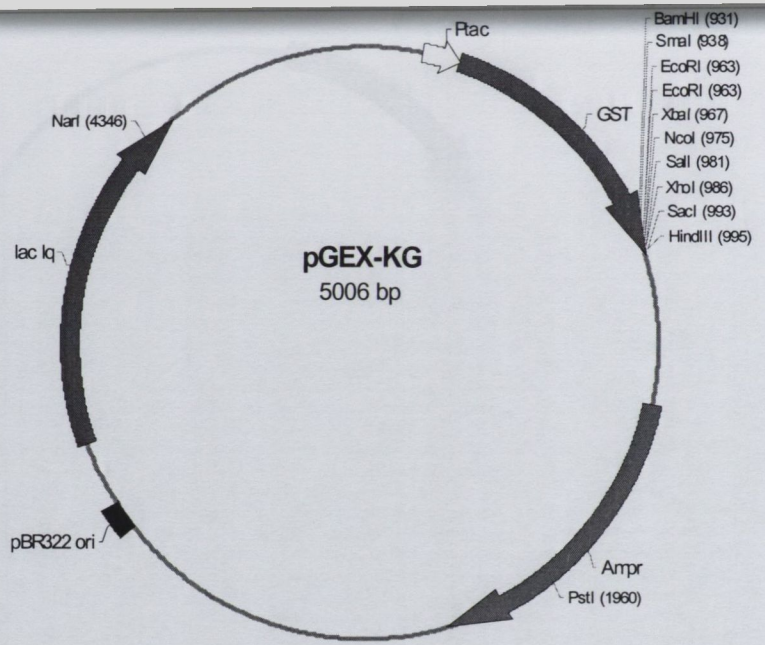


```
                                SmaI                                                                  SalI          SacI
CTG GTT CCG CGT GGA TCC CCG GGA ATT TCC GGT GGT GGT GGT GGA ATT CTA GAC TCC ATG GGT CGA CTC GAG CTC AAG CTT AAT TCA
                 BamHI                                                EcoRI          NcoI           XhoI         HindIII

Leu Val Pro Arg/Gly Ser Pro Gly Ile Ser Gly Gly Gly Gly Gly Ile Leu Asp Ser Met Gly Arg Leu Glu Leu Lys Leu Asn Ser
  Thrombin Cleavage Site                  Polylinker
```

Figure 2 The pGEX-KG Multiple Cloning Vector

The pGEX-KG expression vector (Guan and Dixon 1991) is based on the pGEX-2T expression vector. In frame cloning of target cDNA into the multiple cloning site of the pGEX-KG expression vector produces a GST tagged fusion protein. Target protein cleavage from the GST moiety is facilitated through the thrombin encoded recognition site. Amino acid translation is displayed in red.

Appendix II

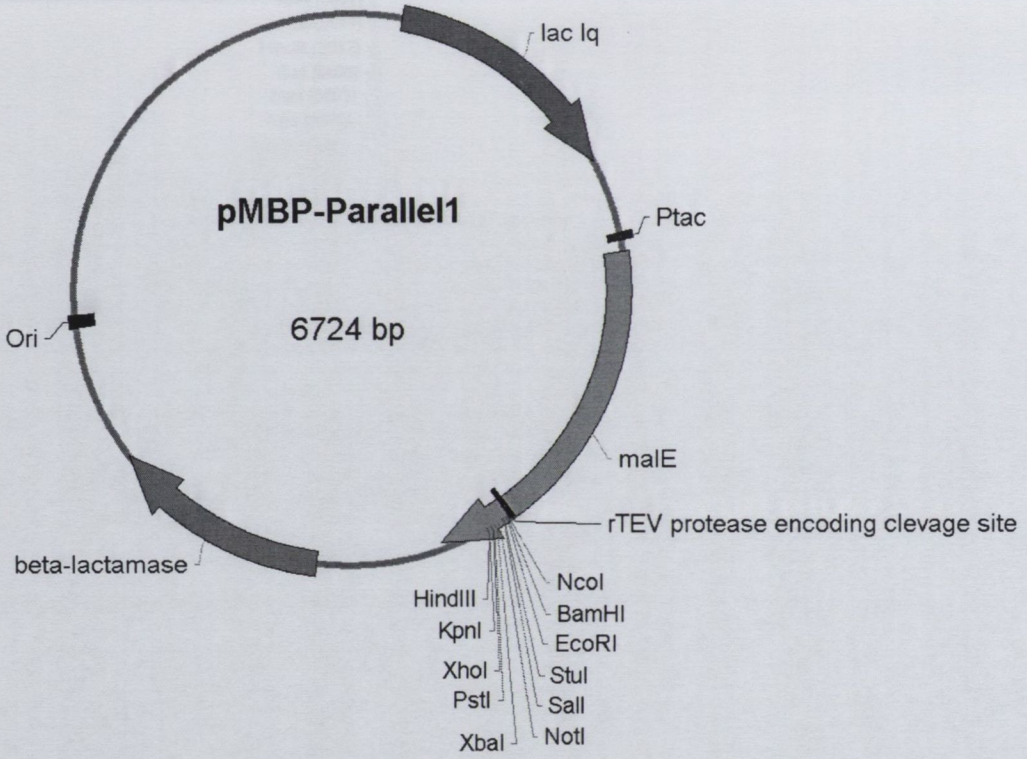


```
                                SacI                                                
```

Appendix II

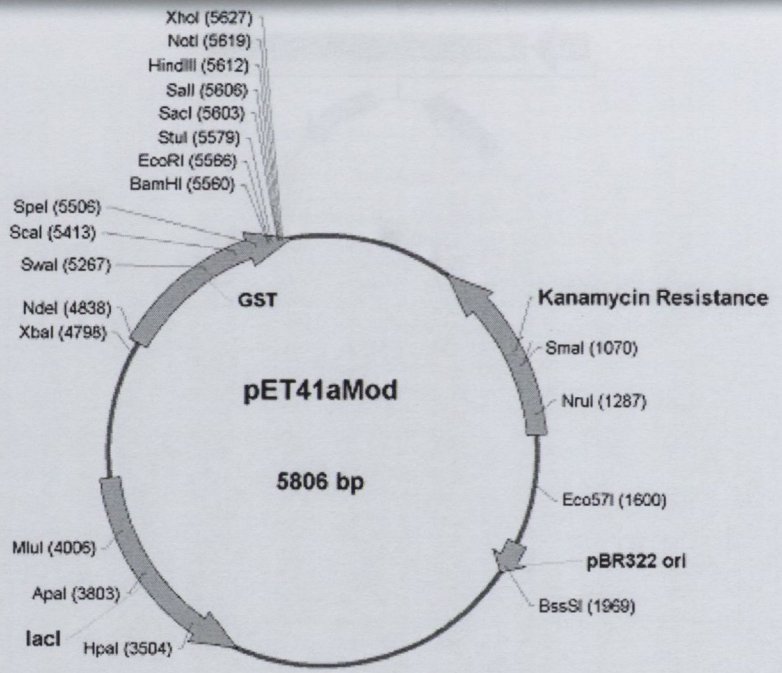


```
GAT.AAG.TAC.TTG.AAA.TCC.AGC.AAG.TAT.ATA.GCA.TGG.CCT.TTG.CAG.GGC.TGG. CAA.GCC.ACG.TTT.GGT.GGT.GGC.GAC.CAT.CCT.CCA.AAA.TCG.GAT.GGT.TCA.ACT.AGT.GGT.
GST encoding    C terminus region----------------------------------------------------------------------Asp His Pro Pro Lys Ser Asp Gly Ser Thr Ser Gly

             6XHis tag         SacII          Thrombin    BamH1    EcoR1         Stu1                Pst1       Sac1     Sal1    Hind III
TCT.GGT.CAT.CAC.CAT.CAC.CAT.CAC.TCC.GCG.GGT.CTG.GTG.CCA.CGC.GGA.TCC.GAA.TTC TGT.ACA.GGC.CTT.GGC.GCG.CCT.GCA.GGC.GAG.CTC.CGT.CGA.CAA.GCT.TGC
Ser Gly His His His His His His Ser Ala Gly Leu Val Pro Arg/Gly.Ser Glu Phe Cys Thr Gly Leu Gly Ala Pro Ala Gly Glu Leu Arg Arg Gln Ala Cys

          Xho1                HIS TAG
GGC.CGC.ACT.CGA.GCA.CCA.CCA.CCA.CCA.CCA.CCA.CTA.ATT.GAT.TAA.TAC. CTA.GGC.TGC.TAA.ACA.AAG.CCC.GAA.AGG.AAG.CTG.AGT.TGG.CTG.CTG.CCA.CCG.CTG.AGC.
Gly Arg Thr Arg Ala Ala.Pro.Pro.Pro.Pro.Pro.Pro.Leu Ile Asp End
```

Figure 4 The pET41aMod expression vector.

In frame cloning of target cDNA into the multiple cloning site (BamHI to HindIII) of the pET41aMod expression vector will produce a 6X histidine tagged GST fusion protein. Target protein cleavage from the His tagged GST is facilitated through the thrombin encoded recognition site. The amino acid translation is displayed in red.

Appendix II

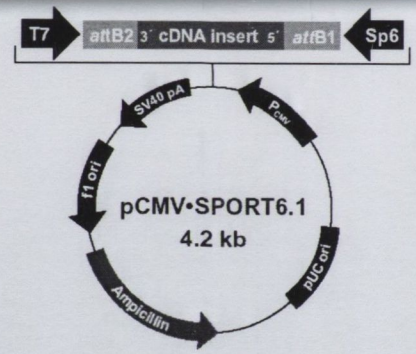

Comments for pCMV•SPORT6.1 (no insert)
4177 nucleotides

SV40 early polyadenylation signal (c): bases 126-392
M13 Forward (-20) priming site: bases 664-679
T7 promoter/priming site: bases 691-710
*att*B2: bases 711-735
*att*B1: bases 807-831
Sp6 promoter/priming site (c): bases 833-850
M13 Reverse priming site (c): bases 861-877
CMV promoter (c): bases 920-1510
pUC origin: bases 1895-2562
Ampicillin (*bla*) resistance gene (c): bases 2729-3589
bla promoter (c): bases 3590-3641
f1 origin (c): bases 3721-4176

(c) = complementary strand

NAME: pCMV-SPORT6.1 (ampicillin resistant; 50-200 ug/ml) SEQUENCING PRIMERS: M13(-21), M13 reverse, sp6 SOURCE: Invitrogen Life Technologies V_TYPE: phagemid POLYLINKER SEQUENCE:

caccacagaagtaaggttccttcacaaagatcccaagctagcagttttcccagtcacgacgttgtaaaacgacggccagtgcctagcttataatacgactcactatagggaccactttgtacaagaaagctgggtacgcgt
aagcttgggcccctcgagggatactctagagcggccgccgatccggcttactaaaagccagataacagtatgcgtatttgcgcgctgatttttgcggtataagaatatatactgatatgtatacccgaagtatgtcaaaaa
gaggtgtgcttctagaatgcagtttaaggtttacacctataaaagagagagccgttatcgtctgtttgtggatgtacagagtgatattattgacacgcccgggcgacggatggtgatccccctggccagtgcacgtctgct
gtcagataaagtctcccgtgaactttacccggtggtgcatatcggggatgaaagctggcgcatgatgaccaccgatatggccagtgtgccggtctccgttatcgggggaagaagtggctgatctcagccaccgcgaaaatga
catcaaaaacgccattaacctgatgttctggggaatataagtcgacgatatcccgggaattccggaccggtaccagcctgctttttttgtacaaacttgttctatagtgtcacctaaataggcctaatggtcatagctgttt
cctgtgtgaaattgttatccgctccgcggcctaggctagagtccggaggctggatcggtcccggtgtcttctatggaggtcaaaacag

Figure 5 Illustration of the pCMV-Sport 6.1 cloning vector.

The I.M.A.G.E cDNA clone (IMAGE: 5308696) consists of the full length xenopus tropicalis biliverdin reductase cloned ligated into the pCMV-Sport6.1 cloning vector. This clone was ordered from the I.M.A.G.E consortium and used as template in subsequent PCR amplification reactions of the putative xenopus BVR-A.

Appendix III

Appendix III

SeqA	Name	Length(aa)	SeqB	Name	Length(aa)	Score
3	Homo	296	9	Pan	296	99
14	Nostoc_sp.PCC	322	15	Anabaena	329	94
3	Homo	296	4	Canis	296	93
4	Canis	296	9	Pan	296	93
3	Homo	296	10	Bos	296	91
4	Canis	296	10	Bos	296	91
9	Pan	296	10	Bos	296	91
5	MOUSE	295	6	Rattus	295	89
3	Homo	296	6	Rattus	295	83
5	MOUSE	295	9	Pan	296	83
6	Rattus	295	9	Pan	296	83
3	Homo	296	5	MOUSE	295	82
4	Canis	296	5	MOUSE	295	81
4	Canis	296	6	Rattus	295	81
5	MOUSE	295	10	Bos	296	81
6	Rattus	295	10	Bos	296	81
11	Nostoc	333	14	Nostoc_sp.PCC	322	76
11	Nostoc	333	15	Anabaena	329	76
1	Gallus	323	2	Xenopus	290	69
7	Zebrafish	292	8	Tetraodon	287	62
1	Gallus	323	10	Bos	296	59
1	Gallus	323	3	Homo	296	58
1	Gallus	323	4	Canis	296	58
1	Gallus	323	5	MOUSE	295	58
1	Gallus	323	8	Tetraodon	287	58
1	Gallus	323	9	Pan	296	58
1	Gallus	323	6	Rattus	295	57
2	Xenopus	290	7	Zebrafish	292	57
11	Nostoc	333	16	Trichodesmium	335	57
1	Gallus	323	7	Zebrafish	292	56
2	Xenopus	290	8	Tetraodon	287	56
15	Anabaena	329	16	Trichodesmium	335	55
2	Xenopus	290	4	Canis	296	54
2	Xenopus	290	10	Bos	296	54
5	MOUSE	295	8	Tetraodon	287	54
14	Nostoc_sp.PCC	322	16	Trichodesmium	335	54
2	Xenopus	290	3	Homo	296	53
2	Xenopus	290	9	Pan	296	53
3	Homo	296	7	Zebrafish	292	53
4	Canis	296	7	Zebrafish	292	53
6	Rattus	295	8	Tetraodon	287	53
7	Zebrafish	292	9	Pan	296	53
7	Zebrafish	292	10	Bos	296	53
2	Xenopus	290	5	MOUSE	295	52
3	Homo	296	8	Tetraodon	287	52
4	Canis	296	8	Tetraodon	287	52
8	Tetraodon	287	9	Pan	296	52
11	Nostoc	333	13	Synechocystis	328	52
2	Xenopus	290	6	Rattus	295	51
5	MOUSE	295	7	Zebrafish	292	51
6	Rattus	295	7	Zebrafish	292	51
8	Tetraodon	287	10	Bos	296	51
13	Synechocystis	328	14	Nostoc_sp.PCC	322	51
13	Synechocystis	328	15	Anabaena	329	51
11	Nostoc	333	17	Crocosphaera	341	50
13	Synechocystis	328	16	Trichodesmium	335	50
14	Nostoc_sp.PCC	322	17	Crocosphaera	341	50
16	Trichodesmium	335	17	Crocosphaera	341	50
15	Anabaena	329	17	Crocosphaera	341	49
13	Synechocystis	328	17	Crocosphaera	341	45
11	Nostoc	333	12	Gloeobacter	332	42
12	Gloeobacter	332	14	Nostoc_sp.PCC	322	42
12	Gloeobacter	332	15	Anabaena	329	42
12	Gloeobacter	332	13	Synechocystis	328	41
12	Gloeobacter	332	16	Trichodesmium	335	38
12	Gloeobacter	332	17	Crocosphaera	341	36
2	Xenopus	290	11	Nostoc	333	24
2	Xenopus	290	14	Nostoc_sp.PCC	322	23
5	MOUSE	295	11	Nostoc	333	23
5	MOUSE	295	13	Synechocystis	328	23
5	MOUSE	295	15	Anabaena	329	23
8	Tetraodon	287	14	Nostoc_sp.PCC	322	23
8	Tetraodon	287	15	Anabaena	329	23
5	MOUSE	295	14	Nostoc_sp.PCC	322	22
8	Tetraodon	287	11	Nostoc	333	22
1	Gallus	323	11	Nostoc	333	21
1	Gallus	323	15	Anabaena	329	21
2	Xenopus	290	13	Synechocystis	328	21
2	Xenopus	290	15	Anabaena	329	21
3	Homo	296	11	Nostoc	333	21

Appendix III

SeqA	Name	Length(aa)	SeqB	Name	Length(aa)	Score
3	Homo	296	13	Synechocystis	328	21
5	MOUSE	295	12	Gloeobacter	332	21
5	MOUSE	295	16	Trichodesmium	335	21
6	Rattus	295	11	Nostoc	333	21
6	Rattus	295	13	Synechocystis	328	21
6	Rattus	295	15	Anabaena	329	21
7	Zebrafish	292	16	Trichodesmium	335	21
9	Pan	296	11	Nostoc	333	21
9	Pan	296	13	Synechocystis	328	21
3	Homo	296	15	Anabaena	329	20
6	Rattus	295	14	Nostoc_sp.PCC	322	20
6	Rattus	295	16	Trichodesmium	335	20
9	Pan	296	15	Anabaena	329	20
1	Gallus	323	14	Nostoc_sp.PCC	322	19
2	Xenopus	290	12	Gloeobacter	332	19
2	Xenopus	290	16	Trichodesmium	335	19
3	Homo	296	12	Gloeobacter	332	19
3	Homo	296	14	Nostoc_sp.PCC	322	19
4	Canis	296	12	Gloeobacter	332	19
6	Rattus	295	12	Gloeobacter	332	19
8	Tetraodon	287	16	Trichodesmium	335	19
9	Pan	296	12	Gloeobacter	332	19
9	Pan	296	14	Nostoc_sp.PCC	322	19
10	Bos	296	13	Synechocystis	328	19
10	Bos	296	15	Anabaena	329	19
4	Canis	296	11	Nostoc	333	18
4	Canis	296	14	Nostoc_sp.PCC	322	18
4	Canis	296	15	Anabaena	329	18
7	Zebrafish	292	14	Nostoc_sp.PCC	322	18
7	Zebrafish	292	15	Anabaena	329	18
8	Tetraodon	287	13	Synechocystis	328	18
10	Bos	296	11	Nostoc	333	18
10	Bos	296	14	Nostoc_sp.PCC	322	18
2	Xenopus	290	17	Crocosphaera	341	17
4	Canis	296	13	Synechocystis	328	17
7	Zebrafish	292	11	Nostoc	333	17
7	Zebrafish	292	12	Gloeobacter	332	17
8	Tetraodon	287	12	Gloeobacter	332	17
10	Bos	296	12	Gloeobacter	332	17
1	Gallus	323	12	Gloeobacter	332	16
4	Canis	296	16	Trichodesmium	335	16
1	Gallus	323	16	Trichodesmium	335	15
3	Homo	296	16	Trichodesmium	335	15
5	MOUSE	295	17	Crocosphaera	341	15
8	Tetraodon	287	17	Crocosphaera	341	15
9	Pan	296	16	Trichodesmium	335	15
10	Bos	296	16	Trichodesmium	335	15
1	Gallus	323	13	Synechocystis	328	14
6	Rattus	295	17	Crocosphaera	341	14
7	Zebrafish	292	13	Synechocystis	328	14
1	Gallus	323	17	Crocosphaera	341	13
7	Zebrafish	292	17	Crocosphaera	341	13
3	Homo	296	17	Crocosphaera	341	12
4	Canis	296	17	Crocosphaera	341	12
9	Pan	296	17	Crocosphaera	341	12
10	Bos	296	17	Crocosphaera	341	12

Figure 1 Amino acid sequence identity shared between all known and putative biliverdin IXα reductase enzymes identified.

Sequences were analysed using the Clustalw Alignment tool available online at www.ebi.ac.uk and alignment scores calculated.

Appendix III

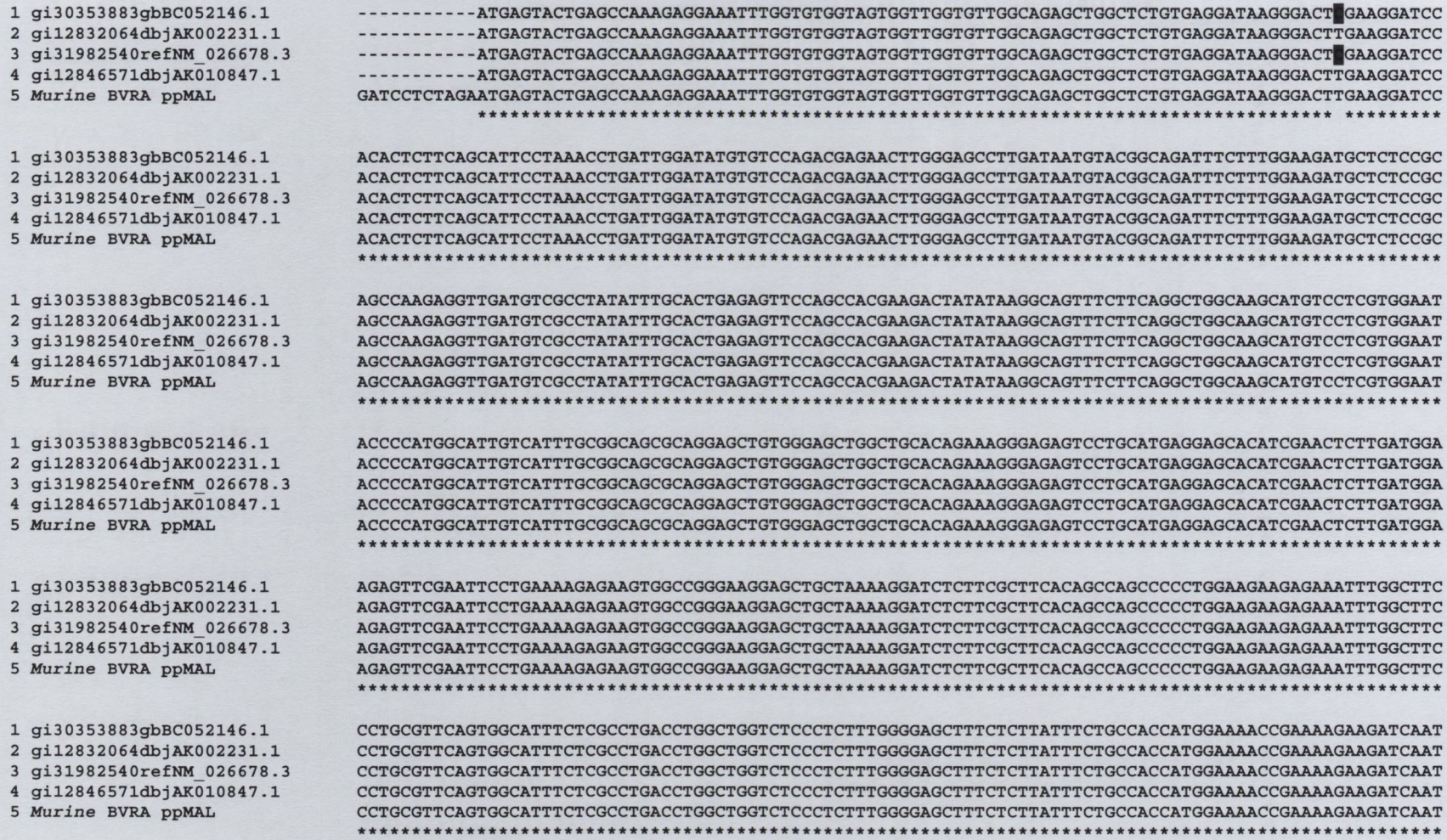

```
1 gi30353883gbBC052146.1        ATATGAAAATGACCGTGCAGCTCGAGACCCAGAACAAAAGTCCATTATCATGGATTGAAGAGAAAGGGCCTGGCTTAAAAAGGAACAGACATATAAGCAT
2 gi12832064dbjAK002231.1       ATATGAAAATGACCGTGCAGCTCGAGACCCAGAACAAAAGTCCATTATCATGGATTGAAGAGAAAGGGCCTGGCTTAAAAAGGAACAGACATATAAGCAT
3 gi31982540refNM_026678.3      ATATGAAAATGACCGTGCAGCTCGAGACCCAGAACAAAAGTCCATTATCATGGATTGAAGAGAAAGGGCCTGGCTTAAAAAGGAACAGACATATAAGCAT
4 gi12846571dbjAK010847.1       ATATGAAAATGACCGTGCAGCTCGAGACCCAGAACAAAAGTCCATTATCATGGATTGAAGAGAAAGGGCCTGGCTTAAAAAGGAACAGACATATAAGCAT
5 Murine BVRA ppMAL             ATATGAAAATGACCGTGCAGCTCGAGACCCAGAACAAAAGTCCATTATCATGGATTGAAGAGAAAGGGCCTGGCTTAAAAAGGAACAGACATATAAGCAT
                                ********************************************************************************************************

1 gi30353883gbBC052146.1        CCACTTCAAATCTGGGTCCTTGGAGGAAGTGCCAAATGTAGGAGTCAATAAGAACATTTTCCTGAAAGATCAGGATATATTTATCCAGAAGCTCTTGGGC
2 gi12832064dbjAK002231.1       CCACTTCAAATCTGGGTCCTTGGAGGAAGTGCCAAATGTAGGAGTCAATAAGAACATTTTCCTGAAAGATCAGGATATATTTATCCAGAAGCTCTTGGGC
3 gi31982540refNM_026678.3      CCACTTCAAATCTGGGTCCTTGGAGGAAGTGCCAAATGTAGGAGTCAATAAGAACATTTTCCTGAAAGATCAGGATATATTTATCCAGAAGCTCTTGGGC
4 gi12846571dbjAK010847.1       CCACTTCAAATCTGGGTCCTTGGAGGAAGTGCCAAATGTAGGAGTCAATAAGAACATTTTCCTGAAAGATCAGGATATATTTATCCAGAAGCTCTTGGGC
5 Murine BVRA ppMAL             CCACTTCAAATCTGGGTCCTTGGAGGAAGTGCCAAATGTAGGAGTCAATAAGAACATTTTCCTGAAAGATCAGGATATATTTATCCAGAAGCTCTTGGGC
                                ********************************************************************************************************

1 gi30353883gbBC052146.1        CAGGTCTCTGCAGAGGACCTGGCTGCTGAGAAGAAGCGCATCCTGCATTGCCTGGAGCTGGCCAGCGACATCCAGAGGCTGTGCCACCGGAAGCAGTGAG
2 gi12832064dbjAK002231.1       CAGGTCTCTGCAGAGGACCTGGCTGCTGAGAAGAAGCGCATCCTGCATTGCCTGGAGCTGGCCAGCGACATCCAGAGGCTGTGCCACCGGAAGCAGTGGG
3 gi31982540refNM_026678.3      CAGGTCTCTGCAGAGGACCTGGCTGCTGAGAAGAAGCGCATCCTGCATTGCCTGGAGCTGGCCAGCGACATCCAGAGGCTGTGCCACCGGAAGCAGTGAG
4 gi12846571dbjAK010847.1       CAGGTCTCTGCAGAGGACCTGGCTGCTGAGAAGAAGCGCATCCTGCATTGCCTGGAGCTGGCCAGCGACATCCAGAGGCTGTGCCACCGGAAGCAGTGAG
5 Murine BVRA ppMAL             CAGGTCTCTGCAGAGGACCTGGCTGCTGAGAAGAAGCGCATCCTGCATTGCCTGGAGCTGGCCAGCGACATCCAGAGGCTGTGCCACCGGAAGCAGTGAG
                                ********************************************************************************************************* *

1 gi30353883gbBC052146.1        GAGGAAGCTTCAGATACCTCTG-
2 gi12832064dbjAK002231.1       GAGGAAGCTTCAGATACCTCTGA
3 gi31982540refNM_026678.3      GAGGAAGCTTCAGAT--------
4 gi12846571dbjAK010847.1       GAGGAAGCTTCAGAT--------
5 Murine BVRA ppMAL             GAGGAAGCTTGGCACTGGCCGTC
                                **********   *
```

Appendix III Figure 2

Shown above are cDNA sequencing results from the ppMAL- mouse BVR-A construct (sequence 5), aligned with some of the murine cDNA sequences available on the NCBI nucleotide database (sequences 1-4). Accession numbers for each sequence are 1; BC052146.1, 2; AK002231.1 3; NM_026678.3 and 4; AK010847.1.

Appendix III

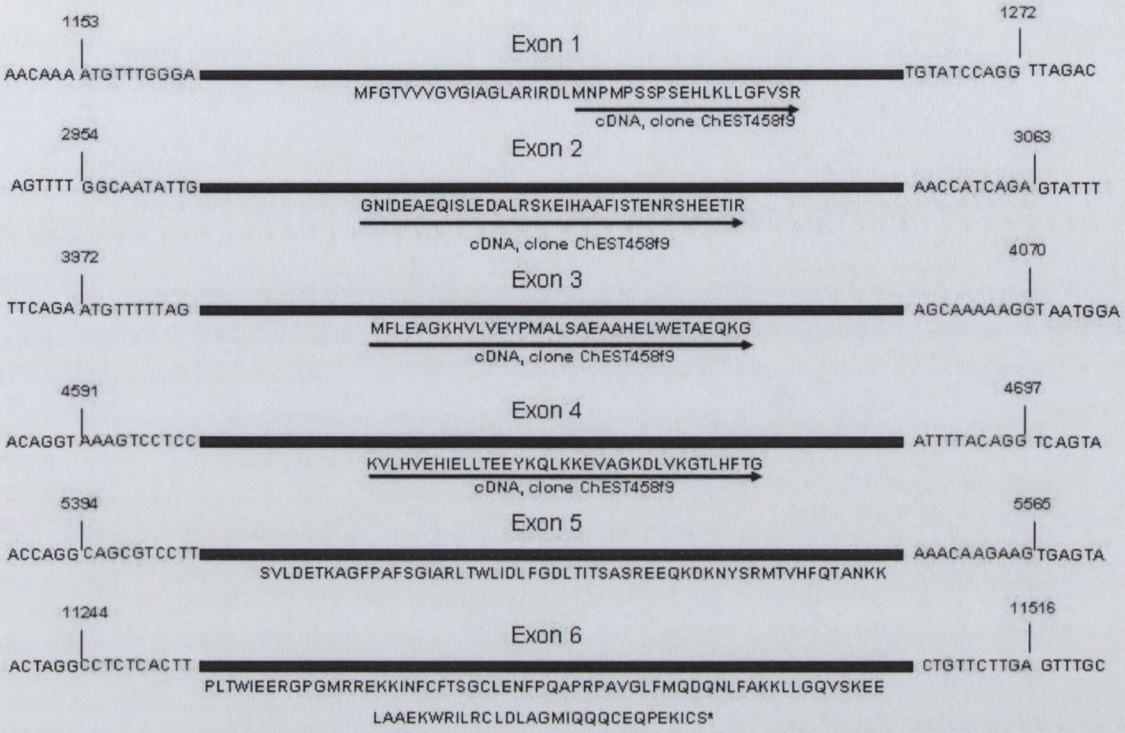

Figure 3.1 Gallus gallus DNA which may encode a BVR-A like protein

Analysis of the chicken chromosome 2 genome (accession number gi|50733099: 20393135-20405371) revealed a gene with exons, detailed in red encoding for a protein similar to other biliverdin reductases. Exon start and end positions are numbered, while their translated products are shown. EST evidence (is represented in blue.

Appendix III

>gi|50733017|ref|XM_418872.1| PREDICTED: Gallus gallus similar to Biliverdin reductase A precursor (Biliverdin-IX alpha-reductase) (BVR A) (LOC420776), mRNA

ATGAGCTTCAAAGATGGCCGTGGTAAAGGTGAGTATTACTGCTGCCTAGAGCTTTCTGATGGGAGGATT
CAGATTAACAAAATGTTTGGGACTGTGGTGGTTGGAGTTGGAATTGCTGGCTTAGCACGGATTCGAGAT
TTGATGAATCCAATGCCTTCTAGCCCTTCAGAGCATCTGAAGCTCCTTGGATTTGTATCCAGGAGAAGT
TTTGGCAATATTGATGAGGCTGAGCAGATTAGCCTGGAAGATGCTCTAAGAAGCAAAGAGATTCATGCA
GCCTTTATCAGCACAGAGAACAGAAGCCATGAAGAAACCATCAGAATGTTTTTAGAAGCTGGGAAACAT
GTCCTTGTTGAGTACCCCATGGCTTTGTCTGCTGAGGCAGCCCATGAGCTCTGGGAGACGGCTGAGCAA
AAAGGTAAAGTCCTCCATGTGGAGCATATTGAACTTCTGACTGAAGAATACAAGCAGCTGAAAAAGGAG
GTGGCTGGGAAAGACCTAGTGAAGGGAACATTACATTTTACAGGCAGCGTCCTTGATGAAACAAAAGCA
GGGTTTCCAGCTTTCAGTGGAATTGCCCGACTGACTTGGCTGATTGACCTCTTTGGAGACCTCACCATT
ACCTCTGCCAGCAGAGAAGAGCAGAAGGATAAGAATTATTCTAGAATGACCGTTCATTTTCAGACTGCA
AACAAGAAGCCTCTCACTTGGATCGAAGAACGAGGACCGGGGATGAGACGTGAAAAGAAAATCAATTTC
TGTTTCACCAGTGGTTGTCTGGAGAACTTCCCTCAAGCCCCAAGGCCTGCTGTGGGCCTTTTCATGCAG
GATCAGAACCTCTTCGCCAAAAAACTGTTGGGACAGGTATCCAAGGAGGAGCTGGCTGCTGAGAAATGG
CGAATTTTGCGGTGTCTTGACCTTGCTGGGATGATTCAACAGCAGTGTGAACAGCCAGAGAAAATCTGT
TCTTGAGTTTGCTCTTCCAAGAGGATCATGGCAGACAGAAAAGCTGTAGGTCTAGAGTTCAGTGTTGCC
ATCAGGTAATTGCTGTTTCTGCCTTATTACATTCTCCTTGACTGAACGTGAATCCTAGGTTCTCTGTGT
GGACTGGAGAGCCTGGGCTATGCCCCATGCCTTCTGGTGTACGCTGGAACACAAAGCAACGTGTTACCC
TGCTCCAATGCATTGCTGTCCTTTCAGCCAGACAGGAACCTAGCAGCAACAAGGTTTCTCATGGTTGCT
TCCAAGCAGTTTAGTTGGTAATGTCCCTGAGGTCAGATCATGGAGGATTGCAAATTTGTAACATGATTT
TTCTTCTTGAGTATTCTTTCTCCTCTATTTAGATATATGTGAAAATGAGACATATTGGATTATCTAGAA
CAAAGCTCTAAATGAATTTTCAACCTCTCTGCTTGATCTGCAAAAGTTGTACCACCTCAGTCCCAACCT
TTTTTTTCTGGGTACTCTGAATTTGTTTGTGTGTTTGCTCTGATTAGAAGTTGTGCCTGTTTTGTTTTG
TGTTTCACACTGGAAATCATCTTCCTTCAACCAGAATCTATAATGGTATCAAACCAGAATAGAAATATC
TTGTTTCTGACAGATGCCATGTTGAATTCATTCTATTTCTCTGGTGTCCTGTGCCAACAGGGAAATGTT
TTTCCAGCAGAGATTAAAACAATACATTAATACATCA

>gi|50733018|ref|XP_418872.1| PREDICTED: similar to Biliverdin reductase A precursor (Biliverdin-IX alpha-reductase) (BVR A) [Gallus gallus]

MSFKDGRGKGEYYCCLELSDGRIQINKMFGTVVVGVGIAGLARIRDLMNPMPSSPSEHLKLLGFVSRRS
FGNIDEAEQISLEDALRSKEIHAAFISTENRSHEETIRMFLEAGKHVLVEYPMALSAEAAHELWETAEQ
KGKVLHVEHIELLTEEYKQLKKEVAGKDLVKGTLHFTGSVLDETKAGFPAFSGIARLTWLIDLFGDLTI
TSASREEQKDKNYSRMTVHFQTANKKPLTWIEERGPGMRREKKINFCFTSGCLENFPQAPRPAVGLFMQ
DQNLFAKKLLGQVSKEELAAEKWRILRCLDLAGMIQQQCEQPEKICS

Figure 3.2 The nucleotide and deduced amino acid sequence of cDNA encoding the putative chicken biliverdin-IXα reductase.

Shown above is the full nucleotide sequences and the amino acid translation of the putative chicken BVR-A (see Section 3.9.1 for further explanation).

Appendix III

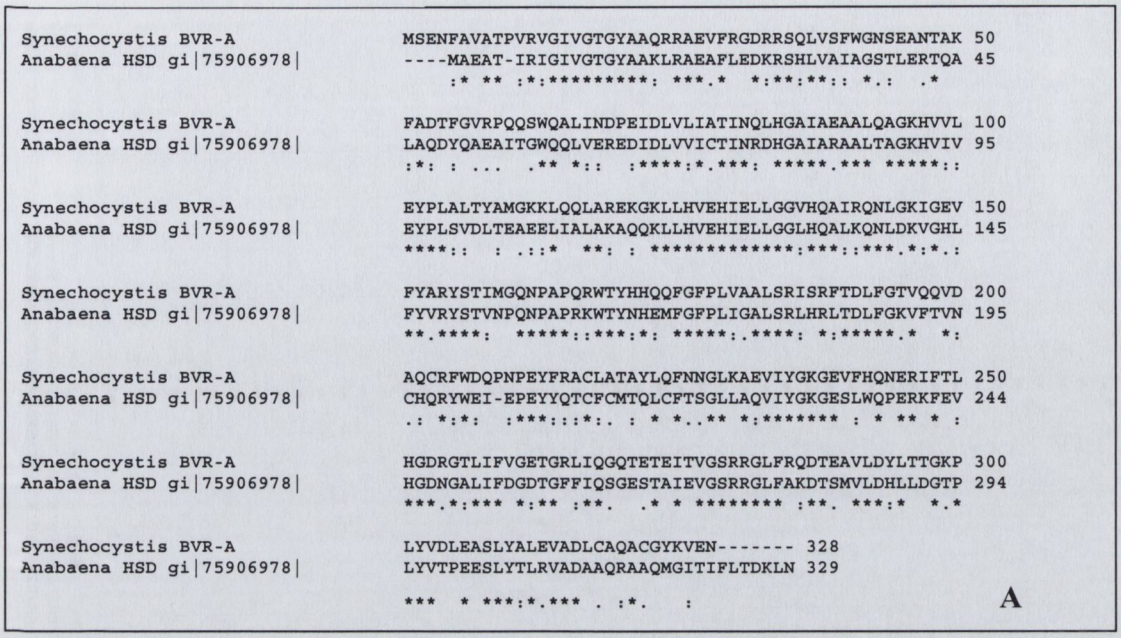

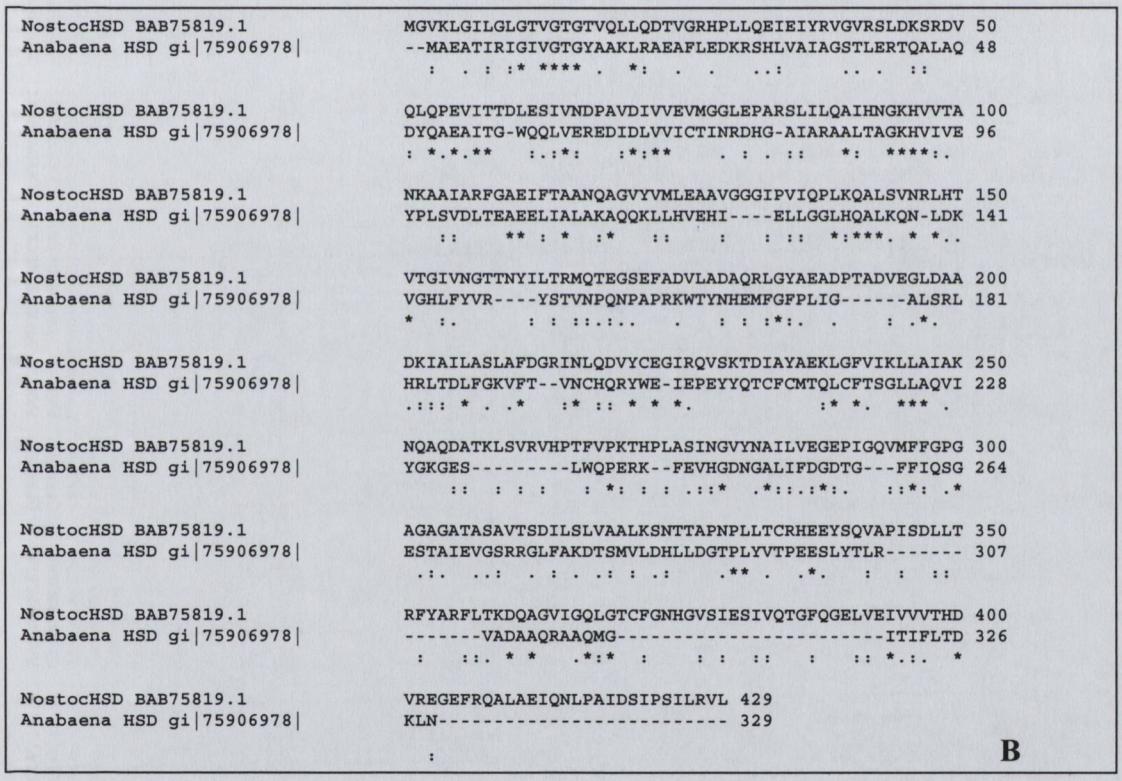

Figure 4

Alignments of the protein sequence accession number gi|75 700731|gb|ABA20407.1 (annotated as an NAD-binding, homoserine dehydrogenase from *Anabaena variabilis ATCC 29413*) against the *Nostoc sp. PCC 7120* homoserine dehydrogenase accession (number BAB75819.1) shown in part B. It is clear that this protein has greater similarity to the synechocystis biliverdin reductase than homoserine dehydrogenase of the *Nostoc sp. PCC 7120.*

Appendix III

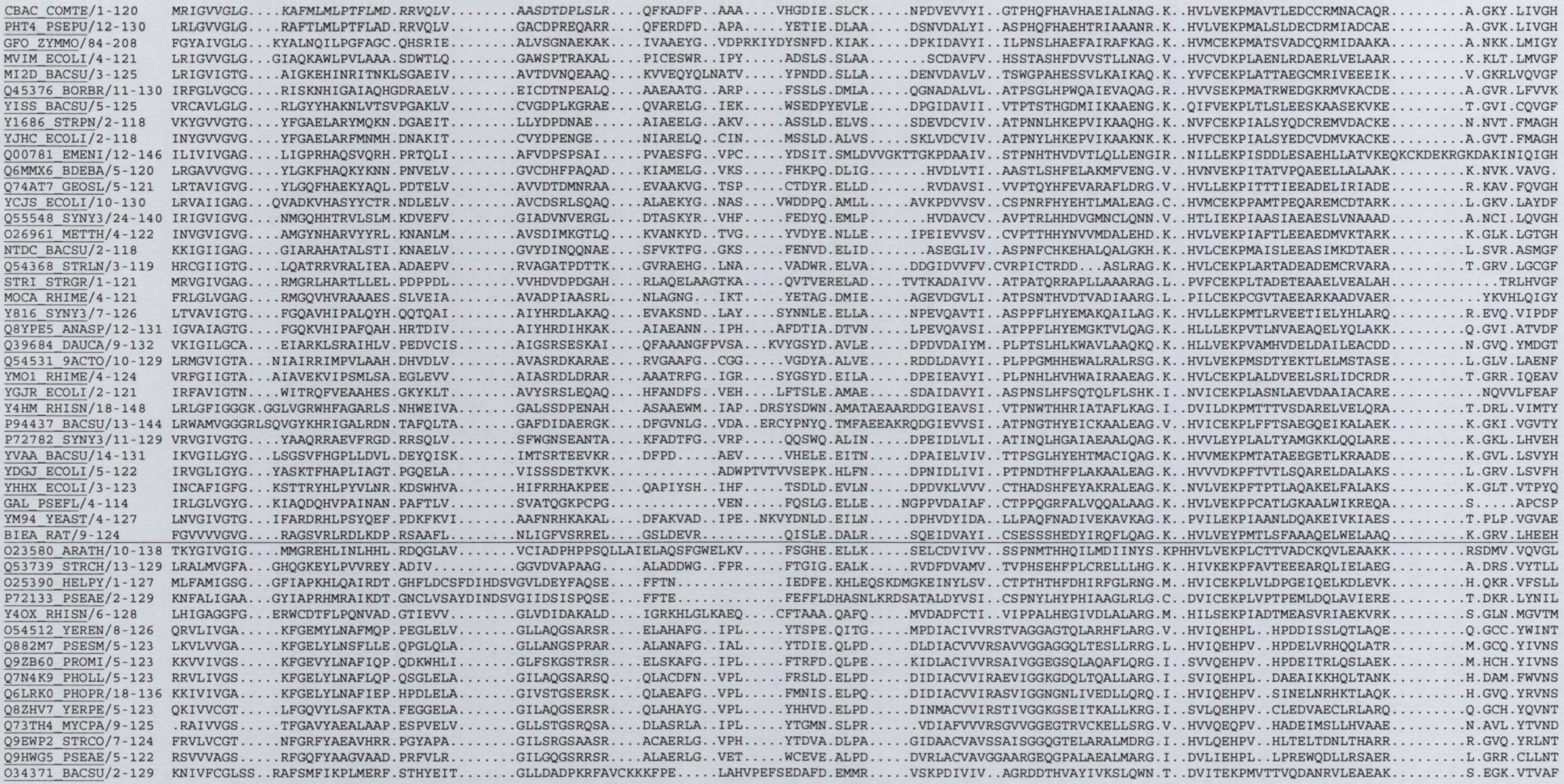

Figure 5 The GFO/IDH/MOCA family

The amino acid sequences of the GFO/IDH/MOCA family consensus sequence. Areas of similarity are evident throughout all sequences. The amino acid sequence of rat BVR-A is underlined.

Appendix IV

Appendix IV Figure 1 The dissociation constant of NAD with rat BVR-A over increasing concentrations of phosphate

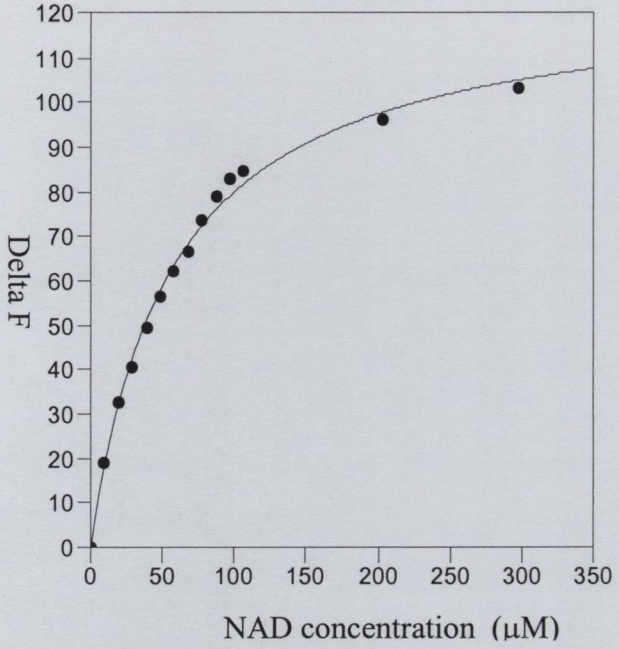

	F(x)=a*b/(x+b)	
a	1.248E+02	2.65E+00
b	5.60E+01	3.04102E+00
R2	0.99561	

(a) The dissociation constant of NAD with rat BVR-A in 50mM Tris pH 7.2 supplemented with 5 mM sodium phosphate. Data points were fitted to the Michaelis equation F(x)=a*b/(x+b) with b representing the $_{app}K_D$ values.

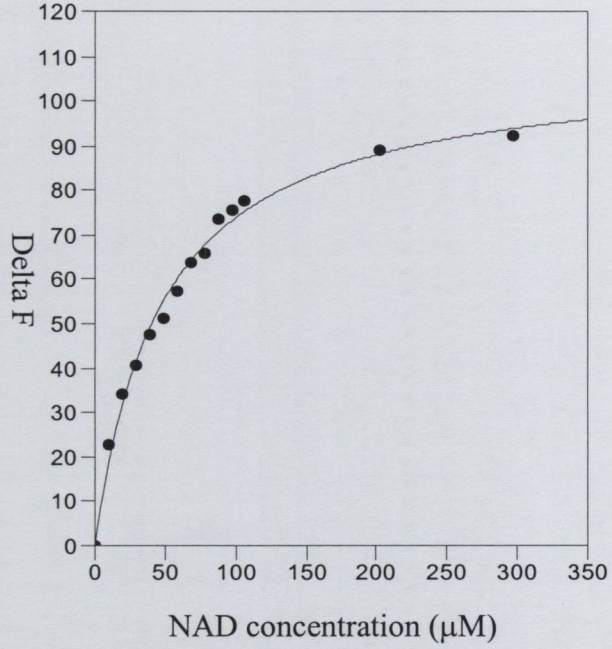

	F(x)=a*b/(x+b)	
a	1.09E+02	3.00E+00
b	4.73E+01	3.57E+00
R2	0.99108	

(b) The dissociation constant of NAD with rat BVR-A in 50mM Tris pH 7.2 supplemented with 10mM sodium phosphate. Data points were fitted to the Michaelis equation F(x)=a*b/(x+b) with b representing the $_{app}K_D$ values.

Appendix IV Figure 1 The dissociation constant of NAD with rat BVR-A over increasing concentrations of phosphate

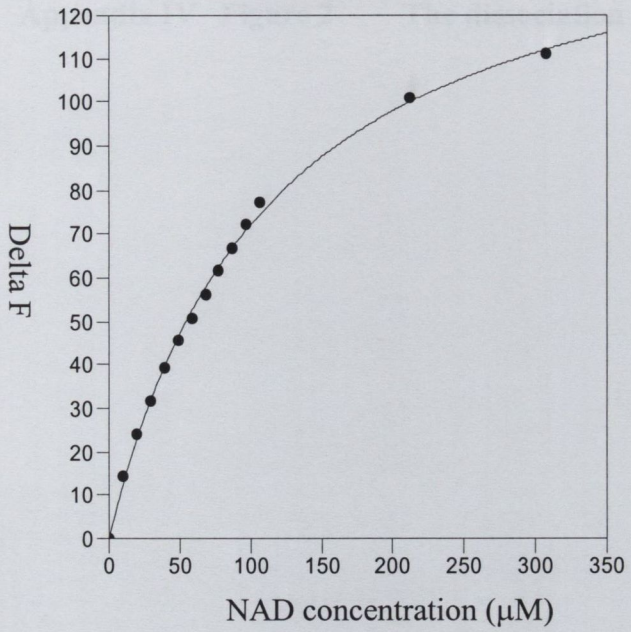

	F(x)=a*b/(x+b)	
a	1.53E+02	2.86518+00
b	1.12E+02	4.18973+00
R2	0.99814	

(c) The dissociation constant of NAD with rat BVR-A in 50mM Tris pH 7.2 supplemented with 50mM sodium phosphate. Data points were fitted to the Michaelis equation F(x)=a*b/(x+b) with b representing the $_{app}K_D$ values.

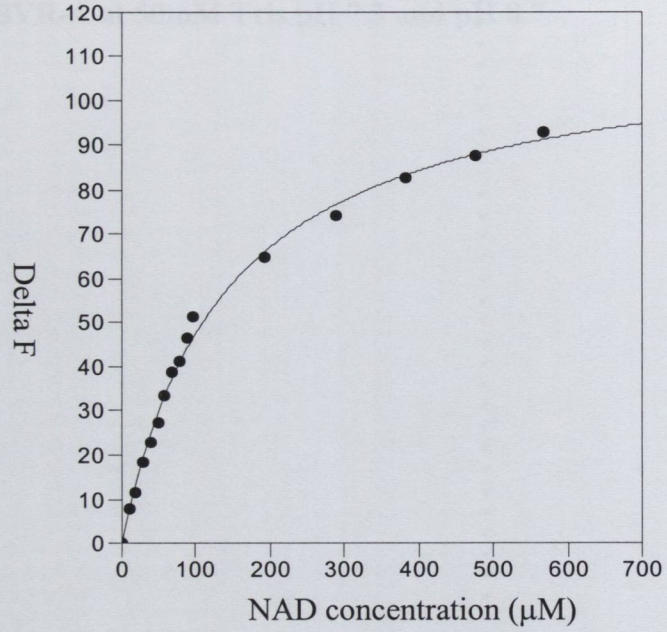

	F(x)=a*b/(x+b)	
a	1.14E+02	2.51211+00
b	1.39E+02	7.51184+00
R2	0.99537	

(d) The dissociation constant of NAD with rat BVR-A in 50mM Tris pH 7.2 supplemented with 100mM sodium phosphate. Data points were fitted to the Michaelis equation F(x)=a*b/(x+b) with b representing the $_{app}K_D$ values.

Appendix IV Figure 2 The dissociation constant of NADP with rat BVR-A at 50mM Tris pH 7.2 and pH 8.7

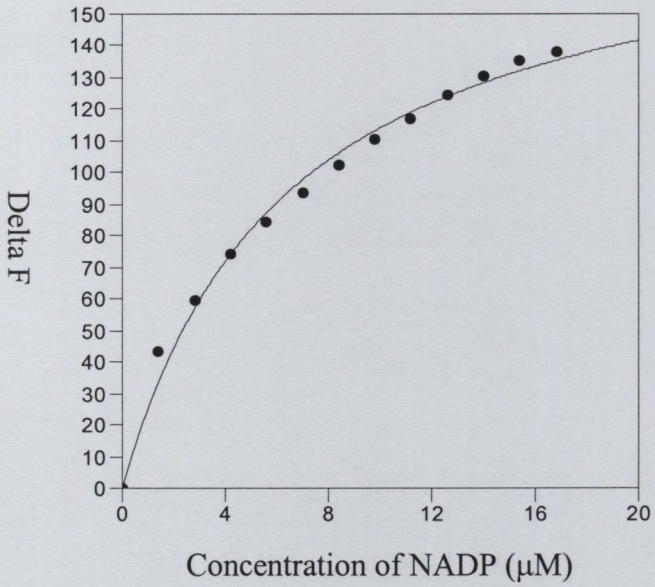

	F(x)=a*b/(x+b)	
a	1.87E+02	7.39E+00
b	6.39E+00	6.37E-01
R2	0.99145	

(a) Determination of the apparent dissociation constant of NADP with rat BVR-A in 50mM Tris pH 7.2. The data was fitted to the Michaelis equation F(x)=a*b/(x+b) where b represents the estimated $_{app}K_D$ values.

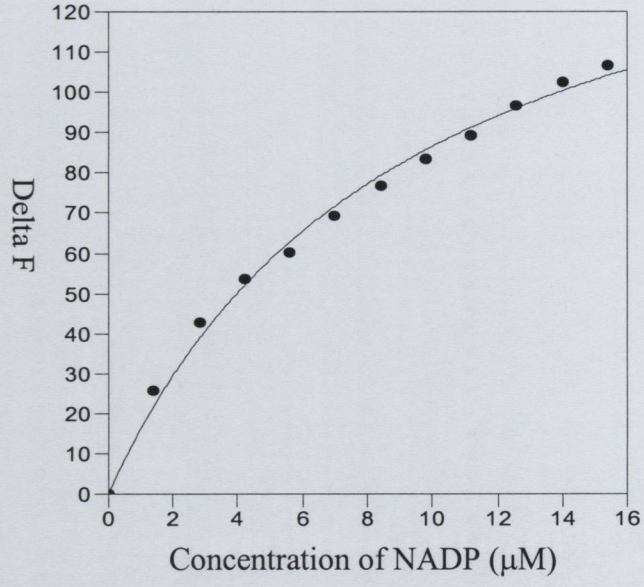

	F(x)=a*b/(x+b)	
a	1.85E+02	1.25E+01
b	1.12E+01	1.49E+00
R2	0.99151	

(b) Determination of the apparent dissociation constant of NADP with rat BVR-A in 50mM Tris pH 8.7. Data was fitted to the Michaelis equation F(x)=a*b/(x+b) where b represents the estimated $_{app}K_D$ values.

Appendix IV Figure 3 The dissociation constant of NAD and NADP with rat BVR-A

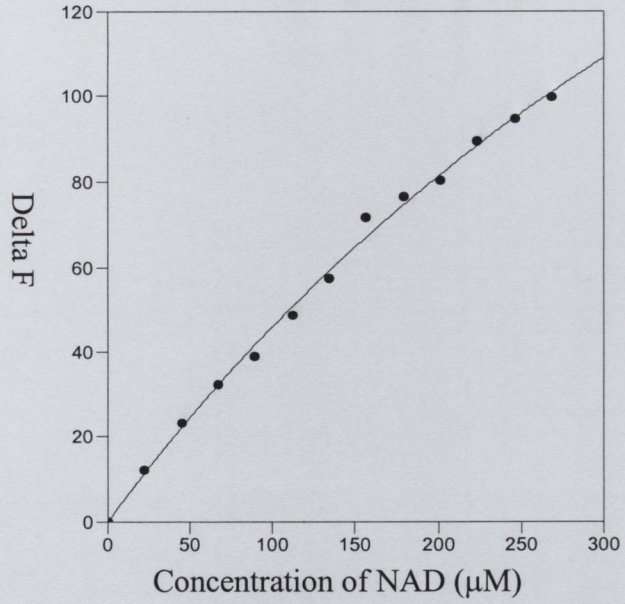

	F(x)=a*b/(x+b)	
a	3.47E+02	4.32E+01
b	6.54E+02	1.06E+02
R2	0.99648	

(a) Determination of the dissociation constant for NAD on rat BVRA in 50 mM Tris pH 8.7. Data points were fitted to the Michaelis equation F(x)=a*b/(x+b) with b representing the $_{app}K_D$ value.

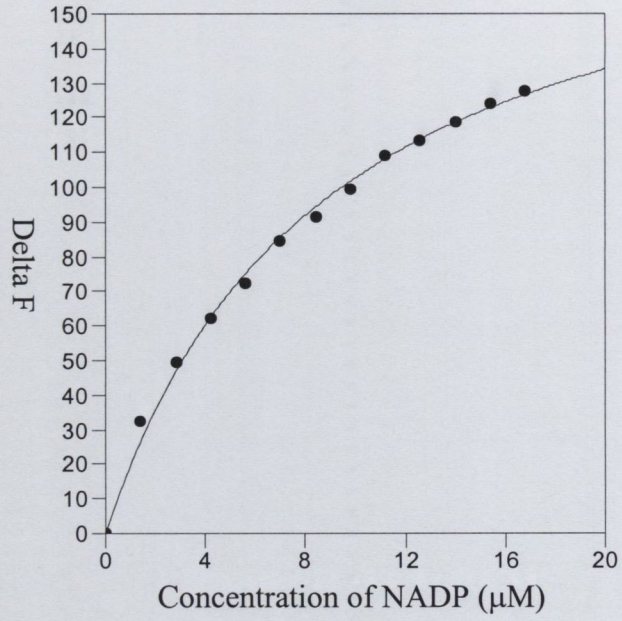

	F(x)=a*b/(x+b)	
a	1.91E+02	6.52E+00
b	8.64E+00	6.45E-01
R2	0.996	

(b) Determination of the dissociation constant for NADP on rat BVRA in 50 mM sodium phosphate pH 7.2. Data points were fitted to the Michaelis equation F(x)=a*b/(x+b) with b representing the $_{app}K_D$ value.

Appendix IV Figure 4 The dissociation constant for NAD with rat BVR-A.

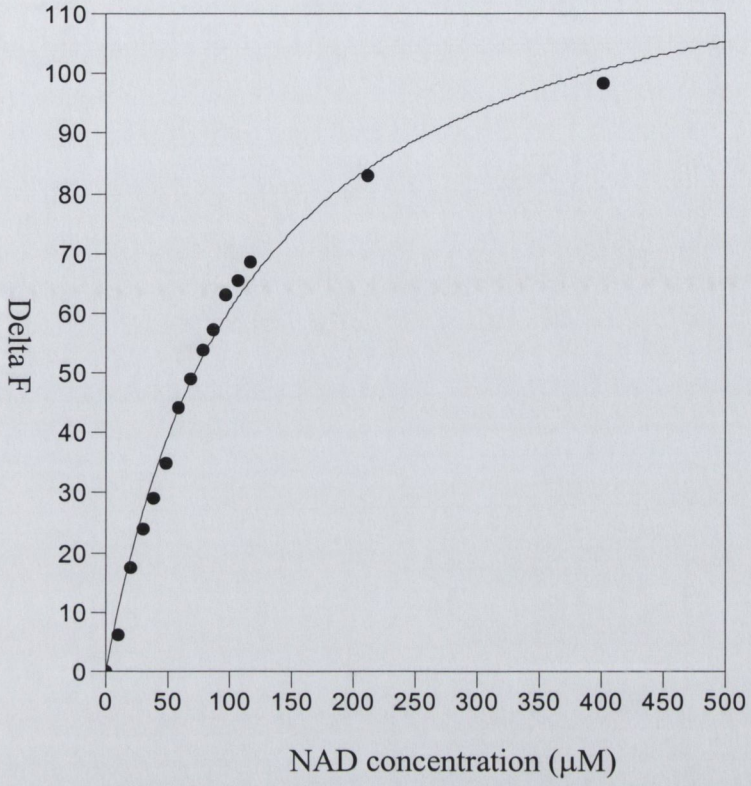

F(x)=a*b/(x+b)		
a	1.29E+02	4.80E+00
b	1.13E+02	8.59E+00
SSE	94.17	
R2	0.99134	

The dissociation constant for NAD with rat BVR-A in 50mM Tris pH 7.2. The fluorescence intensity was measured at 340nm (excitation wavelength 295nm) after each addition of nucleotide. The measured fluorescence intensities were corrected for the 'inner filter effect' to yield the corrected fluorescence F_{corr} which is represented as Delta F in the data presented.

Appendix IV

Hill equation			f(x)=(a*x^b)/c+x^b)
a	1.66463E+00		+/- 1.66463E+00
b	1.85943E+00		+/- 1.91472E-01
c	1.99E+03		+/- 1.32745E+03
SSE	0.01656	R^2	0.9910

Table 1 The effect of phosphate on the activity of human BVR-A.

Assays were performed with 20 μM biliverdin and 700 μM NADH at 30°C with increasing sodium phosphate (Figure 4.6). The reaction was started on addition of enzyme. Experimental data obtained from the effect of phosphate on the activity of human BVR-A is fitted to the Hill equation.

Appendix IV

5 µl	10×Pfu reaction buffer
10 ng (in 5µl)	Rat BVR-A in pHisParallel-1 plasmid
1 µl (10pmol/µl)	Forward mutagenic primer
1 µl (10pmol/µl)	Reverse mutagenic primer
3 µl	dNTP mix (10 mM each nucleotide)
29µl	Nuclease free H_2O
1 µl	PfuTurbo DNA polymerase (2.5 U/µl)

(i)

1	95°C	2 minutes
2	95°C	30 seconds
3	58°C	30 seconds
4	72°C	8 minutes
5	Go to step 2	16 times
6	72°C	10 minutes
7	4°C	10 minutes
8	END	

(ii)

Table 2 Site directed mutagenesis of rat BVR-A

(i) The PCR reaction mixtures used to introduce mutations into the pHis-Parallel 1 vector containing cDNA for rat BVR-A, were prepared with the components detailed above. (see Section 4.6)

(ii) Details of the cycling parameters used for the PCR of these mutants.

	a	b	c	K (s^{-1})	Chisquared	Signal noise
50 mM Tris	-3.112e-03 +/- 5.739e-05	4.511e-03 +/- 1.062e-04	2.829e-03 +/- 5.915e-05	1.514e+01 +/- 6.220e-01	1	0.000071
5 mM phosphate	-7.048e-03 +/- 4.783e-05	2.007e-02 +/- 9.663e-05	4.400e-03 +/- 3.588e-05	1.853e+01 +/- 2.825e-01	1	0.000871775
10 mM phosphate	-7.368e-03 +/- 3.355e-05	2.148e-02 +/- 1.067e-04	4.236e-03 +/- 3.400e-05	1.827e+01 +/- 2.022e-01	0.9999	0.000535814
20 mM phosphate	-9.402e-03 +/- 8.869e-05	2.438e-02 +/- 2.185e-04	6.943e-03 +/- 6.516e-05	2.36e+01 +/- 4.850e-01	0.9999	0.0014017
50 mM phosphate	-1.267e-02 +/- 8.158e-05	2.895e-02 +/- 1.769e-04	1.116e-02 +/- 4.992e-05	2.857e+01 +/- 9.862e-01	0.9999	0.00138655
100 mM phosphate	-1.264e-02 +/- 8.386e-05	3.047e-02 +/- 1.772e-04	1.013e-02 +/- 5.042e-05	2.773e+01 +/- 3.825e-01	1	0.00134688
200 mM phosphate	-1.494e-02 +/- 4.579e-05	3.337e-02 +/- 9.0711e-05	1.446e-02 +/- 4.392e-05	2.681e+01 +/- 2.199e-01	0.99901	0.00154

Table 3 The effects of phosphate concentration on the burst rate constant of human biliverdin reductase in 50mM sodium citrate pH 7.2.

The results of stopped flow experiments discussed in Section 4.4 were fitted with to the single exponential plus slope where $y = a \cdot e^{(-k\,x)} + b \cdot x + c$. As x approaches infinity the equation effectively reduces to $y = b.x + c$, the steady state rate. The burst rate constant (k_b) is represented as k in this equation.

Appendix IV

SSE:	0.69075	
R2:	0.99965	
a:	9.89E+01	+/- 2.9458E+00
b:	2.35E+02	+/- 1.1036E+01

(a)

SSE	1.9524	
R^2	0.99768	
(Km) a:	6.00E+01	+/- 4.10489
(V_{max}) b:	3.77E+02	+/- 4.37680

(b)

Table 4 The effect of increasing NADPH and NADH concentrations on activity of the rat BVR-A R44A mutant.

(a) NADPH was varied over the concentrations 2, 5, 10, 15, 25, 50 100 and 200μM in 50mM Tris pH 8.7.

(b) The activity was measured by monitoring bilirubin production at 460 nm using various NADH concentrations (5, 10, 25, 50 100, 200 and 400 μM) in 50 mM Tris pH 8.7.

Data points from Figure 4.22 were fitted to the Michaelis equation f(x)=(a*x)/(x +b) and estimates for Km and V_{max} are presented in accompanying tables.

f(x) = a*x/(x+b) using NADH as cofactor	
a = 6.00078E+01	+/- 4.1 E+00
b = 3.76995E+02	+/- 4.3E+01
SSE 1.952	
R2 0.99768	

(a)

f(x) = a*x/(x+b) using NADPH as cofactor	
a =9.83707E+01	3.656E+00
b = 2.33047E+02	1.369E+01
SSE 1.09422	
R2 0.9994	

(b)

Table 5 The effect of increasing NADH and NADPH concentrations on activity of the rat BVR-A R44A mutant.

Data sets presented in Figures 4.22 (a) and (b) were fitted to the Michaelis equation f(x)=(a*x)/(x +b) and estimates for the Km and Vmax were detemined.

(a) The activity was measured by monitoring bilirubin production at 460nm using various NADH concentrations (5, 10, 25, 50 100, 200 and 400μM) in 50mM Tris pH 8.7.

(b) NADPH was varied over the concentrations 2, 5, 10, 15, 25, 50 100 and 200 μM in 50mM Tris pH 8.7.

Appendix IV

f(x) = a*x/(x+b) using NADH as cofactor	
a = 3.30706E+00	+/- 6.50030E-02
b = 2.12849E+01	+/- 1.65466E+00
c = 6.19746E-01	+/- 4.65483E-02
SSE 0.01563	
R2 0.9982	

Table 6 The effect of phosphate on the activity of rat BVR-A.

Rat BVR-A was assayed using 700 μM NADH and 10μM BV as substrate in 50 mM Tris pH 7.2 at 30°C with increasing concentrations of phosphate (0, 3.125, 6.25, 12.5, 25, 50, 100, 250mM). Data points presented in Figure 4.20 was fitted to the Michaelis equation f(x)=((a*x)/(x +b))+c, the results of which are presented above.

Appendix V

Appendix V

ZZZanti 18ET biliverdin			
a	7.43E+03	2.61E+06	SSE 0.465
b	1.23E+03	4.32E+05	R2 0.9957
c	1.24E-02	4.36E+00	
d	2.70E+02	9.54E+04	
ZZZ-syn 18ET biliverdin			
a	5.21E+03	7.56E+05	SSE 0.00114
b	1.06E+03	1.54E+05	R2 0.99995
c	4.77E-03	6.93E-01	
d	1.72E+02	2.50E+04	
ZZEanti 18ET biliverdin			
a	3.82E+05	9.21E+10	SSE 0.6595
b	2.12E+04	5.12E+09	R2 0.98761
c	6.52E-05	1.50E+01	
d	5.12E+03	1.23E+09	

Figure 1 The effects of increasing concentrations of locked biliverdin isomers on the activity of human biliverdin-IXα reductase.

The effects of increasing concentrations of 15ZZE-anti 18ET biliverdin, 15ZZZ-syn 18ET biliverdin and 15ZZZ-anti 18ET biliverdin on human biliverdin-IXα reductase are shown in Figures 5.17, 5.14, and 5.12. The curves obtained were fitted with the equation for partial substrate inhibition, the coefficients for which are detailed above.

References

A

Ahmad, Z., Salim, M. & Maines, M. D. (2002) 'Human biliverdin reductase is a leucine zipper-like DNA-binding protein and functions in transcriptional activation of heme oxygenase-1 by oxidative stress'. J Biol Chem. 277, 9226-32.

Angel, P., Okino, S.T., Hattori, K., Boyle, W.J., Hunter, T., Karin, M., (1988) 'Oncogene jun encodes a sequence-specific trans-activator similar to AP-1'. Nature 332, 166-171.

B

Baranano, D.E., Rao, M., Ferris, C.D., Snyder, S.H. (2002) 'Biliverdin reductase: a major physiologic cytoprotectant'. Proc Natl Acad Sci U S A. 99, 16093-16098.

Beale, S.I., Cornejo, J. (1991) 'Biosynthesis of phycobilins. 15,16-Dihydrobiliverdin IX alpha is a partially reduced intermediate in the formation of phycobilins from biliverdin IX alpha'. J Biol Chem. 266, 22341-22345.

Beale SI, Castelfranco, P.A. (1974 a) 'The Biosynthesis of delta-Aminolevulinic Acid in Higher Plants: I. Accumulation of delta-Aminolevulinic Acid in Greening Plant Tissues'. Plant Physiol. 53, 291-296.

Beale SI, Castelfranco, P.A. (1974 b) The Biosynthesis of delta-Aminolevulinic Acid in Higher Plants: II. Formation of C-delta-Aminolevulinic Acid from Labeled Precursors in Greening Plant Tissues., Plant Physiol. 53, 297-303.

Bellamacina, C.R. (1996) 'The nicotinamide dinucleotide binding motif: a comparison of nucleotide binding proteins'. FASEB J. 10, 1257-1269.

Benedikt ,E., Gossauer, A., Kost H.P., Miki, W., Yamaguchi, K. (1988) 'Biliverdin IX delta and neobiliverdin IX delta, isolated from the ovaries of the marine snail, Turbo cornutus'. Eur J Biochem. 175, 643-648.

Berberat, P. O., Katori, M., Kaczmarek, E., Anselmo, D., Lassman, C., Ke, B., Shen, X., Busuttil, R. W., Yamashita, K., Csizmadia, E., Tyagi, S., Otterbein, L. E., Brouard, S., Tobiasch, E., Bach, F. H., Kupiec-Weglinski, J. W. & Soares, M. P. (2003) 'Heavy chain ferritin acts as an antiapoptotic gene that protects livers from ischemia reperfusion injury' Faseb J. 17, 1724-6.

Bissell, D.M., H. L., Schmid R. (1972) 'Hemoglobin and erythrocyte catabolism in rat liver: the separate roles of parenchymal and sinusoidal cells'. Blood. 40, 812-822.

Blauer, G., King, T. (1970) 'Interactions of bilirubin with bovine serum albumin in aqueous solution'. J Biol Chem. 245, 372-381.

Blumenthal, S.G., Stucker, T., Rasmussen, R.D., Ikeda R.M., Ruebner, B.H., Bergstrom, D.E., Hanson, F.W. (1980) 'Changes in bilirubin in human prenatal development'. Biochem J. 186, 693-700.

Bocanegra, J.A., Scrutton, N., Perham, R.N. (1993) 'Creation of an NADP-dependent pyruvate dehydrogenase multienzyme complex by protein engineering'. Biochemistry. 32, 2737-2740.

Bornberg-Bauer, E., Rivals, E., Vingron, M. (1998) 'Computational approaches to identify leucine zippers'. Nucleic Acids Res. 26, 2740-6.

Braggins, P.E., Trakshel. G.M., Kutty, R.K., Maines, M.D. (1986) 'Characterization of two heme oxygenase isoforms in rat spleen: comparison with the hematin-induced and constitutive isoforms of the liver'. Biochem Biophys Res Commun. 141, 528-533.

Brendel, V., Karlin, S. (1989) 'Too many leucine zippers?' Nature. 341, 574-5.

Brodersen, R., Andersen. S., Jacobsen, C., Sonderskov, O., Ebbesen, F., Cashore, W.J., Larsen, S. (1982) 'Determination of reserve albumin-equivalent for ligand binding, probing two distinct binding functions of the protein'. Anal. Biochem. 121, 395-408.

Brodersen, R. (1979) 'Bilirubin. Solubility and interaction with albumin and phospholipid'. J. Biol. Chem. 254, 2364-9.

Bunn, H.F. & Forger, B. (1986) 'Hemoglobin: Molecular, Genetic and Clinical Aspects'. W.B. Saunders & Company, Philadelphia.

Busch, S.J. & Sassone-Corsi, P. (1990) 'Dimers, leucine zippers and DNA-binding domains'. Trends Genet. Feb;6 (2): 36-40.

Busch SJ, Sassone-Corsi, P. (1990) 'Fos, Jun and CREB basic-domain peptides have intrinsic DNA-binding activity enhanced by a novel stabilizing factor'. Oncogene 5, 1549-1556.

C

Caignan, G.A., Deshmukh, R., Wilks, A., Zeng, Y., Huang, H., Moënne-Loccoz, P., Bunce, R.A., Eastman, M.A., and Rivera, M. (2002) 'Oxidation of Heme to beta- and alpha-Biliverdin by Pseudomonas aeruginosa Heme Oxygenase as a Consequence of an Unusual Seating of the Heme'. J. Am. Chem. Soc. Dec 18; 124 (50): 14879-14892.

Carugo, O, Argos, P. (1997 a) 'NADP-dependent enzymes. I: Conserved stereochemistry of cofactor binding'. Proteins. May;28(1): 10-28.

Carugo, O, Argos, P. (1997 b) 'NADP-dependent enzymes. II: Evolution of the mono- and dinucleotide binding domains'. Proteins: Sructure, Function, and Genetics. May 28 (1): 29-40.

Castenholz, R. W., Garrity, G., Boone, D.R. (2001) 'Cyanobacteria. Oxygenic Photosynthetic Bacteria., Bergey's Manual of Systematic Bacteriology. Volume 1: The Archaea and the Deeply Branching and Phototropic Bacteria'. Second Edition.

Choi, A.M., Alam, J. (1996) 'Heme oxygenase-1: function, regulation, and implication of a novel stress-inducible protein in oxidant-induced lung injury'. Am. J. Respir. Cell Mol. Biol. Jul; 15 (1): 9-19.

Chomczynski, P, Mackey, K. (1995) 'Substitution of chloroform by bromo-chloropropane in the single-step method of RNA isolation'. Anal. Biochem. Feb 10; 225 (1): 163-164.

Christensen, K.E., Mirza, A., Berghuis, A.M., Mackenzie, R.E. (2005) 'Magnesium and phosphate ions enable NAD binding to methylenetetrahydrofolate dehydrogenase-methenyltetrahydrofolate cyclohydrolase'. J. Biol. Chem. Oct 7; 280 (40): 34316-34323.

Cline, J., Bramann, J., Hogrefe, H.H. (1996) 'PCR fidelity of pfu DNA polymerase and other thermostable DNA polymerases'. Nucleic Acids Research Vol 24 (18): 3546-3551.

Cole, K.D. & Little, G.H (1983 a) 'UDP-glucuronosyltransferase activity and bilirubin conjugation in the bullfrog' Biochem. J. May 15; 212 (2): 265-269.

Cole, K.D. & Little, G.H. (1983 b) 'Bile pigments and bilirubin UDP-glucuronyl transferase during the metamorphosis of Rana catesbeiana tadpoles'. Comp. Biochem. Physiol. B. 76 (3): 503-506.

Cornelius, C.E. (1981) 'Hepatic Billrubin-IX-alpha-Glycosyltransferase Activities in Animals Excreting Primarily Biliverdin into Bile'. Vet. Clin. Pathol. 10 (1): 27-31.

Cunningham, O., Dunne, A., Sabido, P., Lightner, D., Mantle, T.J. (2000) 'Studies on the specificity of the tetrapyrrole substrate for human biliverdin-IXalpha reductase and

biliverdin-IXbeta reductase. Structure-activity relationships define models for both active sites'. J. Biol. Chem. Jun 23; 275 (25):19009-19017.

D

Didierjean, C., Rahuel-Clermount, S., Vitoux, B., Dideberg, O., Branlant, G., Aubry, A. (1997) 'A crystallographic comparison between mutated glyceraldehyde-3-phosphate dehydrogenases from Bacillus stearothermophilus complexed with either NAD^+ or $NADP^+$'. J. Mol. Biol. May 16; 268 (4): 739-759.

Dohr, O., Paine, M.J.I., Friedberg, T., Roberts, G.C.K., Wolf, C.R. (2001) 'Engineering of a functional human NADH-dependent cytochrome P450 system'. Proc. Natl. Acad. Sci. U.S.A. Jan 2; 98, No.1: 81-86.

Dolphin, D. (Ed.), (1979) 'The Porphyrins' Vol I-VII Academic Press New York.

Drum, D.E., Harrison, J.H., Ting-Kai Li, Bethune, J.L., Vallee, B.L. (1967) 'Structural and functional zinc in horse liver alcohol dehydrogenase'. May 15, Vol 57, No. 5: 1434-1440.

E

Eklund, H., Nordstrom, B., Zeppezauer, E., Soderlund, G., Ohlsson, G., Bowie, T. and Branden, C.I. (1974) 'The structure of liver alcohol dehydrogenase'. FEBS Letters, Aug 25, Vol. 44 (2): 200-204

Elliott, G., Mantle, T.J. (1995) 'Purification and properties of salmon liver biliverdin reductase'. Biochem. Soc. Trans. May; 23 (2): 389S.

Elmore, C.L. & Porter, T.D. (2002) 'Modification of the nucleotide cofactor-binding site of cytochrome P-450 reductase to enhance turnover with NADH in Vivo'. J. Biol. Chem. Vol 277(50): 48960-48964.

Ennis, O.M. & Mantle, T.J. (1995) 'Expression of rat biliverdin reductase as a glutathione-S-transferase fusion protein'. Biochem. Soc. Trans. Aug; 23 (3), 443S.

F

Falchuk, K.H., Contin, J.M., Dziedzic, T.S., Feng, Z., French, T.C., Heffron, G.J. and Montorzi, M. (2002) 'A role for biliverdin IXalpha in dorsal axis development of Xenopus laevis embryos'. Proc. Natl. Acad. Sci. U.S.A. Jan 8; Vol. 99 (1): 251-256.

Fang, L.S. & Lai, C.C. (1987) 'Characterization and purification of biliverdin reductase from the liver of eel, Anguilla japonica'. Comp. Biochem. Physiol. B. Vol. 88: 1151-1155.

Fankhauser, C. (2001) 'The phytochromes, a family of red/far-red absorbing photoreceptors'. J. Biol. Chem. Apr 13; 276 (15): 11453-11456.

Fisher, H. (1937) In Die Chemie des Pyrrols, 2, 486, by Fisher, H. & Orth, H. Leipzig: Akdemische Verlagsgesellschaft M.B.H.

Fisher, C.L. & Pei, G.K. (1997) 'Modification of a PCR-based site-directed mutagenesis method'. Biotechniques. Oct;23 (4): 570-1, 574.

G

Gibson, K.D., Laver W.G., Neuberger, A. (1958) 'Initial stages in the biosynthesis of porphyrins. 2. The formation of delta-aminolaevulic acid from glycine and succinyl-coenzyme A by particles from chicken erythrocytes'. Biochem J. Sep;70 (1): 71-81.

Granick, S. & Beale, S.I. (1978) 'Hemes, chlorophylls, and related compounds: biosynthesis and metabolic regulation'. Adv. Enzymol. Relat. Areas Mol. Biol. 46: 33-203.

Granick, P.S., Sassa, S., Grieninger, G. (1975) 'Effects by heme, insulin, and serum albumin on heme and protein synthesis in chick embryo liver cells cultured in a chemically defined medium, and a spectrofluorometric assay for porphyrin composition'. J. Biol. Chem. Dec 25; 250(24): 9215-9225.

Grodsky, GM, Carbone, J.V., Fanska, R., Peng, C.T. (1962) 'Tritiated bilirubin: preparation and physiological studies'. Am. J. Physiol. Sep; 203: 532-536.

H

Habig, W.H., Pabst, M.J., Jakoby, W.B. (1974) 'Glutathione S-transferases. The first enzymatic step in mercapturic acid formation'. J. Biol. Chem. Nov 25; 249(22): 7130-7139.

Hackley, B.M., Smith, J.A., Halsted, J.A. (1968) 'A simplified method for plasma zinc determination by atomic absorption spectrophotometry'. Clin. Chem. Jan;14 (1): 1-5.

Himes, J.A. & Cornelius, C.E. (1975) 'Biliverdin and bilirubin excretion in the turkey'. Cornell Vet. Jul; 65 (3): 374-9.

Hirst, J.D., Vieth, M., Skolnick, J., Brooks, C.L. 3rd. (1996) 'Predicting leucine zipper structures from sequence' Protein Eng. Aug; 9 (8): 657-662.

Honore, B. (1987) 'Stopped-flow studies of spectral changes in bilirubin-human serum albumin following an alkaline pH jump and following binding of bilirubin'. J. Biol. Chem. Nov 5; 262 (31): 14939-44.

Howe, R.B., Berk, P., Bloomer, J.R., Berlin, N.I. (1970) 'Preparation and properties of specifically labeled radiochemically stable 3H-bilirubin'. J. Lab. Clin. Med. Mar; 75 (3): 499-502.

Huang, T.S., Melefors, O., Lind, M.I., Soderhall, K. (1999) 'An atypical iron-responsive element (IRE) within crayfish ferritin mRNA and an iron regulatory protein 1 (IRP1)-like protein from crayfish hepatopancreas'. Insect Biochem. Mol. Biol. Jan; 29 (1): 1-9.

Hutchinson, D.W., Johnson, B., Knell, A.J. (1972) 'The reaction between bilirubin and aromatic diazo compounds'. Biochem. J. May; 127 (5): 907-8.

I

Ignarro, L.J. (1992) 'Haem-dependent activation of cytosolic guanylate cyclase by nitric oxide: a widespread signal transduction mechanism'. Biochem Soc Trans. May; 20 (2): 465-9.

Immenschuh, S., Hinke, V., Ohlmann, A., Gifhorn-Katz, S., Katz, N., Jungermann, K., Kietzmann, T. (1998) 'Transcriptional activation of the haem oxygenase-1 gene by cGMP via a cAMP response element/activator protein-1 element in primary cultures of rat hepatocytes'. Biochem. J. Aug 15; 334 (Pt. 1): 141-146.

Inomata, K., Hammam, M.A., Kinoshita, H., Murata, Y., Khawn, H., Noack, S., Michael, N., Lamparter, T. (2005) 'Sterically locked synthetic bilin derivatives and phytochrome Agp1 from Agrobacterium tumefaciens form photoinsensitive Pr- and Pfr-like adducts'. J. Biol. Chem. Jul 1; 280 (26): 24491-7.

Inoue, H., Nojima, H., Okayama, H. (1990) 'High efficiency transformation of Escherichia coli with plasmids'. Gene 1990 Nov 30; 96 (1): 23-28.

J

Jansen, P.L., Chowdhury, J.R., Fischberg, E.B., Arias, I.M. (1977) 'Enzymatic conversion of bilirubin monoglucuronide to diglucuronide by rat liver plasma membranes'. J. Biol. Chem. Apr; 252 (8): 2710-2716.

John, M., Briand, J., Granger-Schnarr, M., Schnarr, M. (1994) 'Two pairs of oppositely charged amino acids from Jun and Fos confer heterodimerization to GCN4 leucine zipper'. J. Biol. Chem. Jun 10; 269(23): 16247-53.

K

Kawai, S., Mori, S., Mukai, T., Hashimoto, W., Murata, K. (2001) 'Molecular characterization of Escherichia coli NAD kinase'. Eur. J. Biochem. Aug; 268 (15): 4359-4365.

Kelli, A., Markham, R., Sikorski, S., Kohen, A. (2003) 'Purification, analysis, and preservation of reduced nicotinamide adenine dinucleotides 2'-phosphate' Analytical Biochemistry 322: 26 - 32.

Kikuchi, A., Park, S. Y., Miyatake, H., Sun, D., Sato, M., Yoshida, T. & Shiro, Y. (2001) 'Crystal structure of rat biliverdin reductase'. Nat. Struct. Biol. 8 (3): 221-5.

Kleiger, G. & Eisenberg, D. (2002) 'GXXXG and GXXXA motifs stabilize FAD and NAD(P)-binding Rossmann folds through C(alpha)-H... O hydrogen bonds and van der waals interactions'. J. Mol. Biol. Oct 11; 323 (1): 69-70.

Kleiger, G., Grothe, R., Mallick, P., Eisenberg, D. (2002) 'GXXXG and AXXXA: common alpha-helical interaction motifs in proteins, particularly in extremophiles'. Biochemistry May 14; 41 (19): 5990-5997.

Kravets, A., Hu, Z., Miralem, T., Torno, M.D., Maines, M.D. (2004) 'Biliverdin reductase, a novel regulator for induction of activating transcription factor-2 and heme oxygenase-1'. J. Biol. Chem. May 7; 279 (19): 19916-19923.

Kutty, R.K., Maines, M. (1981) 'Purification and characterization of biliverdin reductase from rat liver'. J. Biol. Chem. Apr 25; 256 (8): 3956-3962.

L

Laemmli, U.K. (1970) 'Cleavage of structural proteins during the assembly of the head of bacteriophage T4'. Nature Aug 15; 227 (5259): 680-685.

Lavitrano, M., Smolenski, R.T., Musumeci, A., Maccherini, M., Slominska E., Di Florio, E., Bracco, A., Mancini, A., Stassi, G., Patti, M., Giovannoni, R., Froio, A., Simeone, F., Forni, M., Bacci, M.L., D'Alise, G., Cozzi, E., Otterbein, L.E., Yacoub, M.H., Bach, F.H., Calise, F. (2004) 'Carbon monoxide improves cardiac energetics and safeguards the heart during reperfusion after cardiopulmonary bypass in pigs'. FASEB J. Jul; 18 (10): 1093-1095.

Lee, P.J., Alam, J., Wiegand, G.W., Choi, A.M. (1996) 'Overexpression of heme oxygenase-1 in human pulmonary epithelial cells results in cell growth arrest and increased resistance to hyperoxia'. Proc. Natl. Acad. Sci. U.S.A. Sep 17; 93 (19): 10393-10398.

Lee, T.S. & Chau, L. (2002) 'Heme oxygenase-1 mediates the anti-inflammatory effect of interleukin-10 in mice'. Nat. Med. Mar; 8(3): 240-246.

Lester, R., & Klein, P. (1966 a) 'Bile pigment excretion: a comparison of the biliary excretion of bilirubin and bilirubin derivatives'. J. Clin. Invest. Dec 45 (12): 1839-1846.

Lester, R., & Klein, P. (1966 b) 'Biosynthesis of tritiated bilirubin and studies of its excretion in the rat'. J. Lab. Clin. Med. Jun; 67 (6): 1000-1012.

Lightner, D.A., An, J.Y., Pu, Y.M. (1988) 'Circular dichroism of bilirubin-amine association complexes: insights into bilirubin-albumin binding'. Arch Biochem Biophys. May 1; 262 (2): 543-559.

Lightner, D.A., Reisinger, M., Landen, G.L. (1986) 'On the structure of albumin-bound bilirubin. Selective binding of intramolecularly hydrogen-bonded conformational enantiomers'. J. Biol. Chem. May 5; 261 (13): 6034-6038.

Lin, G.L., Himes, J.A., Cornelius, C.E. (1974) 'Bilirubin and biliverdin excretion by the chicken'. Am. J. Physiol. Apr; 226 (4): 881-885.

Lind, C.W., Gronwall, R.R., Cornelius, C.E 1967. 'Bile pigments in the chicken'. Res.Vet. Sci. Jul; 8 (3):280-282

Liu, Y. & Ortiz de Montellano, P.R. (2000) 'Reaction intermediates and single turnover rate constants for the oxidation of heme by human heme oxygenase-1'. J. Biol. Chem. Feb 25; 275 (8): 5297-5307.

Llorente, P., Marco, R., Sols, A. (1970) 'Regulation of liver pyruvate kinase and the phosphoenolpyruvate crossroads'. Eur. J. Biochem. Mar 1; 13 (1): 45-54.

M

Maines, MD. (2003) 'Bile pigments: newcomers to the cell signalling arena'. Toxicol. Sci. Jan; 71 (1): 9-10.

Maines, M.D., Polevoda, B.V., Huang, T.J., McCoubrey, W.K. Jr. (1996) 'Human biliverdin IXalpha reductase is a zinc-metalloprotein. Characterization of purified and Escherichia coli expressed enzymes'. Eur. J. Biochem. Jan 15; 235 (1-2): 372-381.

Maines, M.D. (1997) 'The heme oxygenase system: a regulator of second messenger gases'. Annu. Rev. Pharmacol. Toxicol. 37; 517-554.

Makos, B.K. & Youson, J.H. (1988) 'Tissue levels of bilirubin and biliverdin in the sea lamprey, Petromyzon marinus L., before and after biliary atresia'. Comp. Biochem. Physiol. A. 91 (4): 701-710.

Manitto, P. & Monti, D. (1973) 'Acid-catalyzed addition of alcohols and thiols to bilirubin'. Experientia Feb 15; 29 (2): 137-139.

Manitto P. & Monti, D. (1979) 'Addition of sulphydryl groups to biliverdin'. Cellular and Molecular Life Sciences (CMLS) Nov; 35 (11): 1418 – 1420

Marco, R., Pestana, A., Sebastian, J., Sols, A. (1974) 'Oxaloacetate metabolic crossroads in liver. Enzyme compartmentation and regulation of gluconeogenesis'. Mol. Cell. Biochem. Mar 8; 3 (1): 53-70.

Markham, K.A., Sikorski, R., Kohen, A. (2003) 'Purification, analysis, and preservation of reduced nicotinamide adenine dinucleotide 2'-phosphate'. Anal. Biochem. 322: 26-32.

Markham, K.A., Sikorski, R., Kohen, A. (2004) 'Synthesis and utility of ^{14}C-labeled nicotinamide cofactors'. Anal. Biochem. 325: 62-67.

McCoubrey, W. K., Jr. & Maines, M. D. (1994) 'Site-directed mutagenesis of cysteine residues in biliverdin reductase. Roles in substrate and cofactor binding'. Eur. J. Biochem. Vol. 222: 597-603.

McCoubrey, W.K. Jr, Cooklis, M.A., Maines, M.D. (1995) 'The structure, organization and differential expression of the rat gene encoding biliverdin reductase'. Gene. Jul 28; 160(2), 235-240.

McCoubrey, W.K. Jr, Huang T.J., Maines, M.D. (1997) 'Isolation and characterization of a cDNA from the rat brain that encodes hemoprotein heme oxygenase-3'. Eur. J. Biochem. Jul 15; 247(2), 725-732.

McDonagh, A.F., Assisi, F. (1972) 'The ready isomerization of bilirubin IX- in aqueous solution'. Biochem. J. Sep; 129 (3): 797-800.

McDonagh, A.F., Lightner, D. (1985) 'Like a shrivelled blood orange' - bilirubin, jaundice, and phototherapy'. Pediatrics. 75 (2): 443-455.

McDonagh A.F. (1971) 'The role of singlet oxygen in bilirubin photo-oxidation'. Biochem. Biophys. Res. Commun. Sep 17; 44 (6): 1306-1311.

Meera Khan, P., Wijnen, L., Wijnen, J.T., Grzeschik, K.H. (1983) 'Electrophoretic characterization and genetics of human biliverdin reductase (BLVR; EC 1.3.1.24); assignment of BLVR to the p14 leads to cen region of human chromosome 7 in mouse-human somatic cell hybrids'. Biochem. Genet. Feb; 21 (1-2): 123-133.

Melefors, O. (1996) 'Translational regulation in vivo of the Drosophila melanogaster mRNA encoding succinate dehydrogenase iron protein via iron responsive elements'. Biochem. Biophys. Res. Commun. Apr 16; 221 (2): 437-41.

Melefors, O., Goossen, B., Johansson, H.E., Stripecke, R., Gray, N.K., Hentze, M.W. (1993) 'Translational control of 5-aminolevulinate synthase mRNA by iron-responsive elements in erythroid cells'. J. Biol. Chem. Mar 15; 268 (8): 5974-8.

Menken, M., Barrett, P.D., Swarm, R.L., Berlin, N.I. (1966) 'Kernicterus. Development of an experimental model using bilirubin ^{14}C '. Arch. Neurol. 15 (1): 68-73.

Miller, S.R. & Castenholz, R.W. (2000) 'Evolution of thermotolerance in hot spring cyanobacteria of the genus Synechococcus'. Appl. Environ. Microbiol. Oct; 66 (10): 4222-4229.

Miller, S.R. & Castenholz R.W. (2001) 'Ecological physiology of Synechococcus sp. strain SH-94-5, a naturally occurring cyanobacterium deficient in nitrate assimilation'. Appl. Environ. Microbiol. Jul; 67 (7): 3002-3009.

Minning, D.M., Gow, A.J., Bonaventura, J., Braun, R., Dewhirst, M., Goldberg, D.E., Stamler, J.S. (1999) 'Ascaris haemoglobin is a nitric oxide-activated 'deoxygenase'. Nature. 401: 497-502.

Mizobe, M., Kondo, F., Kumamoto K., Kanda, Y., Seguchi, H. (1997) 'High-performance liquid chromatographic analysis of bilirubin and biliverdin from jaundiced broilers'. J. Vet. Med. Sci. Aug; 59 (8): 677-680.

Montorzi, M., Dziedzic, T., Falchuk, KH. (2002) 'Biliverdin during Xenopus laevis oogenesis and early embryogenesis'. Biochemistry. Aug 6; 41 (31): 10115-22.

Muir, H.M., Neuberger, A. (1950) 'The biogenesis of porphyrins. 2. The origin of the methyne carbon atoms'. Biochem. J. Jun-Jul; 47 (1): 97-104.

N

Nakao, A., Otterbein, L., Overhaus, M., Sarady, J.K., Tsung, A., Kimizuka, K., Nalesnik, M.A., Kaizu, T., Uchiyama, T., Liu, F., Murase, N., Bauer, A.J., Bach, F.H. (2004) 'Biliverdin protects the functional integrity of a transplanted syngeneic small bowel'. Gastroenterology. Aug; 127 (2): 595-606.

Nogales, D., Lightner, D. (1995) 'On the structure of bilirubin in solution. 13C[1H] heteronuclear Overhauser effect NMR analyses in aqueous buffer and organic solvents'. J. Biol. Chem. Jan 6; 270 (1): 73-77.

Noguchi, M., Yoshida, T., Kikuchi, G. (1979) 'Purification and properties of biliverdin reductases from pig spleen and rat liver'. J. Biochem. Oct; 86 (4): 833-848.

Noonan, N.E., Olsen, G.A., Cornelius, C.E. (1979) 'A new animal model with hyperbilirubinemia: the indigo snake'. Digestive Diseases and Science. Jul; 24 (7): 521-524.

Novotny, L. & Vitek, L. (2003) 'Inverse relationship between serum bilirubin and atherosclerosis in men: a meta-analysis of published studies'. Exp. Biol. Med. May; 228 (5): 568-571.

O

O'Carra, P. & Colleran, E. (1970) 'Separation and identification of biliverdin isomers and isomer analysis of phycobilins and bilirubin'. J. Chromatogr. Aug 12; 50(3): 458-468.

O'Carra, P. & Colleran, E. (1975) 'Separation and identification of isomeric deuterobiliverdins and mesobiliverdins'. J Chromatogr. May 7; 108(1): 212-215.

Ohyoshi, E., Hamada, Y., Nakata, K., Kohata, S. (1999) 'The interaction between human and bovine serum albumin and zinc studied by a competitive spectrophotometry'. J. Inorg. Biochem. Jun 30; 75 (3): 213-218.

Ortiz de Montellano, P.R. (1998) 'Heme Oxygenase Mechanism: Evidence for an Electrophilic, Ferric Peroxide Species'. Acc. Chem. Res. May; 31 (9): 543-549.

Ott, M.C., Scott, J., Bihari, A., Badhwar, A., Otterbein, L.E., Gray, D.K., Harris, K.A., Potter, R.F. (2005) 'Inhalation of carbon monoxide prevents liver injury and inflammation following hind limb ischemia/reperfusion'. FASEB J. Jan; 19 (1): 106-108.

Otterbein, L.E., Otterbein, S., Ifedigbo, E., Liu, F., Morse, D.E., Fearns, C., Ulevitch, R.J., Knickelbein, R., Flavell, R.A., Choi, A.M. (2003) 'MKK3 mitogen-activated protein kinase pathway mediates carbon monoxide-induced protection against oxidant-induced lung injury'. Am. J. Pathol. Dec; 163 (6): 2555-2563.

Otterbein, L.E., Soares, M., Yamashita, K., and Bach, F.H. (2003) 'Heme oxygenase-1: unleashing the protective properties of heme'. Trends in Immunology. Aug; 24 (8), 449-455.

P

Parrish, J.W. (1984) 'Chemical levels in the serum of captive female House Sparrows'. The Wilson Bulletin. Mar; 96 (1): 138-143.

Pereira PJ, Macedo-Ribeiro S., Parraga, A., Perez-Luque, R., Cunningham, O., Darcy, K., Mantle, T.J., Coll, M. (2001) 'Structure of human biliverdin IXbeta reductase, an early fetal bilirubin IXbeta producing enzyme'. Nat. Struct. Biol. Mar; 8 (3); 198-200.

Petersen, C.E., Ha, C.E., Harohalli, K., Feix, J.B., Bhagavan, N.V. (2000) 'A dynamic model for bilirubin binding to human serum albumin'. J. Biol. Chem. Jul 14; 275 (18): 20985-20995.

Phillips, O., Mantle, T.J. (1981) 'Some kinetic and physical properties of biliverdin reductase'. Biochem. Soc. Trans. Aug; 9(4): 275-278.

Plieninger, H., el-Barkawi, F., Ehl, K., Kohler, R., McDonagh, A.F. (1972) 'New synthesis and 14 C-labelling of bilirubin-IXalpha'. Justus Liebigs Ann Chem. Apr; 758: 195-201.

Ponka, P. (1999) 'Cell Biology of Heme'. American Journal of the Medical Sciences. Oct; 318(4): 241-256.

Pozzoli, G., Mancuso, C., Mirtella, A., Preziosi, P., Grossman, A.B., Navarra, P. (1994) 'Carbon monoxide as a novel neuroendocrine modulator: inhibition of stimulated corticotropin-releasing hormone release from acute rat hypothalamic explants'. Endocrinology. Dec; 135(6): 2314-2317.

Q

Quail, P.H., Boylan, M.T., Parks, B.M., Short, T.W., Xu, Y., Wagner, D. (1995) 'Phytochromes: photosensory perception and signal transduction'. Science. May 5; 268(5211): 675-680.

Quail, P.H., (2002) 'Photosensory perception and signalling in plant cells: new paradigms?' Curr. Opin. Cell. Biol. 14(2): 180-181.

R

Radin, N.S., Rittenberg, D., Shemin, D. (1950) 'The role of glycine in the biosynthesis of heme'. J. Biol. Chem. Jun; 184(2): 745-53.

Radin, N.S, Rittenberg, D., Shemin D. (1950) 'The role of acetic acid in the biosynthesis of heme'. J. Biol. Chem. Jun; 184(2): 755-67.

Randerath, K. & Randerath, E., 'Thin-layer separation methods for nucleic acid derivatives'. Meth. Enzymol. 12A:323-47, 1967.

Rao, A.U., Carta, L.K., Lesuisse, E., Hamza, I. (2005) 'Lack of heme synthesis in a free-living eukaryote'. Proc. Natl. Acad. Sci. U.S.A. Mar 22; 102 (12), 4270-4275.

Rigney, E. (1986) 'Kinetic studies of Ox kidney biliverdin reductase'. Ph.D. Thesis. The University of Dublin, Trinity College, Dublin, Ireland.

Rigney, E. & Mantle T.J., (1988) 'The reaction mechanism of bovine kidney biliverdin reductase'. Biochim. Biophys. Acta. Nov 23;957(2): 237-242.

Rigney, E.M., Phillips, O., Mantle, T.J., (1988) 'Some physical and immunological properties of ox kidney biliverdin reductase'. Biochem. J., Oct 15; 255(2): 431-435.

Rudiger, W., Klose, W., Vuillaume, M., Barbier, M. (1969) 'On the biosynthesis of biliverdin-IX-gamma in Pieris brassicae'. Experientia. May 15; 25(5): 487-8.

Ryter, S.W., Otterbein, L.E., (2004) 'Carbon monoxide in biology and medicine'., Bioessays. Mar; 26(3): 270-280.

Schluchter, W.M., & Glazer, A., (1997) 'Characterization of cyanobacterial biliverdin reductase. Conversion of biliverdin to bilirubin is important for normal phycobiliprotein biosynthesis'. J. Biol. Chem. May 23; 272(21): 13562-13569.

Sedlak, T.W. & Solomon, S., (2004) 'Bilirubin benefits: cellular protection by a biliverdin reductase antioxidant cycle'. Pediatrics. Jun; 113(6): 1776-1782.

Shalloe, F., Elliott, G., Ennis, O., Mantle, T.J. (1996) 'Evidence that biliverdin-IX beta reductase and flavin reductase are identical'. Biochem. J. Jun 1; 316(Pt 2): 385-387.

Shemin, D., London, I.M., Rittenberg D. (1948) 'The in vitro synthesis of heme from glycine by nucleated red blood cells'. J. Biol. Chem. 173(2): 799-800.

Shen, A.L., Sem, D., Kasper, C.B. (1999) 'Mechanistic studies on the reductive half-reaction of NADPH-cytochrome P450 oxidoreductase'. J. Biol. Chem. Feb 26; 274(9): 5391-5398.

Silverstein, E., (1970) 'Separation of NAD^+ and NADH and $NADP^+$ and NADPH by anion exchange on DEAE-cellulose paper'. Biochim. Biophys. Acta. Jul 21; 215(1): 205-6.

Steinberg, D., Vaughan, M., Anfinsen, C.B., Gorry, J., (1957) 'Preparation of tritiated proteins by the Wilzbach method'. Science. Sep. 6; 126(3271), 447-448.

Stocker, R. & Ames, B. (1987) 'Potential role of conjugated bilirubin and copper in the metabolism of lipid peroxides in bile'. Proc. Natl. Acad. Sci. U.S.A. Nov; 84(22): 8130-8134.

Stocker R, M. A., Glazer AN, Ames BN. (1990) Antioxidant activities of bile pigments: biliverdin and bilirubin., Methods Enzymol. 186: 301-9.

T

Tacchini, L., Poglialiagli, G., Radice, L., Anzon, E., Bernelli-Zazzera, A. (1995) 'Differential activation of heat-shock and oxidation-specific stress genes in chemically induced oxidative stress'. Biochem. J. Jul 15; 309(Pt 2): 453-459.

Talbot, C. & Higgins, P. (1982) 'Observations on the gall bladder of juvenile Atlantic salmon Salmo salar L. in relation to feeding'. Journal of Fish Biology; 21: 663-669.

Talbot , C., Higgins, P. J., Shanks, A. M., (1984) 'Effects of pre- and post-prandial starvation on meal size and evacuation rate of juvenile Atlantic salmon, Salmo salar L.' Journal of Fish Biology, 25:5 551

Tenhunen, R., Marver, H., Schmid, R. (1970 a) 'The enzymatic catabolism of hemoglobin: stimulation of microsomal heme oxygenase by hemin'. J. Lab. Clin. Med. Mar; 75(3): 410-421.

Tenhunen, R., Ross, M.E., Marver, H.S., Schmid, R. (1970 b) 'Reduced nicotinamide-adenine dinucleotide phosphate dependent biliverdin reductase: partial purification and characterization'. Biochemistry. Jan 20; 9(2): 298-303.

Tenhunen, R., Marver, H. S., Schmid, R. (1968) 'The enzymatic conversion of heme to bilirubin by microsomal heme oxygenase'. Proc. Natl. Acad. Sci. U.S.A. Oct; 61(2): 748-755.

V

Vajro P, Thaler M.M., Blanckaert, N. (1995) 'Bile pigment composition and bilirubin esterification in the developing chick'. Pediatr. Res. Sept; 38(3), 349-355.

Verma, A., Hirsch D.J., Glatt, C.E., Ronnett, G.V., Snyder S.H. (1993) 'Carbon monoxide: a putative neural messenger'. Science. Jan 15; 259(5093): 381-384.

W

Wagniere, G. & Blauer, G. (1976) 'Calculations of optical properties of biliverdin in various conformations' J. Am. Chem. Soc. Nov 24; 98(24): 7806-7810.

Wang, J., de Montellano, P.R. (2003) 'The binding sites on human heme oxygenase-1 for cytochrome p450 reductase and biliverdin reductase' J. Biol. Chem. May 30; 278(22): 20069-20076.

Wen-qi L, Yong-long L. (2004) 'Detection of biliverdin reductase activity of Schistosoma japonicum' Journal of parasitology and parasitic diseases (Chinese)'. 22(2): 106-108.

Whitby, F.G., Phillips J.D., Hill, C.P., McCoubrey W., Maines, M.D. (2002) 'Crystal structure of a biliverdin IXalpha reductase enzyme-cofactor complex'. Jun 21; 319(5): 1199-1210.

Wilks, A. & Ortiz de Montellano, P.R. (1993) 'Rat liver heme oxygenase. High level expression of a truncated soluble form and nature of the meso-hydroxylating species'. J. Biol. Chem. Oct 25; 268(30): 22357-22362.

Wittenberg, J., Shemin, D. (1950) 'The location in protoporphyrin of the carbon atoms derived from the alpha-carbon atom of glycine'. J. Biol. Chem. Jul; 185(1): 103-16.

Woolley, P.V., Hunter, M.J., Arias, I.M. (1976) 'Bilirubin and biliverdin binding to rat Y protein (ligandin)'. Biochem. Biophys. Acta. Sept 28; 446(1): 115-123

Wu, J.T., Wu L.H., Knight, J.A. (1986) 'Stability of NADPH: effect of various factors on the kinetics of degradation'. Clin Chem. Feb; 32(2): 314-319.

Y

Yamaguchi T, Komuro, A., Nakano, Y., Tomita, M., Nakajima, H. (1993) 'Complete amino acid sequence of biliverdin-IX beta reductase from human liver'. Biochem. Biophys. Res. Commun. Dec 30; 197(3): 1518-1523.

Yamaguchi, T., Komoda, Y., Nakajima, H. (1994) 'Biliverdin-IX alpha reductase and biliverdin-IX beta reductase from human liver. Purification and characterization'. J Biol Chem. Sept 30; 269(39): 24343-24348.

Yamaguchi, T. & Nakajima, H. (1995) 'Changes in the composition of bilirubin-IX isomers during human prenatal development'. Eur. J. Biochem. Vol 233: 467-472.

Sakamoto, H., Omata Y., Palmer G., Noguchi, M. (1999) 'Ferric alpha-hydroxyheme bound to heme oxygenase can be converted to verdoheme by dioxygen in the absence of added reducing equivalents'. Biol. Chem. Jun 25; 274(26): 18196-18200.

Z

Zeng X, Zhu H, Lashuel HA, Hu JC., (1997) 'Oligomerization properties of GCN4 leucine zipper e and g position mutants' Protein Sci. Oct; 6(10):2218-26.

Zucker, S.D., Goessling, W., Ransil, B.J., Gollan, J.L. (1995) 'Influence of glutathione S-transferase B (ligandin) on the intermembrane transfer of bilirubin. Implications for the intracellular transport of nonsubstrate ligands in hepatocytes'. J. Clin. Invest. Oct; 96(4), 1927-1935.

Zuckerbraun, B.S., Billiar, T.R., Otterbein, S.L., Kim, P.K., Liu, F., Choi, A.M., Bach, F.H., Otterbein, L.E. (2003) 'Carbon monoxide protects against liver failure through nitric oxide-induced heme oxygenase 1'. J. Exp. Med. 198(11): 1707-1716.